

## Durham E-Theses

---

### *Some aspects of the time dependent strength behaviour of a range of tungsten carbide - cobalt materials*

Barrie David Wright

#### How to cite:

---

Wright, Barrie David (1983) Some aspects of the time dependent strength behaviour of a range of tungsten carbide - cobalt materials. Doctoral thesis, Durham University.

#### Use policy

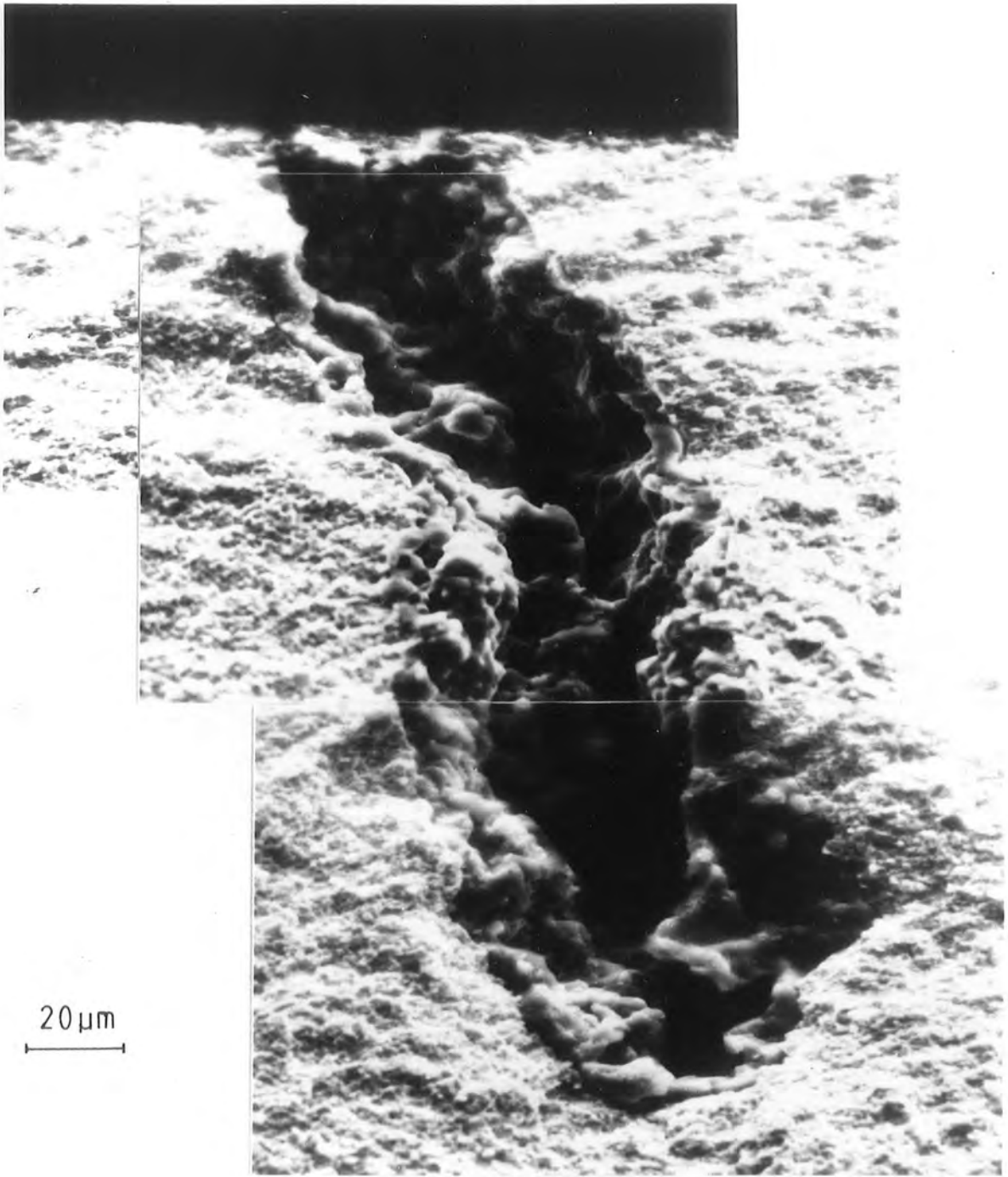
---

The full-text may be used and/or reproduced, and given to third parties in any format or medium, without prior permission or charge, for personal research or study, educational, or not-for-profit purposes provided that:

- a full bibliographic reference is made to the original source
- a <https://etheses.durham.ac.uk/id/eprint/7189/> is made to the metadata record in Durham E-Theses
- the full-text is not changed in any way

The full-text must not be sold in any format or medium without the formal permission of the copyright holders.

Please consult the [full Durham E-Theses policy](#) for further details.



Frontispiece.

Large surface flaw on fracture face of WC-16% Co bend specimen.

The copyright of this thesis rests with the author.  
No quotation from it should be published without  
his prior written consent and information derived  
from it should be acknowledged.

SOME ASPECTS OF THE TIME DEPENDENT  
STRENGTH BEHAVIOUR OF A RANGE OF  
TUNGSTEN CARBIDE - COBALT MATERIALS

by

Barrie David Wright

A thesis submitted for the degree of Doctor of Philosophy in  
the Faculty of Science, University of Durham.

March 1983



28 NOV 1983

## ABSTRACT

Delayed fracture, slow crack growth and corrosion in sintered WC-Co alloys containing 6, 13 and 16% cobalt by weight, have been observed and evaluated at room temperature in a variety of environments including laboratory air, distilled water and dilute nitric acid. Data from strength tests and double torsion tests have been analysed using theories of stress corrosion and brittle fracture, to obtain estimates of the stress corrosion parameter,  $n$ , which best describe the behaviour. A statistical method has been developed for analysing strength data. Observation of specimens in soak tests has shown corrosion to occur in some environments. Inspection of bend strength specimen fracture faces has indicated the source of fracture initiation. A simple, and reliable method of precracking WC-Co double torsion specimens has been developed.

## ACKNOWLEDGEMENTS

I would like to thank all who have provided support during the period of study. In particular, special thanks go to Dr.P.M.Braiden for his guidance, unceasing encouragement and lively discussions; to Mr.Campbell and the technicians in the Engineering Science department workshops for their help and advice on more practical matters; to Dr.P.J.Green of the Mathematics department for his invaluable assistance with the statistics; and to members of the departments of Chemistry and Applied Physics and Electronics for their help with specimen preparation and tuition in the use of the scanning electron microscope. I also gratefully acknowledge the financial support provided by the Science Research Council. Finally, I would like to offer my sincere apologies to all who have suffered with me during the long arduous hours spent writing up; I greatly appreciate their patience and understanding.

## CONTENTS

1.	Introduction	1
2.	Stress Corrosion	4
2.1	Introduction	4
2.2	Effects of stress corrosion on strength and lifetime and factors influencing the degree of delayed fracture	4
2.2.1	Applied Load	5
2.2.2	Environment	5
2.2.3	Temperature	5
2.3	Theories and models of stress corrosion	6
2.4	Stress corrosive slow crack growth	8
2.5	Use of the $K_I - v$ diagram to predict strength and lifetime	10
2.6	Summary	13
3.	Properties of WC-Co materials	14
3.1	Introduction	14
3.2	Factors influencing the strength	14
3.2.1	Material composition and grain size	14
3.2.2	Temperature	15
3.2.3	Microstructural factors	15
3.3	Factors influencing the fracture toughness and its measurement	17
3.4	Crack resistance	19
3.5	Mechanisms of failure	20
3.6	Delayed fracture and slow crack growth	23
3.7	Summary	28
4.	Manipulation and analysis of strength data	29
4.1	Introduction	29
4.2	Brittle fracture model	29

4.3	Stress corrosion model	32
4.3.1	The failure model	32
4.3.2	Comparison of average behaviour	33
4.3.3	Statistical representation of the random variable, $a_I$	34
4.3.4	A technique to analyse strengths originating from tests involving different stress rates to failure	37
4.4	Development of the "maximum likelihood" technique	38
4.4.1	The failure model	39
4.4.2	Use of the model to estimate unknown parameters $n, m, B$	40
4.4.3	Assessing the validity of the model	43
4.5	Transformation of strength data	45
4.6	Graphical representation of delayed fracture behaviour	51
4.7	Summary	52
5.	Characterisation of materials	53
5.1	Introduction	53
5.2	Hardness	53
5.3	Crack resistance	54
5.4	Coercive force	54
5.5	Microstructural investigation	54
6.	Strength tests	56
6.1	Introduction	56
6.2	Experimental details	56
6.2.1	Measurement of strength	56
6.2.2	Test rig	57
6.2.3	Specimen preparation	57
6.2.4	Loading and associated errors	58
6.3	Time-dependent loading tests	59

6.4	Stress rate tests	59
6.4.1	Test details	59
6.4.2	Analysis and discussion of results	60
6.5	Stepped loading tests	62
6.5.1	Test details	62
6.5.2	Analysis and discussion of results	63
6.6	Comparison of results from stress rate and stepped loading tests	65
6.7	Environmental tests	67
6.8	Preliminary environmental tests	68
6.8.1	Test details	68
6.8.2	Analysis and discussion of results	68
6.9	Main environmental tests	72
6.9.1	Test details	72
6.9.2	Analysis and discussion of results	73
6.10	A Comparison of the influence of environment on the strength of WC-Co and alumina materials	75
6.11	Inspection of fractured specimens	76
6.11.1	The specimen side	76
6.11.2	The tensile face	76
6.11.3	The fracture face	77
6.11.4	Relation of observations to strength test results	78
6.12	Summary of strength test results	82
7.	Crack propagation tests	84
7.1	Introduction	84
7.2	Choice of test configuration	84
7.3	The double torsion test	86
7.4	Use of the double torsion test to measure slow crack growth	89

7.5	Experimental details	92
7.5.1	Test rig	92
7.5.2	Specimen preparation	93
7.5.3	Precracking tests and techniques	94
7.5.4	Procedure to ensure reliability of results	97
7.5.5	The guiding groove	98
7.5.6	Observation of the crack	99
7.5.7	Compliance measurements	100
7.5.8	Estimation of errors	101
7.6	Preliminary tests on soda-lime glass specimens	102
7.7	A note on "jumps" observed on load relaxation curves	102
7.8	WC-Co double torsion test results and discussion	104
7.9	Inspection of double torsion specimen fracture faces	105
7.10	Evidence of environmentally assisted slow crack growth in WC-Co materials	106
7.10.1	Crack growth in dilute nitric acid	106
7.10.2	Environmental crack resistance tests	108
7.11	Summary of crack propagation test results	109
8.	Discussion	110
9.	Conclusions	116
10.	Future Work	119

## References

## Tables

## Figures

## Plates

LIST OF TABLES

- 5.1 Characterisation of materials - manufacturer's specifications.
- 5.2 Characterisation of materials - laboratory test results.
- 6.1 Largest estimated errors in variables used to calculate the bend strength.
- 6.2 Maximum likelihood estimates of  $m$  and  $n$ , related confidence intervals and the significance of observed rate effect using bend strength data from stress rate tests in laboratory conditions on soda-lime glass and WC-Co materials.

## LIST OF FIGURES

- 2.1 Typical form of the  $K_{I1} - v$  diagram, showing the three regions of slow crack<sup>1</sup> growth behaviour lying between the lower threshold,  $K_{I0}$ , and the critical limit,  $K_{IC}$ .
- 4.1 Typical form of the SPT diagram.
- 5.1 Inverse crack resistance plotted against Vickers hardness for the three grades of WC-Co material studied.
- 6.1 Strengths recorded from stress rate tests at 20°C in laboratory air on WC-6% Co specimens with ground faces.
- 6.2 As Figure 6.1 for WC-6% Co specimens with polished faces.
- 6.3 As Figure 6.1 for WC-13% Co specimens with ground faces.
- 6.4 As Figure 6.1 for WC-13% Co specimens with polished faces.
- 6.5 As Figure 6.1 for WC-16% Co specimens with ground faces.
- 6.6 As Figure 6.1 for WC-16% Co specimens with polished faces.
- 6.7 Probability integral transform,  $U_i$ , of residual,  $Z_i$ , plotted against  $i/N$ , ( $i = 1, 2, 3, \dots, N$ ), for strength - stress rate data from stress rate tests on soda-lime glass specimens.
- 6.8 As Figure 6.7 for WC-6% Co specimens with ground faces.
- 6.9 As Figure 6.7 for WC-6% Co specimens with polished faces.
- 6.10 As figure 6.7 for WC-13% Co specimens with ground faces.
- 6.11 As Figure 6.7 for WC-13% Co specimens with polished faces.
- 6.12 As Figure 6.7 for WC-16% Co specimens with ground faces.
- 6.13 As Figure 6.7 for WC-16% Co specimens with polished faces.
- 6.14 As Figure 6.7 for examples of two artificial data sets.
- 6.15 Strengths recorded from stepped loading tests at 20°C in laboratory air on WC-16% Co specimens with ground faces.
- 6.16 As Figure 6.15 for WC-16% Co specimens with polished faces.
- 6.17 Mean strengths of WC-16% Co specimens tested using each constant stress duration.
- 6.18  $\sigma_{ISEC}$  Weibull curves for WC-16% Co stress rate and stepped loading data, transformed using a value of  $n = 10$ .
- 6.19 As Figure 6.18 using a value of  $n = 30$ .
- 6.20 As Figure 6.18 using a value of  $n = 100$ .

- 6.21 As Figure 6.18 using a value of  $n = 1000$ .
- 6.22  $\sigma_{ISEC}$  Weibull curves for WC-6% Co, and WC-13% Co stress rate data, transformed using a value of  $n = 10$ .
- 6.23 As Figure 6.22 using a value of  $n = 30$ .
- 6.24 As Figure 6.22 using a value of  $n = 100$ .
- 6.25 As Figure 6.22 using a value of  $n = 1000$ .
- 6.26 Strengths recorded from stress rate tests on WC-13% Co specimens at  $20^{\circ}\text{C}$ , in laboratory air and in distilled water, both with and without a presoak in distilled water - preliminary environmental test data.
- 6.27 Weibull diagrams for preliminary environmental test data, according to use of presoak, or not, but independent of test environment, and according to test environment, but independent of use of presoak, or not.
- 6.28 Strengths recorded from stress rate tests on WC-16% Co specimens at  $20^{\circ}\text{C}$  in laboratory air with no presoak, in laboratory air with a presoak, and in distilled water with no presoak - main environmental test data.
- 6.29 Weibull diagrams for main environmental test data.
- 6.30 Strengths recorded from stress rate tests on  $\text{Al}_2\text{O}_3$  specimens at  $20^{\circ}\text{C}$  in laboratory air, and Ringers Solution, both with and without a presoak in Ringers Solution.
- 6.31 External views of a fractured bend specimen drawn diagrammatically.
- 7.1 Common large crack technique configurations.
- 7.2 The double torsion specimen.
- 7.3 Double torsion crack front, drawn diagrammatically to show direction of cracking.
- 7.4 Double torsion crack growth model.
- 7.5 Impact loading technique for precracking double torsion specimens.
- 7.6 Typical load-time record for crack growth through a double torsion specimen loaded under a constant displacement rate.
- 7.7 Approximate shape, in cross-section, of crack-guiding grooves in double torsion specimens used in this study.
- 7.8 Compliance calibration diagram for double torsion specimens.
- 7.9  $K_I - v$  diagram for soda-lime glass at  $20^{\circ}\text{C}$  in laboratory air.

- 7.10 Typical form of load relaxation curves for soda-lime glass and WC-Co materials.
- 7.11 Typical form of  $K_I - v$  diagram for WC-Co materials showing the effects of "jumps" in load relaxation curves.
- 7.12  $K_I - v$  diagram for WC-6% Co at 20°C in laboratory air.
- 7.13  $K_I - v$  diagram for WC-16% Co at 20°C in laboratory air.
- 7.14 Ranges of  $K_I$  measured from double torsion slow crack growth tests on WC-6% Co and WC-16% Co compared with values of  $K_{IC}$  for WC-Co materials, found in the literature.
- 7.15 Cracked surfaces of the first WC-16% Co specimen to be soaked in a 10% solution of nitric acid - after 3 days.
- 7.16 Cracked surfaces of the first WC-13% Co specimen to be soaked in a 10% solution of nitric acid - after 1 day.
- 7.17 Cracked surfaces of the second WC-13% Co and WC-16% Co specimens to be soaked in a 10% solution of nitric acid - after 2 and 5 days.
- 8.1 Typical SPT diagram for WC-Co materials in ambient conditions.
- 8.2 SPT diagram for soda-lime glass at 20°C in laboratory air.

## LIST OF PLATES

- Frontispiece            Large surface flaw on the fracture face of a WC-16% Co bend specimen.
- 5.1                    Etched surface of WC-6% Co.
- 5.2                    Etched surface of WC-13% Co.
- 5.3                    Etched surface of WC-16% Co.
- 6.1                    The three point bend rig.
- 6.2                    Scanning electron micrographs of the surfaces of bend specimens with a ground finish.
- 6.3                    Scanning electron micrographs of the surfaces of bend specimens with a polished finish.
- 6.4                    WC-13% Co specimen loaded to failure after a presoak of 150 hours in distilled water.
- 6.5                    WC-16% Co specimen fracture face showing the approximate location of fraction initiation, the smooth elliptical region, the outer rough region and the final ligament to be broken.
- 6.6                    Scanning electron micrographs of a WC-16% Co specimen fracture face containing a large surface flaw.
- 6.7                    Scanning electron micrographs of a WC-16% Co specimen fracture face containing an extremely large surface flaw.
- 6.8                    Scanning electron micrographs of a WC-16% Co specimen fracture face containing a large sub-surface flaw.
- 6.9                    Scanning electron micrographs of a WC-6% Co specimen fracture face containing a large sub-surface multiple flaw system.
- 6.10                   Scanning electron micrographs of a WC-16% Co specimen fracture face on which no large flaw was detected.
- 7.1                    The double torsion rig.
- 7.2                    WC-6% Co double torsion specimen with a machined notch sharpened by spark erosion.
- 7.3                    The "kink" on the compressive ungrooved face of a double torsion specimen, highlighted by the reflected boundary of a dark object.
- 7.4                    Observation of the "kink" using reflections of a parallel line grid seen in the surface of the specimen.

- 7.5 Fracture face of a WC-6% Co double torsion specimen.
- 7.6 Matching portions of the two fracture faces of a WC-16% Co double torsion specimen.
- 7.7 The first WC-13% Co specimen to be soaked in a 10% solution of nitric acid - after 14 days.
- 7.8 The second WC-13% Co specimen to be soaked in a 10% solution of nitric acid - after 14 days.

1. INTRODUCTION

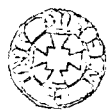
The object of this study was to observe and evaluate time dependent effects on the strength of tungsten carbide-cobalt (WC-Co) materials with particular emphasis on stress corrosion.

This range of alloys has found considerable use in shaping and forming tools and in wear resistant applications. So extensive is their usage that even a modest increase in tool performance would greatly increase the profitability of manufacturing industry (Lardner, 1981). Since the introduction of WC-Co materials, cutting speeds, for example, have increased by approximately an order of magnitude over those achieved by conventional cutting steels (Schwartzkopf, Kieffer, 1960).

To maximise performance, component behaviour must be well understood. However, such an understanding can rarely be achieved through experience gained from studies of existing usage. Invariably, tests on the materials from which the components are made must be performed in the laboratory, where individual factors influencing the behaviour, can be isolated and studied in depth. Only then is it possible to build up a comprehensive picture of material behaviour from which component behaviour can be reliably predicted.

The success of WC-Co materials lies in their high strength, retention of hardness at elevated temperatures, and good wear properties. However, of equal importance to the production engineer is an estimate of the likely component life. To obtain this, the material properties must be studied in relation to time dependent factors - how strength varies with time and hence, the influence of such mechanisms as fatigue, creep, wear, ageing and corrosion.

Another time dependent mechanism is stress corrosion. The resulting slow crack growth inducing delayed fracture has received



much attention in glasses and ceramics (see, in review, Wachtman, 1974; Wiederhorn, 1974; Adams, McMillan, 1977) and in metals (also in review, Logan, 1966; Scully, 1971). However little is known of its effects in WC-Co materials. Searches through the literature for data which might indicate the presence of stress corrosive mechanisms, yield information which, firstly, is extremely limited, and secondly is, for the most part, either contradictory or inconclusive. (A review may be found in Section 3.6).

The first to investigate delayed fracture in WC-Co materials in terms of stress corrosion were Braiden et al (1977). Although a significant dependence of strength on rate of loading to fracture was detected at elevated temperatures, results at ambient temperatures were somewhat inconclusive, and, as a result, led to the study reported here.

The effects of stress corrosion may be investigated using two distinct approaches. The first involves the measurement of strength degradation under the action of stress corrosive cracking, and the second, an investigation of the crack growth itself. By carefully controlling influential factors, which include applied stress, test environment, and temperature, throughout the duration of the test, and by analysing the resulting strength or crack growth data using theories of stress corrosion, estimates may be made of parameters characterising the behaviour. Since two approaches are available parameters obtained from each can be compared, thereby increasing confidence and reliability in observations and parameter estimates. A brief review of typical stress corrosion behaviour is given in Chapter 2.

A test programme to investigate stress corrosive slow crack growth and consequent delayed fracture was therefore developed to highlight these features whilst avoiding, or taking into account influences from other factors which might cause misinterpretation of the results.

Obviously delayed fracture induced by fatigue can be easily avoided by ensuring that loads are not cyclic. However, identifying stress corrosion when say, corrosion independent of stress is also present, is not so easy. Further, the behaviour may be obscured by non-time dependent factors, such as small changes in material composition, or specimen surface finish. In this respect an outline of general WC-Co behaviour with particular emphasis on strength and fracture, is given in Chapter 3.

One factor which cannot be avoided is the strength dependence of WC-Co materials upon inherent flaws. Their random, and in most cases, unpredictable nature induces a degree of uncertainty into results. In consequence, analysis of delayed fracture requires both the use of fracture mechanics (Pook, 1970; Knott, 1973) to model the effect of flaws, and also a statistical approach to model their randomness (Weibull, 1951; Stanley et al, 1973; Braiden, 1975). This is particularly necessary when effects of delayed fracture are expected to be little larger than random variations due to material flaws, and as such, are likely to be obscured. The delayed fracture model and the methods of analysis are developed in Chapter 4.

In this work, the primary concern has been the influence of applied stress and its variation with time in laboratory air. In addition, effects of different environments, namely distilled water and dilute nitric acid, have been investigated briefly. All tests were performed at room temperature.

Throughout this report, the term "strength" refers to the stress, calculated using linear elastic continuum mechanics, applied to a specimen at the point of catastrophic failure. No account is taken of any microstructural features such as flaws or cracks. Unless otherwise stated, the strength is measured in bending.

## 2. STRESS CORROSION

### 2.1 Introduction

Stress corrosion is discussed in terms of its effects on strength and lifetime, factors influencing the degree of delayed fracture, mechanisms, slow crack growth and mathematical models representing the behaviour quantitatively. The review provides details of expected behaviour, investigatory approaches and analytical techniques for use in the development of a test programme to study stress corrosion in WC-Co materials.

The discussion is based to a large extent upon reports of tests on what are traditionally considered more brittle materials, such as glasses and ceramics. It is from their behaviour, however, that modern stress corrosion theories were developed. Even so, the theories appear to model relatively well various types of slow crack growth for which widely different mechanisms, some based on more ductile behaviour, have been proposed (Evans, Langdon, 1976).

### 2.2 Effects of stress corrosion on strength and lifetime, and factors influencing the degree of delayed fracture

Grenet (1889) first observed that glass which had supported a constant load for some time, suddenly failed without warning. Since then, this delayed fracture phenomenon, dubbed "static fatigue" at an early stage (although now more correctly called stress corrosion) has been found to be controlled by three major factors - applied load, environment and temperature.

### 2.2.1 Applied Load

Much early work involved the application of constant loads until failure occurred. Experiments on various glasses and porcelain (Baker, Preston, 1946; Gurney, Borysowski, 1948) revealed that the time to fracture decreased when specimens were subjected to a higher constant load.

Work on similar materials in which the load was increased at a constant rate showed that the strength was greater at higher loading rates (Kropschot, Mikesell, 1957; Creyke, 1968).

Thus, in general, the strength diminishes as both the magnitude of the load and period of application prior to failure are increased.

### 2.2.2 Environment

The strength and lifetime under prolonged loading were also found to be influenced by the test environment. A major factor appeared to be the quantity of water present.

From tests on various glasses in vacuum (Baker, Preston, 1946) including heat treatments to remove absorbed, or surface water (Gurney, Pearson, 1949) and tests in a range of relative humidities (Mould, Southwick, 1951-61) and liquid water (Baker, Preston, 1946), the strength was found to decrease as the water content in the test environment was increased. The materials were also found to become more susceptible to delayed fracture.

### 2.2.3 Temperature

The test temperature was also found to be influential (Vonnegut, Glathart, 1946; Kropschot, Mikesall, 1957) although the relationship between strength and temperature was not simple. The strength reached a minimum at around 200<sup>o</sup>C for the glasses studied and increased as the

temperature was raised up to 520°C and down to 20K. Again delayed fracture was more pronounced when the strength was low.

These results were corroborated by Proctor et al (1967) who suggested that two mechanisms were present - a thermally controlled interaction between material and environment, limited by the availability of water both in the environment and absorbed in the material. They also noted that at high temperatures (>200°C) an additional factor was present, namely a chemical change in the material.

### 2.3 Theories and models of stress corrosion

Many theories have been proposed to explain the mechanisms of stress corrosion ranging from the early theories of Orowan (1944); Murgatroyd and Sykes (1944, 1947); Taylor (1947); Gurney (1947); Stuart and Anderson (1953) involving viscous pockets of material within an elastic matrix, rearrangement of atomic lattices and environmental corrosion, to the modern theories of Weidmann and Holloway (1974) and Lawn (1975) incorporating concepts of limited plastic deformation, and atomically kinked cracked fronts. However, perhaps most widely adopted for practical usage are the theories of Charles and Hillig (1958, 1962).

Charles (1958) proposed that a thermally activated chemical reaction takes place at the tip of an atomically sharp crack, the reactants being the material at the tip and a corrosive species in the environment. Further, for stress corrosive crack growth to occur, the material at the tip has to experience tensile stresses tending to open the crack, although magnitudes are less than the critical level for catastrophic failure. The reaction breaks material bonds revealing new sites for stress corrosion, and hence elongates the crack.

The longer this relatively slow crack propagation is allowed to

continue, then the greater is the crack length when the critical conditions for catastrophic failure are reached. Hence the corresponding applied stress at this point, and therefore the fracture strength as measured using continuum mechanics are smaller. Thus all factors which tend to increase the rate of chemical reaction between material and environment, such as higher applied stresses for longer durations, greater concentration of corrosive species in the environment, and higher temperatures, increase the rate of crack growth and hence cause reductions to strength and lifetime.

Charles attempted to express the behaviour mathematically. Relating the velocity of sub-critical crack growth,  $v$ , to the crack length,  $a$ , the critical crack length,  $a_I$ , an activation energy term,  $A$ , the gas constant,  $R$ , the temperature,  $T$  such that

$$v = \alpha \left[ \beta \left( \frac{a}{a_I} \right)^{n/2} + k \right] e^{-A/RT}$$

where  $\alpha$ ,  $\beta$  and  $n$  are constants and  $k$  is a term representing stress-independent corrosion, and by assuming a simple relationship to hold between  $v$  and the tensile stress,  $\sigma_m$ , at the crack tip, such that

$$v = \check{V} (\sigma_m)^n + k$$

where  $\check{V}$  is a constant, he was able to develop simple equations relating strength or lifetime to test conditions.

For example, the mean lifetime,  $\bar{t}$ , of specimens held under a constant applied stress,  $\sigma_c$ , until failure, is given by

$$\log(\bar{t}) = -n \log(\sigma_c) + \text{constant} \quad \dots\dots\dots 2.1$$

Also the mean fracture strength,  $\bar{\sigma}_f$  of specimens loaded at a constantly increasing rate of stress,  $\dot{\sigma}$ , is given by

$$\log(\bar{\sigma}_f) = \frac{1}{(n+1)} \log(\dot{\sigma}) + \text{constant} \quad \dots\dots\dots 2.2$$

It is evident from Equations 2.1 and 2.2 that the term  $n$  plays an important part in specifying the degree of stress corrosion. Charles compared values of  $n$  (now commonly called the stress corrosion parameter) obtained from constant stress, and constant stress rate tests on soda-lime glass specimens in saturated water vapour at room temperature and found them to be in good agreement ( $n \approx 16$ ).

Charles and Hillig (1962) developed the theory further and demonstrated the possible existence of a set of limiting conditions below which stress corrosion cracking would not occur. This supported the experimental findings of Mould and Southwick (1959-61).

#### 2.4 Stress corrosive slow crack growth

A major step forward in the investigation of stress corrosion came with the development of test techniques involving large artificially induced cracks, for fracture toughness measurements. Adapting the techniques to allow observation of slow crack growth, early workers in this field (Wiederhorn, Bolz, 1967, 1970; Schonart et al, 1970; Kies, Clark, 1970; Mostovoy et al, 1971; Carter, 1971) demonstrated that when a material was tested in a particular environment, a unique curve could be achieved experimentally relating crack tip velocity to a parameter incorporating both the applied load and the crack length. The shape was similar to that predicted theoretically (for example, by Shand (1961)) from the theories of Charles and Hillig (1958, 1962).

The commonest parameter plotted against the crack tip velocity,  $v$ , is the plane strain stress intensity factor,  $K_{I}$ , in the crack opening mode I (see Knott (1973)). It is related to the applied stress,  $\sigma$ , and the crack length,  $a$ , by

$$K_I = Y \cdot \sigma \cdot a^{\frac{1}{2}} \quad \dots\dots\dots 2.3$$

where Y is a geometrical factor associated with the test technique.

Rapid crack growth at the onset of catastrophic failure occurs when

$K_I = K_{IC}$ , the critical stress intensity factor, or fracture toughness.

The general shape of the curve may be seen on the  $K_I - v$  diagram shown schematically in Figure 2.1. Three regions are evident lying between two limiting values of  $K_I$ . The lower limit represents a stress corrosion limit,  $K_{IO}$ , below which slow crack growth cannot occur (see Section 2.3). The upper limit is the critical stress intensity factor  $K_{IC}$ . In between,  $v$  increases with  $K_I$  in region 1, remains approximately constant during further increases of  $K_I$  in region 2, and increases again with  $K_I$  in region 3.

Wiederhorn (1967) explained the three regions in the following way. In region 1, crack growth is controlled by the rate of chemical reaction between the material at the crack tip and a corrosive species in the test environment. In region 2, crack growth is limited by the rate at which the corrosive species can be transported to the crack tip. Crack growth in region 3 is probably controlled by a combination of mechanical tearing and chemical action.

Wiederhorn found that for glass specimens tested using the double cantilever beam technique, general levels of crack velocities in regions 1 and 2, increased as the amount of water in the test environment rose. Further work by Wiederhorn and Bolz (1970) demonstrated a similar effect when the temperature was raised (up to 90°C). These results support the findings from strength tests discussed in Section 2.2.

Since these first studies, many materials have been tested in a similar way using various test configurations.  $K_I - v$  diagrams (or their

equivalent) have been produced for such materials as glasses (Evans et al, 1972, 1973; Freiman et al, 1973; Weidmann, Holloway, 1974), silicon carbide (Evans, Lange, 1975; Kotchick, Tressler, 1975; McHenry, Tressler, 1977), silicon nitride (Evans, Wiederhorn, 1974), alumina (Evans, 1973) graphite (Freiman, Mecholsky, 1978) and epoxy resins (Phillips, Scott, 1974; Young, Beaumont, 1976). They all display one or more of the regions shown in Figure 2.1.

## 2.5 Use of the $K_I$ -v diagram to predict strength and lifetime

The uniqueness of the  $K_I$ -v curve provides a useful basis for quantitative representation of stress corrosion behaviour. Evans (1972) proposed that each region be expressed in the form

$$v = AK_I^n \quad \dots\dots \quad 2.4$$

where A is the intercept, and n the gradient of each region when drawn as a straight line using logarithmic axes.

Using Equation 2.4 and the fracture mechanics relationship for  $K_I$  given by Equation 2.3, equations may be formulated relating strengths and lifetimes to various types of loading and test conditions.

The task may be made easier by assuming that for simple types of loading, regions 2 and 3 of the  $K_I$  - v diagram can be ignored. High velocities in these regions indicate that the specimen passes through to the critical level for catastrophic failure, so quickly that the extent of crack growth is negligible. The effects of regions 2 and 3 have been described by Evans and Johnson (1974, 1975).

Thus, considering region 1 alone, Equations 2.3 and 2.4 may be combined and integrated to form the expression

$$\int_{a_i}^{a_f} \frac{da}{a^{n/2}} = AY^n \int_{t_i}^{t_f} \dot{\sigma}^n dt \dots 2.5$$

where integration is carried out between times  $t = t_i$  and  $t = t_f$  where the crack lengths are  $a = a_i$  and  $a = a_f$  respectively. The suffix  $i$  refers to the initial application of stress  $\sigma$ , which is a function of  $t$ , and  $f$  the final application, not necessarily representing the point of failure.

One example of simple loading is a constant stress rate test, where the stress is raised at a constant rate,  $\dot{\sigma}$ , until the specimen fails, at a stress,  $\sigma_f$ . Equation 2.5 may be used to show, to a close approximation, that

$$\sigma_f = \left[ \frac{2 \dot{\sigma} (n+1)}{AY^n (n-2) a_i^{(n-2)/2}} \right]^{1/(n+1)} \dots 2.6$$

The various elements of Equation 2.6 may be seen clearer in its logarithmic form

$$\log(\sigma_f) = \frac{1}{(n+1)} \log(\dot{\sigma}) + \frac{(n-2)}{(n+1)} \log\left(\frac{1}{a^{1/2}}\right) + \frac{1}{(n+1)} \log \left[ \frac{2(n+1)}{AY^n (n-2)} \right] \dots 2.7$$

The first term on the right-hand side of Equation 2.7 shows the dependence of strength upon the stress rate, the second indicates the brittle dependence of strength on the crack length, and the third is a constant scaling factor.

Applying Equation 2.7 to batches of specimens failing at a mean stress of  $\bar{\sigma}_f$  under stress rate  $\dot{\sigma}$ , and assuming that the mean initial crack length,  $\bar{a}_i$  is the same for all batches

$$\log (\bar{\sigma}_f) = \frac{1}{(n+1)} \log (\dot{\sigma}) + \text{constant} \quad \dots \quad 2.8$$

Likewise, the mean lifetime,  $\bar{t}$ , of a batch of specimens tested at a constant stress,  $\sigma_c$ , is given by

$$\log (\bar{t}) = -n \log (\sigma_c) + \text{constant} \quad \dots \quad 2.9$$

Equations 2.8 and 2.9 are exactly the same as those derived by Charles (1958) (see Equations 2.2 and 2.1 respectively in Section 2.3).

These equations not only permit the prediction of strength and lifetime, but conversely allow estimation of the stress corrosion parameter,  $n$ , from strength tests for comparison with estimates from crack propagation tests using a large crack specimen.

There are few reports of both approaches being applied to the same material. However, Evans and Johnson (1975) found good agreement between  $n$  - values obtained from stress rate tests and double torsion crack propagation tests on soda-lime silicate glass. In contrast, tests performed by Davidge et al (1973) on alumina gave quite different  $n$ -values from each type of test -  $n = 21.5$  from bend strength tests and  $n = 30-60$  from double torsion tests.

At present, the cause of this difference is unknown. However, strength tests and crack propagation tests are fundamentally dissimilar in a number of respects. Firstly, the crack size and extent of cracking are considerably greater in crack propagation tests. Secondly, crack growth in crack propagation tests is effectively in one direction, whereas in strength tests it is likely to be three dimensional. Thirdly, there may be a need for crack initiation prior to propagation in strength tests, whereas crack growth in crack propagation tests is invariably from an existing sharp crack - Davidge and Tappin (1968) have

shown that for some materials, energy required for initiation may be significantly greater than for propagation. Finally two different large crack techniques used for fracture toughness measurements do not always give comparable results when applied to the same material (Simpson, 1974; Meredith, Pratt, 1975).

## 2.6 Summary

Stress corrosion is a thermally activated chemical reaction between the material and a corrosive species in the environment, occurring at the tip of a crack subjected to tensile stresses tending to open it. The resulting slow crack growth, at a level of stress intensity factor less than that required for catastrophic failure, reduces the continuum strength of a specimen and its lifetime.

Major factors influencing the degree of stress corrosion, and hence delayed fracture, include the applied stress, the test environment including temperature, and the variation of these with time.

Experimental evidence of stress corrosion may be obtained using two approaches. Firstly, variations in strength and lifetime are evident from traditional bend tests. Secondly, recently developed large crack techniques have enabled slow crack growth to be studied directly.

Data from both strength tests involving simple types of loading, and the  $K_I$ - $v$  diagram obtained from crack propagation tests may be analysed to provide estimates of the stress corrosion parameter,  $n$ .

### 3. PROPERTIES OF WC-Co MATERIALS

#### 3.1 Introduction

The properties of WC-Co materials are discussed with particular emphasis on strength, fracture and mechanisms of failure, and the influence of material composition, temperature and microstructural factors. The limited information available on delayed fracture in WC-Co materials is also considered.

The review provides details of the general behaviour of WC-Co materials and indicates factors to be controlled in the test programme so that their influence does not obscure any delayed fracture effects.

#### 3.2 Factors influencing the strength

Factors influencing the strength of WC-Co alloys include the composition and structure of the material, the temperature at which the tests are performed, and local factors such as material flaws, impurities and residual stresses in the specimen.

##### 3.2.1 Material composition and grain size

The major constituents of WC-Co materials are a hard ceramic granular phase of tungsten carbide (WC), set in a softer metallic matrix of cobalt (Co). In general, the materials are specified by the cobalt content (either by volume,  $V_{Co}$  or by weight,  $W_{Co}$ ) and the mean WC grain diameter,  $\bar{d}_{WC}$ . Their mechanical properties are controlled by the manufacturing process, and to some extent by subsequent machining.

At a constant value of  $\bar{d}_{WC}$  the strength increases with  $V_{Co}$  until a maximum is reached. Further increases in  $V_{Co}$  cause the strength to decrease. A similar variation is observed when  $V_{Co}$  is held constant and  $\bar{d}_{WC}$  increased; again there is a particular value of  $\bar{d}_{WC}$  for optimum strength. The interaction between these two factors is such that the value of  $V_{Co}$  required to maximise the strength depends on the value of

$\bar{d}_{WC}$  (Gurland, Bardzil, 1955, Suzuki, Tanase, 1976; Chermant et al, 1977).

Attempts have been made to find a single parameter characterising the material which displays a unique relationship with the strength. One example is the mean free path in the cobalt matrix,  $\lambda_{Co}$  (Gurland, Bardzil, 1955; Chermant et al, 1977). Although some degree of correlation appears to exist for low  $\lambda_{Co}$ , this is not apparent for higher values. Here, a relationship proposed by Drucker (1964) seems more suitable, in which the strength is related primarily to  $\bar{d}_{WC}$ :

### 3.3.2 Temperature

The effects of temperature on strength are fairly similar for all commercial grades of WC-Co. As the temperature is raised above ambient, the strength remains relatively constant (Platov, 1960) or shows a slight increase (Kreimer et al, 1955) up to a transition temperature, the level of which tends to decrease with increasing  $V_{Co}$ . Beyond this, the strength drops rapidly. The transition temperature is typically between 200°C and 600°C.

### 3.2.3 Microstructural factors

Microstructural factors range from large holes or pores, through impurities and phase boundaries, to microscopic "flaws" such as dislocation pile-ups.

Porosity is present in all WC-Co alloys, although to a much lesser extent in hot-isostatically pressed materials than in sintered materials (Lardner, 1974).

Impurities are of two main types. The first are "foreign bodies" introduced with the starting materials, or from the surroundings during

manufacture. The second are composed of the elements found in the major constituents, and originate primarily from the manufacturing process. These include free carbon, the embrittling eta phase, and tungsten dissolved in the cobalt phase. All influence the strength to some extent (Suzuki, Kubota, 1966; Ueda et al, 1977a; Suzuki et al, 1978).

Phase boundaries and microscopic flaws have received considerable attention in the search for a fracture model. Their influence on crack initiation and preferred paths of propagation are discussed in Section 3.5.

The general effect of all the local factors listed above is to attract stress concentrations around them. Since commercial grades of WC-Co materials do not contain sufficient dislocation mobility for significant stress relief, local factors or flaws, have a considerable influence upon the site of initial failure and the fracture strength. The wide range of types of flaws and their generally random size, shape, orientation and distribution through the material induce a correspondingly wide variability in strength. Employing Weibull statistics (see Section 4.2) to model the variability, Chermant et al (1977) found that the Weibull modulus,  $m$ , increased both with increasing  $V_{Co}$ , and decreasing  $\bar{d}_{WC}$  (a low value of  $m$  indicates a wide variability in strength, and hence a strong dependence on flaws, or a wide range of flaw sizes).

The influence of flaws introduces two additional factors affecting the strength - specimen size, and surface finish. As specimen dimensions increase, the strength tends to decrease (Gurland, 1961); a bigger critical flaw controlling failure is more likely to be found in larger specimens. A decrease in strength is also apparent with increasingly severe surface finishes (Gurland, 1961; Chermant et al, 1977).

A diamond polished surface gives a higher strength than a ground one which in turn is better than a spark eroded surface. Again the critical flaw is likely to be larger with rougher surface finishes.

### 3.3 Factors influencing the fracture toughness and its measurements

The earliest report of fracture toughness measurements in WC-Co materials is by Kenny (1971). He used a simple bend technique, inducing precracks with a row of Knoop indentations across the width of the specimen. However, doubts have been expressed (Inglestrom, Nordberg, 1974) on the validity of the method of precracking since indenting, in addition to introducing small cracks, also induces large residual stresses which may influence subsequent propagation. The method is also limited in the grades of material that may be studied, because cracks are not formed around indentations in large cobalt content alloys at room temperatures.

In an attempt to overcome the problems of initiating a sharp precrack, Chermant et al (1974,1976) investigated crack propagation from notches cut with diamond wheels of varying thicknesses. However, the apparent values of fracture toughness decreased with notch root radius, until a certain value was reached below which no further decrease was observed. The low level was also achieved using spark eroded notches, prompting the authors to suggest that such notches satisfactorily represent a sharp precrack. This evidence led Pickens and Gurland (1978) and Nakamura and Gurland (1980) to use a similar technique in their own investigations.

Murray and Perrott (1976) however, found that upon loading double torsion specimens with spark eroded notches, the load reached a high level which, after the start of crack propagation dropped rapidly to a lower level. The authors proposed that the high level represents crack

initiation, necessary because the spark eroded notch was not immediately suitable for crack propagation.

A further problem associated with fracture toughness tests using spark eroded notches as alternatives to precracks is that initial crack growth occurs through a region of material severely damaged by spark erosion (Almond, Roebuck, 1978). Since this region is unrepresentative of the bulk, estimates of fracture toughness so measured are obviously suspect.

Greater reliability, then, should be accorded to the values of fracture toughness obtained from techniques involving a sharp precrack. Lueth (1974) induced precracks into double cantilever beam specimens by opening a machined notch with a steadily advancing wedge. Berry (1975, 1976) also used a wedge to precrack notched bend specimens, although he applied the precrack load using an impact technique. To retain the crack inside the specimen, he added compressive loads to the specimen sides, tending to close the crack. This technique was used by Inglestrom and Nordberg (1974) to precrack compact tension specimens. However they found the apparent fracture toughness to be dependent upon the magnitudes of the side loads; below a certain magnitude the apparent value remained constant but above that level, it increased. Why this should happen is still unclear, although the compressive stress field may, in addition to halting the crack within the specimen, produce a crack front which is unsuitable for immediate propagation - some re-initiation may be necessary.

Recently Almond and Roebuck (1978) have returned to the Knoop indenting methods of Kenny (1971). They improved the technique by removing material containing residual stresses induced during indenting, by diamond grinding (annealing proving unsuccessful) and induced cracks

around indentations in high cobalt alloys by performing the operation in liquid nitrogen.

Despite the various test configurations, precracking techniques and their relative, suitability, similar trends have been observed. Fracture toughness,  $K_{IC}$  increases both with cobalt content,  $V_{Co}$ , and mean WC grain size,  $\bar{d}_{WC}$  (Inglestrom, Nordberg, 1974; Chermant et al, 1974, 1976). Unlike the variation in fracture strength,  $K_{IC}$  continues to rise at high values of  $V_{Co}$  and  $\bar{d}_{WC}$ . Further a unique relationship between the mean free path in the cobalt phase,  $\lambda_{Co}$ , and the critical strain energy release rate,  $G_{IC}$  where

$$G_{IC} = K_{IC}^2 \frac{(1 - \nu^2)}{E}$$

and  $E$  and  $\nu$  are Young's modulus and Poisson's ratio respectively, has been proposed by Murray (1977) of the form

$$G_{IC} = \alpha \lambda_{Co} + \beta \dots\dots\dots 3.1$$

where  $\alpha$  and  $\beta$  are constants. The relationship fits well the experimental data obtained by Murray and others (Lueth, 1974; Pickens, Gurland, 1978; Nakamura, Gurland, 1980).

### 3.4 Crack resistance

The uncertainty of predicting fracture from strength data led to the development of large crack techniques and the use of fracture toughness as a comparative measure. However, the experimental difficulties encountered in such tests have resulted in the search for another alternative.

When an indenter is pressed into some materials such as glass or

WC-Co alloys, cracks are produced around the indentation. This is the basis for Kenny's precracking technique discussed in Section 3.3.

Palmqvist (1957) proposed that the total lengths,  $L$ , of cracks emanating from the corners of a Vickers pyramid indentation, produced under a load,  $P$ , was related to the resistance of the material to cracking. He defined the Palmqvist toughness, or crack resistance,  $W$ , as

$$W = P/L \quad \dots \quad 3.2$$

Workers (Vis wanadham, Venables, 1977; Peters, 1979) finding experimentally that  $W$  increased with  $\lambda_{Co}$  for WC-Co alloys containing less than about 16% cobalt by weight, proposed that a linear relationship exists of such a form that when combined with Murray's (1977)  $G_{IC} - \lambda_{Co}$  relationship (Equation 3.1) demonstrates that  $W$  is proportional to  $G_{IC}$ .

If the proposal can be accepted then the test provides a simple method of obtaining estimates of fracture toughness. However, great care has to be taken in preparing the specimen surfaces for indentation since residual stresses influence the value of  $W$  (Exner, 1969; French, 1969).

### 3.5 Mechanisms of failure

The thickness of cobalt binder film separating two adjacent WC grains depends both upon the cobalt content,  $V_{Co}$ , and the WC grain size,  $\bar{d}_{WC}$ . At large  $V_{Co}$  and  $\bar{d}_{WC}$ , the film thickness is relatively large and capable of significant plastic deformation. Yielding tends to transfer load from the matrix to the grains, and assuming the preferential crack path to be transgranular, makes grain fracture more likely. (Gurland, Norton, 1956). This supports the findings of

Drucker (1964) who proposed that fracture of high  $V_{Co}$  and  $\bar{d}_{WC}$  grades and hence their strength was influenced almost entirely by crack initiation in WC grains and hence  $\bar{d}_{WC}$ .

As the film thickness decreases (through a reduction in  $V_{Co}$  or  $\bar{d}_{WC}$ ), the yield strength of the film increases because of the proximity of the hard WC grains. Hence less plastic deformation occurs prior to transgranular fracture. (Gurland, Bardzil, 1966; Gurland, Norton, 1956).

With further decreases in film thickness, the cobalt appears to play a much lesser part in controlling fracture. The binder may become discontinuous resulting in contiguous grains and areas devoid of material. These areas of weakness cause a transferal of the type of preferential fracture path from transgranular to intergranular (Gurland, Bardzil, 1955).

Early workers, referenced above, suggested that a carbide skeleton may be present in low  $V_{Co}/\bar{d}_{WC}$  alloys allowing crack propagation to proceed through the specimen with the minimum of crack blunting by the softer cobalt phase. Recent work by Lee and Gurland (1978) indicated a high probability of such a skeleton existing.

To summarise the corresponding variation in strength and fracture toughness, the types of fracture path delineated by Chermant and Osterstock (1976) have been used. They proposed four types - transgranular cleavage (which they labelled) W/C; intergranular fracture between contiguous grains, WC/WC; intergranular fracture at matrix - grain boundaries, WC/Co; and intergranular fracture completely within the matrix, Co/Co.

In low cobalt alloys where the binder film thickness is thin, fracture is predominantly of the WC/WC type through areas of weakness.

Consequently strength and fracture toughness are both low.

As the binder film thickness increases, areas of weakness disappear, cobalt begins to toughen the material and W/C fracture becomes more evident. Failure is governed by a combination of the plasticity of the cobalt film and its thickness, and the increase in yield strength of the film imposed by the proximity of hard carbide grains. The compromise of constrained plasticity produces the highest strengths and a high fracture toughness.

With large binder thickness, W/C fracture is seen less frequently. Instead, a large proportion of crack growth is of the WC/Co and Co/Co type, demonstrating that for fracture to occur, the crack must necessarily pass through a considerable volume of cobalt, because the binder thickness is large, with little or no grain contiguity. Since a large amount of energy is required to propagate a crack through the cobalt region, the fracture toughness is very high. Conversely the strength is relatively low. But in this case the criterion appears to be crack initiation rather than propagation; substantial yielding of the matrix passes load to the grains making initiation of the W/C type more likely, and both reduce the load bearing ability of the material.

A mathematical model has been developed by Murray (1977) to describe the relationship between critical strain energy release rate,  $G_{IC}$ , in the crack opening mode I (see Knott (1973)) and the mean free path in the cobalt matrix,  $\lambda_{Co}$ . He proposed that fracture is controlled by plasticity of the cobalt phase at the crack tip, even for extremely small binder thicknesses. Further the plasticity is constrained by the proximity of hard carbide grains such that the

matrix yield strength is considerably higher than that found in single phase cobalt material. Murray found that the matrix yield strength was constant for all grades of WC-Co studied and approximately equal to twice the theoretical shear stress,  $\tau_{th}$ .

Hence, introducing terms to represent internal stresses,  $\bar{\sigma}_{Co}$  in the matrix, and roughness factor,  $\phi$  to describe the deviatoric nature of crack growth, Murray derived a relationship between  $G_{IC}$  and  $\lambda_{Co}$  such that

$$G_{IC} = \left[ \frac{12\pi\phi(1-\nu^2)}{E} \left( 1 - \frac{\bar{\sigma}_{Co}}{2\tau_{th}} \right)^2 \tau_{th}^2 \right] \lambda_{Co} + \lim_{\lambda_{Co} \rightarrow 0} (G_{IC})$$

where  $E$  and  $\nu$  are Young's modulus and Poisson's ratio respectively for the material.

The intercept is considered to be influenced by the surface energy of cobalt, mode II and III crack growth (see Knott (1973)) and slip at Co-WC interfaces.

Thus, to summarise, the fracture behaviour of WC-Co materials may be thought of as a complex mixture of brittle cracking and constrained plasticity, the degree of each being dependent upon the composition and structure of the alloy.

### 3.6 Delayed fracture and slow crack growth

Delayed fracture has been investigated in WC-Co materials both in respect to fatigue (for example, Dawihl, 1941; Kreimer et al, 1958; Hara, Yazu, 1968; Evans, Linzer, 1976) and high temperature creep (for example Ueda et al, 1975; Suzuki et al, 1977a). However, reports

of behaviour which might be caused by stress corrosion are scarce. Of these, most involved the measurement of bend strength in ambient conditions under different rates of loading. Some cannot be considered because other delayed fracture mechanisms may have been present. In this respect, high temperature work has to be discarded because of the possible influence of creep (Ueda et al, 1977b, 1977c; Suzuki et al, 1977b; Braiden et al, 1977) or toughening through crack blunting (see work on  $\text{Si}_3\text{N}_4$  by Evans and Wiederhorn (1974)).

The remaining reports are by no means consistent. Gurland (1961) applied three loading rates (6, 600, 6000 lb/sec) to WC-10% Co specimens and found no influence on the strength. Conversely, Smaglenko and Loshak (1973) found considerable rate effect. Applying deformation rates between 0.5 and  $5 \times 10^3$  mm/sec to alloys containing 6-25% cobalt, they observed a significant increase in strength with deformation rate in all but the 6% cobalt alloy. The change in strength with deformation rate increased as the cobalt content became greater.

The rate effect noticed by Knotek et al (1978) was not as straightforward. The strength tended to decrease as the rate was raised, until a minimum was reached. At higher rates, the strength began to increase again. Doi et al (1975) however, recorded a rise in strength with crosshead speeds up to 10 mm/sec, above which the strength dropped rapidly. The drop was more pronounced in large grain alloys. Scanning electron microscopy revealed that low rate fracture surfaces showed a preference for crack propagation along Co-WC boundaries whereas at high rates, grain cleavage and crack nucleation at the boundaries of contiguous grains were evident. The authors explained this phenomenon in terms of embrittlement at high strain rates caused by

the time between initial load application and failure being so short as to limit the extent of stress relieving plastic deformation.

Braiden et al (1977) specifically set out to investigate delayed fracture in WC-Co materials in terms of stress corrosion and used many of the concepts and techniques developed for use on other materials. Initial tests on WC6% Co specimens under crosshead rates of 0.005, 0.05 and 0.5 mm/min proved inconclusive; the authors pointed out the difficulty of drawing reasonable conclusions because of the scatter of strengths in any one test case, caused by the brittle dependence on materials flaws. They calculated the Weibull modulus for the variability in strength to be approximately 9.

To investigate further, Braiden et al employed a form of stepped loading used by Davidge et al (1973) for tests on alumina (details of this type of loading are given in Section 6.3). The tests provided evidence of delayed fracture during periods of constant load, and data which, when compared with results from rate tests, produced an estimate of the stress corrosion parameter,  $n$ , of approximately 200.

Similar tests were performed on WC-16%Co specimens, but although delayed fracture was observed, insufficient data were available for conclusions to be drawn.

Braiden et al also attempted to study slow crack growth in WC-Co materials using the double torsion technique. However tests proved unsuccessful because of the difficulties encountered in precracking the plate specimens - a precrack once initiated, travelled rapidly through the complete specimen. The authors suggested that such rapid propagation indicated a steep slope on the  $K_I$ - $V$  diagram and hence a large value of  $n$  - which was in agreement with their strength test results.

Almond et al (1976) found slow crack growth when WC-6% Co specimens containing pyramid indentations with cracks emanating from each corner (see Section 3.4), were exposed to hydrogen fluoride (HF) vapour. Prolonged exposure caused flakes to break away from around the indentation. The authors proposed that the phenomenon was stress corrosive since crack enlargement and flaking only occurred when the residual stresses, introduced by indenting, were left in specimens during exposure to HF vapour; if the residual stresses were removed by annealing, crack growth was not observed. However annealing may also have caused crack blunting, which would tend to inhibit further crack growth.

Further evidence of slow crack growth may be present in the work of Murray (1977). He produced a diagram of load against time for double torsion specimens with spark eroded notches loaded at a constant crosshead speed. The load rose initially to a high level, when crack growth began, reducing the load to a lower level. This remained roughly constant for a short while before dropping to zero as the crack emerged from the specimen. Murray proposed that the high level of load represented that required to induce crack initiation and the low level, that for rapid propagation and hence representative of the critical conditions for catastrophic failure. However, the high level can also be explained in terms of end effects unrepresentative of general behaviour which are peculiar to the double torsion specimen as described by Trantina (1977), Bruce and Koepke (1977) and Shetty and Virkar (1978). Further, the persistence of the lower level indicates a relatively slow rate of crack growth, and is similar to the theoretical stress corrosive crack growth behaviour predicted by Evans (1972); if

crack growth was rapid, then the load might be expected to drop from the high level immediately to zero.

Given the evidence detailed above, it is apparent that few conclusions may be drawn as to the presence of stress corrosive mechanisms. Results from strength tests are contradictory or inconclusive, and there are few reports of slow crack growth. The strength behaviour reported by Loshak and Smaglenko (1973) and Braiden (1977) and possible slow crack growth seen in the work of Murray (1977) can be satisfactorily modelled using stress corrosion theories. However, the theories cannot describe the complex variation of strength with rate of loading observed by Knotek et al (1978) and Doi et al (1975).

Further, there is no information as to whether the behaviour discussed above is in any way environmentally assisted; apparent stress corrosive cracking in HF vapour reported by Almond et al (1976), provides little supporting evidence since the test environment is so different, chemically, from laboratory air used by the other workers.

General fracture mechanisms in WC-Co materials, discussed in Section 3.5, likewise give few clues as to the expected behaviour. The materials have a brittle phase capable of supporting slow crack growth but also have a potentially ductile phase which may inhibit, or prevent crack propagation under conditions less than those required for catastrophic failure.

However, giving consideration to the degree of variation observed in strengths under the ranges of loading rates employed in the tests discussed above, delayed fracture, if present in WC-Co materials when tested in laboratory air at room temperature, is likely to be small, and comparatively much smaller than stress corrosive delayed fracture observed in glasses and alumina (see Chapter 2).

### 3.7 Summary

The strength, fracture toughness and crack resistance of WC-Co materials are influenced by the cobalt content and the mean WC grain size. The strength is further influenced by temperature and structural factors including pores, impurities and surface damage.

Fracture of WC-Co materials may be considered a complex mixture of brittle cracking and constrained plasticity, the dominance of each depending upon the composition and structure of the alloy.

Evidence of delayed fracture, or slow crack growth which may be induced by stress corrosion, is extremely limited. Delayed fracture, if present in ambient conditions, is likely to be small. Nothing is known regarding any environmental, or thermal influence under these conditions. Further there is no evidence to indicate whether reported variations of strength with loading rate are controlled by stress corrosive mechanisms, or not.

#### 4. MANIPULATION AND ANALYSIS OF STRENGTH DATA

##### 4.1 Introduction

In this chapter, analytical techniques are developed to compare the distributions of strengths obtained from bend tests involving different types of loading to failure, to assess the significance of any observed delayed fracture effects, and to estimate parameters describing the behaviour.

The techniques are based on a failure model developed from theories of brittle fracture and stress corrosion, using Weibull statistics to account for the variability in strength due to material flaws. The method of maximum likelihood is incorporated for parameter estimation, and transformation equations are developed to enable results from tests involving different types of time dependent loading, to be compared.

In addition, a graphical method of displaying delayed fracture - the SPT diagram - is discussed.

##### 4.2 Brittle fracture model

The analysis of brittle fracture is commonly approached using the model developed by Griffith (1921). He represented a material flaw, or crack by an ellipse with major and minor axes of lengths  $2a$  and  $2b$  respectively. Using the model to represent a crack of zero thickness and of length  $a$ , Griffith proposed that one condition for brittle fracture was that the decrease in strain energy due to the formation of a crack must be at least equal to the energy required to create the new surfaces, such that the continuum stress,  $\sigma_I$ , at fracture is given by

$$\sigma_I = \left( \frac{2E\gamma_s}{\pi a} \right)^{1/2} \dots\dots\dots 4.1$$

where  $E$  and  $\gamma_s$  are Young's modulus and the surface energy per unit length, respectively, for the material. Thus the strength is directly proportional to a function of the model flaw size.

Although the model flaw cannot be considered a direct representation of real material flaws - which are in the majority of cases, far too complex in size, shape, orientation and distribution, for mathematical representation - it may be thought of as an equivalent. Thus, if material flaws are assumed to be random by nature, then through the equivalent model flaw, the corresponding strengths should likewise be random.

The representation of this variability requires a statistical approach. Consider a variable,  $X$ , demonstrating variability in a number of observations. The probability,  $P$ , of an observed value of  $X$  being equal to, or less than a fixed value,  $x$ , is defined as the cumulative distribution function (cdf),  $F(x)$  such that

$$P \left\{ X \leq x \right\} = F(x) \quad \dots\dots 4.2$$

In general a cdf may be expressed in the form

$$F(x) = 1 - e^{-f(x)} \quad \dots\dots 4.3$$

where  $f(x)$  is some function of  $x$ .

One such function proposed by Weibull (1951) is of the form

$$f(x) = \frac{(x - x_u)^m}{x_o} \quad \dots\dots 4.4$$

where  $x_u$  is a lowest limit of possible  $x$ ,  $x_o$  is a normalising, or scaling factor, and  $m$  is a shape factor, now commonly called the Weibull modulus.

This distribution has been applied to observations of brittle strength,  $\sigma_I$ , (Güçer, Gurland, 1962; Davies, 1973) where  $x_u$  is taken as zero, and  $F$  generally referred to as the cumulative failure probability (cfp). Using  $\sigma_o$  as the corresponding scaling factor

$$F(x) = P \left\{ \sigma_I \leq x \right\} = 1 - \exp \left[ - \left( \frac{x}{\sigma_o} \right)^m \right] \dots\dots 4.5$$

Consider a sample of  $N$  observations of  $\sigma_I$ , where  $(\sigma_I)_i$  is the  $i$ 'th when the data are ranked in ascending order of magnitude.

If  $(\sigma_I)_i$  is plotted against the corresponding median, or mean rank value (obtained from standard tables (Johnson, 1964)) assigned to the cdf,  $F(\sigma_I)_i$ , for the whole sample, then, from Equation 4.6, the points should lie along a curve given by

$$F(\sigma_I) = 1 - \exp \left[ - \left( \frac{\sigma_I}{\sigma_0} \right)^m \right] \quad \dots \quad 4.6$$

or in its logarithmic form

$$\log \log \left[ \frac{1}{1 - F(\sigma_I)} \right] = m \log (\sigma_I) - m \log (\sigma_0) \quad \dots \quad 4.7$$

When Weibull paper is used, where axes are adjusted in the manner of Equation 4.7, the relationship should be linear with a gradient of  $m$ . Obviously, since the  $N$  observations represent only a sample of the behaviour, the points are unlikely to lie exactly along a straight line; the deviation from it represents errors due to sampling. However, the exact location of the straight line is unknown, but may be estimated by drawing a best straight line by eye through the plotted points.

Confidence bands can be added (Johnson, 1964) to produce an area on the Weibull diagram in which the true straight line is, say, 99% certain to lie. Also, simple formulae have been developed by Sivill (1974) to assess the possible error in the Weibull modulus,  $m$ .

Thus, the distribution of strengths may be characterised using the Weibull diagram to obtain estimates of the parameters describing the best straight line - usually the Weibull modulus,  $m$ , and the median strength,  $\sigma_M$ , corresponding to a cumulative failure probability of 50% ( $F(\sigma_I) = 0.5$ ) - and the confidence that may be placed in them.

The significance of  $m$  may be seen by rearranging Equation 4.7, so that

$$\log (\sigma_I) = \frac{1}{m} \log \log \left[ \frac{1}{1-F(\sigma_I)} \right] + \log (\sigma_0) \quad \dots \quad 4.8$$

The first term on the right-hand side of Equation 4.8 represents the variability in  $\sigma_I$  and is governed by the magnitude of  $m$ . The smaller  $m$  becomes, the greater the variability in  $\sigma_I$  is seen. The second term on the right-hand side acts as a scaling factor on  $\sigma_I$ .

#### 4.3 Stress corrosion model

With the inclusion of stress corrosion effects in the failure model, consideration must be given to time as a variable. When stress corrosion does not occur, only the stress at failure is important, whereas when it does, consequent sub-critical slow crack growth introduces the need for the loading prior to failure and its variation with time to be defined.

Development of the failure model, described below, has been based on an applied continuum stress raised at a constant rate to failure. However, similar procedures may be adopted, in principle, for other types of loading, where mathematical representation is simple.

##### 4.3.1 The failure model

In section 2.5, the applied stress of fracture,  $\sigma_f$ , under a constant stress rate  $\dot{\sigma}$  was shown to be given by

$$\sigma_f = \left[ \frac{2(n+1)\dot{\sigma}}{AY^{n(n-2)}a_i^{(n-2)/2}} \right]^{1/(n+1)} \quad \dots \quad (\text{Equation 2.6})$$

where  $a_i$  is the initial theoretical flaw size at the start of loading,  $n$  is the stress corrosion parameter, and  $A, Y$  are constants -

Rewriting Equation 2.6 in logarithmic form

$$\log(\sigma_f) = \frac{1}{(n+1)} \log(\dot{\sigma}) + \frac{(n-2)}{(n+1)} \log\left(\frac{1}{a_i^{1/2}}\right) + \log(C^I)$$

where  $\log(C^I) = \frac{1}{(n+1)} \log\left[\frac{2(n+1)}{AY^n(n-2)}\right] = \text{constant} \dots$  4.9

Equation 4.9 shows the dependence of strength upon time dependent loading, the initial flaw size, and a constant scaling factor.

Potentially Equation 4.9 could be used to estimate the stress corrosion parameter,  $n$ , given experimental data, but the operation is impeded by the unknown quantity  $a_i$ .

#### 4.3.2 Comparison of average behaviour

One method of avoiding the measurement of  $a_i$  is to compare the average behaviour of a number of identical specimens rather than of individuals. If the total number of specimens to be tested is split into several batches, then the average size of the equivalent theoretical flaw for each batch will be approximately the same. Then, if all specimens in each batch are tested to failure using the same stress rate,  $\dot{\sigma}$ , and different batches are tested at different stress rates, then the relationship between mean strength  $\bar{\sigma}_f$ , for each batch, and stress rate is given, from Equation 4.9, by

$$\log(\bar{\sigma}_f) = \frac{1}{(n+1)} \log(\dot{\sigma}) + \log(C^{II})$$

where  $\log(C^{II}) = \log(C^I) + \frac{(n-2)}{(n+1)} \log\left(\frac{1}{a_i^{1/2}}\right) = \text{constant} \dots$  4.10

Thus, a plot of  $\log(\bar{\sigma}_f)$  against  $\log(\dot{\sigma})$  should yield a straight line relationship, where  $n$  may be calculated from the gradient of the best line through the points.

However, errors are potentially high. Firstly the behaviour of each batch is represented by only one number - the mean strength - and thus, no account is taken of the distribution or the presence of any "extreme" values, which tend to have a considerable effect on the mean. Secondly, the average equivalent flaw size of each batch is unlikely to be exactly the same, particularly when batch sizes are small, because the specimens form only a random sample of the whole. Thirdly, the total number of specimens available for testing, limits not only the batch size but also the number of batches, and hence the number of stress rates employed. Thus, some error must be expected when trying to fit a best straight line through relatively few points on the graph of  $\log(\bar{\sigma}_f)$  against  $\log(\dot{\epsilon})$ .

#### 4.3.3 Statistical representation of the random variable $a_i$

The method can be improved if the random variable  $a_i$  is approached statistically. This may be achieved by considering the material behaviour under a different set of conditions.

If the specimens are loaded to failure in such a way that stress corrosion is prevented from occurring, say, in an inert environment, then the inert strength,  $\sigma_I$ , may be related to the initial theoretical flaw size,  $a_i$ , and the critical stress intensity factor,  $K_{IC}$ , (see Section 2.4) by

$$K_{IC} = Y \cdot \sigma_I \cdot a_i^{1/2} \quad \dots \quad 4.11$$

where Y is the same geometrical constant used in Equation 2.6.

Combining Equations 4.9 and 4.11 to eliminate  $a_i$  produces

$$\log (\sigma_f) = \frac{1}{(n+1)} \log (\dot{\sigma}) + \frac{(n-2)}{(n+1)} \log (\sigma_I) + \log (C^{III})$$

$$\text{where } \log (C^{III}) = \log (C^I) + \frac{(n-2)}{(n+1)} \log \left( \frac{Y}{K_{IC}} \right) = \text{constant} \dots \quad 4.12$$

Now the strength is dependent upon the unknown inert strength,  $\sigma_I$ . However,  $\sigma_I$  is identical to the brittle strength discussed in Section 4.2. Thus Weibull statistics may be introduced once again, to represent the variability in  $\sigma_I$ .

Consider a sample of N observations obtained from tests at a single stress rate. Then Equation 4.12 reduces to

$$\log (\sigma_f) = \frac{(n-2)}{(n+1)} \log (\sigma_I) + \log (C^{IV})$$

$$\text{where } \log (C^{IV}) = \log (C^{III}) + \frac{1}{(n+1)} \log (\dot{\sigma}) = \text{constant} \dots \quad 4.13$$

If  $(\sigma_f)_i$  is the  $i$ 'th observation when the data are ranked in ascending order of magnitude, then by noting that  $\sigma_f$  is directly proportional to  $\sigma_I$ , the ranked order of  $\sigma_I$  is the same as that of  $\sigma_f$ . Thus  $(\sigma_f)_i$  may be plotted against the corresponding median, or mean rank value assigned to the cfp,  $F(\sigma_I)_i$ , for the whole sample.

The points should lie along a curve described by a combination of Equations 4.7 and 4.13 to eliminate  $\sigma_I$  such that

$$\log \log \left[ \frac{1}{1-F(\sigma_I)} \right] = \frac{m(n+1)}{(n-2)} \log (\sigma_f) - \log (C^V)$$

$$\text{where } \log (C^V) = m \log (\sigma_0) + \frac{m(n+1)}{(n-2)} \log (C^{IV}) = \text{constant} \dots \quad 4.14$$

Hence, once again, on Weibull paper with logarithmic axes, the relationship should be linear, but this time with a slope of  $m(n+1)/(n-2)$ . However, for large  $n$ , this approximates to  $m$ .

Estimates of the median strength,  $\sigma_M$ , and  $m$  may be made from the Weibull diagram for each batch of specimens and hence for each stress rate employed.

At this stage also, each distribution can be studied for unexpected trends and the presence of any "extreme" values. In the case of the latter, a more suitable straight line might be drawn if they are ignored.

The procedure to estimate the stress corrosion parameter,  $n$  continues by observing that estimated values of  $\sigma_M$  for each stress rate correspond to the same cumulative failure probability of 0.5 and hence the same median inert strength,  $(\sigma_I)_M$ .

Hence, returning to equation 4.12

$$\log (\sigma_M) = \frac{1}{(n+1)} \log (\dot{\sigma}) + \log (C^{VI})$$

$$\text{where } \log (C^{VI}) = \log (C^{III}) + \frac{(n-2)}{(n+1)} \log (\sigma_I) = \text{constant...} \quad 4.15$$

This may be compared with Equation 4.10 used in the first method to describe the relationship of mean strength with stress rate. Here, a plot of  $\log (\sigma_M)$  against  $\log (\dot{\sigma})$  should yield a straight line relationship where  $n$  may be calculated from the gradient of the best line through the points.

This method benefits over the first, in that the representation of a batch - still using a single number,  $\sigma_M$  - is based not only on mathematical analysis of the data, but also upon a study of the distributions and any peculiarities that may be present in them.

This method is still limited in that only a relatively few results are analysed statistically at any one time; sampling errors are therefore likely to be large. Although Davidge et al (1973) found the technique useful for analysing strength data from tests on alumina, where  $n$  is relatively low, Braiden et al (1977) could place little significance in their results from tests on WC-Co materials in ambient conditions; their estimates of  $n \approx 200$  for WC6% Co indicated that the expected changes

in strength under different rates of loading were similar in size to possible errors due to sampling. The authors also noted that reasonable increases in batch size were likely to reduce sampling errors only slightly.

#### 4.3.4 A technique to analyse strengths originating from tests involving different stress rates to failure

One alternative is to develop a technique which analyses all data together irrespective of the stress rate employed. Since the single large batch to be operated on statistically is considerably larger than individual stress rate batches, significant reductions in sampling errors might be expected.

An analytical technique of this type was developed by Jakus et al (1978). Using as a failure model a combination of Equations 4.7 and 4.12 (which eliminates  $\sigma_I$ ) of the form

$$\left[ \log (\sigma_f) - \frac{1}{(n+1)} \log (\dot{\sigma}) \right] = \frac{(n-2)}{m(n+1)} \log \log \left[ \frac{1}{1-F(\sigma_I)} \right] + \text{constant}$$

..... 4.16

they ranked data according to the magnitude of the left-hand side of Equation 4.16 treated as a single term. To do this they had to guess an initial value of n.

Rearranging Equation 4.16 to the form

$$\log (\sigma_f) = \frac{1}{(n+1)} \log (\dot{\sigma}) + \frac{(n-2)}{m(n+1)} \log \log \left[ \frac{1}{1-F(\sigma_I)} \right] + \text{constant}$$

they performed a multivariate regression analysis to obtain estimates of  $1/(n+1)$ ,  $(n-2)/m(n+1)$ , and the constant, from which they calculated a new value of n.

The initial guessed value of  $n$  was replaced by the new value and the whole operation repeated in an iterative loop, until a best "regression" estimate of  $n$  was obtained.

The technique was applied to WC-Co data obtained in the present study, but the outcome differed in one respect from the reports of Jakus et al. Whereas they indicate a single best estimate of  $n$ , the WC-Co data yielded a range of "best" estimates at which the iteration process stopped. The final value depended upon the guessed value used at the start of iteration.

Further, the technique appears to involve a multivariate regression using the "least squares" method. Since this requires all data to have an equal degree of confidence, and since the multivariate regression is performed on ranked data where more extreme values have less confidence attached to them, the statistical validity of the analysis appears to be in doubt. The authors were approached by letter with a request for clarification of these points but declined to answer.

#### 4.4 Development of the "maximum likelihood" technique

In the light of the various shortcomings associated with existing methods of obtaining estimates of the stress corrosion parameter,  $n$ , from stress rate tests, an alternative technique has been developed (Wright et al, 1982). It employs theories of brittle fracture and stress corrosion, with Weibull statistics, using the method of maximum likelihood to analyse unranked strength data within a single analysis irrespective of the stress rate employed. The technique makes maximum use of the data, by minimising possible sampling errors, whilst maintaining statistical validity, and obtains estimates of the stress corrosion

parameter, the Weibull modulus, the confidence attached to them, and the significance of any rate effect on the strength. A further development, incorporating the Monte Carlo method assesses the suitability of the failure model in representing the material behaviour. A similar technique has been developed by Trustrum and Jayatilaka (1979) to estimate parameters of brittle fracture.

#### 4.4.1 The failure model

The failure model is based on Equations 4.5 and 4.12 describing brittle, and stress corrosion behaviour respectively.

The two equations may be combined by first writing

$$Z = m \log \left( \frac{\sigma_I}{\sigma_0} \right) \quad \dots \quad 4.17$$

The cumulative distribution function (cdf) of  $Z$  may be obtained from Equation 4.6 such that

$$\begin{aligned} P \left\{ Z \leq x \right\} &= P \left\{ \sigma_I \leq \sigma_0 \cdot \exp \left( \frac{x}{m} \right) \right\} \\ &= 1 - \exp \left( - e^x \right) \dots \quad 4.18 \end{aligned}$$

This probability distribution with no parameters, is known as the Gumbel or "extreme-value" distribution (Fraser, 1976).

The elimination of  $\sigma_I$  from Equation 4.12 using Equation 4.18 gives

$$\log (\sigma_f) = \frac{1}{(n+1)} \log (\dot{\sigma}) + \frac{(n-2)}{m(n+1)} \cdot Z + B$$

$$\text{where } B = \log (C^{III}) + \frac{(n-2)}{(n+1)} \log (\sigma_0) = \text{constant} \quad 4.19$$

Equation 4.19 demonstrates that the model predicts a linear regression of  $\log (\sigma_f)$  on  $\log (\dot{\sigma})$ , the slope of which is  $1/(n+1)$ . The second term, involving the random variable,  $Z$ , represents the variability in  $\sigma_f$ .

The final term - the intercept, B - involves a number of unknown parameters, all constant.

The distinctive features of this model are:

(i) the "error" distribution is "extreme value" rather than the more commonly encountered Normal or Gaussian. In consequence, the standard "least squares" theory is not applicable.

(ii) The "errors" in the fracture strength data are more properly systematic random variation caused by the variability in material flaws, the size of which cannot be measured. Thus, these errors are not expected to be negligible, and close fit of a straight line to the  $(\log(\dot{\sigma}), \log(\sigma_f))$  data will not be obtained. In this context, measurement error may be neglected.

#### 4.4.2 Use of the model to estimate unknown parameters, n, m, B

Although the "least squares" method of linear regression is not applicable in this case, another standard statistical procedure - the method of maximum likelihood estimation (Fraser, 1976) - is valid. It may be used to obtain not only estimates of the unknown parameters in the model (given by Equation 4.19) but also confidence limits for them.

Consider a sample of N observations  $(X_i, Y_i)$  where

$$X_i = \log(\dot{\sigma})$$

for the i'th observation,

$$Y_i = \log(\sigma_f)$$

where  $i = 1, 2, 3, \dots, N$ .

From Equation 4.19,

$$Y_i = \frac{1}{(n+1)} X_i + \frac{(n-2)}{m(n+1)} Z_i + B \quad \dots \quad 4.20$$

For temporary notational convenience, this may be written

$$Z_i = rX_i + sY_i + t$$

where  $r = m/(n-2)$

$$s = m(n+1)/(n-2) \quad \dots \quad 4.21$$

$$t = -mB(n+1)/(n-2)$$

The cdf of  $Y_i$  for a given  $X_i = x_i$  (i.e. a fixed preset stress rate) is given from Equations 4.18 and 4.21 by

$$\begin{aligned} P \left\{ Y_i \leq y_i \right\} &= P \left\{ Z_i \leq (r x_i + s y_i + t) \right\} \\ &= 1 - \exp \left[ - \exp (r x_i + s y_i + t) \right] \end{aligned}$$

Now the probability density function (pdf) of  $Y_i$ ,  $g(y_i)$  is the derivative of the cdf. Thus

$$g(y_i) = \exp \left[ - \exp(r x_i + s y_i + t) \right] \cdot \exp(r x_i + s y_i + t) \cdot s$$

The likelihood is the product of these terms over the whole sample so that the log-likelihood, or support,  $\mathcal{L}$ , is given by

$$\begin{aligned} \mathcal{L} &= \log \prod_{i=1}^N g(Y_i) \\ &= \sum_{i=1}^N \log g(Y_i) \\ &= \sum_{i=1}^N \left[ (rX_i + sY_i + t) - \exp(rX_i + sY_i + t) + \log s \right] \end{aligned}$$

$$= \sum_{i=1}^N \left[ -r \log (\hat{\sigma}_i) + s \log (\hat{\sigma}_{f_i}) + t \right] \\ - \exp \left\{ r \log (\hat{\sigma}_i) + s \log (\hat{\sigma}_{f_i}) + t \right\} + \log (s) \Bigg]$$

The maximum likelihood estimates of  $r$ ,  $s$ ,  $t$  are obtained by maximising  $\hat{S}$ . Exact formulae are not available, but the maximisation can be carried out easily using a standard numerical technique. The estimates of  $n, m, B$  may then be obtained from Equation 4.21.

The values assigned to  $n, m, B$  at the end of the maximisation procedure are only estimates. Thus an indication of the confidence that may be placed in them is required. To this end, a likelihood ratio test may be employed, (Fraser, 1976). Suppose that  $\hat{S}_r$  is the maximum support obtained when the parameters  $n, m, B$  are restricted by one fixed constraint. If  $\hat{S}$  is the maximum unrestricted support, then

$$\chi^2 = 2(\hat{S} - \hat{S}_r)$$

has approximately a  $\chi^2$  distribution on one degree of freedom, under the null hypothesis that the constraint actually holds.

For example, if the constraint is that the stress corrosion parameter,  $n = n_0$ , where  $n_0$  is some preassigned number, and if the maximum support under this restriction is denoted by  $\hat{S}_{n_0}$ , then  $2(\hat{S} - \hat{S}_{n_0})$  has a  $\chi^2$  distribution with one degree of freedom if  $n = n_0$ . The upper 5% point of this distribution is 3.84, so that the collection of values of  $n_0$ , such that

$$2(\hat{S} - \hat{S}_{n_0}) \leq 3.84$$

provides a 95% confidence interval for  $n$ .

A similar procedure may be adopted to obtain confidence intervals for  $m$  and  $B$ . If simultaneous confidence statements about two or three of the parameters are required, then the resulting  $\chi^2$  distribution will have two or three degrees of freedom respectively.

Sometimes it may be necessary to show that the fracture stress is being influenced by the stress rate to a significant degree, so that any apparent correlation between the two is not merely an effect of sampling. In this case, the null hypothesis is that the fracture stress is not influenced by the stress rate, so that a single constraint applies, namely that  $n = \infty$ . If  $\bar{S}$  and  $\bar{S}_{\infty}$  are the unrestricted, and restricted supports respectively, then

$$\chi^2 = 2(\bar{S} - \bar{S}_{\infty}) \quad \dots \quad 4.22$$

Whether there is a significant departure from the null hypothesis that no rate effect exists is assessed by comparing  $\chi^2$  calculated using Equation 4.22 with the distribution of  $\chi^2$  in one degree of freedom given in standard tables.

#### 4.4.3 Assessing the validity of the model

Up to this point, the validity of the model and in particular, the Weibull assumption, has not been questioned. Some attempt to do so may be made by examining the residuals,  $Z_i$ , in Equation 4.20, which may be expressed in the form

$$Z_i = \frac{m(n+1)}{(n-2)} \left[ Y_i - \frac{1}{(n+1)} \cdot X_i - B \right]$$

$Z_i$  is evaluated for each  $(X_i, Y_i) = (\log(\dot{\sigma}), \log(\sigma_f))$ , given the estimated values of  $m, n, B$ . If the Weibull assumption is correct, then

$Z_i$ , ( $i = 1, 2, 3 \dots N$ ) should appear to follow approximately the "extreme-value" distribution. This may be checked graphically by first transforming the  $Z_i$  using the probability integral transform

$$U_i = 1 - \exp(-\exp(Z_i)).$$

The resulting  $U_i$  ( $i = 1, 2, 3 \dots N$ ) should be approximately uniformly distributed in the interval (0,1). If these  $N$  values are ordered in magnitude and then plotted against  $i/N$  ( $i = 1, 2, 3 \dots N$ ) the points should lie close to the  $45^\circ$  line from (0,0) to (1,1).

Obviously, sampling fluctuations tend to generate departures from this ideal form. If the discrepancies yielded by the data are large, then this would indicate the Weibull model was unsatisfactory.

To assess the significance of the discrepancies, a Monte Carlo technique (Fraser, 1976) may be used. Artificial data sets of similar size to the real data sets are constructed with pseudo-random numbers using the failure model defined by Equations 4.5 and 4.12, and predefined values of  $m, n$ , and  $B$ . The maximum likelihood method is applied and the graphs displaying the standardised residuals plotted as for the real data. It may be shown (Fraser, 1976) that the distribution of the residuals does not depend on the values of  $m, n, B$ , so it is immaterial what values are chosen for the simulation.

The graphs displaying the standardised residuals for the artificial data sets are combined to form an envelope for comparison with the curves for the real data sets. If the curves do not lie to any significant extent, outside the envelope, then there is no justification for rejecting the Weibull hypothesis.

#### 4.5 Transformation of strength data

Comparison of results from tests in which specimens are fractured using different types of time dependent loading can indicate the presence of a delayed fracture mechanism and may be used to obtain estimates of parameters describing the behaviour (see Section 2.5).

Simple transformation equations relating data from constant stress, and constant stress rate tests, from which the stress corrosion parameter,  $n$ , may be assessed, have already been discussed (see Equations 2.8 and 2.9). Other transformations have been developed for more complex types of loading. Davidge et al (1973) used the stepped loading test (see Section 6.3) on alumina specimens, but treated the results as if coming from a constant stress test. If a specimen had withstood more than one constant level, only the highest was used; lower levels and periods of increasing load were assumed to have insignificant effect on the lifetime.

Braiden et al (1977) accommodated failure of WC-Co specimens on periods of both constant stress and constant stress increase. Failures during initial loading up to the first constant level were treated as rate failures; Davidge's approach was adopted for failures during constant load periods; and specimens which failed during a period of increasing load after one or more constant stress periods were assumed to have suffered negligible slow crack growth during the short period of load increase and were therefore assigned the full lifetime of the constant load period.

Both Davidge et al and Braiden et al used transformations to reduce loading rate data and stepped loading data to equivalent stresses,  $\sigma_{1\text{SEC}}$ , which if applied instantaneously, and held constant, would give each specimen a lifetime of one second. To do this, they needed to guess a

value of  $n$ . If the two sets of  $\sigma_{1\text{SEC}}$  data were not coincident, the transformations were repeated using a different value of  $n$ . A best estimate of  $n$  was obtained when the two sets of  $\sigma_{1\text{SEC}}$  were coincident.

The transformations chosen for the present study are, in some cases, more fundamental in that they take into account the complete loading history of each specimen from the time of initial loading to the point of fracture. This technique has been employed by Evans and Fuller (1974) to estimate failure times under cyclic loads. Assumptions include the sole importance of region 1 on the  $K_I$ - $v$  diagram; the non-existence of any lower stress corrosion limit; and the absence of any time-dependent failure mechanisms, other than stress corrosion.

The fundamental equation governing region 1 slow crack growth is given by Equation 2.5 (see Section 2.5). The left-hand side of this equation, governing crack growth from initial loading, when  $a = a_i$  to failure when  $a = a_f$ , may be reduced if significant slow crack growth is assumed (Evans, Johnson, 1975) so that

$$\frac{1}{AY^n} \int_{a_i}^{a_f} \frac{da}{a^{n/2}} \approx \frac{2}{AY^n (n-2) a_i^{(n-2)/2}}$$

where  $A$  and  $Y$  are constants and  $n$  is the stress corrosion parameter.

Since this is independent of parameters associated with loading, or final conditions, the left-hand side of Equation 2.5 is approximately constant for all types of loading. Thus, when a stress,  $\sigma$ , which is a function of time,  $t$ , is applied between times  $t = t_i$  and  $t = t_f$ ,

$$\int_{t_i}^{t_f} \sigma^n dt \approx \text{constant} \quad \dots \quad 4.23$$

Consider a constant stress,  $\sigma_c$  applied until failure, after time  $t_c$ . Then from Equation 4.23

$$\sigma = \sigma_c$$

$$t_i = 0$$

$$t_f = t_c$$

$$\text{and } \int_{t_i}^{t_f} \sigma^n dt = \sigma_c^n t_c \quad \dots \quad 4.24$$

Consider now, a constant stress rate,  $\dot{\sigma}$ , applied from an initial stress,  $\sigma_i$ , at times,  $t = 0$  until failure at a stress,  $\sigma_f$  at time  $t = t_r$

$$\text{Then } \sigma = \sigma_i + \dot{\sigma} t$$

$$t_i = 0$$

$$t_f = t_r$$

$$\text{and } \int_{t_i}^{t_f} \sigma^n dt = \frac{(\sigma_i + \dot{\sigma} t_r)^{n+1}}{\dot{\sigma}^{n+1}}$$

By allowing  $\sigma_i = 0$  and noting, then, that  $\sigma_f = \dot{\sigma} t_f$

$$\int_{t_i}^{t_f} \sigma^n dt = \frac{\sigma_f^{n+1}}{\dot{\sigma}^{n+1}} \quad \dots \quad 4.25$$

Using Equation 4.23, strength and lifetimes from one type of loading (denoted by the suffix 1) may be compared with those from another (denoted by suffix 2), such that

$$\int_{t_{i1}}^{t_{f1}} \sigma_1^n dt = \int_{t_{i2}}^{t_{f2}} \sigma_2^n dt \dots\dots \quad 4.26$$

Thus comparing tests at two different constant stresses, from Equation 4.24

$$\sigma_{c1}^n t_{c1} = \sigma_{c2}^n t_{c2}$$

or

$$\frac{t_{c1}}{t_{c2}} = \left( \frac{\sigma_{c2}}{\sigma_{c1}} \right)^n \dots\dots \quad 4.27$$

Comparing tests at two different constant stress rates from Equation 4.25

$$\frac{\sigma_{f1}^{n+1}}{\dot{\sigma}_1^{n+1}} = \frac{\sigma_{f2}^{n+1}}{\dot{\sigma}_2^{n+1}}$$

or

$$\left( \frac{\sigma_{f1}}{\sigma_{f2}} \right)^{n+1} = \frac{\dot{\sigma}_1}{\dot{\sigma}_2} \dots\dots \quad 4.28$$

Comparing the lifetime,  $t_r$ , under a constant stress rate where the fracture stress is  $\sigma_f$ , with the equivalent lifetime,  $t_c$ , that would be seen if instead of a constant stress rate, the fracture stress,  $\sigma_f$ , is applied instantaneously and held constant until fracture, then from Equations 4.24 and 4.25, with  $\sigma_c = \sigma_f$

$$\sigma_f^n t_c = \frac{\sigma_f^{n+1}}{\dot{\sigma}^{n+1}}$$

or, by noting that  $\sigma_f = \dot{\sigma} t_f$

$$t_c = \frac{t_f}{n+1} \dots\dots \quad 4.29$$

Equations 4.27, 4.28 and 4.29 form the basic transformations used by Davidge et al (1973) and Braiden et al (1977).

Now consider stepped loading which may be thought of as a constant stress rate,  $\dot{\sigma}$ , initially from stress,  $\sigma_i$ , interrupted by periods of constant stress. Each period,  $p_j$ , of which there are M in total (i.e.  $j = 1, 2, 3, \dots, M$ ), involves a constant stress  $\sigma_{cj}$ , held for a time  $t_j$ .

Each period of loading, whether under constant stress rate, or constant stress may be considered to induce a small amount of crack growth.

Thus for the first period under a stress rate, from time  $t=0$  to time  $t = t_I$ , the crack grows from  $a = a_i$  to  $a = a_I$ .

Then from Equation 2.5

$$\begin{aligned} \frac{1}{AY^n} \int_{a_i}^{a_I} \frac{da}{a^{n/2}} &= \int_0^{t_I} (\sigma_i + \dot{\sigma} t)^n dt \\ &= \frac{(\sigma_I)^{n+1} - (\sigma_i)^{n+1}}{\dot{\sigma} (n+1)} \end{aligned}$$

For the next period - at a constant stress  $\sigma_{cl}$ , - the crack grows from  $a_I$  to  $a_{II}$  in time  $t_I$  to  $t_{II}$ . Then

$$\begin{aligned} \frac{1}{AY^n} \int_{a_I}^{a_{II}} \frac{da}{a^{n/2}} &= \int_{t_I}^{t_{II}} \sigma_{cl}^n dt \\ &= \sigma_{cl}^n (t_{II} - t_I) \\ &= \sigma_{cl}^n t_1 \end{aligned}$$

since  $(t_{II} - t_I) = t_1$ , the duration of the first period.

Applying this technique to all periods, and by noting that

$$\frac{1}{AY^n} \int_{a_i}^{a_f} \frac{da}{a^{n/2}} = \frac{1}{AY^n} \int_{a_i}^{a_I} \frac{da}{a^{n/2}} + \frac{1}{AY^n} \int_{a_I}^{a_{II}} \frac{da}{a^{n/2}} + \dots$$

$$\text{then } \frac{1}{AY^n} \int_{a_i}^{a_f} \frac{da}{a^{n/2}} = \frac{(\sigma_f)^{n+1} - (\sigma_i)^{n+1}}{\dot{\sigma}^{(n+1)}} + \sum_{p=1}^M \sigma_{cp}^n t_p$$

where  $\sigma_f$  is the final stress at fracture.

Thus, from Equation 4.23 and allowing loading to commence from zero stress (i.e.  $\sigma_i = 0$ )

$$\int_{t_i}^{t_f} \sigma^n dt = \frac{(\sigma_f)^{n+1}}{\dot{\sigma}^{(n+1)}} + \sum_{p=1}^M \sigma_{cp}^n t_p \quad \dots \quad 4.30$$

Equation 4.30 may be compared with the equivalent equations governing constant stress and constant stress rate loading - Equations 4.24 and 4.25 respectively.

The procedure used by Davidge et al (1973) and Braiden et al (1977) of transforming all data to  $\sigma_{ISEC}$ , the equivalent constant stress, which when instantaneously applied would give each specimen a lifetime of one second, has also been adopted in the present study.

Using Equations 4.24, 4.25 and 4.30 and by noting from Equation 2.24 that

$$\int_{t_i}^{t_f} \sigma^n dt = \sigma_{1\text{SEC}}^n$$

then, the following transformation equations may be derived

for constant stress,

$$\sigma_{1\text{SEC}} = \sigma_c \cdot t_c^{1/n} \quad \dots \quad 4.31$$

for constant stress rate,

$$\sigma_{1\text{SEC}} = \left[ \frac{(\sigma_f)^{n+1}}{\dot{\sigma}^{(n+1)}} \right]^{1/n} \quad \dots \quad 4.32$$

for stepped loading,

$$\sigma_{1\text{SEC}} = \left[ \frac{(\sigma_f)^{n+1}}{\dot{\sigma}^{(n+1)}} + \sum_{p=1}^M \sigma_{cp}^{n t_p} \right]^{1/n} \quad \dots \quad 4.33$$

#### 4.6 Graphical representation of delayed fracture behaviour

When strength is dependent upon a nominal constant, variability due to material flaws, and the degree of stress corrosive slow crack growth, a relatively large number of parameters are required for its specification. In such a case, the information is far better displayed graphically.

Davidge et al (1973) constructed an SPT diagram relating a constant applied stress (S) to the cumulative failure (or survival) probability (P) for a range of possible lifetimes (T).

The diagram shown schematically in Figure 4.1 comprises a series of lines, each for a different lifetime, the slope of each being governed by the Weibull modulus, m, and their separation by the stress corrosion parameter, n.

As well as providing information for prediction of behaviour, it also allows quick assessment of strength characteristics. For example, lines for lifetimes increasing by orders of magnitude which lie close together indicate little delayed fracture, and lines with steep gradients indicate little variability in strength due to material flaws.

The SPT diagram is easily constructed using transformation equations (see Section 4.5) when the median strength, Weibull modulus and stress corrosion parameter are all known. However it only applies to specimens of the same material, shape and size as those tested to obtain the parameters from which the SPT diagram was constructed. If the specimens or the test conditions are different, corrections need to be introduced, (Stanley et al, 1973; Braiden, 1975) or another diagram constructed more suited to the conditions.

#### 4.7 Summary

Techniques have been developed to allow comparison of data from tests involving different types of loading to failure, and hence obtain estimates of parameters describing the behaviour. The techniques use theories of brittle fracture and stress corrosion within a statistical framework based on the Weibull distribution, incorporated to take into account the random variability of strength caused by its dependence upon material flaws.

The parameters of brittle fracture and stress corrosion, once estimated, may be used to construct an SPT diagram which displays the behaviour graphically.

## 5. CHARACTERISATION OF MATERIALS

### 5.1 Introduction

WC-Co alloys containing 6, 13 and 16% cobalt by weight, all having a nominal mean WC grain size of  $1\mu\text{m}$ , were chosen for bend strength and double torsion tests.

To minimise any variations in strength due to small differences in the material (see Chapter 3) bend specimens were prepared using tool tips from a single manufactured batch for each grade.

Although the double torsion specimens could not be prepared from the same material used for bend specimens, they were obtained from the same manufacturer and were, in themselves, from a single manufactured batch for each grade.

The manufacturer's specifications are given in Table 5.1. As a check, and to provide further information, some material properties were measured in the laboratory. A summary of the results is given in Table 5.2 and details of tests are discussed briefly below.

### 5.2 Hardness

Hardness was measured on an Avery Hardness Testing machine fitted with a Vickers diamond indenter. Prior to testing, the machine was checked using a standard slab of known hardness.

Tests were performed using loads of 50kg and 100kg, and the Vickers hardness values obtained from standard tables. At least ten indentations were made on each type of specimen for each material. Indentations were put into specimen faces polished using a  $6\mu$  diamond paste, (see Section 6.2.3).

### 5.3 Crack resistance

The lengths of cracks emanating from the corners of pyramid indentations were measured during hardness tests. The crack resistance was assessed graphically according to Equation 3.2.

A plot of inverse crack resistance,  $1/W$ , against hardness shown in Figure 5.1, shows that although values of  $1/W$  are a little low, they do follow the general trend found by Viswanadham and Venables (1977). Occasionally the precise location of the crack tip was difficult to see, and crack lengths possibly underestimated. As such, this may explain the low values of  $1/W$ .

### 5.4 Coercive force

Facilities were not available in the department to measure either coercivity or coercive force. Instead, the manufacturer performed the tests. Four bend specimens of each material were packaged individually and left unidentified apart from a code number which had no connection with the material composition. The manufacturer's results showed quite distinctly the specimens of each material.

### 5.5 Microstructural investigation

Polished specimens were etched with a mixture of equal quantities of sodium hydroxide and potassium ferricyanide, each in 20% solution.

The etched surfaces were viewed under a Vickers microscope, photographed - see Plates 5.1 - 5.3 - and analysed to obtain estimates of the mean free path in the cobalt phase,  $\lambda_{Co}$ , and the mean WC grain size,  $\bar{d}_{WC}$  (Murray, 1977).

Straight lines were drawn, some at right angles to each other, on the photographs, and the grains intercepting each line were counted. Hence, the average number of grains per unit length,  $N_L$ , was calculated. A similar procedure where grains were counted within squares drawn on the photographs, obtained estimates of the average number of grains per unit area,  $N_S$ . Five lines and five squares were analysed for each material and specimen type, involving at least 18 grains per line, and at least 200 grains per square.

The values of  $\bar{d}_{WC}$  and  $\lambda_{Co}$  were estimated using

$$\bar{d}_{WC} = \frac{4N_L}{\pi N_S}$$

and  $\lambda_{Co} = \frac{V_{Co}}{N_L}$

where  $V_{Co}$  is the volumetric cobalt content. (Fullman, 1953).

## 6 STRENGTH TESTS

### 6.1 Introduction

In this chapter, work to investigate the presence of delayed fracture in WC-6% Co, WC-13% Co and WC-16% Co loaded in laboratory air at room temperature, is described. Strength tests are performed using different types of loading, with respect to time, prior to fracture. The results are analysed, and parameters describing the behaviour evaluated using the various techniques discussed in Chapter 4.

Tests are also performed in distilled water to assess the influence of environment and hence the presence of environmentally-assisted stress corrosion. Also included is a brief study of the effects of soaking specimens in distilled water prior to loading to identify the presence of corrosion which may be uninfluenced by stress.

Finally details of the fracture process are discussed in terms of observations through the microscope of the fractured specimens.

### 6.2 Experimental details

#### 6.2.1. Measurement of strength

All strengths were measured in bending. This type of loading was considered beneficial to the study of stress corrosion since continuum mechanics indicate the maximum tensile stresses to lie on the specimen surface, where any chemical reaction between material and environment must necessarily occur.

The three point bend configuration was chosen for its practical simplicity and consequent potential high accuracy of loading. An alternative - four point bending - although inducing high stresses over a large proportion of the specimen (the strength thereby being controlled

by a greater volume of material) was rejected because of the difficulties of alignment and consequent lack of loading accuracy.

The continuum bend strength,  $\sigma_f$ , was calculated from the fracture load, P, the specimen dimensions of width, b, and depth, d, and the three point bend span, L, using the standard relationship

$$\sigma_f = \frac{3}{2} \frac{PL}{bd^2} \quad \dots \quad 6.1$$

### 6.2.2 Test rig

The rig designed to carry out three point bending is shown in Plate 6.1.

Particular aspects of the design include accurate alignment of the loading rods using non-load-bearing brass formers machined as one; a device secured in the top jaw of the testing machine to ensure that the centre loading rod remains in contact with the specimen across the whole width; a horizontally mounted load cell and frame to measure, and minimise any horizontal components of the load; a perspex container for environmental tests in liquids; and trip gear to remove the load immediately fracture occurs, thereby minimising any further damage to the specimen.

Load was applied using a Dartec M1000 servo-hydraulic testing machine.

### 6.2.3 Specimen preparation

Material for specimens was obtained in the form of cutting tool tips, commercially available. Initial specimen preparation was performed by contractors outside the department. Specifications included each specimen to have nominal dimensions of 20 x 5 x 2mm. An additional constraint was placed on the thickness such that variations

between specimens of the same material should not exceed  $\pm 0.01\text{mm}$ . To minimise variability in surface finish, the contractors were instructed to grind all specimens of each material together.

Upon return, the surface texture, although consistent for all specimens of one material, showed differences between materials - see Plate 6.2. Straight ridges were apparent on WC6% Co specimens and to a lesser extent on WC16% Co specimens, whereas the surfaces of WC13% Co specimens had a roughness which was non-directional. The contractors later revealed that some lapping, with a SiC paste had been necessary to achieve the specified tolerances on specimens of the higher grade materials.

Half the specimens of each material were diamond polished within the department, leaving the other half with the ground finish. By so doing, the effects of surface finish could be assessed.

Polishing was performed in two stages. Firstly a  $23\mu\text{m}$  diamond paste was used to remove approximately  $50\mu\text{m}$  of material. Then polishing continued with a  $6\mu\text{m}$  paste until the majority of scratches had been removed, as observed under a microscope at a magnification of 400.

This process gave specimens a mirror finish. Scanning electron micrographs, shown in Plate 6.3, indicate that polishing preferentially removed cobalt from the surface leaving WC grains standing slightly proud.

Prior to testing, all specimens were cleaned in acetone which was removed by evaporation using a hot air blower.

#### 6.2.4 Loading and associated errors

Each test involves the identical testing of a number of specimens.

Following the approach of Evans (1972), the stress, or change of stress was maintained constant for each batch, and the loads required to achieve this calculated using individual specimen dimensions.

Errors in the calculated fracture strength arise from variations of dimensions over the specimen, the definition of measuring equipment, off-centre loading and thermal drift of the test machine servo-system.

Estimates of these errors, summarised in Table 6.1 give a maximum estimated error in the fracture strength (using Equation 6.1) of approximately  $\pm 3\%$ .

### 6.3 Time dependent loading tests

One of the most direct methods of observing delayed fracture is to apply a constant stress which is maintained until the specimen fails. However, because of the variability in strength of WC-Co materials, the test is not particularly suitable; some specimens will fail after a few seconds, whereas others, although stressed at the same level, may survive for days.

The range of test durations may be reduced using a constant stress rate to failure. The use of this type of test, expected behaviour and analysis of results have been discussed in detail in Chapter 4.

Another practical improvement on the constant stress test is the stepped loading test, used by Davidge et al (1973) and Braiden et al (1977). A constant load is applied for a prescribed time, after which, if the specimen has not failed, the load is raised to a higher load and held constant again. Increments are applied (using a constant stress rate) until failure occurs.

### 6.4 Stress rate tests

#### 6.4.1 Test details

Five stress rates were chosen for the tests ranging from 0.1

$\text{MN/m}^2\text{s}$  increasing by an order of magnitude each time up to  $1000 \text{ MN/m}^2\text{s}$ .

The test duration governed the lowest rate, while the possibility of errors due to testing machine response limited the upper rate.

Fracture times were typically 20,000 and 2 seconds at each extreme.

24 specimens of each grade of WC-Co were tested at each stress rate, 12 with a ground finish and 12 with a polished finish.

#### 6.4.2 Analysis and discussion of results

The results are presented in Figures 6.1 - 6.6. Overall a trend of increasing strength with stress rate is apparent, as predicted by stress corrosion theory.

Closer inspection reveals considerable differences between, and within batches. For example, strengths of WC6% Co specimens with a polished finish, tested at  $100 \text{ MN/m}^2\text{s}$  display a greater variability than strengths obtained at other rates. Also, the strengths of WC13% Co specimens with a rough finish, form very uneven distributions at all stress rates; although the majority of results fall into a relatively small band, a few are much lower.

Considering these differences of distribution, due most probably to sampling, analytical methods involving the representation of a batch by a mean, or median strength (see Section 4.3) were thought inappropriate. Instead, the data were analysed using the maximum likelihood technique described in Section 4.4. For comparison, data from stress rate tests on soda-lime glass were also analysed.

To check that the failure model involved in the analysis was suitable to represent the results from tests on both soda-lime glass and WC-Co materials, the Monte Carlo technique was employed (see Section 4.4.3). The residuals from the real data sets when superimposed on the envelope

of residuals from 36 artificial data sets of similar size - see Figures 6.7 - 6.13 - gave no justification for rejecting the model. Examples of graphs for the artificial data sets are shown in Figure 6.14.

Results of the maximum likelihood analysis are summarised in Table 6.2.

A similarity in estimates of the Weibull modulus,  $m$ , from WC-Co and glass specimens indicate the distributions of strength to be much the same. Thus the behaviour of WC-Co materials, like glass, is relatively brittle and hence influenced by inherent flaws. Estimates of  $m$  from WC-Co data increase with cobalt content; this agrees with the work of Chermant et al (1977).

A trend is also apparent with surface finish. Estimates of  $m$  are higher from polished specimens than from ground specimens, indicating that a rougher surface induces a greater variability in strength. However, the effect is small, and may be insignificant - the 95% confidence intervals overlap to a considerable extent, particularly for WC-6% Co and WC-13% Co.

Estimates of  $n$  for the WC-Co materials are higher than for soda-lime glass, indicating stress corrosion, or at least, delayed fracture to be much less evident. Even so, a significant stress rate effect on the strength is indicated in all but one case - WC6% Co with polished surfaces. The reason why this batch is different remains unknown.

Variations of estimated  $n$  between different grades of WC-Co and between different surface finishes are not straightforward. Considering first polished specimens,  $n$  for WC-6% Co is much lower than the values of  $n$  for WC-13% Co and WC-16% Co which are similar. From ground specimens,  $n$  tends to decrease with increasing cobalt content, a trend which has been

reported by Smaglenko and Loshak (1973).

Comparing all the results, and giving consideration to the large confidence intervals, a maximum likelihood estimate of  $n \approx 100$  is apparent in all but two cases; estimates from polished WC-6% Co and ground WC-16% Co specimens are much lower.

Now the strength of WC-16% Co specimens appears to be surface sensitive as indicated by the trend in estimated  $m$ . Perhaps surface flaws introduced by grinding are sharper, or larger, and hence more critical than both flaws in the bulk of the material and flaws introduced by diamond polishing. If so then fracture is more likely to initiate from the surface than from within the bulk in ground specimens. Hence any stress corrosive influence should be more noticeable and a lower value of  $n$  expected. This hypothesis, however, cannot explain the low value of  $n$  obtained from polished WC-6% Co specimens. At present, no possible mechanism has been found to explain this.

Nonetheless, all the above observations must be treated with caution. The maximum likelihood technique obtains, solely, estimates of parameters which best fit the data. If sample sizes are small, or the data not perfectly modelled by the Weibull distribution, then errors may arise. The extreme sensitivity of estimates of  $n$  to error is illustrated by the wide 95% confidence intervals shown on Table 6.2. Thus although trends have become apparent, little significance can be given to them at present. They are discussed further in conjunction with the results from stepped loading tests in Section 6.6.

## 6.5 Stepped loading tests

### 6.5.1 Test details

A constant stress rate of  $10 \text{ MN/m}^2 \text{ s}$  was used to raise the stress

to ten predetermined constant levels.

The magnitude of stress for each level were obtained from a Weibull diagram of the data from stress rate tests at  $10 \text{ MN/m}^2 \text{ s}$  on WC-16% Co specimens with ground surfaces, corresponding to cumulative failure probabilities of 5, 10, 20, 30, 40, 50, 60, 70, 80, 90%.

Tests were performed using one of three maximum times for the periods of constant stress - 50, 500 and 5000 seconds.

Only specimens of WC-16% Co were available for these tests being part of the same manufactured batch from which the stress rate test specimens were prepared. As with the rate tests, half the specimens were polished and the rest left with <sup>a</sup>ground finish (see Section 6.2.3). Twelve specimens with each finish were tested to failure using each of the three maximum constant stress periods.

#### 6.5.2 Analysis and discussion of results

The results are presented in Figures 6.15 and 6.16. Also included are the corresponding results from the  $10 \text{ MN/m}^2 \text{ s}$  stress rate tests - effectively stepped loading tests with a maximum constant stress period of zero. Data from specimens failing during a period of increasing stress are shown as lines whereas those failing during a period of constant stress are shown as crosses.

In each test case, at least 50% of the specimens failed during a constant stress period, indicating the presence of delayed fracture mechanisms.

Mean strengths for each batch are shown on Figure 6.17a. Although representation by mean values was not entirely suitable, particularly since many of the original data were confined to particular values governed by the predefined constant stress levels, it was hoped that any gross trends would become evident.

A decrease in strength with increasing constant stress duration is apparent for ground specimens, this being the expected behaviour predicted by theories of stress corrosion. The trend is similar in polished specimens apart from those tested using 5000 second constant stress periods. Here, the mean strength is much higher - similar to the mean from the stress rate tests with no constant stress periods.

However, the mean strengths compared above are to some extent biased by a number of data originating from specimens which did not reach the first constant stress level. To overcome this, these data were removed and the means recalculated. For purposes of comparison, stress rate fracture strengths below the 5% failure probability stress - the first constant stress level - were also removed. This operation is considered fair in that all batches were treated alike.

The adjusted means are shown in Figure 6.17b. A similar trend is apparent for both surface finishes, although not that predicted by stress corrosion theories. A decrease in mean strength (with little apparent influence of surface finish) accompanies an increase in constant stress duration up to 500 seconds. The mean strength rises again at durations of 5000 seconds although this is less apparent for polished specimen results.

A number of possible causes of this phenomenon were investigated. Firstly, the random distribution of material flaws may have induced the effect and thus the trends observed are merely differences due to sampling. However, this seems unlikely (although not impossible), since the effect appears in two sets of data analysed separately.

Secondly, the test itself was investigated. Whereas 50 and 500 second tests lasted a relatively short time (in the order of minutes), tests involving 5000 second constant stress durations lasted most of a working

day, and tests on the whole spanned two weeks. One possible variable was the laboratory environment, but no correlation between strength and relative humidity, or temperature (the variation of both being extremely small) could be found. Even so, small changes in the zero position of the testing machine were detected. However, these produced an error in the loading of less than 0.5% which is too small to account for the variation in mean strength.

Thirdly, a slow acting relaxation mechanism tending to inhibit crack propagation, perhaps by blunting, may be active, the effect of which becomes significant only over long periods of time. However, at present, there is no evidence to support this.

#### 6.6 Comparison of results from stress rate and stepped loading tests

Stress rate, and stepped loading data were compared using the  $\sigma_{1\text{SEC}}$  - transformation analysis described in Section 4.5. Data from each type of test were analysed together irrespective of stress rate, or constant stress duration employed. However data from specimens with different surface finishes were not combined.

Transformation was carried out using a range of possible  $n$  - values - 10, 30, 100, 1000. The distributions of  $\sigma_{1\text{SEC}}$  so obtained from stress rate and stepped loading data from WC-16% Co specimens, are shown in Figures 6.18 - 6.21. Individual points have not been plotted; instead the points (60 in number from stress rate tests, and 36 from stepped loading tests for each surface finish) have been joined by a continuous line to preserve clarity. Curves from WC-6% Co and WC-13% Co stress rate data are shown in Figures 6.22 - 6.25.

Contrary to the results of the maximum likelihood analysis, no significant difference in  $m$  is apparent between polished and ground specimens; large differences in curve gradients (from which  $m$  is measured)

occur only at high, and low cumulative failure probabilities, where confidence in the curve position is low. The gross deviation seen in the ground WC-13% Co curves, for example, is caused by just a few data from specimens containing a large surface flaw on the fracture face.

For all three grades of WC-Co no significant difference in median strengths is apparent between polished and ground specimens. Either the difference in surface finish is not sufficient to induce a significant change in strength, or the materials are not surface sensitive, the strength possibly being controlled more by flaws throughout the volume.

The above mentioned observations are apparent for all values of  $n$  used to calculate  $\sigma_{1\text{SEC}}$ .

The WC-16% Co curves from stress rate data are similar in shape to curves from stepped loading data. Only the positions of the curves are different, changing with the value of  $n$  used in the  $\sigma_{1\text{SEC}}$  - transformation. With  $n = 10$ , the stepped loading curves appear to the right of the stress rate curves, and when  $n = 1000$ , they appear to the left.

If delayed fracture mechanisms are the same in both types of test, then the stress rate, and stepped loading curves should be coincident when the correct value of  $n$  has been used to obtain  $\sigma_{1\text{SEC}}$ . This occurs when  $n \approx 45$ , although it is subject to error for reasons of material flaw variability, and suitability of fracture model discussed previously. Indeed, if the range of maximum likelihood estimates of  $n$  for WC-16% Co obtained from stress rate data -  $n = 45-110$  - are used for transformation, the stress rate, and stepped loading curves are still sufficiently close for the difference between them to be considered insignificant.

To summarise, the following deductions have been made concerning the behaviour of WC-6% Co, WC-13% Co, and WC-16% Co when loaded in

laboratory air at room temperature.

The strength depends upon the loading history prior to failure. Although the effect is small, it is statistically significant, and estimates of the stress corrosion parameter,  $n$ , which best describe the behaviour lie between 30 and 120.

So far, no evidence has been found of any significant variation of  $n$  with material composition, although an increase in cobalt content tends to reduce the variability in strength indicated by an increase in  $m$ .

No significant influence of specimen surface finish, has been detected, upon the mean strength or its variability or upon delayed fracture.

Unusual distributions or levels of strength recorded in stress rate, and stepped loading tests probably arose merely because of small samples and the particular distributions of flaws in specimens within each batch; another batch, or a larger batch might have produced quite different results. This highlights the difficulties of assessing the significance of delayed fracture effects when variations due to random material flaws are of a similar order of magnitude. The tests have demonstrated that for characterisation of behaviour, mathematical analysis for parameter estimation must be accompanied by a graphical method whereby the effects of extreme values and unusual distributions can be assessed.

#### 6.7 Environmental tests

The search for an environmental influence on delayed fracture requires not only an investigation of any corrosive effects on the strength but also the separation of effects that are stress-enhanced from those which occur independent of the stress in the material.

Distilled water was chosen as an alternative test environment to laboratory air because it induces considerable stress corrosion cracking in other materials (see Sections 2.2.2 and 2.4).

## 6.8 Preliminary environmental tests

### 6.8.1 Test details

A stress rate of  $2\text{MN/m}^2\text{s}$  was used to test to failure a batch of WC13% Co specimens with ground faces.

To investigate environmental effects on the strength, half the specimens were tested in laboratory air and the other half in distilled water. To differentiate between stress-independent, and stress-enhanced corrosion, half the specimens to be tested in each environment were soaked in distilled water for approximately 150 hours before being loaded. As such, the soak time was considerably longer than the time under load ( $\sim 20$  minutes), so that any effects of stress-independent corrosion during loading could be considered negligible.

If stress-independent corrosion occurs, then all soaked specimens irrespective of the test environment should show a degradation in strength. Similarly if stress-enhanced corrosion is present, then specimens loaded in distilled water should be weaker than those tested in air, irrespective of whether they were presoaked or not. (This assumes that water is, in general, a more corrosive environment than laboratory air.)

These tests formed part of a preliminary series to develop techniques. Consequently, the specimens tested, were not from the same manufactured batch as those used in the main stress rate tests. However, they were from a single manufactured batch from the same manufacturer.

All specimens to be tested in air after a presoak in distilled water, were dried by evaporation using a hot air blower, prior to loading.

### 6.8.2 Analysis and discussion of results

After one day of soaking, small brown spots were seen on specimen faces. Further soaking increased the discolouration until

whole surfaces were covered to various degrees - see Plate 6.4. The thickest deposits were found in the vicinity of the original brown spots where microscopic inspection revealed the presence of a surface flaw.

A similar phenomenon had been noticed when distilled water was placed on recently polished surfaces of WC16% Co specimens. Small brown deposits appeared after approximately one hour. Surface flaws found at these sites were estimated from further polishing to be between 10 and 20  $\mu\text{m}$  deep.

In both cases, surface discolouration indicated corrosion to have taken place during soaking, and the colours, in extreme cases ranging from yellow, green and blue to brown, suggest that the deposits were compounds of cobalt.

Why corrosion should occur preferentially in the vicinity of a surface flaw is still unclear. Perhaps the confined space within a flaw increases the activity of chemical reaction between the material and a corrosive species in the environment.

Another possible explanation is that residual stresses were present in the surface, and locally concentrated by a flaw, such that their presence enhanced corrosion in that area - in other words, a stress corrosive mechanism.

However, residual stresses introduced during sintering and subsequently modified by machining and surface preparation, tend to be compressive (French, 1969; Jaensson, 1971) and hence unsuitable for stress corrosive crack opening. It is possible, though, that the stress concentrating effect of flaws may produce tensile components in the residual stress field. Murray (1977) reports that although residual stresses in the WC phase are both compressive on the surface and internally, in the cobalt, they are compressive on the surface but tensile internally. It is

possible, then that at the deepest point of the surface flaw, the stress field may be suitable for stress enhanced corrosion.

The strengths of specimens both soaked and unsoaked are displayed in Figure 6.26. A first inspection of the data reveals a much wider distribution of strengths from specimens which were soaked prior to testing. In particular, a greater number of low strengths are evident.

To investigate further the effects of soaking, results were grouped together as to whether specimens were soaked or unsoaked, but independent of loading environment. Each set was ranked and plotted on a Weibull diagram - see Figure 6.27a.

Little confidence may be placed in the slightly lower range of data recorded from soaked specimens at the high failure probability/high strength end of the curves. However, the difference between soaked and unsoaked data becomes considerable at the lower end.

Microscopic inspection of the fractured pieces of soaked specimens revealed in almost all those failing at a low stress, the presence of a large heavily corroded surface flaw along the line of fracture (see for example Plate 6.4). Inspection of the fracture face indicated the flaw to be the likely site of crack initiation (see Section 6.11.4). Few large surface flaws in the vicinity of crack initiation were observed in soaked specimens failing at higher strengths. A similar inspection of unsoaked specimens revealed far fewer critical surface flaws.

The low strengths recorded from soaked specimens could be due, merely, to the presence of a large critical surface flaw, and by chance, the soaked batch contained more specimens with such a flaw. However, the correlation between low strength and the critical surface flaw being heavily corroded, indicates that the flaw has been enlarged, or sharpened by the chemical reaction. This action makes the flaw more likely

to become critical than other flaws elsewhere in the material, and also tends to reduce the failure strength. This may explain the greater number of surface flaws being critical in soaked specimens than in unsoaked specimens.

Soaked specimens in which fracture initiated away from heavily corroded surface flaws tended to fail at much higher stresses - similar in magnitude to the strengths of unsoaked specimens. Thus general corrosion over the surface away from heavily corroded areas does not appear to have any significant influence on the strength.

Regrouping, re-ranking and replotting the results according to the loading environment but irrespective of whether specimens were presoaked or not, produced the Weibull curves shown in Figure 6.27b. The two curves are relatively similar apart from the mid failure probability/mid strength region.

However little significance can be attached to the difference. Grouping of results independent of soaking, or not, assumes there to be no soak effect. But this appears not to be the case from the previous grouping. Inspection of both curves revealed almost all soaked specimen results to lie at the low strength ends. The curves, therefore, are biased by the predominant effect of soaking. A similar investigation of the soak/no soak curves in Figure 6.27a revealed the data from specimens loaded in air and water to be fairly evenly distributed. Hence, there is no evidence of any influence of loading environment and therefore, of any stress-enhanced corrosion. If present, its effect on the strength must have been extremely small - too small to distinguish from the general variability in strength due to material flaws, and certainly much smaller than the effect of long term soaking in the absence of externally applied loads.

To summarise, the preliminary environmental tests have indicated corrosion to occur when WC-Co specimens are soaked in distilled water, particularly around surface flaws. The strength is lower than expected when failure initiates from a heavily corroded flaw, indicating the flaw to have been enlarged, or sharpened. No evidence of environmentally assisted stress corrosion has been found.

## 6.9 Main Environmental tests

### 6.9.1 Test details

In consideration of the preliminary test results, the main environmental tests were designed to enhance any environmentally assisted stress corrosion present, whilst minimising corrosion effects during soaking, (this is not simple, since magnification of any stress enhanced corrosion requires a longer period of loading in the corrosive environment, which also increases the degree of stress-independent corrosion). To minimise effects of sampling, all remaining WC16% Co specimens (all with ground faces) of the material used to provide specimens for stress rate and stepped loading tests, were tested. To increase the batch size still further, no specimens were subjected to long presoaks.

Hence, thirty specimens were loaded to failure using a stress rate of  $1\text{MN/m}^2\text{s}$  (half the rate used in preliminary tests), in laboratory air, and another thirty similarly tested in distilled water.

Since specimens tested in water effectively experienced a duration of soaking equal to the loading time to failure (approximately 40 minutes), specimens to be loaded in air were, therefore, presoaked for a similar time, and dried prior to loading (see Section 6.8.1 for details).

Since materials were the same, results from stress rate tests and environmental tests could be directly compared.

### 6.9.2 Analysis and discussion of results

As expected, with so short an exposure to distilled water, specimens showed no visible signs of corrosion.

The recorded strengths are displayed in Figure 6.28. Included for comparison are the results from the equivalent  $\text{MN/m}^2$  stress rate tests in air (in which no presoak of any sort was used). Since no influence of surface finish was detected (see Section 6.6), data from specimens with polished and ground faces have been combined to reduce possible sampling errors.

One extremely low strength ( $1460 \text{ MN/m}^2$ ) recorded during environmental tests in air, originated from a specimen containing a large surface flaw 0.2 mm deep (see Plate 6.7). Because it is so different from the rest it has been treated as an extreme value and, consequently, ignored in the following discussion. It has, however, been included in the accompanying diagrams for completeness.

Taking this into account, the range of strengths from both stress rate and environmental tests in air are similar. The range from environmental tests in water is slightly larger, extending further particularly at the low strength end.

The data in each set were ranked and plotted on a Weibull diagram - see Figure 6.29. As for previous diagrams, individual points have been joined together to form a continuous line, so that clarity is improved. Also included in Figure 6.29 are 5% and 95% confidence bands calculated for the best straight line passing through data from the environmental tests in air (thus there is a 90% probability that the true behaviour lies within the area bounded by the confidence bands).

No significant difference is apparent between the curves from stress rate tests and environmental tests in air. (The small portion of the former lying outside the confidence bands can be ignored - no evidence

has been found to suggest that this is caused by anything other than effects of sampling. Also data from stress rate tests were fewer in number than data from environmental tests and hence confidence bands should be slightly further apart.) Thus, the short soak period in environmental tests appears to have had a negligible effect on the strength. This implies that any strength degradation seen in results from environmental tests in water (where effective soak times were similar), is unlikely to have been caused by corrosion independent of the applied load.

The high failure probability/high strength portion of the curve for environmental tests in water is similar to the other two curves. However, the low strength end deviates to lower strengths for the same failure probability. The shape is similar to the soaked specimen curve in Figure 6.27a from preliminary environmental tests, although not so pronounced. Even so, since the lower portion of the curve lies outside the confidence bands for the environmental tests in air, a degree of significance in the deviation is indicated.

The apparent link between low strength and fracture initiation from heavily corroded flaws found in preliminary soak tests (see Section 6.8.2) prompted a similar microscopic inspection of fracture faces here. However, specimens in which fracture appeared to initiate from large surface flaws were not so numerous (18% instead of 26% of the total). Further, there was no predominance of surface initiation in specimens loaded in water; indeed slightly (although, not significantly) more specimens of this type were found from tests in air. The inspection also indicated approximately 50% of all specimens to have failed initially from sub-surface flaws, and therefore, presumably uninfluenced by the test environment (assuming WC-Co materials to be impervious to distilled

water); six of the ten weakest specimens loaded to failure in water were of this type.

Thus, although a trend of reduced strength has been noticed tending to indicate the existence of stress corrosion mechanisms, at present there is no additional evidence to support this. Hence, little significance can be attached to it. Further work is required to check that the trend is not merely a coincidental effect of sampling.

#### 6.10 A Comparison of the influence of environment on the strength of WC-Co and alumina materials

Tests on WC-Co materials have shown that, at room temperature, a change of test environment from laboratory air to distilled water produces little, if any, effect on delayed fracture when specimens are loaded to failure. Far more significant is the degradation in strength found after long-term soaking with no externally applied loads.

This behaviour is quite different from that observed in environmental tests on alumina ( $\text{Al}_2\text{O}_3$ ). Bend specimens, similar in size to the WC-Co specimens, were loaded to failure using a range of stress rates, in laboratory air and in Ringers Solution (commonly used to simulate body fluid, and as such, considered relatively corrosive), both with and without a presoak. Results, all obtained at room temperature, are shown in Figure 6.30.

The degradation in strength with decreasing stress rate in Ringers Solution may be represented by a value of the stress corrosion parameter,  $n \approx 40$ . This indicates that delayed fracture is likely to be less obvious in an  $\text{Al}_2\text{O}_3$ /Ringers Solution system than in a glass/laboratory air system but more obvious than in a WC-Co/laboratory air system (comparable estimates of  $n$  are given in Table 6.2).

Alumina is approximately 15% weaker when tested in Ringers Solution

instead of laboratory air, although fractured under the same rate of loading. The effect is stress corrosive since tests involving a presoak of one hour (considerably longer than the time taken to load the specimen to fracture) did not influence the strength significantly. Thus, any effect of corrosion which is independent of applied stress, if present, must be extremely small. The dominant influence appears to be stress-enhanced corrosion. The behaviour is opposite to that of WC-Co materials tested in air, or water, where corrosion during soaking is predominant.

#### 6.11 Inspection of fractured specimens

All fractured specimens were inspected by eye and under the microscope. Both the region of initial fracture, and subsequent crack propagation became evident by viewing each specimen from the side, the tensile face and the fracture face.

##### 6.11.1 The specimen side

Fracture rarely initiated exactly at mid-span. In a few specimens, it occurred almost 2mm off centre on the tensile face.

The crack propagated initially at approximately  $90^{\circ}$  from the tensile face. As it approached mid-thickness it turned towards mid-span, eventually travelling almost parallel to the tensile face (see Figure 6.31). When the crack reached mid-span, the remaining unbroken ligament fractured, again perpendicular to the tensile face.

##### 6.11.2 The tensile face

Cracking seen across the width of the tensile face followed a distinctive pattern common to all specimens. The characteristics were symmetrical about a point, the position of which across the width appeared

to be random. When the point lay close to one edge, the pattern appeared predominantly on one side only, between the point and the other edge. The following description follows the crack path from the point of symmetry to one edge (see Figure 6.31).

Initially the crack path from the point was virtually straight, lying perpendicular to the edge. Then it deviated in a zig-zag fashion with increasing amplitude. Eventually crack branching was seen at peak deviations. Most branches were just a few micrometers long but some extended much further, sometimes reaching the edge. Occasionally severe crack branching produced a chip completely separated from the main fractured pieces. Near the edge, both the major crack and crack branches tended to turn inwards towards the original line of crack growth.

The fracture strength appeared to influence the extent of the cracking. If it was low, the straight region of cracking from the point of symmetry was long, with little deviation or crack branching. At high strengths, the straight regions were hardly discernible, and crack branching severe, producing a large delta of branches near the edge and as many as three separate chips.

Crack branching was seen repeatedly to occur at approximately  $30^{\circ}$ , an angle given some significance by Kalthoff (1971).

### 6.11.3. The fracture face

The fracture face also displayed characteristics common to all specimens (see Plate 6.5) with a point of symmetry coincident with the point of symmetry observed on the tensile face.

Around the point was seen a smooth semi-elliptical region with the major axis lying along, or parallel to the tensile face. It corresponded to the region of straight cracking observed on the tensile face. Beyond the smooth region, the surface undulated with increasing roughness as the distance

from the point of symmetry became greater.

A thin strip of the fracture face adjacent to the compressive face displayed a different texture comprising ridges running parallel to that face. This region corresponded to the final ligament to be broken, as described in Section 6.11.1.

Closer inspection of the smooth elliptical region often revealed a flaw near its centre. This was particularly evident in WC 6% Co specimens. The flaw was almost always a pore, or hole.

Observing the smooth region under the microscope revealed feint lines radiating outwards from the centre and away from the tensile face. When the region contained a surface flaw, lines near the flaw radiated away from its perimeter. Away from the flaw lines appeared to radiate more from the tensile face, although still in a direction away from the flaw - see Plates 6.6 and 6.7. A similar pattern was seen when the flaw lay sub-surface. In the ligament between the tensile face and the flaw, lines, although indistinct, appeared to radiate from the flaw, diverging as they approached the tensile face - see Plates 6.8 and 6.9. An example of a smooth region in which a large flaw could not be found is shown in Plate 6.10.

In general, a low fracture strength was accompanied by the observation in the smooth region of a large flaw, lying on, or near the tensile face. The smooth region was usually large. As strengths increased, flaws became smaller, and less frequently seen. In addition the size of the smooth region decreased; at high strengths it was almost impossible to identify.

#### 6.11.4 Relation of observations to strength test results

If a "weakest link" concept is applied to brittle fracture, then a crack initiates at a point where the stress first reaches or exceeds the

the level required to separate two adjacent atoms. Rapid propagation follows, resulting in immediate catastrophic failure of the specimen. Introducing also a continuum mechanics approach to the three point bend specimen, a crack should initiate simultaneously across the width at mid-span on the tensile face, along the line of maximum tensile stress. Propagation then follows uniformly in a direction perpendicular to the tensile face, up through the thickness of the specimen, towards the compressive face.

This model must be modified on two accounts when applied to WC-Co materials. Firstly, the model assumes the material to be homogeneous. WC-Co materials by their very nature are not; a propagating crack may be passing through a WC grain at one instant followed immediately by a period spent in the cobalt matrix. In this respect, observations made by Gurland and Bardzil (1955) of grain cleavage just prior to fracture probably indicate conditions of crack initiation having been met in the WC grain, but subsequent propagation halted at the grain boundary by the cobalt matrix which is far more crack resistant.

A second modification is necessary to take into account the effect of flaws both on crack initiation and propagation. A flaw tends to attract concentrations of stress such that critical conditions for fracture are likely to be reached there rather than in a region without a flaw. Consequently, if the critical flaw lies sub-surface, away from mid-span, and somewhere across the width of the bend specimen, then propagation is very different from that predicted by the model. The crack, once initiated, must travel downwards towards the tensile face, outwards across the width, and inwards towards mid-span, as well as upwards through the thickness towards the compressive face.

This concept of multidirectional cracking radiating outwards from a point may be compared with the description of fracture and points of symmetry

given in Sections 6.11.1 - 6.11.3. The centre of symmetry lies in the smooth region seen in the fracture face. Following the crack growth backwards towards its origin, it is not unreasonable to assume that the radiating lines seen in the smooth region follow the direction of cracking. Further, when the lines are seen to radiate from a large flaw, then the flaw is likely to be the stress concentrator which first became critical, and hence, initiated fracture (Almond, Roebuck, 1980).

A investigation of this type has a direct bearing on the bend strength results. Firstly, fracture strengths observed in environmental tests incorporating a long presoak in distilled water (see Section 6.8), were lower than expected when a heavily corroded surface flaw was seen on the fracture face. Observations of the fracture face, the patterns of cracking, and particularly the position of the flaw at the centre, or point of symmetry, indicated that it was the initiator of fracture. Observations of presoaked specimens failing at higher stresses showed in most cases, failure to initiate either from a subsurface, and therefore uncorroded flaw, or from a region where a large flaw could not be found.

The "weakest link" concept appears to be applicable here. Assuming failure to initiate at a point where critical conditions are first met, or exceeded, the sharpening or enlarging effect of corrosion on a surface flaw, tends to increase the stress concentration in that area, thereby, both increasing the likelihood of failure initiation from that flaw, and lowering the applied stress necessary to cause failure. If, however, the critical conditions are reached elsewhere - say, at a large subsurface flaw - then since the critical region is unaffected by corrosion (assuming the material to be impervious) the stress concentration and hence fracture strength remain unaltered. Thus, corrosion, although occurring in all presoaked specimens may not always have a significant effect on their strength.

A second observation concerns specimens tested using stepped loading. When failure occurs during a period of constant stress, the presence of a delayed fracture mechanism is indicated. However, fracture faces of some specimens which had failed in this manner, indicated failure to have initiated from a sub-surface flaw. The direction of radiating lines on the smooth region, between the flaw and the tensile face (see Section 6.11.3) indicate cracking to be from the former to the latter, and this is supported by elastic theory (Roark, Young, 1975). Using as a model, a beam in bending with a hole near the tensile face, the highest theoretical stress occurs at the edge of the hole nearest the tensile face.

If this is the case, then the test environment is unlikely to have had any influence on fracture; the relative imperviousness of WC-Co materials prevents any corrosive species in the air from reaching a crack propagating from a subsurface flaw. Once the crack reaches the tensile face, where the corrosive species first comes into contact with the crack tip, the critical crack length has probably been exceeded, and propagation is rapid. Thus, delayed fracture in this case appears to be independent of test environment with controlling mechanisms lying solely within the behaviour of the material.

An alternative explanation might be that environmental corrosion on the surface modified the stress field in the rest of the specimen, including around the critical sub-surface flaw. However, this is unlikely, given the negligible visible evidence of corrosion in stepped loading tests in air. By comparison, the heavily corroded flaws seen in environmental tests produced significant reductions in strength only when failure initiated from them, and even then reductions were small.

Another alternative is that the "constant" load during which failure occurred was not, in fact, constant. However test records showed no trace of deviation or perturbation. It is conceivable that slight

oscillations of the servo-system in the testing machine - usually much too small to be seen - were the source. However this would require the constant applied stress to lie just fractionally below the fracture stress of the specimen. Since approximately 40% of all specimens failing during a period of constant stress contained a critical sub surface flaw, it is extremely unlikely the predetermined constant stress levels should repeatedly lie so close.

#### 6.12 Summary of strength test results

Time dependent loading tests in laboratory air have shown that delayed fracture occurs in WC-Co alloys containing 6, 13 and 16% cobalt by weight. An increase in strength with stress rate to failure is similar to that predicted by stress corrosion theories. No differences in behaviour have been detected between specimens tested using either constant stress rates or stepped loading.

Estimates from maximum likelihood, and transformation techniques, of the stress corrosion parameter,  $n$ , which best describe the behaviour, lie between 30 and 120. No significant influence of material composition or specimen surface finish has been found.

The degree of delayed fracture in WC-Co materials in air is much less than in others such as soda lime glass and alumina for which  $n$  has been estimated to be approximately 19 and 40 respectively (see also Evans (1974)).

The influence of test environment on delayed fracture has yet to be ascertained. Although a trend of decreasing strength was noticed when specimens were loaded to failure in distilled water instead of laboratory air, no supporting evidence has been found. If such an influence exists, then it is extremely small, and certainly much smaller than the effects of testing alumina in Ringers Solution instead of laboratory air.

Distilled water, however, had a significant effect on the strength

when unloaded specimens were soaked in it, prior to being tested. Prolonged soaking caused severe corrosion particularly around surface flaws, which were shown, in subsequent strength tests to have been enlarged or sharpened by the action. The mechanisms are not known at present, although possible factors influencing the degree of corrosion include residual stresses in the specimen surface. By comparison, the strength of alumina was not significantly degraded when specimens were soaked in Ringers Solution prior to testing; strength reduction was predominantly stress corrosive requiring the presence of an applied load.

Observations of the fractured pieces of bend specimens have shown fracture faces to display a common pattern of varying roughness which appears symmetrical about a point. The frequent presence in that location, of a large material flaw indicates that it is the critical flaw governing failure. The symmetrical pattern, hence, follows the progression of crack growth through the specimen.

The investigation led to the conclusion that unexpected low strengths recorded in environmental tests including a long presoak in distilled water, were caused by fracture initiating from heavily corroded flaws. Also sub-surface initiation was sometimes observed in specimens failing during a period of constant stress in stepped loading tests, thereby suggesting that delayed fracture in air was not necessarily environmentally assisted.

## 7. CRACK PROPAGATION TESTS

### 7.1 Introduction

A simple method of introducing precracks into specimens is developed for double torsion tests, chosen to investigate slow crack growth in WC-Co materials at room temperature.

Measurements of crack growth rates and corresponding stress intensity factors are used to construct  $K_I$ - $v$  diagrams from which slow crack growth behaviour is evaluated.

Details are also given of slow crack growth observed in WC-Co bend specimens soaked in dilute nitric acid.

### 7.2 Choice of test configuration

Various test configurations have been developed to study crack propagation. Most commonly employed are edge-cracked three, or four point bend, compact tension, double cantilever beam, tapered double cantilever beam, constant moment, and double torsion - see Figure 7.1. (Pook, 1970; Braiden, 1976; Jayatilaka, 1979). The relative suitability of each depends upon the properties of the material to be investigated. Of particular relevance in choosing a configuration for WC-Co materials, is their poor machineability, and the difficulty of sintering large specimens. Also, many configurations designed, primarily, to measure fracture toughness are not suitable for the study of slow, sub-critical crack growth.

Bend specimens with a large precrack initiated at mid-span are relatively easy to prepare, but permit little slow crack growth because the critical crack length is short. Also the specimen is wide in relation to its depth, allowing non-uniform crack growth across the width, which is difficult to both measure and represent mathematically.

The compact tension configuration, likewise allows little slow crack growth. Additional problems arise in applying the tension loads necessary to open the crack. The use of jaws gripping the specimen, runs the risk of it slipping and becoming misaligned (overtightening can induce bending), and holes drilled in the specimen to allow insertion of loading rods, tend to act as stress concentrators such that failure initiates from them rather than from the precrack.

Both the straight and tapered types of double cantilever beam suffer from similar loading problems. However they do sustain considerable slow crack growth.

In all the configurations so far described, except the tapered double cantilever beam, measurements of velocity and stress intensity factor used to construct the  $K_I$ - $v$  diagram, must be obtained by continuously monitoring the crack length. In some configurations, however, the stress intensity factor is independent of crack length, and relies only upon specimen dimensions, material properties and the applied load.

One such "constant K" specimen is the tapered cantilever beam although in addition to loading problems already mentioned, the techniques requires large specimens and accurate machining of the taper.

The constant moment configuration is also of the "constant K" type. The rectangular plate specimen, although simple to manufacture, and able to contain considerable slow crack growth, must be loaded through two moment arms. A method must be found of fixing the arms to the specimen so that the joint is strong enough to withstand the high bending moments required to induce crack growth.

"Constant K" specimens of the double torsion type, again rectangular plates and, thus, simple to manufacture, are far easier to load. A four-point bend configuration is used to provide torsion in two arms. Since loading is totally compressive, neither tension grips nor holes for

loading rods are required. The specimen can sustain slow crack growth along the whole length of the plate. Thus for reasons noted above, the double torsion configuration was chosen for the present study. One possible disadvantage is the relatively complex type of crack growth - this is discussed in Section 7.3.

### 7.3 The double torsion test

The double torsion specimen, shown schematically in Figure 7.2 consists of two arms with the crack acting as a common boundary. Torsion is applied to each arm, but in opposite directions. The consequent deflection of the arms tends to open the crack, propagating it along the length of the specimen.

The configuration was originally devised by Outwater and Jerry (1966) and developed first by Kies and Clark (1969) and later by Evans (1972). It has been successfully employed for the study of slow crack growth in many materials, including glass (Weidmann, Holloway, 1974; Mai, Gurney, 1975), graphite (Freiman, Mecholsky, 1978), silicon carbide (Evans, Wiederhorn, 1974; Evans, Lange, 1975; McHenry, Tressler, 1977), and in epoxy resins (Phillips, Scott, 1974; Young, Beaumont, 1976.)

Torsion is applied to the specimen of depth,  $d$ , and width,  $W$ , containing a crack of length  $a$ , using a four-point bend arrangement. A total load,  $P$ , applied to the inner points, is split equally between each arm. Each outer point then takes the reaction load,  $P/2$ , from the specimen. The distance between inner and outer points,  $W_m$ , acts as the moment arm providing the torsion.

Treating each arm as a rectangular bar under pure torsion, the angle of twist,  $\theta$ , is given by

$$\theta = \frac{6PaW_m(1+\nu)}{E W d^3} \dots\dots\dots 7.1$$

where  $E$  and  $\nu$  are Young's modulus and Poisson's ratio respectively for the material.

Assuming  $\theta$  to be small, so that the deflection,  $y$ , of each inner loading point is obtained approximately from  $y = \theta \cdot W_m$ , and specifying the specimen compliance,  $C$ , to be the value of  $y$  for unit load (i.e.  $C = y/P$ ), then from Equation 7.1

$$C = \frac{6a(W_m)^2 (1 + \nu)}{E W d^3} \dots\dots\dots 7.2$$

Often a groove is cut into the specimen to guide the crack (see Figure 7.2). The thickness,  $d_n$ , of material through which the crack passes is therefore less than the thickness of the rest of the specimens.

As the crack passes along the groove, it releases strain energy, induced into the specimen by the load. The strain energy release rate per unit thickness,  $G$ , for the specimen is given by

$$G = \frac{1}{2} \frac{P^2}{d_n} \cdot \left( \frac{dC}{da} \right) \dots\dots\dots 7.3$$

Combining Equations 7.2 and 7.3 to eliminate  $C$  gives

$$G = \frac{3(1+\nu) (P W_m)^2}{E W d_n d^3} \dots\dots\dots 7.4$$

Under plane strain conditions, the stress intensity factor,  $K$ , is related to  $G$  by

$$K^2 = \frac{GE}{(1-\nu^2)} \dots\dots\dots 7.5$$

Thus by combining Equations 7.4 and 7.5

$$K = P W_m \left[ \frac{3}{(1-\nu) W d_n d^3} \right]^{\frac{1}{2}} \dots\dots\dots 7.6$$

K, therefore, depends only upon specimen dimensions, material properties and the applied load. Since K is not influenced by the crack length, the configuration is a "constant K" type.

Some concern has been expressed by Evans (1973) as to the mode of crack growth in the double torsion specimen. The general direction of propagation along the length is perpendicular to the direction of loading, and hence would appear to be Mode III crack growth (see Knott (1973)). However, Evans proposed that at any instant the crack is in fact travelling perpendicularly from the tensile face to the compressive face.

The characteristic curved crack front seen in double torsion specimens (shown in Figure 7.3) supports this view. At the greatest extent of crack growth along the tensile face - point A in Figure 7.3 - the crack has just emerged from the tensile face, whereas a short distance back (B), the crack has travelled further through the thickness. Thus a thin width-wise section cut from the specimen passing through the crack front - CC' on figure 7.3 - is effectively a beam loaded in four-point bending, with a mid-span crack travelling upwards through the thickness. In this case crack growth is of type Mode I.

Since the difference between the extent of crack growth in the tensile face and on the compressive face is generally much greater than the specimen thickness (Evans, 1972), it is reasonable to assume that plane strain conditions are present.

Estimates of  $G_c$ , the critical strain energy release rate, for soda lime glass using the double torsion configuration are in good agreement with  $G_{IC}$ , the critical strain energy release rate for Mode I cracking measured using other configurations (Evans, 1973). Thus Equation 7.6 may be rewritten in terms of the plane strain stress intensity factor for Mode I cracking,  $K_I$ , such that

$$K_I = P W_m \left[ \frac{3}{(1-\nu)W d_n d^3} \right]^{\frac{1}{2}} \dots\dots\dots 7.7$$

However, Jayatilaka (1979) questions whether sufficient evidence has been amassed to support the argument.

#### 7.4 Use of the double torsion test to measure slow crack growth

First studies of slow crack growth using the double torsion test involved the estimation of propagation rates from optical measurements of the crack front as it progress along a specimen subjected to a constant load (Kies, Clark, 1969).

Evans (1972, 1974) improved the experimental technique by transferring control from load to displacement of the inner loading points, and by noting the following relationships.

A controlled displacement,  $y$ , induces a load  $P$  into the specimen containing a crack of length,  $a$ . Evans showed experimentally that the specimen compliance,  $C$ , ( $= y/P$ ) is linearly related to  $a$  such that

$$C = A_1 a + A_2 \dots\dots\dots 7.8$$

where  $A_1, A_2$  are constants.

Thus

$$y = P(A_1 a + A_2) \dots\dots\dots 7.9$$

If a constant displacement rate,  $\dot{y}_c$ , is applied to the specimen, then from Equation 7.9

$$\dot{y}_c = \frac{dy}{dt} = \frac{dP}{dt} (A_1 a + A_2) + A_1 P \frac{da}{dt} \dots\dots 7.10$$

Assuming that the specimen is "constant K" and that a stress corrosive relationship exists between the stress intensity factor,  $K_I$ , and crack tip velocity,  $v$ , ( $= da/dt$ ) of the form

$$v = A K_I^n \quad (\text{Equation 2.4})$$

where A is a constant, and n is the stress corrosion factor, then a constant displacement rate should induce a constant crack tip velocity. Further  $K_I$  and P should remain constant such that Equation 7.10 reduces to

$$v = \frac{da}{dt} = \frac{1}{A_I P} \left( \frac{dy}{dt} \right) \quad \dots\dots\dots 7.11$$

Hence, estimates of both stress intensity factor and crack velocity, do not require the measurement of crack length or rate of propagation.

By calculating  $v$  and  $K_I$  using Equations 7.11 and 7.7 respectively, a single point may be plotted on the  $K_I$ - $v$  diagram. By performing tests at a range of displacement rates, the  $K_I$ - $v$  curve can be constructed.

This technique, however does not make efficient use of the specimen; only one point of the  $K_I$ - $v$  diagram is obtained from each period of constant displacement rate, during which some considerable crack growth may have occurred.

The efficiency is greatly improved if a constant displacement technique is used instead. A constant displacement rate is applied to raise the load to some predetermined level. When reached the displacement is held constant. Initially the crack velocity is high, and the consequent increase in crack length raises the compliance of the specimen, thereby reducing the load. As the specimen progressively relaxes, the crack velocity decreases inducing a lower rate of unloading.

Under a constant displacement  $dy/dt = 0$ , and equation 7.10 reduces to

$$v = \frac{da}{dt} = \frac{L}{A_1 P} (A_1 a + A_2) \cdot \left( -\frac{dP}{dt} \right) \dots\dots\dots 7.12$$

Letting  $P_f$  and  $a_f$  represent the load and crack length, respectively, at the end of relaxation, then from Equation 7.9, since  $y$  is constant,

$$\frac{P}{P_f} = \frac{(A_1 a_f + A_2)}{(A_1 a + A_2)} \dots\dots\dots 7.13$$

where  $P$  and  $a$  now represent load and crack length at some intermediate point during relaxation.

Combining Equations 7.12 and 7.13 to eliminate  $a$

$$v = \frac{(A_1 a_f + A_2)}{A_1} \cdot \frac{P_f}{P^2} \cdot \left( -\frac{dP}{dt} \right) \dots\dots\dots 7.14$$

Denoting the compliance at the end of relaxation by  $C_f$  and noting from Equation 7.8 that  $C_f = A_1 a_f + A_2$  then Equation 7.14 reduces to

$$v = \frac{C_f \cdot P_f}{A_1 P^2} \cdot \left( -\frac{dP}{dt} \right) \dots\dots\dots 7.15$$

Again  $v$  may be calculated *without* the need to measure crack lengths or propagation rates.  $P$ ,  $P_f$  and  $dP/dt$  are easily measured from a load-time record of the test;  $C_f$  is obtained by lowering the load under a constant displacement rate at the end of relaxation, and noting the relationship between  $P$  and  $y$  ( $C = y/P$ , hence  $C = \dot{y}/\dot{P}$ ); and  $A_1$  is calculated from a prior compliance calibration.

Hence, by analysing a number of points along a single relaxation curve, a large portion of the  $K_I$ - $v$  diagram may be constructed.

A final note must be made concerning the direction of crack propagation. Equations 7.11 and 7.15 give the velocity of crack propagation in a direction along the length of the specimen. However, as shown in Section 7.3 the validity of the double torsion test requires crack propagation to be considered perpendicular to this.

Let the crack front be represented approximately by a diagonal straight line - see Figure 7.4 - jointing the crack tips seen on the tensile face and the compressive face. If the difference in the extent of cracking on each face is denoted by  $\Delta a$ , and  $d_n$  is the thickness of the specimen through which the crack passes, then the through-thickness velocity  $v_t$ , is related to the lengthwise velocity,  $v_L$ , by

$$\frac{v_t}{v_L} = \frac{d_n}{\Delta a} = \phi$$

Thus  $\phi$  is the correction factor that must be applied to Equations 7.11 and 7.15 such that for a constant displacement rate

$$v = \frac{\phi}{A_1 P} \cdot \left( \frac{dy}{dt} \right) \quad \dots\dots\dots 7.16$$

and for a constant displacement

$$v = \frac{\phi C_f P_f}{A_1 P^2} \cdot \left( - \frac{dP}{dt} \right) \quad \dots\dots\dots 7.17$$

## 7.5 Experimental details

### 7.5.1 Test rig

The double torsion rig is shown in Plate 7.1.

Particular aspects of the design include the maximisation of rig stiffness, so that deflections of a relatively stiff specimen could

be easily seen; in this respect also, making all joints metal-to-metal contact (to increase stiffness, and avoid time-dependent effects, adhesive used at the joints was carefully placed so as not to lie in the path of the load); and finally, allowing as much access as possible to the specimen, whilst loaded for observation and measurement of crack growth.

Load was applied using an Instron 1195 testing machine which could provide both a constant displacement and constant rate of displacement through the crosshead on the loading frame, Load was continuously recorded through a load cell on a pen recorder.

#### 7.5.2 Specimen preparation

Rectangular specimens were prepared from plates,  $3\frac{1}{2}$ " x 1" x  $\frac{1}{8}$ " of WC-Co alloys containing 6,13 and 16% cobalt by weight.

Sintering of such large plates had introduced considerable distortion. A few specimens were prepared from less distorted plates by diamond polishing, but the operation was extremely time consuming and expensive in polishing materials. The majority were prepared by contractors.

Specimens were requested to be nominally 80x25x2mm with opposite faces and edges ground flat and parallel. However, when distortion was severe, grinding was to continue until all surface undulations had been removed. Next, a groove 1mm wide with a depth equal to half the specimen thickness, was to be cut lengthwise down the middle of one face. Finally a through-thickness notch, 1mm wide and 5mm long was to be cut into each end of the specimen in line with the groove.

After initial preparation, the ungrooved face of each specimen was diamond polished to produce a mirror finish (see Section 6.2.3). Final checks on the thickness - the most critical dimension - showed that, although differences existed between specimens, variation over the surface of any one specimen did not exceed  $\pm 0.01$ mm. This was also

found to be true for the grooved region.

Further refinements were made as a result of preliminary tests and these are described in Section 7.5.3.

### 7.5.3 Precracking tests and techniques

To introduce a precrack into a specimen, a crack must be initiated and then subsequent propagation minimised. The problems encountered by others in precracking WC-Co specimens have been discussed in Section 3.3.

In the present study, precracking was first attempted using an impact loading technique. A wedge made from tool steel was placed in a notch cut into the end of the specimen mounted vertically such that the other end rested on a firm base. Compressive loads to halt propagation once the crack had been initiated were applied to the specimen sides by placing it in the jaws of a vice. The impact load was applied by hitting the wedge with a fibre-headed mallet. The technique is shown schematically in Figure 7.5a.

Tests were first performed on soda-lime glass microscope slides which were similar in size to the WC-Co specimens. Some degree of success was achieved with precracks as short as 5mm in length being produced. Approximately 50% of ungrooved WC6% Co specimens, similarly tested, were successfully precracked. However, precracks were appreciably longer (20-40mm) than in glass specimens (higher loads required for crack initiation were less easy to control), and some deviated to one side.

A few tests on grooved specimens were all unsuccessful. Although the groove stopped deviation, crack propagation could not be stopped within the specimen. A possible explanation is that the groove tends to induce bending moments in the specimen under the action of the compressive side loads, which tend to open the crack on the opposite

face, and hence aid its progress through the specimen (see Figure 7.5b).

Precracks could not be initiated in WC13% Co and WC16% Co specimens. Instead the wedge chipped pieces of material from the side of the notch, indicating that the notch was not sharp enough to induce crack initiation at the tip.

The narrowness of a machined notch is limited by the thickness of the cutting wheel. Hence to achieve finer notches, spark erosion was used to sharpen existing machined notches. By using copper shim, 12 $\mu$ m thick, notches approximately 0.2 mm wide and 1 mm deep were spark eroded - see Plate 7.2. The operation was performed in paraffin to dissipate the heat, and consequently all specimens were thoroughly cleaned in acetone afterwards.

With the sharpened notch, cracks were initiated in specimens of all three grades of WC-Co although not all could be stopped from propagating completely through.

In Section 3.3, the effect of spark erosion on crack propagation tests has been discussed in terms of the damage it does to the material, and some damage was found around the tips of sharpened notches in the present study. However, unlike Chermant et al (1974,1976) and others, who used spark eroded notches as substitute precracks, here they were used merely as stress concentrators to aid crack initiation. The tip of each precrack once initiated lay some distance from the region of damaged material.

Two observations made after the introduction of spark eroded notches, led to the discontinuation of the impact loading technique.

Firstly, successfully precracked specimens when placed in the double torsion rig and loaded using a constant displacement rate, gave an audible "click" at the onset of crack growth, accompanied by a rapid drop in load.

In some cases crack growth was so rapid that the specimen broke into two pieces and the load dropped to zero. In cases where immediate removal of the load had retained the crack within the specimen, subsequent crack growth under a reapplied load was far easier to control.

It appeared that some degree of crack re-initiation was required for propagation to start from the precrack. Possibly the shape of the precrack tip produced by one loading configuration - impact loading through a wedge - was unsuitable for subsequent propagation under a different loading configuration - in the double torsion test. Hence a method of precracking using the double torsion configuration was required.

The second observation was made during the precracking of WC 16% Co specimens. A precrack could be introduced with a single large impact load, but also just as successfully, with a number of smaller impacts. This indicated the possible presence of a slow crack growth mechanism.

Taking into account both observations a new test was devised whereby a specimen with a notch sharpened by spark erosion was placed in the double torsion rig and loaded using a cyclic displacement to induce fatigue crack growth.

As the displacement amplitude was raised, the onset of crack growth became evident when the amplitude of the recorded load cycles, showing initially a corresponding increase, suddenly ceased to rise so quickly and occasionally decreased. By immediately removing the load precracks as short as 5mm were introduced. These were obviously too short for crack growth tests since the tip still lay in the region damaged by spark erosion. However, by reapplying a load, not necessarily cyclic, subsequent crack propagation occurred without an "audible" click, and was found to be extremely controllable so that a precrack of suitable size was easily attained.

The technique proved completely successful on the few specimens precracked in this way. Subsequent tests showed that cyclic displacements were not necessary and that a simple constant displacement rate was just as effective. The modified technique proved repeatable and reliable for all subsequent specimens.

Its success seems to be dependent upon two factors. Firstly, the smoothness with which a crack propagated from a spark eroded notch - with no indication, in most cases, of any initiation being required - indicates that a tiny precrack was already present, introduced during spark erosion. Secondly, the controllability of subsequent crack propagation indicated the presence of slow crack growth mechanisms.

#### 7.5.4 Procedure to ensure the reliability of results

Evans (1972,1974) described the load-time curve expected theoretically from a double torsion specimen loaded under a constant displacement rate, as follows. After an initial rise, the load remains constant as the crack propagates along the length of the specimen. However Trantina (1977) from stress analysis of the test, and Shetty and Virkar (1978) from experiments on soda-lime glass, have shown that a constant load is unlikely to be observed when either the crack, or the remaining unbroken ligament is short. In both cases, mixed mode cracking takes place, and hence, the theories used by Evans become invalid.

Displacement rate tests were performed on precracked specimens of soda-lime glass and Wc-Co materials. The load time record, shown schematically in Figure 7.6, was similar for all, and followed the behaviour described above.

After an initial rise in load (region A in Figure 7.6) during which crack propagation was negligible, the load decreased (region B). Sometimes the change occurred in a single drop, sometimes in a number of small

jumps, and sometimes in a smooth curve. Why jumps should be present in some tests and not in others is still unclear.

When no further drops in load were observed, the crack length was found to be between 20 and 30mm for both glass and WC-Co specimens.

The region of jumps was followed by a period of constant load (region C), which displays the behaviour predicted theoretically by Evans (1972, 1974).

When the crack came within 20mm of the end of the specimen, the load began to fall again (region D), this time in a smooth curve. As the crack approached the end of the specimen the rate of change of load increased until final fracture.

It is essential therefore that the precrack tip lies in region C before crack propagation tests begin. In the present study, this requirement provided not only the conditions for valid theoretical analysis, but also ensured that propagation occurred away from material damaged by spark erosion around the notch.

#### 7.5.5 The guiding groove

In the past, the need for a groove to guide crack growth down the middle of the specimen has been considered essential. Indeed, its presence has been assumed in the majority of relevant diagrams and theoretical formulae found in the literature. Without a groove, slight inaccuracies in loading alignment, and small variations in specimen thickness across the width cause the crack to deviate to one side.

However, a groove introduces new problems. Schematic diagrams of the groove represent it as rectangular in cross-section with a flat base, through the middle of which runs the crack. Practically, it is difficult to machine a groove of this shape and, hence, any deviation of the crack takes it into a region with a slightly greater thickness.

Further, groove corners act as stress concentrators tending to attract crack growth towards them.

Pabst and Weich (1981) compared  $K_I$ -v diagrams obtained from alumina double torsion specimens both with and without a groove. The grooves, all precision machined, comprised some with a rectangular cross-section and others with a more rounded cross-section. The authors found that specimens containing grooves of either cross-section gave a far wider scatter of results than those ungrooved.

Murray (1977) chose to replace a machined groove with a spark eroded "scratch" for fracture toughness measurements. However, spark erosion can severely damage the material and possibly influence slow crack growth.

A few ungrooved specimens of soda-lime glass and WC 6% Co were tested at the beginning of the present study but crack growth, central for a short distance, eventually deviated to one side in every case.

All other specimens contained grooves with slightly sloping walls, a relatively flat base and rounded corners - see Figure 7.7. In almost all WC 6% Co and WC 16% Co, the crack remained at the base of the groove. In the remaining few of these materials, and in all the WC 13% Co specimens, the crack deviated into the groove wall. This became immediately apparent during the test from the load-time record. As soon as the crack passed into a thicker part of the specimen, the load tended to rise under displacement rate control. When this was seen, the test was abandoned. The susceptibility of WC 13% Co specimens to this has yet to be explained.

#### 7.5.6 Observation of the crack

Observation of a crack in a WC-Co double torsion specimen is difficult for a number of reasons: the crack opening displacement is small, -

dye penetrants cannot be used because of their possible corrosive influence on crack growth; when the specimen is grooved the crack is invariably obscured on that side by the roughness of the base, - polishing inside the groove is difficult; and on the compressive ungrooved side, the crack rarely penetrates the surface (Murray, 1977), - a thin ligament of material remains unbroken.

However, if the ungrooved face is diamond polished to a mirror finish, an impression of the crack is visible in the form of a "kink" - see Plate 7.3.

Measurements from ungrooved specimens, polished both sides, of the "kink" length in relation to the crack length on the tensile face, revealed a consistent difference of 3mm. The "kink" length was therefore considered a good representative of the extent of crack growth (and the difference used to calculate the correction factor,  $\phi$ , in Equations 7.16 and 7.17).

Observation and measurement of the "kink" during a test were aided by placing behind the specimen, a piece of card on which was drawn a grid of straight parallel lines. When the reflection of a line in the polished specimen surface, crossed the "kink" a discontinuity was observed - see Plate 7.4. The extent of the kink was lightly marked at the edges of the specimen, using a felt-tipped pen, allowing accurate measurement at the end of the test. The ability to measure the length of the "kink" with load applied, gave much better estimates of the extent of crack growth. When the load was removed, the crack closed and the "kink" appeared shorter.

#### 7.5.7 Compliance measurements

The compliance of a double torsion specimen depends upon the specimen dimensions; material properties, dimensions of the loading

configuration and the crack length - see Equation 7.2.

The dimensions of the loading configuration are constant since the same rig was used for all specimens, and material properties assumed constant for specimens of the same grade of WC-Co.

Further, little variation in dimensions was found in specimens of the same grade although significant differences in mean thickness were recorded between specimens of different grades - 1.75, 1.60 and 1.07mm for WC-6% Co, WC-13% Co and WC-16% Co respectively (representing the relative distortion of original plates and subsequent degree of machining in specimen preparation - see Section 7.5.2).

Hence a compliance calibration diagram was constructed using measurements of compliance at various crack lengths, taken from all specimens - see Figure 7.8.

The compliance was calculated using the testing machine crosshead position as a measure of displacement. Consequently, it included a contribution from the test rig. The compliance of the double torsion rig alone is indicated in Figure 7.8 and was subtracted from compliance measurements to obtain an estimate of the specimen compliance.

Assuming a relationship between specimen compliance,  $C$ , and crack length,  $a$ , of the form

$$C = A_1 a + A_2 \quad \dots \quad (\text{Equation 7.8})$$

the constant,  $A_1$ , was estimated to be 7,5 and 25  $\text{MN}^{-1}$  for WC-6%Co, WC-13% Co and WC-16% Co respectively, and the constant,  $A_2$  was 0.06m/MN with no apparent influence of material composition.

#### 7.5.8 Estimation of errors

The characteristic shape of a  $K_I$ - $v$  diagram is of a curve spanning



a range of crack velocities several orders of magnitude wide, but only a short range of  $K_I$ . Hence errors in  $v$  are likely to have much less effect on the estimation of the stress corrosion parameter,  $n$ , than errors in  $K_I$ .

Possible errors in  $K_I$  arise from a lower limit to the sensitivity of measuring equipment; variations of specimens dimensions along its length, particularly the thickness; and drift of the testing machine control system. Largest estimates of errors are summarised in Table 7.1 and compared with smallest measured values of each parameter. Combining these according to Equation 7.7, a maximum possible error in  $K_I$  is estimated to be ~4%.

One further parameter - Poisson's ratio,  $\nu$  - is required for the calculation of  $K_I$ . This could not be measured in the department. Instead values found in the literature (Lardner, McGregor, 1951-2) were used -  $\nu = 0.21$  for WC 6% Co and  $\nu = 0.24$  for WC16% Co.

#### 7.6 Preliminary tests on soda-lime glass specimens

To evaluate the double torsion rig, constant displacement tests were first performed on soda-lime glass specimens prepared from the same batch of microscope slides used to produce the bend specimens for comparative strength tests (see Section 6.4.2).

The resulting  $K_I$ - $v$  diagram - see Figure 7.9 - shows clearly the three regions of crack growth described by Wiederhorn (1967). The curves lie, as expected, between the curves obtained by Evans (1972) from tests in distilled water and toluene, and display a similar degree of scatter.

Estimates of the stress corrosion parameter,  $n$ , for region 1, lie in the range 15-19, which is in good agreement with both the maximum likelihood estimate of 19 obtained from the bend strength tests and published data (Adams, McMillan, 1977).

#### 7.7 A note on "jumps" observed on load relaxation curves

Load relaxation curves obtained from constant displacement tests on

soda-lime glass specimens, displayed a steadily decreasing rate of change of load, shown schematically in Figure 7.10a. In corresponding curves from WC-Co specimens, however, the decrease in load was interrupted by a series of "jumps" - see Figure 7.10b. The position of the "jumps" appeared to be random along the relaxation curve.

When  $K_I$ -v diagrams were constructed from the curves, the shape was of a straight line of increasing crack velocity, v, with stress intensity factor  $K_I$ , interrupted with spikes which, as  $K_I$  decreased, showed first a decrease in v followed by an increase, and then a final decrease back to the straight line, - see Figure 7.11.

At present, the cause of this phenomenon is unknown. One possibility is that the crack front comes up against a small area of material more resistant to cracking. As cracking continues around it, the unbroken ligament maintains the stiffness of the specimen and, hence, the load supported under a constant displacement. When the ligament finally breaks, the specimen suddenly relaxes to a level governed by the extent of crack growth around the obstacle, and the load drops.

However, no visual evidence of any obstacles could be found when the fracture faces were inspected (see Section 7.10). Similarly no evidence was found of crack arrest lines which had been observed accompanying jumps in the load during tests on epoxy resins by Phillips and Scott (1974), and Young and Beaumont (1976).

Despite the source remaining unknown, the random occurrences of the "jumps" indicate them to be localised effects and not representative of the general behaviour. Hence they were removed wherever possible during the construction of the  $K_I$ -v diagrams.

Occasionally a drop in velocity was noticed at the end of the relaxation curve. However, observations of other curves showed this to be due to a "jump" rather than a threshold of slow crack growth.

### 7.8 WC-Co double torsion test results and discussion

The  $K_I$ - $v$  diagrams obtained from constant displacement tests on WC 6% Co and WC 16% Co are presented in Figures 7.12 and 7.13. (Similar tests on WC 13% Co had to be abandoned because of crack deviation into the guiding groove wall - see Section 7.5.5).

Curves were rejected if effects of a short crack, or short unbroken ligament were detected (see Section 7.5.4). This was easily detected from the  $K_I$ - $v$  diagram since curves from those regions displayed a lower gradient.

A number of relaxations were applied to each specimen. The curves in Figures 7.12 and 7.13 are labelled both with the test number of the specimen and the number of the relaxation. (Intermediate numbers which do not appear, were attached to specimens in which the crack travelled into the groove wall, or to relaxations in which load "jumps" were too numerous or too large to permit analysis.)

The  $K_I$ - $v$  curves <sup>for</sup> both WC-Co materials display a number of similar characteristics within the range of  $K_I$  and  $v$  studied.

Firstly, the levels of  $K_I$  over which slow crack growth has been recorded are much higher than for soda-lime glass (see Figure 7.9). The materials are obviously more resistant to crack growth.

The ranges of  $K_I$  lie close to the critical level for rapid propagation. This may be seen by comparing the results with values of  $K_{Ic}$  obtained from the literature - see Figure 7.14.

No evidence of a lower threshold, or limit to slow crack growth has been found.

Finally, slow crack growth behaviour displayed on  $K_I$ - $v$  diagrams using logarithmic axes, may be described by a straight line. There is no evidence of more than one region. Measurements of  $n$  from the gradients range from 60-150 for WC 6% Co and 75-180 for WC 16% Co. At present, the extent of each range disallows any conclusions as to a relationship

between  $n$  and material composition. However the general levels are considerably higher than estimates of  $n$  (=15-19) for soda-lime glass, indicating slow crack growth to be much less in evidence.

Inspection of the  $K_I$ - $v$  curves for each grade of WC-Co reveals considerable variability in  $K_I$ . Variations between curves from the same specimen come within expected error bands (see Section 7.5.8), and as such may be considered insignificant. Variations between specimens, however, are much larger. They may be caused by small differences in material and specimen preparation, or by the presence of a guiding groove - see Section 7.5.5.

A more precise estimate of  $n$  was not obtainable for a number of reasons. Firstly, the slopes of the  $K_I$ - $v$  lines are steep (corresponding to high values of  $n$ ); even a slight error in measurement, or judgement as to the best line fitting the data causes a considerable change in the magnitude of  $n$  calculated from the slope. Secondly, each line spans a very small range of  $K_I$ ; since  $K_I$  is extremely sensitive to specimen dimensions, particularly the thickness, the estimate is likely to be influenced by small undetected variations along the path of the crack. Thirdly, the load relaxation curves used to obtain the  $K_I$ - $v$  lines were "adjusted" to remove irregular "jumps" in the load; the estimate of  $n$  is influenced by the judgement used in deciding where "jumps" begin and end, particularly when they are small, or close together.

#### 7.9 Inspection of double torsion specimen fracture faces

Inspection of the fracture faces by eye revealed a finish similar in texture to that of the smooth region on the fracture faces of bend specimens (see Section 6.10). The surfaces were virtually featureless, with a notable absence of material flaws - see Plate 7.5.

Viewing the surfaces under the microscope at high magnification (x 900) individual WC grains could be seen. The faces of some were shiny and lightly scored indicating grain cleavage. When two corresponding areas from

each face were photographed - see Plate 7.6 - differences between the two, indicated considerable intergranular fracture. However, apparent matching grains with shiny surfaces did not necessarily indicate transgranular fracture; one side could have been the impression of a grain left on the cobalt matrix if fracture occurred along a grain boundary.

The surfaces were also viewed through a scanning electron microscope. However, at high magnification the two phases were not easily distinguishable.

#### 7.10 Evidence of environmentally assisted slow crack growth in WC-Co materials

Double torsion specimens were not available in sufficient numbers to allow an investigation of slow crack growth in environments other than laboratory air. However, evidence of environmentally assisted slow crack growth was found when fractured pieces of bend specimens were soaked in dilute nitric acid. Crack growth seen emanating from pyramid indentations previously introduced into these specimens, led to a brief survey of the crack resistance test as a possible method of identifying and evaluating slow crack growth.

##### 7.10.1 Crack growth in dilute nitric acid

Four fractured pieces of WC-Co bend specimens with polished faces were soaked in a 10% solution of nitric acid.

The first specimen - of WC 16% Co - contained pyramid indentations from an earlier hardness test. After it had been soaked for a day, some discolouration of the surfaces was noticed, particularly around the indentations. Cracks at the four corners of the pyramid, also introduced during the hardness test (see Section 3.4) appeared to have grown slightly.

After three days' soaking, discolouration was widespread, indentation cracks were enlarged and crack growth was observed away from the indentations - see Figure 7.15. The face which had been in tension during the bend test,

(and which did not contain indentations), was cracked to a far greater extent than the compressive face, and in one place a chip had come away. At this stage, the acid solution had turned a pale maroon colour, indicating a reaction with the cobalt in the specimen, and contained a sediment of tiny particles of material which had broken away from the bulk.

A second specimen, this time of WC 13% Co, soaked in nitric acid, displayed substantial cracking after one day. The pattern of cracking was different from that seen in the first specimen, in that the cracks tended to lie parallel to the specimen edges - see Figure 7.16. Further soaking led to chips falling away from all edges to leave the specimen in the shape of a lozenge (see Plate 7.7).

Another two specimens, one each of WC-13% and WC-16% Co, were soaked and the crack patterns are shown in Figure 7.17, after two and five days. Preferential cracking around edges in the WC-13% Co specimen is evident once more (see Plate 7.8).

Differences in crack patterns between the two grades of WC-Co indicate either a fundamental difference in material response to acid attack, or more probably, an influence of the specimen structure and preparation. Specimens of the same grade of WC-Co were prepared together (see Section 6.2.3) although different grades were prepared separately. Thus, slight variations in, say, grinding or polishing, might have induced different degrees of surface damage, or residual stresses, tending to promote or inhibit crack growth.

Cracking in WC-13% Co specimens was observed to follow not only the specimen edges but also the fractured edge. This evidence coupled with preferential cracking seen on the tensile face, indicates that the previous strength test was an influencing factor. This supports the view that controlling mechanisms are associated more with the condition of the specimen than with the material alone.

However, at present, the mechanisms are unknown. Almond et al (1976), who observed spalling around hardness indentations when specimens were exposed to hydrogen fluoride vapour, proposed that crack growth was controlled by stress corrosive mechanisms whereby residual stresses introduced during indenting, enhanced corrosion. Although this may explain crack growth around indentations in the present study, it does not explain crack growth away from indentations. Microstructural and chemical approaches to the investigation of material damage and reaction with corrosive species are required to find out more about this behaviour.

#### 7.10.2 Environmental crack resistance tests

Evidence of surface cracking led to the development of the crack resistance test to study slow crack growth in different environments.

Normally, cracks emanating from the corners of a pyramid indentation are considered to be stationary after the initial application of the indenting load, and their combined length a function of that load (see Section 3.4). However, in a corrosive medium, it was hoped that slow crack growth would occur and that the total crack length would be influenced by not only the indenting load, but also the duration of its application, and the test environment.

Hardness tests were performed on soda-lime glass microscope slides and fractured halves of WC-Co double torsion specimens, in laboratory air and distilled water, employing a range of loads and indenting durations. Some specimens were soaked in water after indenting to promote any stress corrosive crack growth enhanced by residual stresses.

Estimates of crack resistance, however, showed no significant dependence on test environment, load duration or the inclusion of a period of soaking after indenting. In hindsight, the maximum load duration (5

minutes) was probably too short to promote a significant degree of slow crack growth. Time was not available for further tests.

#### 7.11 Summary of crack propagation test results

Slow crack growth has been observed in WC-6% Co and WC-13% Co materials in laboratory air, using the double torsion technique. The success of these tests was due, primarily, to the development of a new technique for introducing pre-cracks into specimens, using a constant displacement rate to induce crack growth from a machined notch sharpened by spark erosion.

Crack growth behaviour, when displayed on a  $K_I$ -v diagram using logarithmic axes, may be characterised by a single straight line, with a series of spikes of rapidly decreasing and increasing crack tip velocity, dispersed randomly along it. The spikes are assumed to be due to local inhomogeneities and, therefore, have been ignored during analysis of the behaviour.

The value of the stress corrosion parameter,  $n$ , is estimated to lie between 60 and 180. No significant influence of material composition has been detected.

The degree of slow crack growth in WC-Co materials in air is much less than in soda-lime glass, for which estimates of  $n$  from double torsion tests lie between 15 and 19.

Soak tests on pieces of fractured bend specimens in a 10% solution of nitric acid, have produced evidence of considerable slow crack growth, the extent and location of which appears to be influenced by specimen preparation and the previous strength test.

## 8. DISCUSSION

Delayed fracture in sintered WC-Co materials has been investigated using two approaches - its influence on bend strength, and its dependence upon slow subcritical crack growth.

Bend strength tests involving both constant rates of stress increase, and stepped loading, have displayed delayed fracture and the time dependent nature of strength in WC-Co alloys containing 6, 13 and 16% Co by weight, in laboratory air at room temperature. Characterising the behaviour using the stress corrosion parameter,  $n$ , estimates lie between 30 and 120. If confidence bands associated with each estimate are also included, the range of possible  $n$  is much larger. No evidence has been found of a significant influence of material composition or specimen surface finish, nor has any variation in behaviour been detected between specimens tested using different types of loading.

Double torsion tests have revealed slow crack growth in WC-6wt% Co and WC-16wt% Co, in laboratory air at room temperature. The general behaviour when displayed on a  $K_I$ - $v$  diagram with logarithmic axes, may be represented by a single straight line. Estimates of  $n$  from the gradient, lie between 60 and 180. No significant influence of material composition has been detected. Further, no evidence has been found of a limiting value of stress intensity factor below which slow crack growth does not occur.

Both approaches have produced ranges of estimated  $n$  in the same order of magnitude, and not very different from the estimate of 200 by Braiden et al (1977). Although estimates from double torsion tests are slightly higher than those from bend strength tests (as found by Davidge et al (1973) in similar tests on alumina), the extent of each range disallows any significance to be placed in the difference. However, if a real difference exists, then it may be due to the fundamental

ways in which strength tests differ from crack propagation tests, as discussed in Section 2.5.

Both approaches have also shown an apparent lack of influence of material composition. If such an influence exists, then its effect must be small.

These results common to both approaches, suggest that in laboratory air at room temperature, delayed fracture and the time dependent nature of strength observed in bend tests, and slow subcritical crack growth seen in double torsion tests are all controlled by similar failure mechanisms.

To investigate the influence of environment on delayed fracture, bend strength tests were also performed in distilled water, incorporating various presoaks. A trend of reduced strength was noticed in some specimens, possibly indicating a stress corrosive reaction. However, no evidence was found to support this. Indeed, inspection of the fracture faces of some low-strength specimens indicated sub-surface fracture initiation where environmental influence is unlikely.

Evidence suggesting that delayed fracture in WC-Co materials in ambient conditions, does not require environmental assistance, came from stepped loading tests. Inspection of the fracture faces of some specimens which failed during a period of constant stress, thereby displaying delayed fracture, indicated the critical flaw to lie sub-surface. Assuming the materials to be impervious, slow crack growth apparently occurred without the need for a corrosive species from the test environment to be present at the crack tip.

However, both the effects of environment on strength and the source of fracture need to be studied further. At present, there is insufficient evidence for conclusions to be drawn, and thus, the influence of environment on delayed fracture; mechanisms of slow crack growth; and hence, whether stress corrosion occurs in WC-Co materials in ambient conditions, all remain unknown.

Even so, the effects of delayed fracture mechanisms, whether stress corrosive or not, have been observed and evaluated. The time dependent nature of the strength of WC-Co materials in ambient conditions may be seen by constructing an SPT diagram (see Section 4.6). Typical values of the Weibull modulus,  $m=10$ , the stress corrosion parameter,  $n = 100$ , and a constant stress of  $2500 \text{ MN/m}^2$  applied to a specimen to give it a 50% cumulative probability of failure after one second, were used to construct the diagram shown in Figure 8.1.

The diagram illustrates that a decade increase in the lifetime requires the applied stress to be reduced by just 2%; equivalent reductions for soda-lime glass and alumina are approximately 11% and 6% respectively. An equivalent STP diagram for soda-lime glass in air is shown in Figure 8.2. Delayed fracture in WC-Co alloys in ambient conditions, therefore, is almost insignificant. Even for a lifetime increase of many decades, the required reduction in applied stress is still far less than the variability in strength due to material flaws. Safety factors introduced to reduce the probability of failure will automatically lower the applied stress to a level where delayed fracture effects may be ignored.

Far more significant is the slow degradation of unloaded specimens when soaked in distilled water, or a 10% solution of nitric acid. In distilled water, particularly severe corrosion occurred around surface flaws tending to enlarge, or sharpen them. In nitric acid, corrosion was accompanied by extensive slow crack growth across the surface. In both cases, corrosion appeared to be controlled by structural aspects of the specimen and material. Possible influencing factors include the presence of a material flaw on the surface, and also surface damage and residual stresses introduced during specimen preparation.

The importance of this phenomenon lies in the way in which specimen degradation - and, hence, reduction in strength and lifetime - occurs

over a period of time, even when no external loads are applied. Hence, relating this to components in service, the useful life may not only be influenced by working loads and environments, but also by conditions of storage.

Larger than all changes due to different types of loading, or test environment, is the variability in strength caused by material flaws. The random nature of the variation not only tends to obscure effects due to other factors but also introduces the need for a level of difference to be achieved before each effect can be called significant. Thus, if the effect is small, it may not be possible to prove its existence with a given number of specimens, since the difference in strength does not exceed the variability that might be expected due to material flaws. This was seen in the main environmental tests (see Section 6.92) where an apparent trend of strength reduction occurred at the low cumulative failure probability/low strength end of the Weibull line. Since confidence in the line is low at either end, the trend, although noted, could not be classed as significant without supporting evidence.

Variability in strength also limits the precision to which parameters describing the behaviour can be calculated. Further, each estimate must be accompanied by an indication of the confidence that may be placed in it.

One method of reducing uncertainty is to increase the number of specimens tested. However, to make any significant improvements, the increase would have to be extremely large (Braiden, et al, 1977) which, in the majority of cases, is impossible given limited time and finance.

An alternative might be to perform tests on hot isostatically pressed (HIP) WC-Co materials where variability in flaw sizes is reported to be much smaller (Lardner, 1974). However, conclusions drawn from HIP materials may not necessarily apply to sintered materials.

The alternative chosen for the present study was to maximise the efficiency of data analysis. Hence the maximum likelihood analysis was developed to analyse stress rate data from strength tests. By combining strengths irrespective of the stress rate employed, the number of data analysed together was increased by a factor of five, thereby considerably increasing the confidence in estimated parameters.

However, the technique merely provides estimates of parameters which best fit the data. Since the recorded strengths come from random samples of specimens, extreme values might be present, tending to distort the analytical results, especially if sample sizes are small. A major drawback of mathematical techniques is that such occurrences are not immediately obvious.

The low-strength variation in soaked bend specimens from the preliminary environmental tests, for example, would have been wrongly identified by a mathematical technique, since the behaviour was unexpected. Instead a graphical method of analysis using the Weibull diagram was more suitable. Further, by using a transformation analysis in conjunction with the Weibull diagram, a trend of decreasing Weibull modulus with increasing surface roughness indicated by the maximum likelihood analysis, was shown to be of little significance.

The use of a crack propagation technique such as the double torsion test, avoids the variability due to material flaws by ensuring propagation occurs in a controlled and measurable manner from a large artificially induced crack. However, the test involves a degree of practical difficulty. In this respect, the development of a reliable and repeatable method of precracking WC-Co plates has made the test far easier. Nonetheless, improvements are still required, particularly regarding the method of crack guiding. Grooves, used in the present study because cracks in ungrooved specimens could not be stopped from deviating to one side, were

not entirely satisfactory. In addition to causing occasional abandonment of the test when the crack travelled into the groove wall, they were probably responsible for the wide scatter in  $K_I$ -v lines obtained from specimens of nominally the same material.

Other possible causes of scatter are slight variations in material composition or specimen preparation. This highlights another problem with large crack techniques in that large specimens are required for accurate crack growth measurement. However, the sintering of large WC-Co plates is relatively difficult, often resulting in severe distortion. Consequently, considerable machining is needed to produce a suitable double torsion specimen, with the obvious likelihood of introducing surface damage and residual stresses.

Finally, a phenomenon peculiar to double torsion tests on WC-Co materials is the observation of "jumps" in load relaxation curves (none were found in similar curves from soda-lime glass specimens). They not only obscure a more general behaviour upon which they are superimposed, but may also affect that behaviour and, hence, influence the estimation of  $n$ . At present, neither their source, nor their influence is known.

9. CONCLUSIONS

Aspects of the time dependent strength behaviour of sintered WC-Co alloys containing 6,13 and 16% cobalt by weight, have been studied. Bend strength tests, double torsion tests and soak tests have been used to observe, and evaluate delayed fracture, slow crack growth and corrosion, at room temperature, in a variety of environments including laboratory air, distilled water and dilute nitric acid.

Results of bend strength tests in air, indicate the presence of delayed fracture mechanisms, in that the strength increases with the rate of loading to fracture in stress rate tests, and that delayed fracture has been observed directly during periods of constant stress in stepped loading tests.

Double torsion tests in air have shown evidence of stable sub-critical slow crack growth. When the behaviour is displayed on a  $K_I$ - $v$  diagram using logarithmic axes, it may be represented by a single straight line lying close to the critical stress intensity factor. No lower threshold for slow crack growth has been detected. Superimposed on the general behaviour are randomly dispersed 'spikes' of rapidly increasing and decreasing velocity, which are ascribed to local material inhomogeneities.

Using the stress corrosion parameter,  $n$ , to describe strength and crack growth behaviour, estimates lie between  $n = 30-120$  and  $n = 60-180$  from bend strength tests and double torsion tests respectively. The similarity of both ranges suggests that failure mechanisms are the same in both types of test.

No significant influence of material composition, or specimen surface finish on  $n$  has been detected. Material composition has, however, been shown to affect the Weibull modulus,  $m$ , and, hence, the variability in strengths induced by random inherent flaws :  $m$  increases and the variability decreases in alloys with higher cobalt contents.

Compared with soda-lime glass in air, or alumina in Ringers Solution, the grades of WC-Co studied display very little delayed fracture. An increase in lifetime of one order of magnitude is accompanied by a decrease in strength of approximately 2% - this is far less than the expected variability in strength due to material flaws.

Strength tests in distilled water and laboratory air have provided no evidence to suggest that delayed fracture is significantly influenced by one environment more than the other and, hence, no evidence of delayed fracture being significantly environmentally assisted. In contrast, the strength and delayed fracture of alumina is influenced to a considerable extent when tests are performed in Ringers Solution instead of laboratory air.

Corrosion of WC-Co materials has been observed when unloaded specimens are soaked in both distilled water and in a 10% solution of nitric acid. Corrosion in distilled water is particularly severe around surface flaws. Subsequent bend tests have shown unexpectedly low strengths to accompany failure initiated from heavily corroded surface flaws, indicating the flaws to have been enlarged and/or sharpened by the corrosive action. Soaking pieces of previously fractured bend specimens in dilute nitric acid causes considerable slow crack growth, the extent and location of which is apparently influenced by specimen preparation and the previous strength test.

Corrosion independent of externally applied loads is far more significant than stress enhanced corrosion in distilled water for the WC-Co materials studied. This may be compared with alumina in Ringers Solution where stress corrosion is dominant - no evidence of stress - independent corrosion has been found.

A simple technique has been developed for the efficient analysis of delayed fracture effects in data obtained from bend strength tests performed over a range of stress rates. The fracture model, incorporating theories of stress corrosion and brittle fracture, with Weibull statistics, has an "extreme value" error distribution. Parameter estimation is accomplished using the method of maximum likelihood. The technique obtains the significance of any rate effect; estimates of the stress corrosion parameter,  $n$ , and the Weibull modulus,  $m$ ; confidence intervals for these parameters; and an assessment of the validity of the model.

Another technique has been developed to compare strength data from tests involving different types of loading to failure. Again using theories of stress corrosion and brittle fracture, with Weibull statistics, strength data are transformed to values that would be expected under a common type of loading. The complete loading history is analysed from the initial application of load to the point of fracture. This obtains a graphical representation of the distributions of strength allowing the immediate observation of any deviations from expected behaviour, and extreme values which might distort the evaluation of parameters. It may also be used to obtain estimates of the stress corrosion parameter,  $n$ .

A simple and reliable method of precracking WC-Co double torsion specimens has been developed. A constant displacement rate is applied to propagate a precrack from a machined notch which has been sharpened by spark erosion. The method permits easy control of the precrack length, so that the crack tip can be precisely placed both outside the region of material damaged by spark erosion and inside a region of the specimen where stress corrosion theories are valid.

## 10. FUTURE WORK

Delayed fracture, slow crack growth and corrosion need to be studied over a wider range of environments and at various temperatures. By so doing, laboratory tests can approach service conditions met by WC-Co components.

The present study has involved observation and evaluation of the effects of time dependent failure mechanisms. However, to investigate the mechanisms directly, microstructural and chemical approaches are needed to discover the corrosive chemical reactions and factors controlling reaction rates.

Individual items arising from the present study, which are likely to benefit from further work include an investigation of sub-surface fracture initiation in bend specimens failing during a period of constant stress; the development of a suitable method of guiding cracks in double torsion specimens; an analysis of "jumps" seen in load relaxation curves from double torsion tests on WC-Co materials; an investigation of the role of flaws and cracks in controlling corrosion and the possible influence of residual stresses; and further development of the crack resistance test to study slow crack growth.

REFERENCES

- Adams, R., McMillan, P.W. 1977 J. Mat. Sci. 12, 643
- Almond, E.A., Mai, A.T.,  
Roebuck, B. 1976 J. Mat. Sci. 11, 565
- Almond, E.A., Roebuck, B. 1978 J. Mat. Sci. 13, 2063; Metals Tech. 5, 92
- Almond, E.A., Roebuck, B. 1980 Trans. J. Brit. Ceram. Soc. 79, 53
- Baker, T.C., Preston, F.W.,  
Glathart, J.L. 1946 J. Appl. Phys. 17, 162; *ibid* 17, 170;  
*ibid* 17, 179; *ibid* 17, 189
- Berry, G. 1975 New Tool Mater. Cutting Techn.  
Int. Conf. 4.
- Berry, G. 1976 Metal Sci. 10, 361
- Braiden, P.M. 1975 "An Introduction to Weibull  
Statistics", AERE, Harwell, Rept. 7165
- Braiden, P.M. 1976 "Fracture Mechanics of High Temperature  
Ceramics", AGARD Rept. 651.
- Braiden, P.M., Davidge, R.W.,  
Airey, R. 1977 J. Mech. Phys. Solids 25, 257
- Bruce, J.G., Koepke, B.G. 1977 J. Amer. Ceram. Soc. 60, 284
- Carter, C.S. 1971 Corrosion 27, 471
- Charles, R.J. 1958 J. Appl. Phys. 29, 1549; *ibid* 29, 1554;  
*ibid* 29, 1657
- Charles, R.J., Hillig, W.B. 1962 "Proceedings, Symposium sur la  
resistance mecanique du verre et les  
moyens de l'ameliorer", Union Sci.  
Continetale du Verre, Charleroi,  
Belgium, 511
- Chermant, J.L., Deschanvres, A.,  
Iost, A. 1974 "Fracture Mechanics of Ceramics"  
Plenum Press, New York, 2, 347
- Chermant, J.L., Deschanvres, A.,  
Osterstock, F. 1977 Powder Met. 20, 63
- Chermant, J.L., Osterstock, F. 1976 J. Mat. Sci. 11, 1939
- Creyke, W.E.C. 1968 Trans. Brit. Ceram. Soc. 67, 339
- Davidge, R.W., McLaren, J.R.,  
Tappin, G. 1973 J. Mat. Sci. 8, 1699
- Davidge, R.W., Tappin, G. 1968 J. Mat. Sci. 3, 165

- |  |      |   |
|--|------|---|
| Davies, D.G.S.                                   | 1973 | Proc.Brit.Ceram.Soc. 22, 429  |
| Dawihl, W.                                       | 1941 | Stahl und Eisen 61, 909   |
| Doi, H., Ueda, F., Fujiwara, Y.,<br>Masatomi, H. | 1975 | Grain Boundaries Eng.Mater. Proc.<br>Bolton Landing Conf., 4th, 1974, 235                                       |
| Drucker, D.C.                                    | 1964 | Division of Engineering, Brown Univ.,<br>Tech Rept. 7. J.S. Atomic Energy<br>Commission, Contract AT(30-1)-2394 |
| Evans, A.G.                                      | 1972 | J.Mat.Sci. 7, 1137  |
| Evans, A.G.                                      | 1973 | I.J.Fract. 9, 267   |
| Evans, A.G.                                      | 1974 | I.J.Fract. 10, 251  |
| Evans, A.G.                                      | 1974 | Metal. Trans. 5, 27   |
| Evans, A.G., Johnson, H.                         | 1975 | J.Mat.Sci. 10, 214  |
| Evans, A.G., Langdon, T.G.                       | 1976 | Progress in Materials Science 21, 171   |
| Evans, A.G., Lange, F.F.                         | 1975 | J.Mat.Sci. 10, 1659   |
| Evans, A.G., Linzer, M                           | 1976 | I.J.Fract. 12, 217  |
| Evans, A.G., Wiederhorn, S.M.                    | 1974 | J.Mat.Sci. 9, 270   |
| Exner, H.E.                                      | 1969 | Trans TMS-AIME 245, 677   |
| Fraser, D.A.S.                                   | 1976 | "Probability and Statistics",<br>Duxbury Press, North Scituate, MA  |
| Freiman, S.W., Mecholsky, J.J.                   | 1978 | J.Mat.Sci. 13, 1249   |
| Freiman, S.W., Mulville, D.R.,<br>Mast, P.W.     | 1973 | J.Mat.Sci. 8, 1527  |
| French, D.N.                                     | 1969 | Trans TMS-AIME 245, 2351  |
| Fullman, R.L.                                    | 1953 | Trans AIME (J.Metals) 197, 447  |
| Grenet, L.                                       | 1899 | Bull.Soc.Enc.Industr.Nat.Paris<br>(Ser.5) 4, 838  |
| Griffith, A.A.                                   | 1921 | Phil.Trans.Roy.Soc. A221, 163   |
| Güçer, D.E., Gurland, J.                         | 1962 | J.Mech.Phys.Solids 10, 365  |
| Gurland, J.                                      | 1961 | "Powder Metallurgy" (ed.W.Leszynski)<br>Interscience, 661   |
| Gurland, J., Bardzil, P                          | 1955 | Trans AIME (J.Metals) 7, 311  |
| Gurland, J., Norton, J.T.                        | 1956 | Proc.2nd.Plansee Seminar, 99  |

- |   |        |  |
|---|--------|--|
| Gurney, C.  | 1947   | Proc.Phys.Soc.59, 169  |
| Gurney, C., Boryscowski, Z                        | 1948   | Proc.Phys.Soc. 61,446  |
| Gurney, C., Pearson, S.                           | 1949   | Proc.Phys.Soc.62B, 469   |
| Hara, A., Yazu, S.                                | 1968   | J.Japan Soc.Powders Powder Met.<br>15, 356   |
| Inglestrom, N., Nordberg, H.                      | 1974   | Eng.Fract.Mech. 6,597  |
| Jaensson, B.O.                                    | 1971   | Mat.Sci.Eng. 8,41  |
| Jakus, K., Coyne, D.C.,<br>Ritter Jr., J.E.       | 1978   | J.Mat.Sci. 13,2071   |
| Jayatilaka, A.S.                                  | 1979   | "Fracture of Engineering Brittle<br>Materials", Applied Science, London                |
| Johnson, L.G.                                     | 1964   | "Theory and Technique of Variation<br>Research", Elsevier, Amsterdam                   |
| Kalthoff, J.F.                                    | 1971   | I.J.Fract.Mech. 7,478  |
| Kenny, P.   | 1971   | Powder Metall., 14,22  |
| Kies, J.A., Clark, B.J.                           | 1970   | Proc.2nd.Int.Conf. on Fracture, 1969<br>(ed.P.L.Pratt) Chapman and Hall,<br>London 483 |
| Knotek, O., Lugscheider, E.,<br>Stabrey, H.       | 1978   | Prepr.Eur.Symp.Powder Metall. 5th.<br>2, 82  |
| Knott, J.K.                                       | 1973   | "Fundamentals of Fracture Mechanics",<br>Butterworth                                   |
| Kotchick, D.M., Tressler, R.E.                    | 1975   | J.Mat.Sci. 10,608  |
| Kreimer, G.S., Sidorin, I.I.,<br>Tishenkova, E.F. | 1958   | Izvest.Akad.Nauk.SSSR Met. i Toplivo<br>113  |
| Kropschot, R.H., Mikesell, R.P.                   | 1957   | J.Appl.Phys. 28,610  |
| Lardner, E.                                       | 1974   | The Production Engineer 13   |
| Lardner, E.                                       | 1981   | Proc.TIPTOM Conference, 1981 NPL.<br>The Metals Society, London                        |
| Lardner, E., McGregor, N.G.                       | 1951-2 | J.Inst.Metals 80,369   |
| Lawn, B.R.  | 1975   | J.Mat.Sci. 10,469  |
| Lee, H.C., Gurland, J.                            | 1978   | Mat.Sci.Eng. 33, 125   |
| Logan, H.L.                                       | 1966   | "The Stress Corrosion of Metals",<br>Wiley, New York                                   |
| Lueth, R.C.                                       | 1974   | "Fracture Mechanics of Ceramics"<br>Plenum Press, New York 2,791                       |

- McHenry, K.D., Tressler, R.E. 1977 J.Mat.Sci.12; 1272
- Mai, Y.W., Gurney, C. 1975 Phys.Chem.Glasses 16, 70
- Meredith, H., Pratt, P.L. 1975 "Special Ceramics", (ed.P.Popper), BCRA Publ. 6, 107
- Mostovoy, S., Smith, H.R. 1971 Eng.Fract.Mech. 3, 291  
Lingwall, R.G., Ripling, E.J.
- Mould, R.E., Southwick, R.D. 1959-61 J.Amer.Ceram.Soc. 42(1959) 542;  
ibid 42 (1959) 582; ibid 43(1960)  
160; ibid 44(1961) 481
- Murgatroyd, J.B., 1944 J.Soc.Glass.Tech. 28, 406
- Murgatroyd, J.B., Sykes, R.F.R. 1947 J.Soc.Glass.Tech 31, 17
- Murray, M.J. 1977 Proc.R.Soc.Lond.A. 356, 483
- Murray, M.J., Perrott, C.M. 1976 Proc.1976 Int.Conf. on Hard  
Material Tool Techn. Carnegie  
Press. 314
- Nakamura, M., Gurland, J. 1980 Metall.Trans A11, 141
- Orowan, E. 1944 Nature (Lond.) 154, 341
- Outwater, J.O., Jerry, D.J. 1966 Interim Rept.Contract NONR-3219  
(ONX) Univ. of Vermont
- Pabst, R.F., Weick, J. 1981 J.Mat.Sci. 16, 836
- Palmqvist, S. 1957 Jernkontorets, Ann. 141, 300
- Peters, C.T. 1979 J.Mat.Sci. 14, 1619
- Phillips, D.C., Scott, J.M. 1974 J.Mat.Sci. 9, 1202
- Pickens, J.R., Gurland, J. 1978 Mat.Sci.Eng. 33, 135
- Platov, A.B. 1960 Izvest.Akad.Nauk.SSSR. Met.i  
Toplivo 136
- Pook, L.P. 1970 "Linear Fracture Mechanics - What  
it is, What it does" NEL Rept.  
465, Glasgow
- Proctor, B.A., Whitney, I., 1967 Proc.Roy.Soc.(Lond).A. 297, 534  
Johnson, J.W.
- Roark, R.J., Young, W.C. 1975 "Formulas for Stress and Strain,"  
5th Edn., McGraw-Hill, Kogakusha
- Schönert, K., Umhauer, H., 1970 Proc.2nd Int.Conf.on Fracture, 1969,  
Klemm, W. (ed.P.L.Pratt), Chapman and Hall,  
London, 474

- Schwarzkoepf, P., Kieffer, R. 1960 "Cemented Carbides", Macmillan, New York, 1960
- Scully, J.C. (ed.) 1971 "The Theory of Stress corrosion Cracking in Alloys", NATO Scientific Affairs Division, Brussels
- Shand, E.G. 1961 J.Amer.Ceram.Soc. 44,21
- Shetty, D.K., Virkar, A.V. 1978 J.Amer.Ceram.Soc. 61,93
- Simpson, L.A. 1974 J.Amer.Ceram.Soc. 57,151; "Fracture Mechanics of Ceramics", Plenum Press, New York, 2,567
- Sivill, A.D. 1974 Ph.D. Thesis, University of Nottingham, England.
- Smaglenko, F.P., Loshak, M.G. 1973 Sverkhtrverdye, Mater. Prom-sti. 197
- Stanley, P., Fessler, H., Sivill, A.D. 1973 Proc.Brit.Ceram.Soc. 22,453
- Stuart, D.A., Anderson, O.L. 1953 J.Amer.Ceram.Soc. 36,416
- Suzuki, H., Hayashi, K., Lee, W.J. 1977a Planseeber. Pulvermetall. 25,186
- Suzuki, H., Hayashi, K., Taniguchi, Y. 1977b Sogo Shikensho Nempo 36,223
- Suzuki, H., Hayashi, K., Taniguchi, Y. 1978 Funtai Oyobi Funmatsuyakin 25,94
- Suzuki, H., Kubota, H. 1966 Planseeber, Pulvermetall. 14,96
- Suzuki, H., Tanase, T. 1976 Planseeber, Pulvermetall. 24,271
- Taylor, N.W. 1947 J.Appl.Phys. 18,943
- Trantina, G.G. 1977 J.Amer.Ceram.Soc. 60,338
- Tristram, K., Jayatilaka, A.S. 1979 J.Mat.Sci. 14,1080
- Ueda F., Doi, H., Fujiwara, Y., Masatomi, H. 1977a Powder Metall.Int. 9,32
- Ueda, F., Doi, H., Fujiwara, Y., Masatomi, H. 1977c Trans.Japan Inst.Met.18,247
- Ueda, F., Doi, H., Fujiwara, Y., Masatomi, H., Oosawa, Y. 1975 Trans.Japan Inst.Met.16,591
- Ueda, F., Doi, H., Fujiwara, Y., Masatomi, H., Suzuki, H., Hayashi, K. 1977b Funtai Oyobi Funmatsuyakin 24,183

Viswanathan, R.K., Venables, J.D.	1977	Metall. Trans. A8, 77
Vonnegut, B., Glathart, J.L.	1946	J. Appl. Phys. 17, 1083
Wachtman, Jr., J.B.	1974	J. Amer. Ceram. Soc. 57, 509
Weibull, W.	1951	J. Appl. Mech. 18, 293
Weidmann, G.W., Holloway, D.G.	1974	Phys. Chem. Glasses 15, 116
Wiederhorn, S.M.	1967	J. Amer. Ceram. Soc. 50, 407
Wiederhorn, S.M.	1974	"Fracture Mechanics of Ceramics", Plenum Press, New York, 2, 613
Wiederhorn, S.M., Bolz, L.H.	1970	J. Amer. Ceram. Soc. 53, 543
Wright, B.D., Green, P.J., Braiden, P.M.	1982	J. Mat. Sci. 17, 3227
Young, R.J., Beaumont, P.W.R.	1976	J. Mat. Sci. 11, 776

	WC-6wt%Co	WC-13wt%Co	WC-16wt%Co
Nominal composition by weight	6%Co 94%WC	13%Co 87%WC	16%Co 84%Co
Chemical analysis - C	5.70/5.85%	5.2/5.4%	5.0/5.2%
- Co	6.00/6.50%	12.5/13.5%	15.5/16.5%
- Ti	< 0.05%	< 0.05%	< 0.05%
- Fe	< 0.03%	< 0.02%	< 0.20%
Porosity (ASTM)	A2,B1-,C1-	A2,B1-,C1-	A2,B1-,C1-
Hardness (HV)	1500-1600	1175-1275	1050-1150
Density (gm/cm <sup>3</sup> )	14.8-15.0	14.16-14.35	13.80-14.00
Coercivity (KA/m)	13.5-15.9	7.5 - 9.5	6.7 - 8.4
Bend Strength (KN/mm <sup>2</sup> )	1.54-1.85	2.39-2.70	2.47-2.93

TABLE 5.1: Characterisation of Materials - Manufacturer's specifications

	BEND SPECIMENS			DOUBLE TORSION SPECIMENS		
	WC6%Co	WC13%Co	WC16%Co	WC6%Co	WC13%Co	WC16%Co
Mean free path in cobalt, $\lambda_{Co}$ ( $\mu m$ )	0.16	0.35	0.44	0.12	0.26	0.31
Mean WC grain size $\bar{d}_{wc}$ ( $\mu m$ )	1.4	1.3	1.3	1.1	1.0	0.9
Mean hardness (Hv) (Std. Dev. $n \approx 2\%$ )	1700	1280	1150	1630	1280	1170
Mean crack resistance W(kg/mm) (Std.Dev. $n \approx 30\%$ )	0.12	0.34	0.63	0.12	0.39	1.09
Coercive Force Hc(Oe)	240	108	95	-	-	-

TABLE 5.2: Characterisation of materials - laboratory test results

Variable	Typical Value	largest estimated error
Load, P (N)	2000	15
Three-point bend span, L (mm)	16	0.005
Specimen width, b (mm)	5	0.05
Specimen depth, d (mm)	2	0.01

TABLE 6.1. Largest estimated errors in variables used to calculate the bend strength.

Material	No. of specimens tested	Range of stress rates (MNm <sup>-2</sup> sec <sup>-1</sup> )	No. of different stress rates	ML estimate of n	95% conf. interval for n	ML estimate of m	95% conf. interval for m	Significance, P of rate effect <i>ff</i>
Soda-lime glass (abraded)	68	4-260	7	19	14-28	8.6	7.2-10.2	5 x 10 <sup>-8</sup>
WC-6wt%Co(1)*	60	0.1-1000	5	110	46- <i>f</i>	6.5	5.3-7.8	0.12
WC-6wt%Co(2)*	60	0.1-1000	5	34	24-56	6.8	5.6-8.1	7 x 10 <sup>-6</sup>
WC-13wt%Co(1)	58	0.1-1000	5	93	50-620	9.1	7.3-11.2	0.023
WC-13wt%Co(2)	58	0.1-1000	5	120	59-1100	10.0	8.0-12.2	0.028
WC-16wt%Co(1)	60	0.1-1000	5	45	34-70	8.8	7.2-10.6	2 x 10 <sup>-6</sup>
WC-16wt%Co(2)	60	0.1-1000	5	110	64-330	12.4	9.9-15.0	0.0047

TABLE 6.2: Maximum likelihood estimates of m and n, related confidence intervals and the significance of observed rate effect using bend strength data from stress rate tests in laboratory conditions on soda-lime glass and WC-Co materials.

\* Surface finish of specimens: (1) ground; (2) diamond polished.

*f* No finite upper limit exists.

*ff* P = probability of rate effect being at least as large as that observed when the null hypothesis is true (conventionally, P < 0.05 is termed "significant")

Variable	Typical Value	Largest Estimated Error
Load, P(N)	100	0.3
Specimen thickness, d (mm)	1.0	0.015
Thickness in grooved region, d <sub>n</sub> (mm)	0.5	0.015
Specimen width, W (mm)	25	0.06
Moment arm, W <sub>m</sub> (mm)	7.5	0.01

TABLE 7.1. Largest estimated errors in variables used to calculate the stress intensity factor,  $K_I$

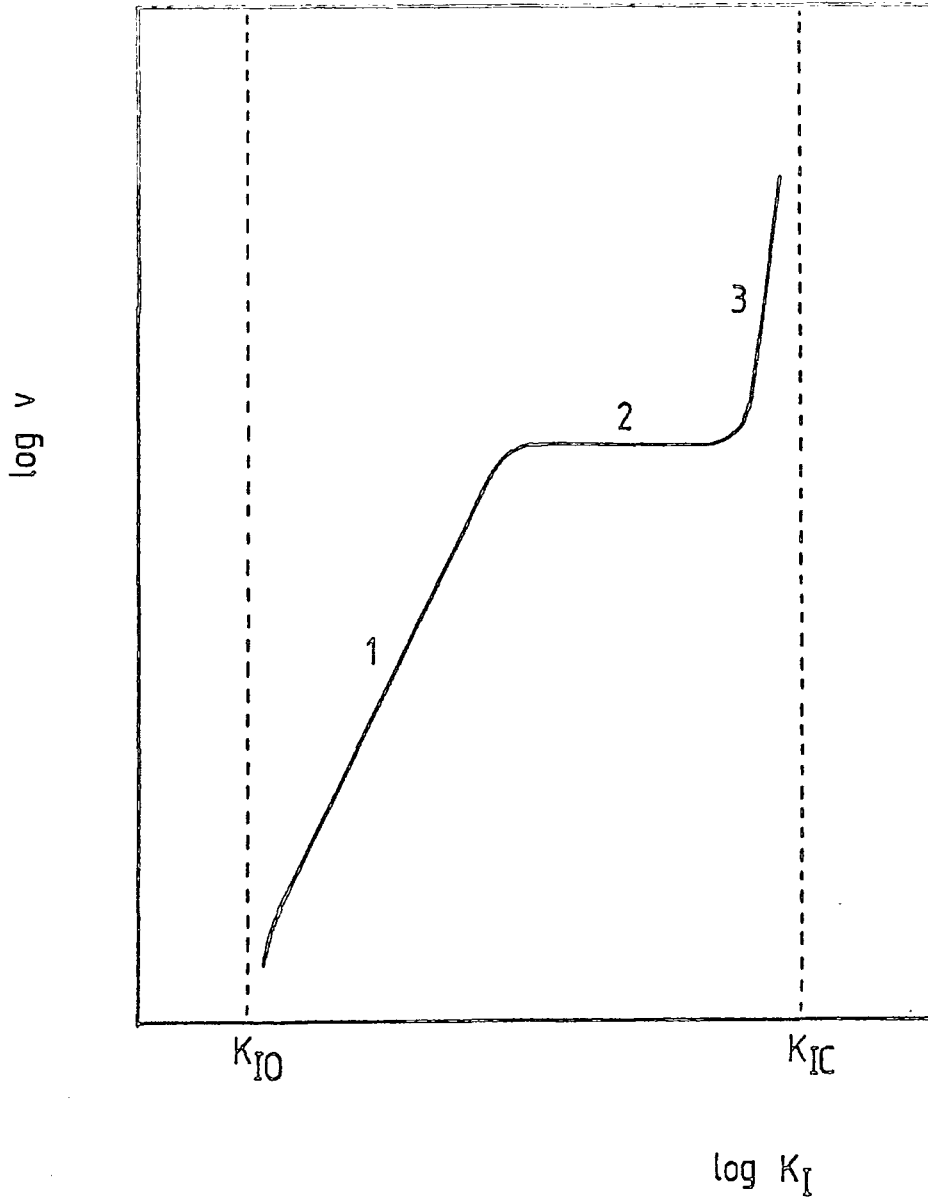


FIGURE 2.1: Typical form of the  $K_I$ - $v$  diagram, showing the three regions of slow crack growth behaviour lying between the lower threshold  $K_{I0}$ , and the critical level,  $K_{IC}$ .  $K_I$  - plane strain stress intensity factor in the crack opening mode, I;  $v$  - crack tip velocity.

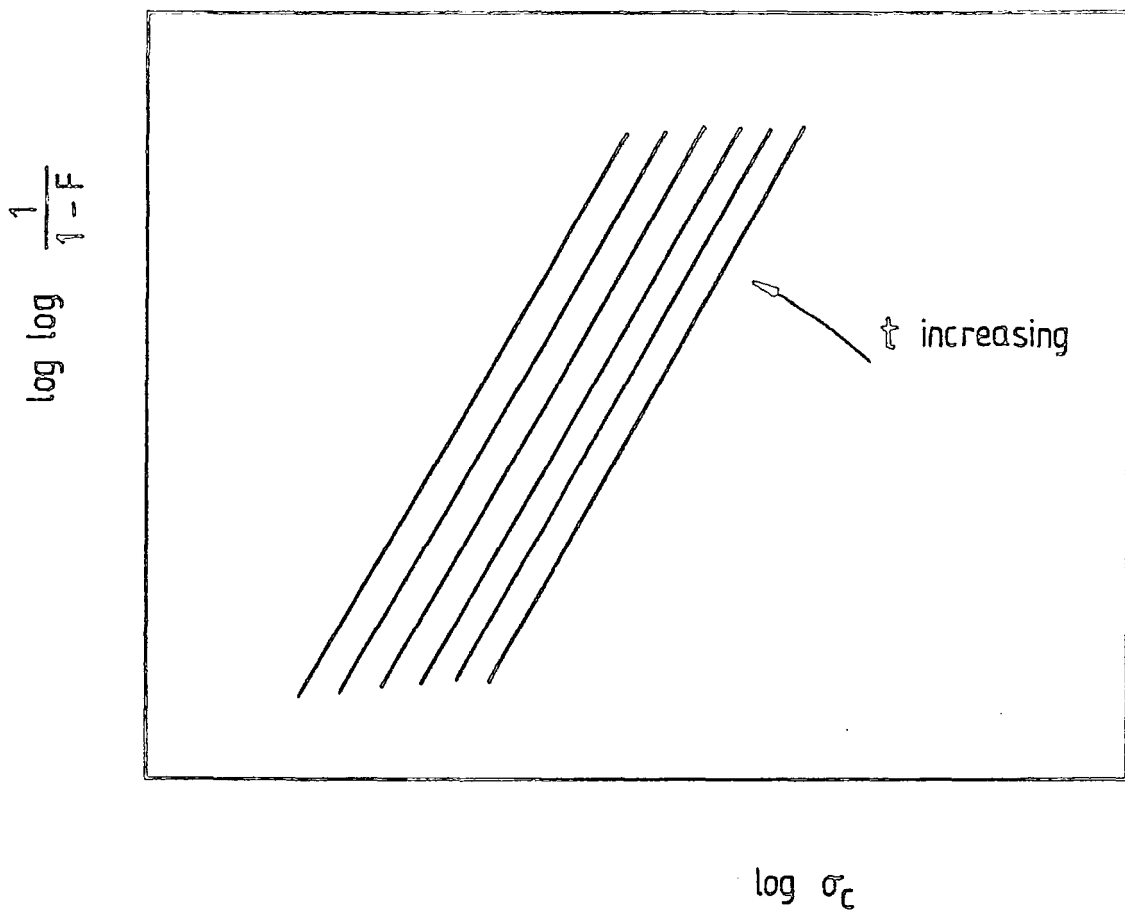


FIGURE 4.1: Typical form of the SPT diagram.  $\sigma_c$  - constant applied stress;  $F$  - cumulative failure probability;  $t$  - lifetime.

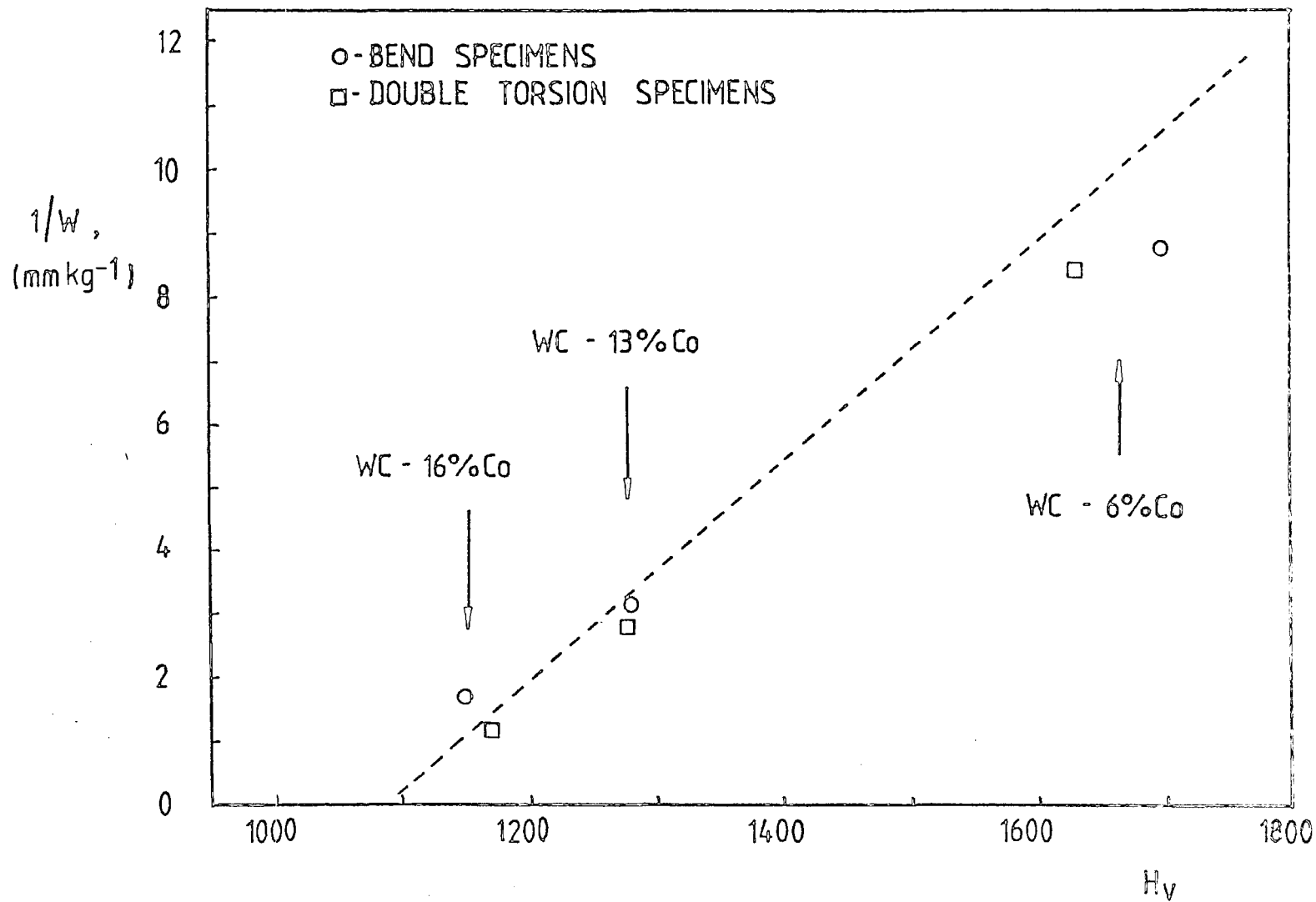


FIGURE 5.1: Inverse crack resistance ( $1/W$ ) plotted against Vickers hardness ( $H_v$ ) for the three grades of WC-Co material studied.

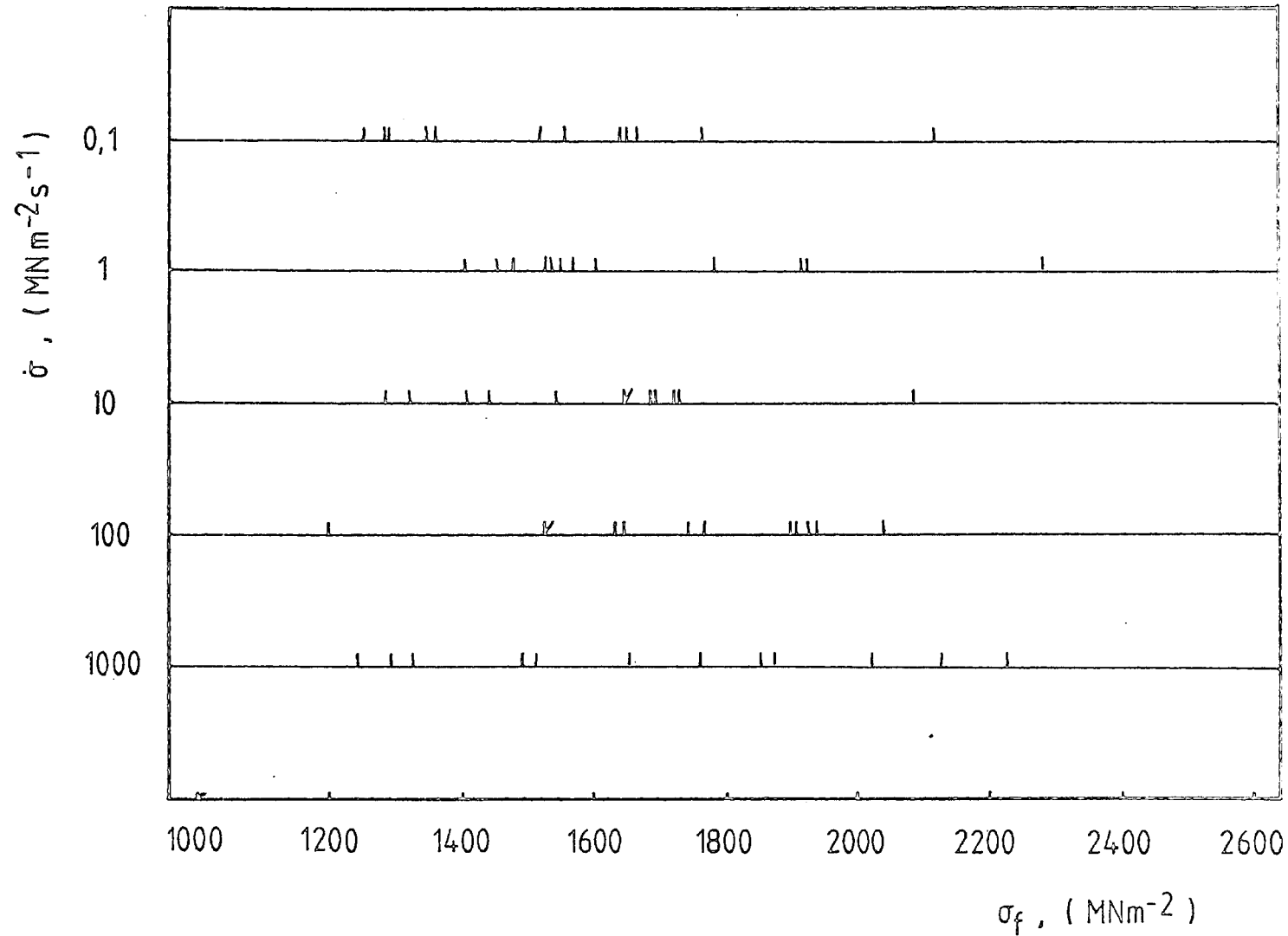


FIGURE 6.1: Strengths ( $\sigma_f$ ) recorded from stress rate ( $\dot{\sigma}$ ) tests at 20°C, in laboratory air, on WC-6% Co specimens with ground faces.

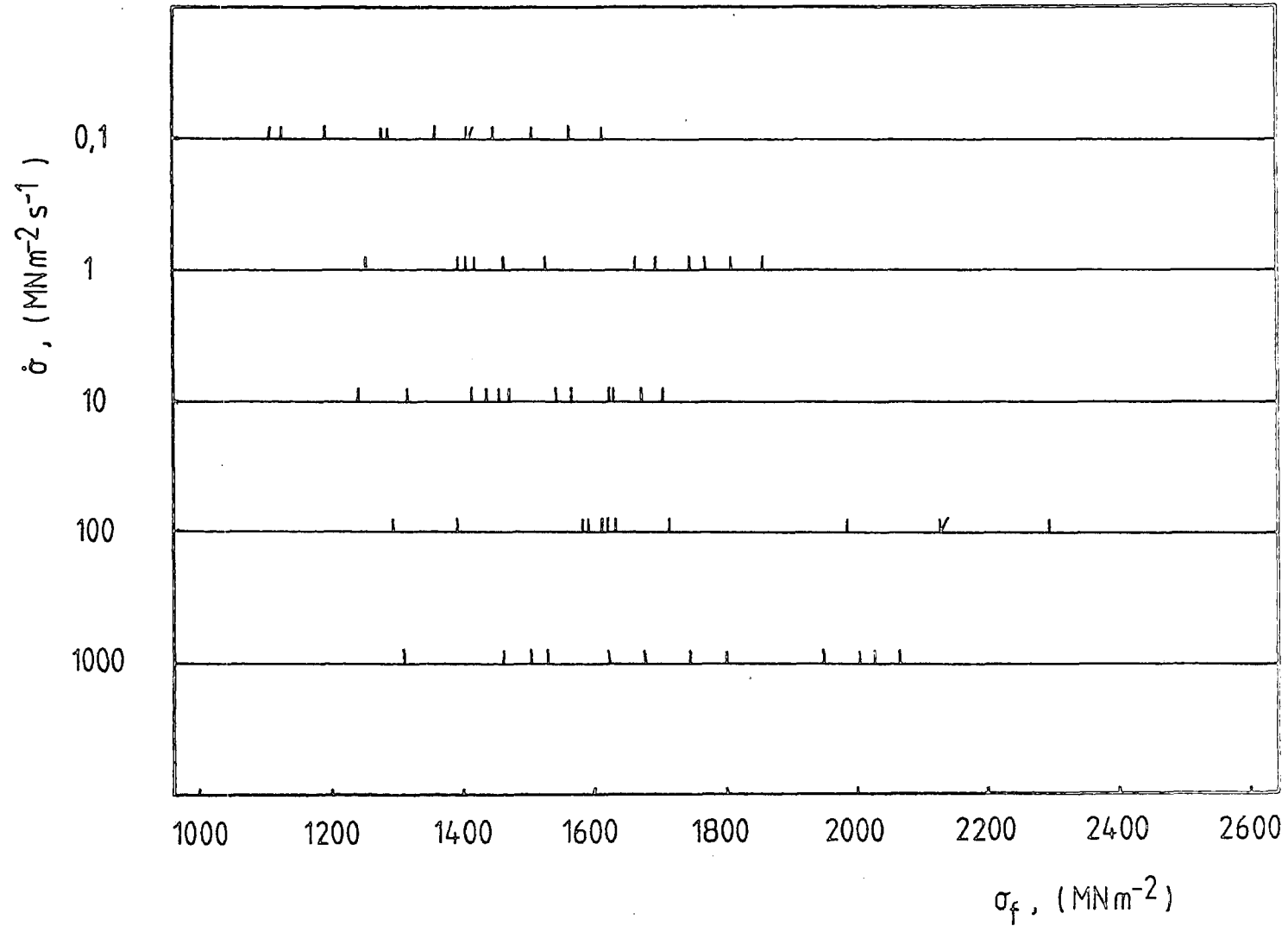


FIGURE 6.2: As Figure 6.1 for WC - 6% Co specimens with polished faces.

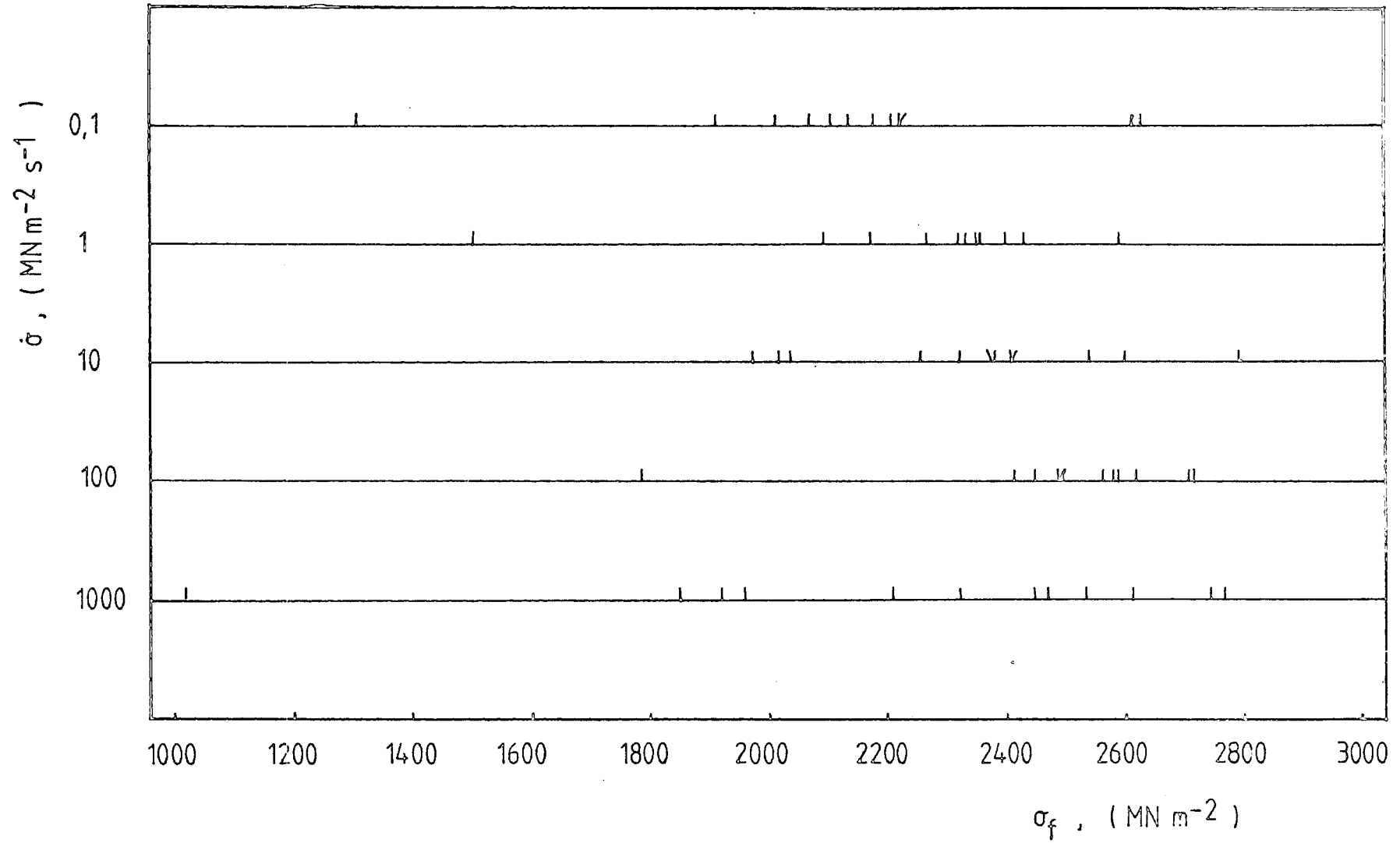


FIGURE 6.3: As Figure 6.1 for WC-13% Co specimens with ground faces.

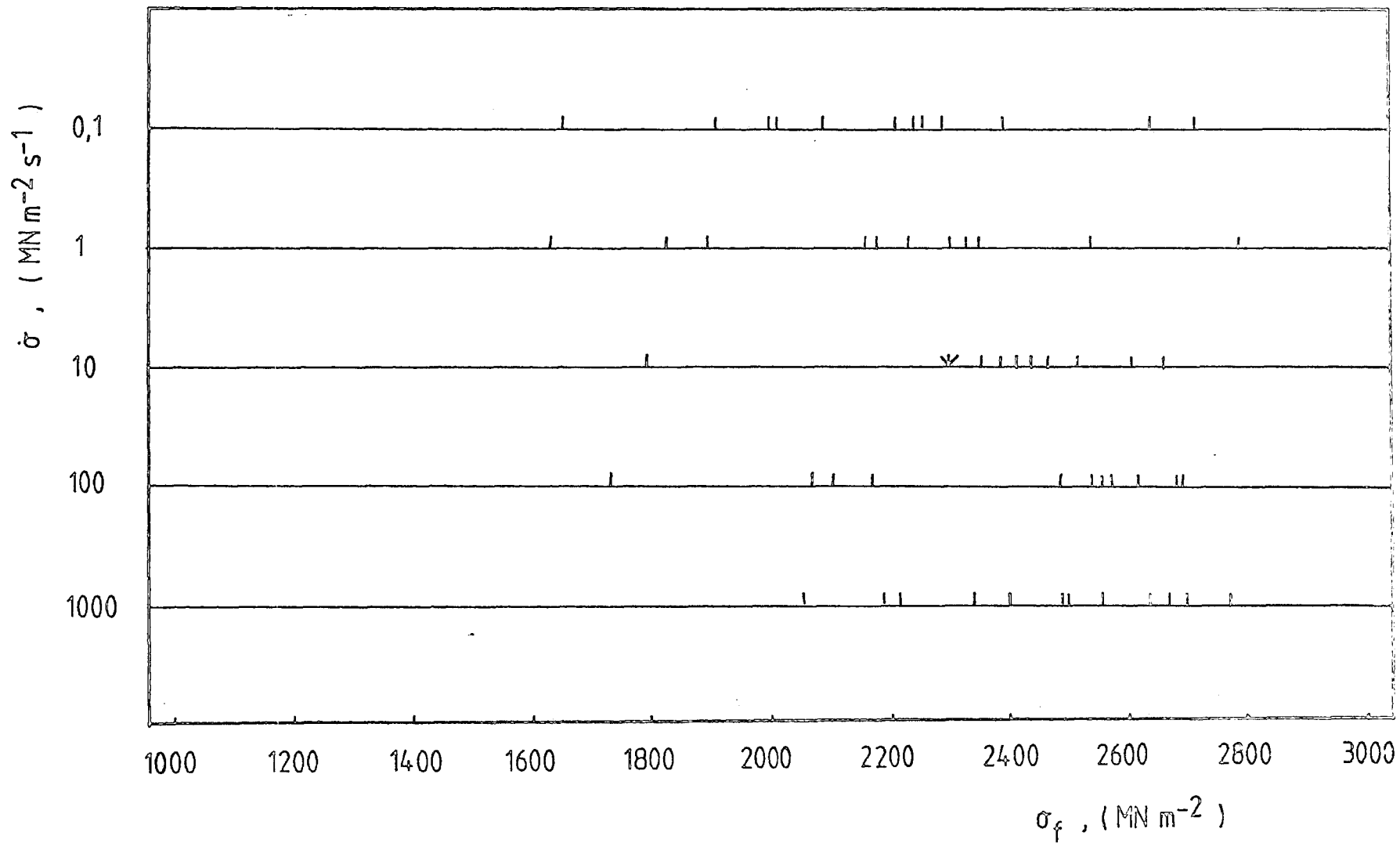


FIGURE 6.4: As Figure 6.1 for WC-13% Co specimens with polished faces.

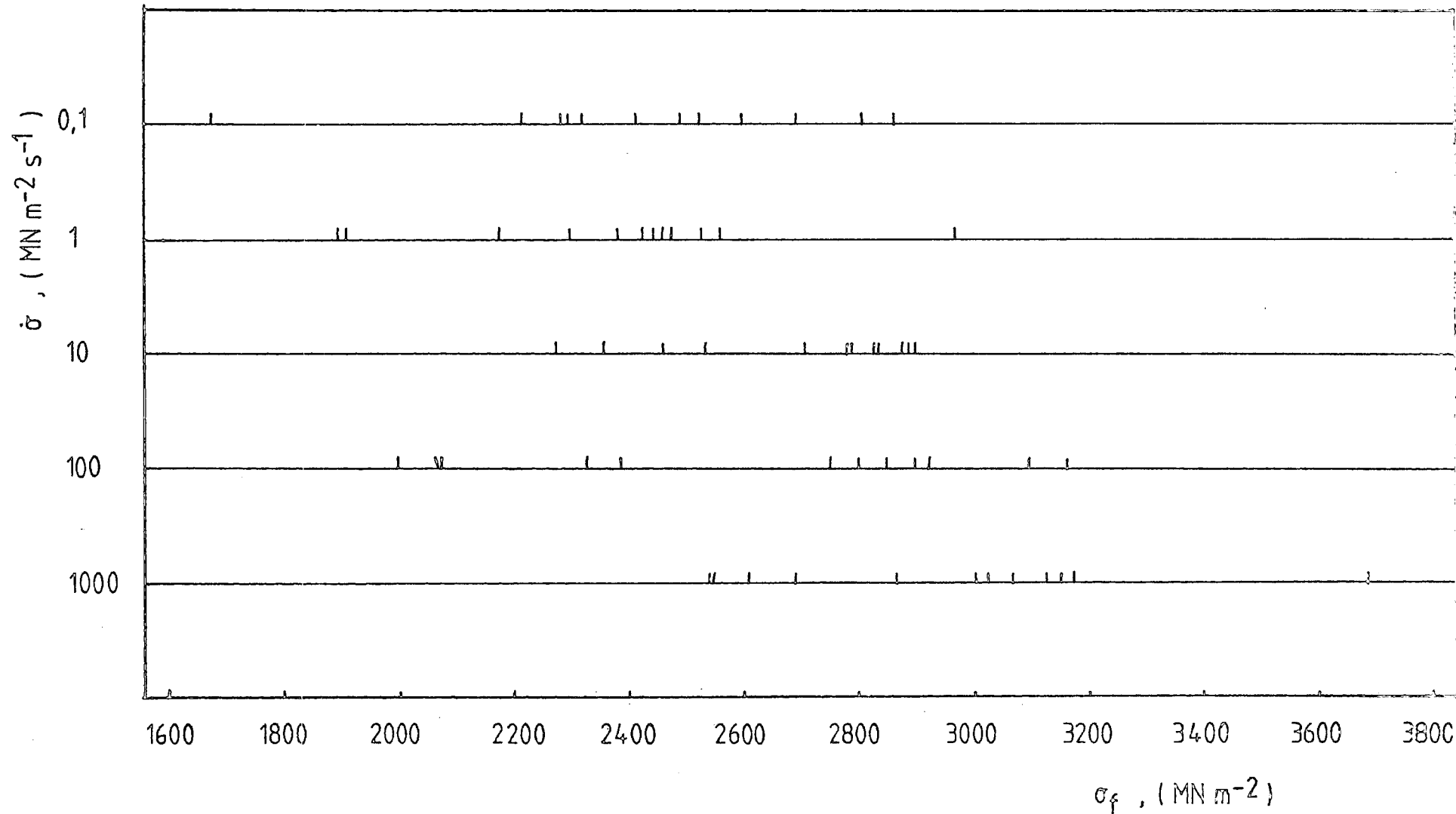


FIGURE 6.5: As Figure 6.1 for WC-16% Co specimens with ground faces.

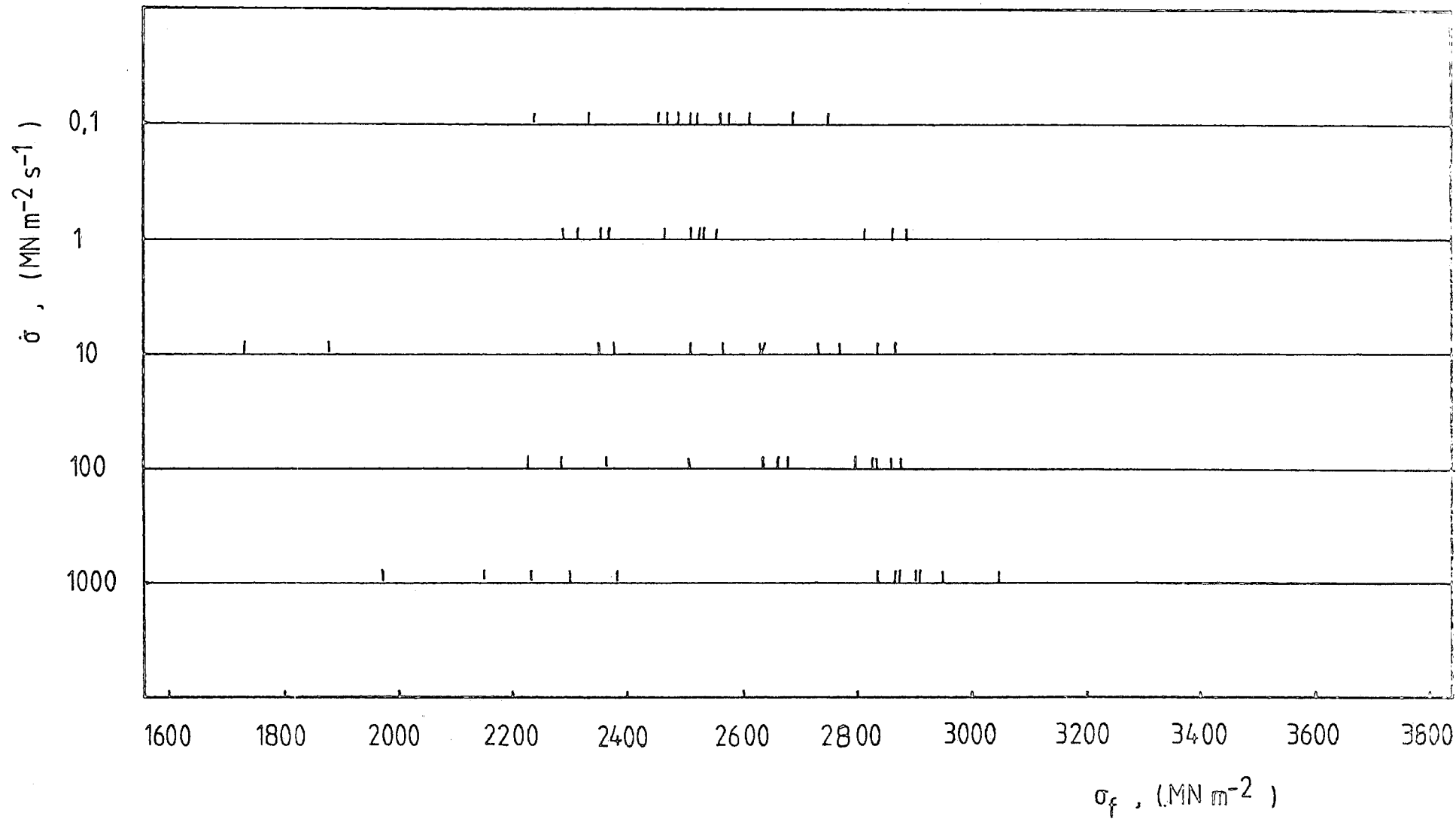


FIGURE 6.6: As Figure 6.1 for WC-16% Co specimens with polished faces.

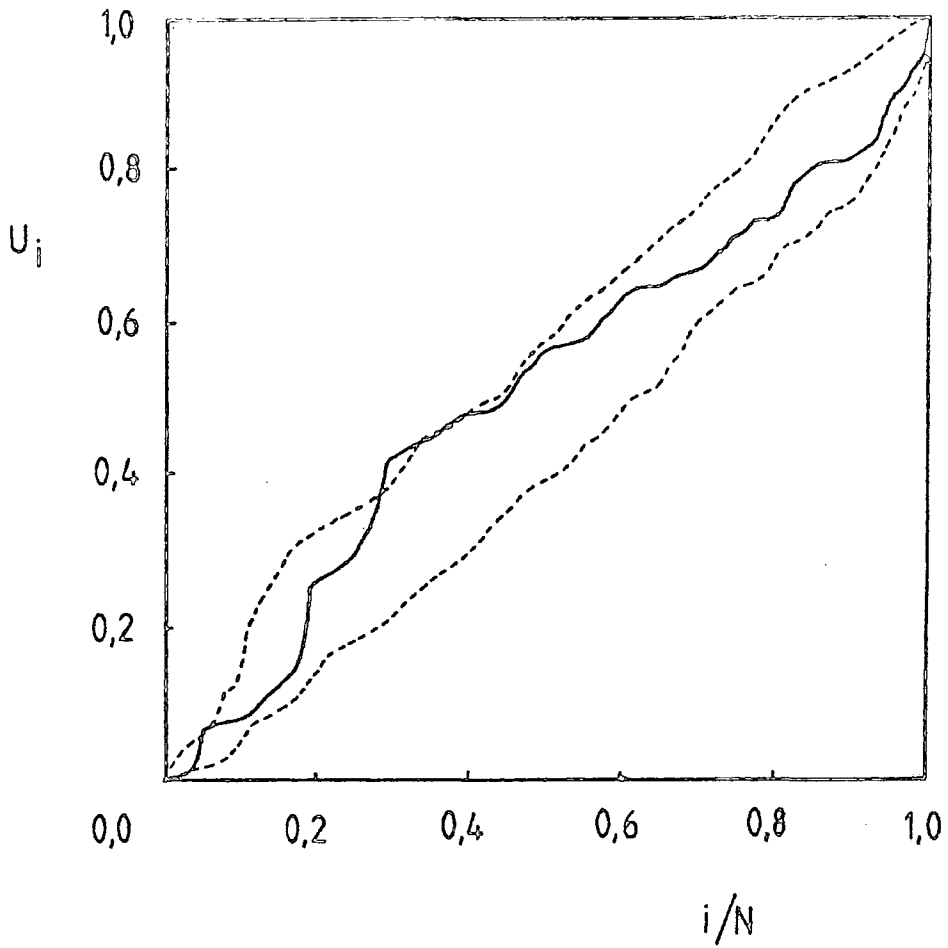


FIGURE 6.7: Probability integral transform,  $U_i$ , of residual,  $Z_i$ , plotted against  $i/N$ , ( $i = 1, 2, 3 \dots N$ ), for strength data from stress rate tests on soda-lime glass specimens. Dotted line - envelope of 36 artificial data sets.

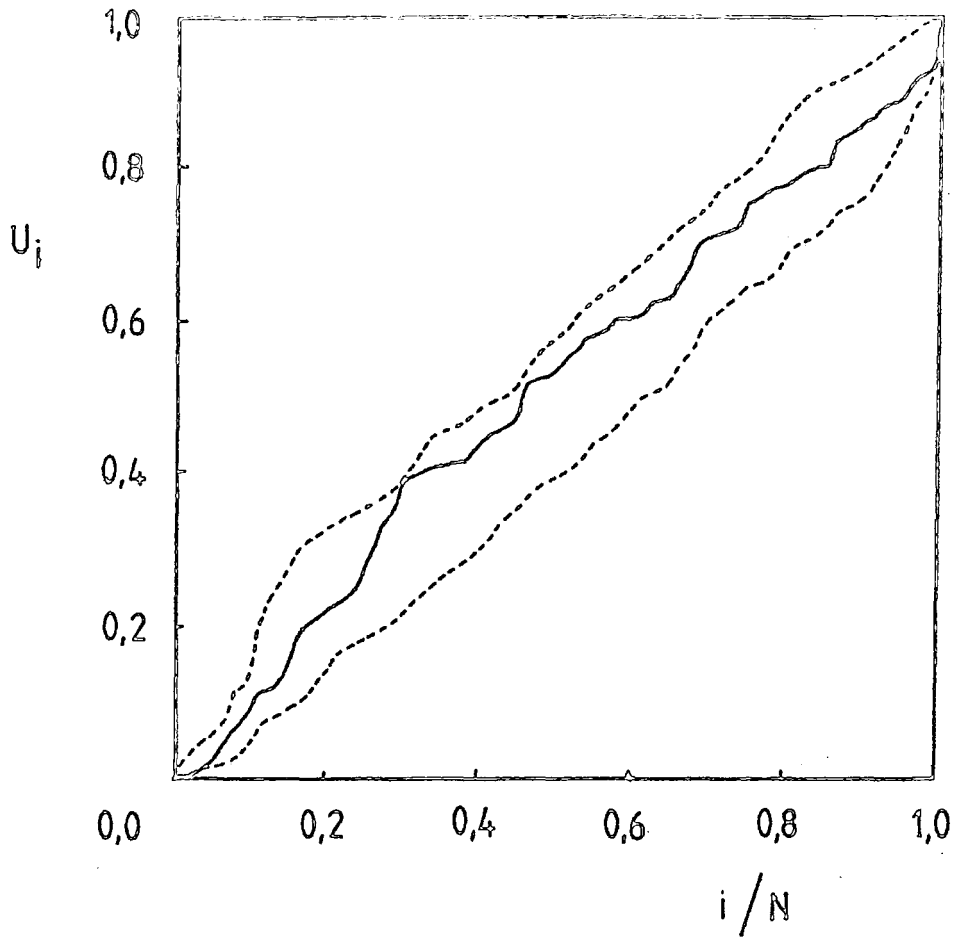


FIGURE 6.8: As Figure 6.7 for WC-6% Co specimens with ground faces.

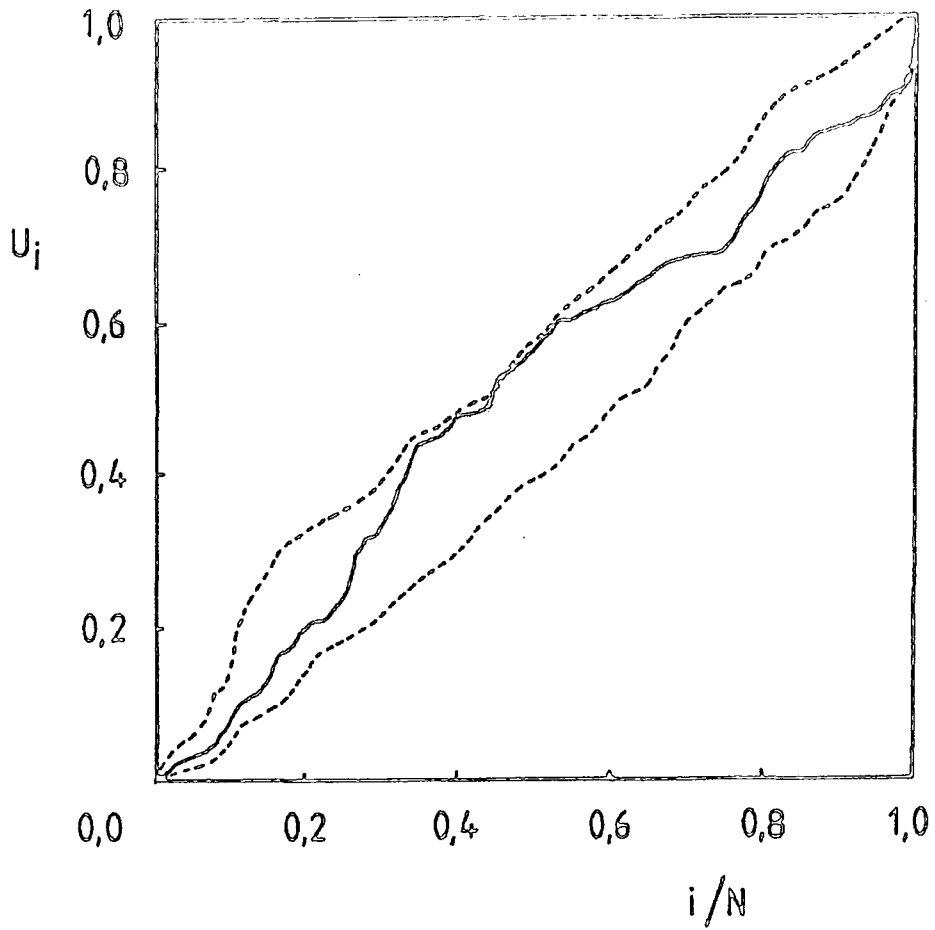


FIGURE 6.9: As Figure 6.7 for WC-6% Co specimens with polished faces.

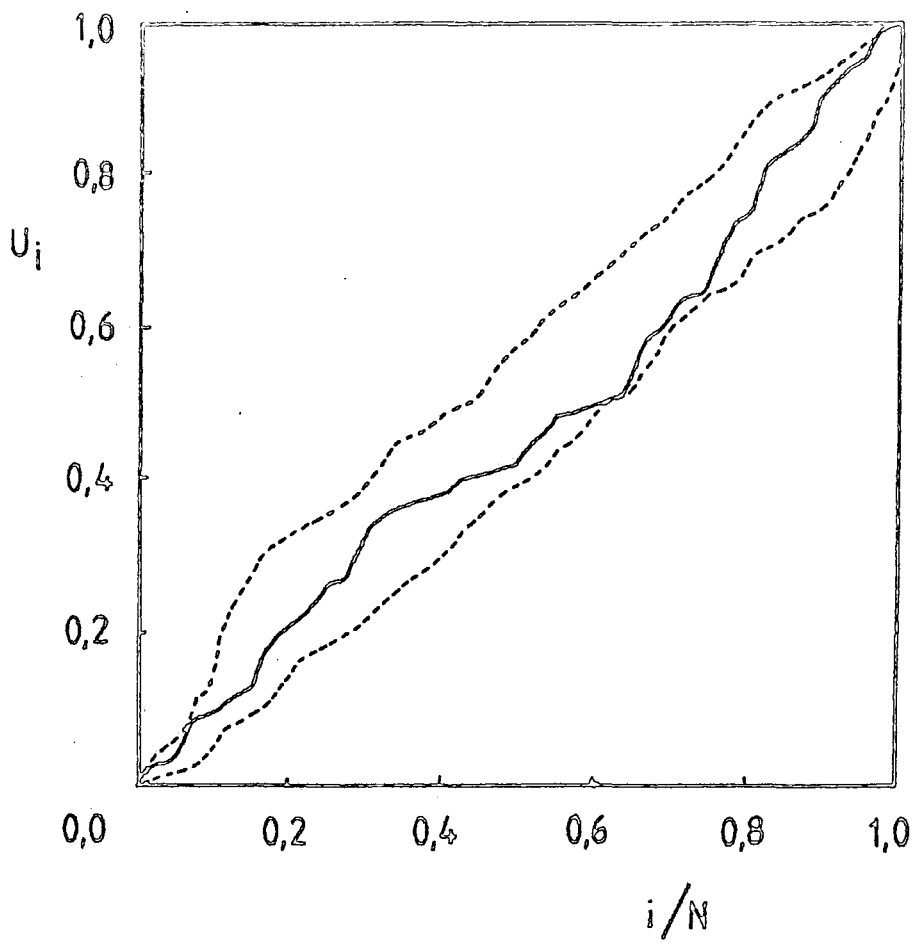


FIGURE 6.10: As Figure 6.7 for WC-13% Co specimens with ground faces.

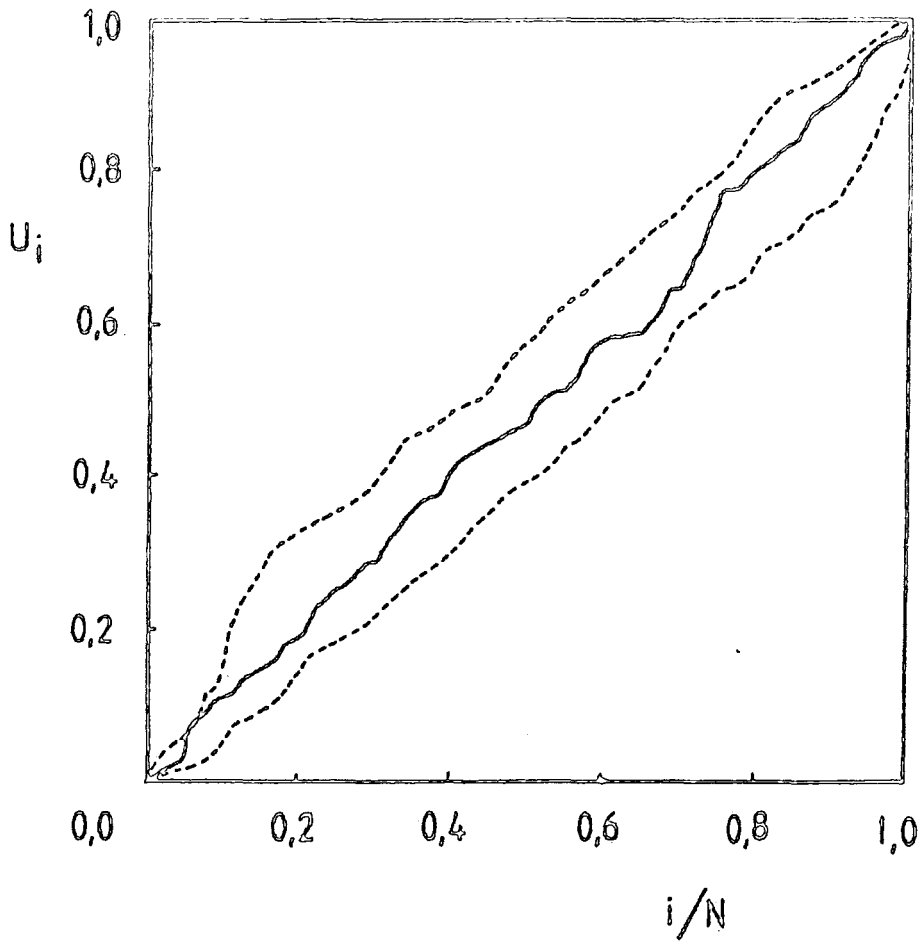


FIGURE 6.11: As Figure 6.7 for WC-13% Co specimens with polished faces.

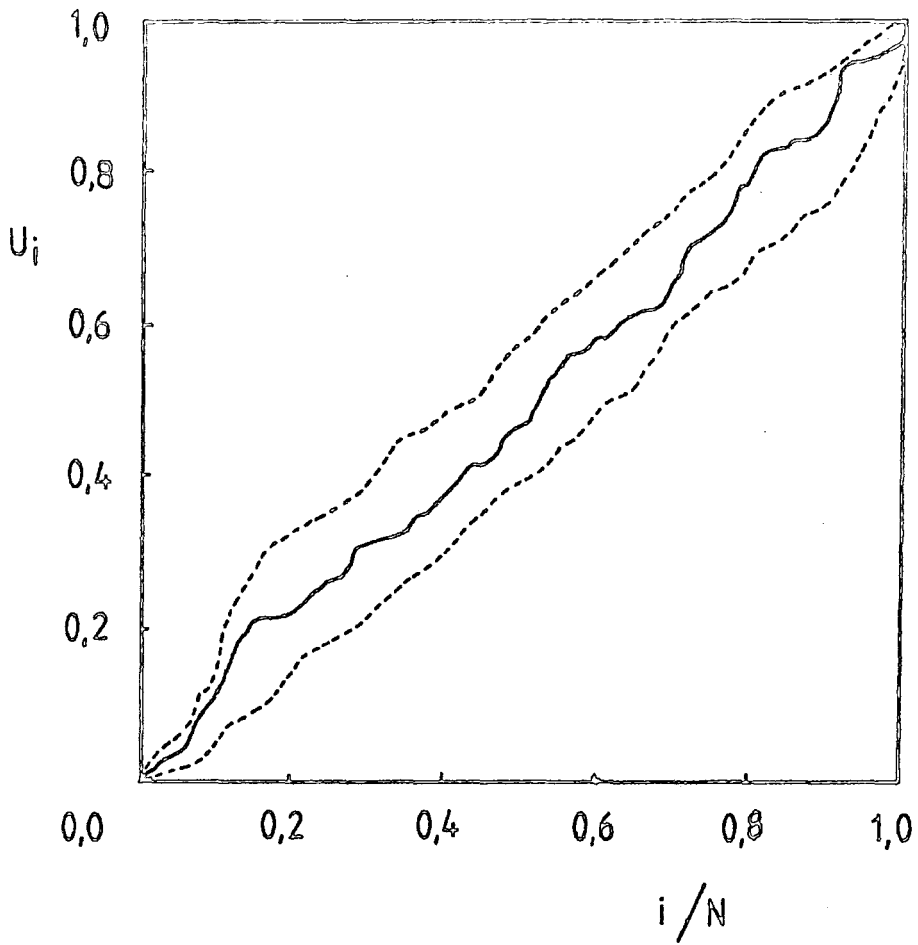


FIGURE 6.12: As Figure 6.7 for WC-16% Co specimens with ground faces.

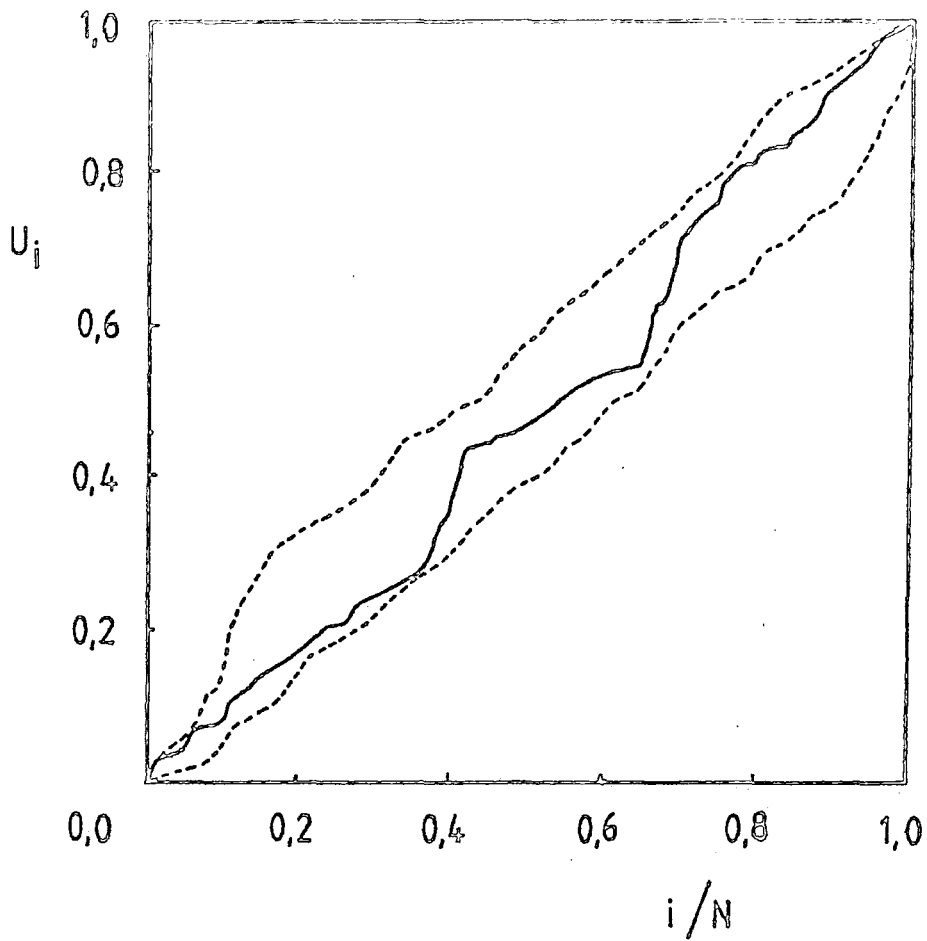


FIGURE 6.13: As Figure 6.7 for WC-16% Co specimens with polished faces.

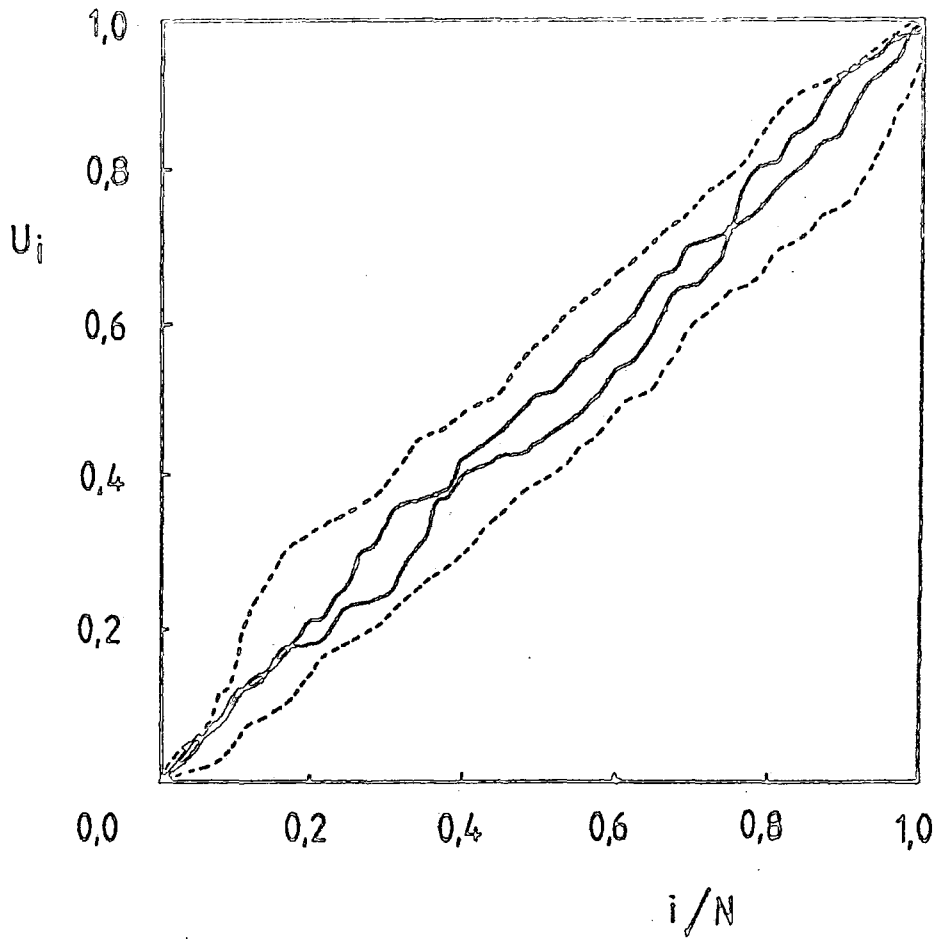


FIGURE 6.14: As Figure 6.7 for examples of two artificial data sets.

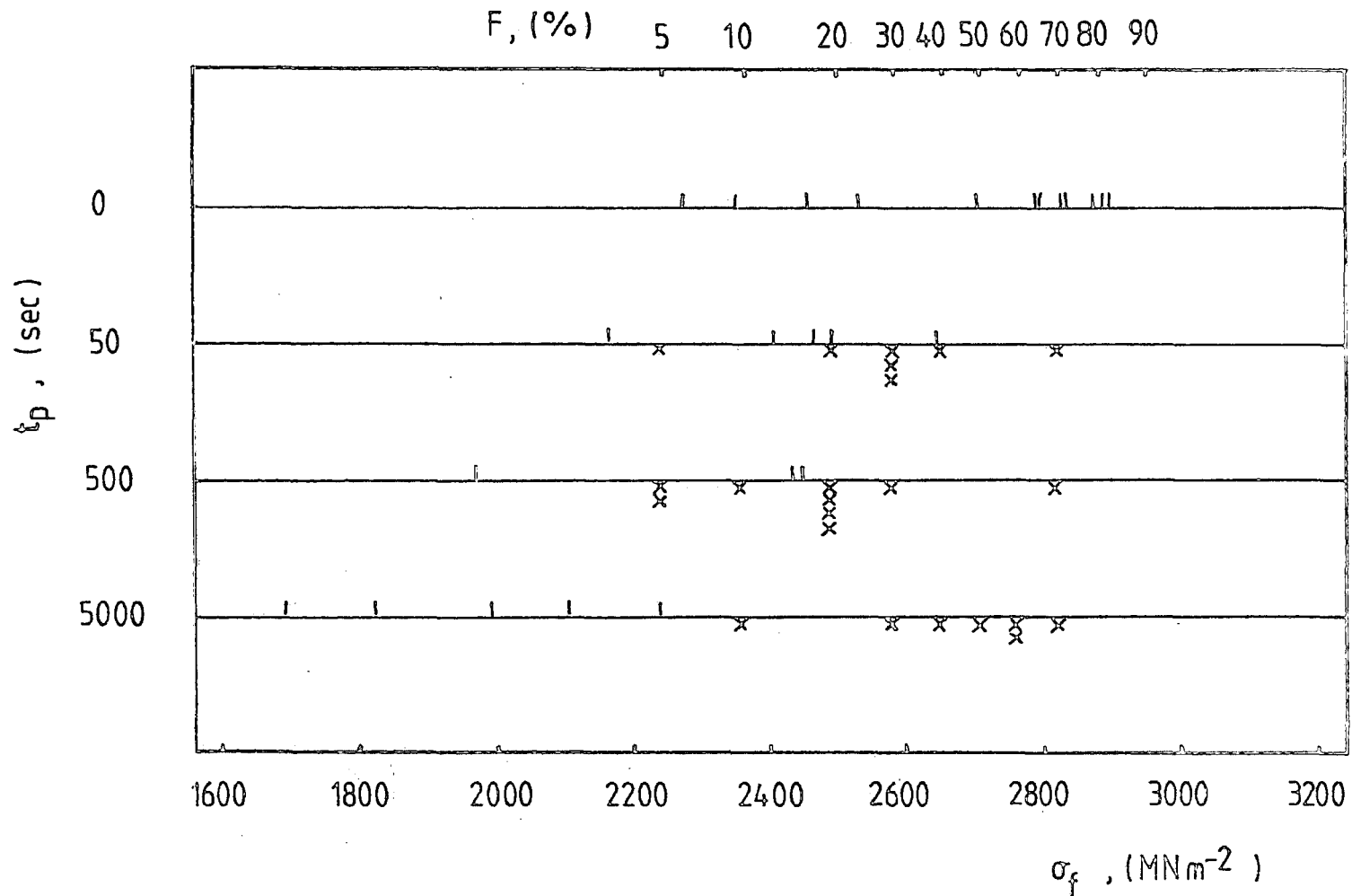


FIGURE 6.15: Strengths ( $\sigma_f$ ) recorded from stepped loading tests at 20°C in laboratory air, on WC-16% Co specimens with ground faces.  $t_p$  - constant stress duration; F - listed values indicate levels of cumulative failure probability, taken from stress rate tests, to determine constant stress levels. Crosses below the line indicate a failure during a period of constant stress.

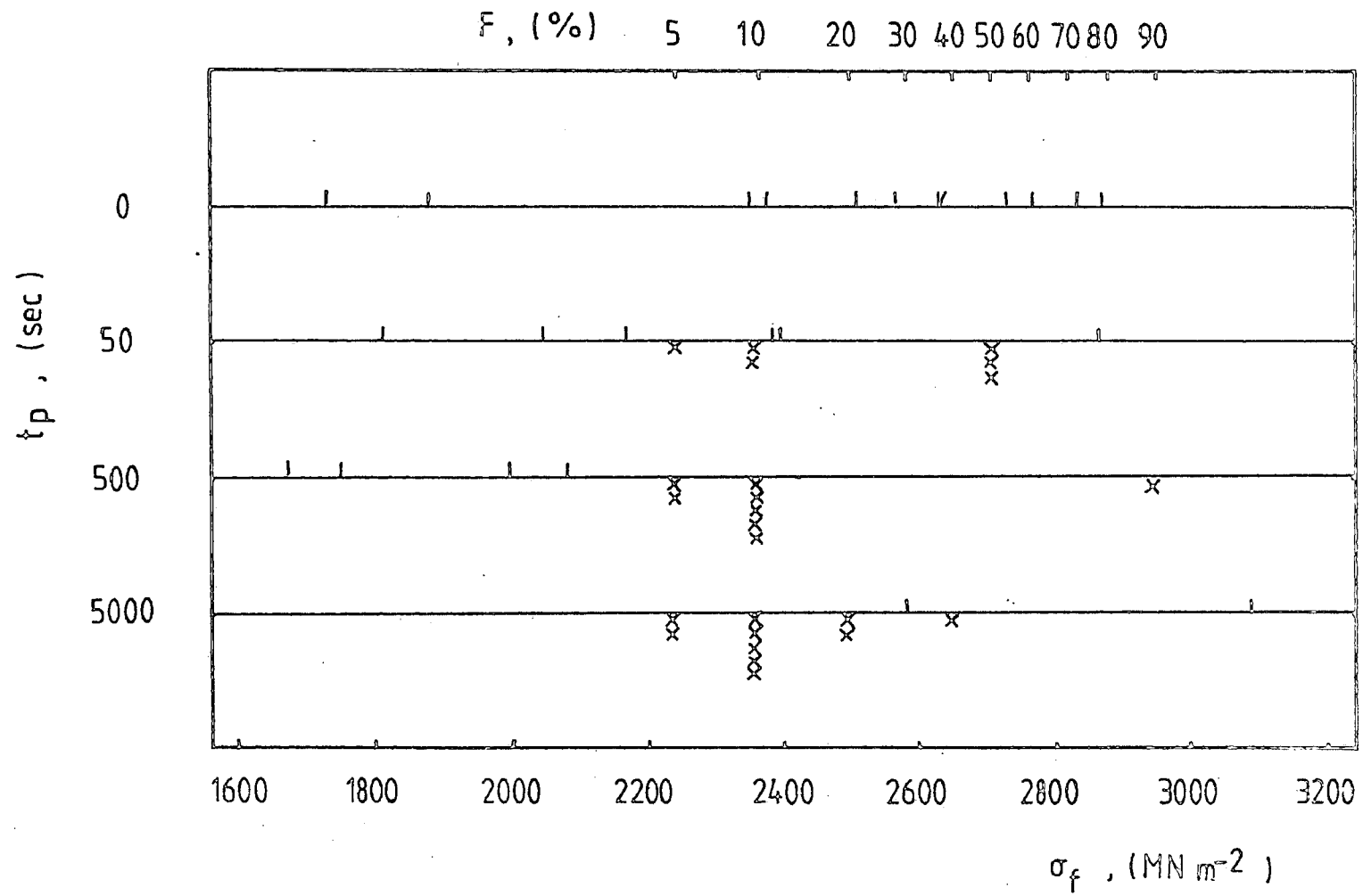
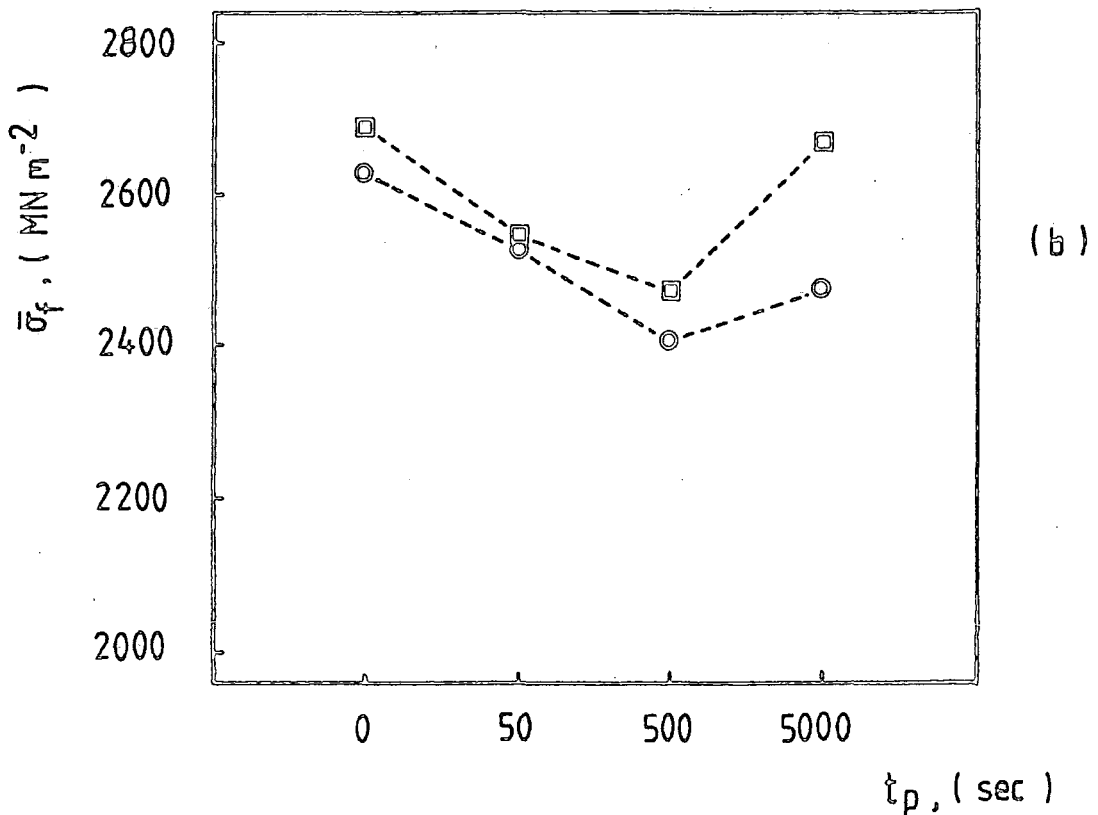
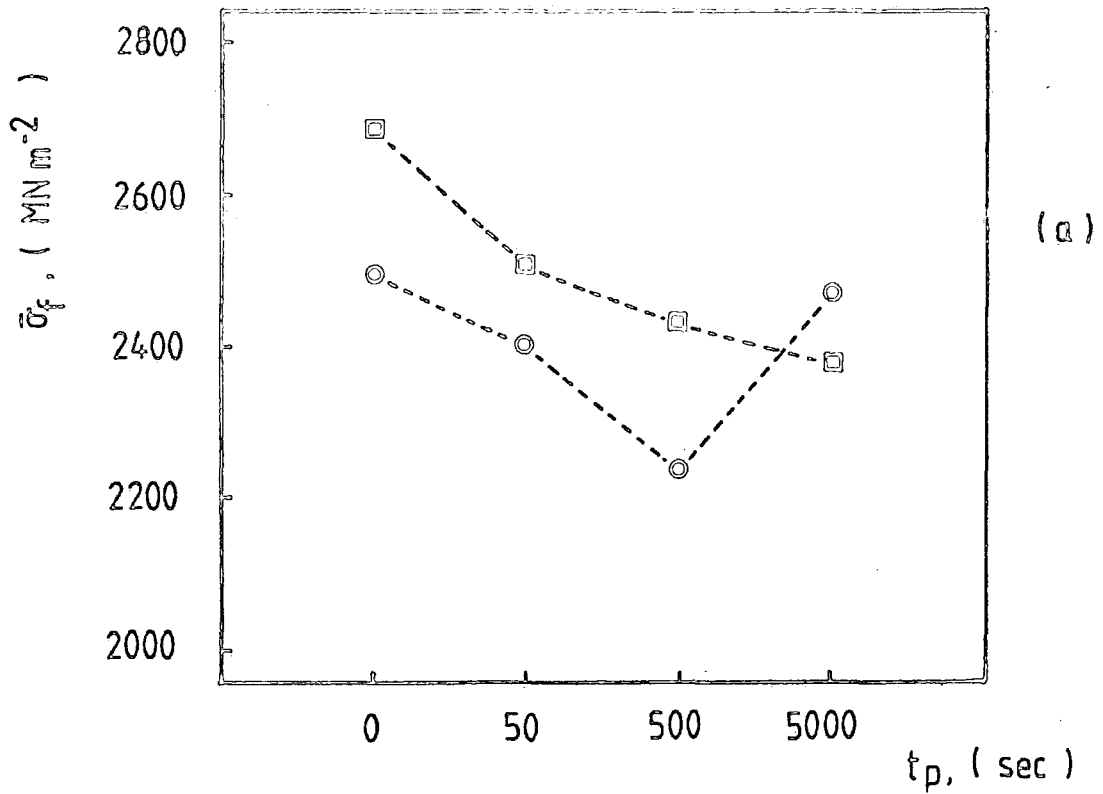


FIGURE 6.16: As Figure 6.15 for WC-16% Co specimens with polished faces.



□ - GROUND FINISH ; ○ - POLISHED FINISH

FIGURE 6.17: Mean strengths ( $\bar{\sigma}_f$ ) of WC-16% Co specimens tested using each constant stress duration ( $t_p$ ). (a), all results analysed; (b), with strengths below the first constant stress level omitted.

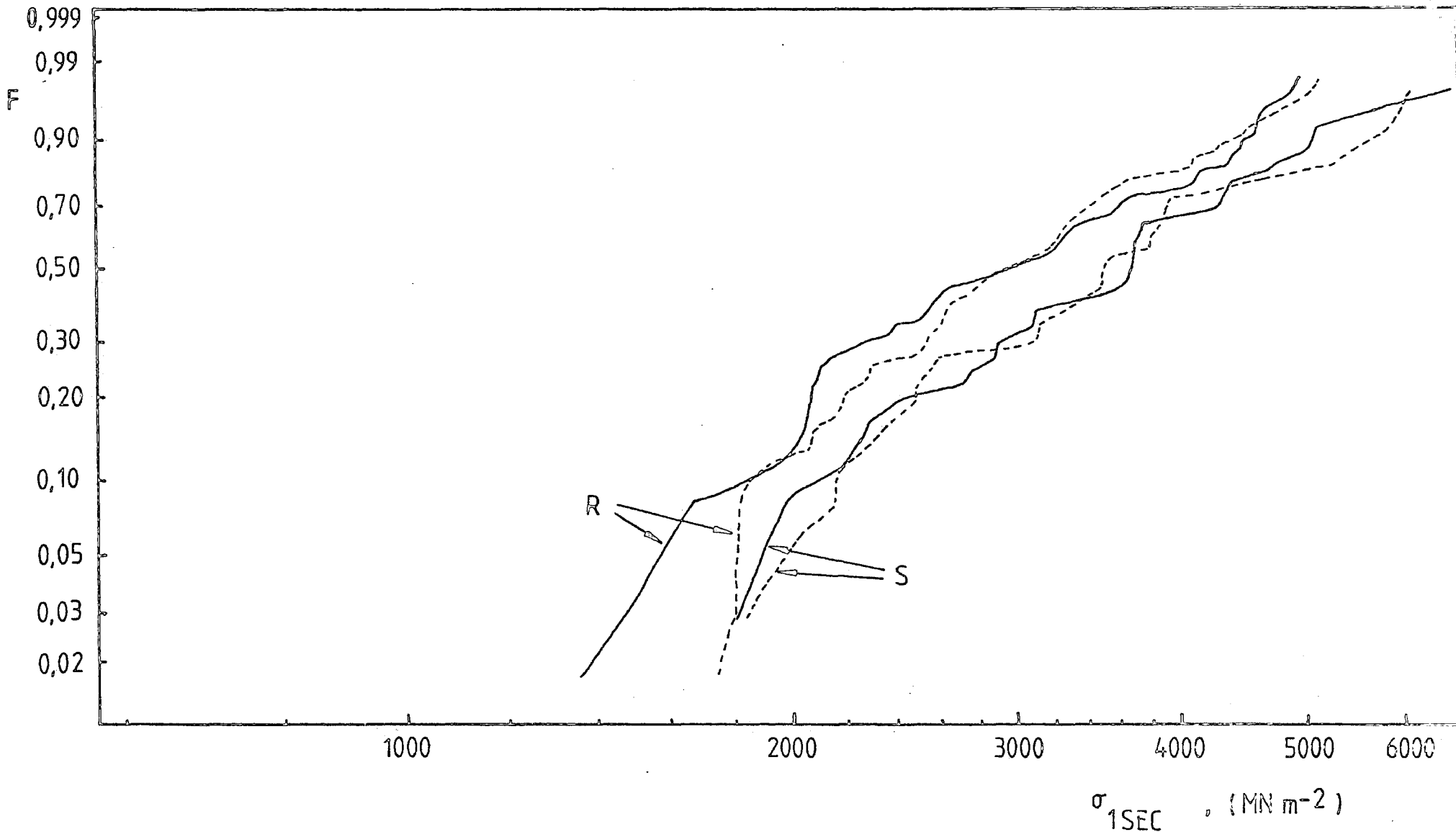


FIGURE 6.18:  $\sigma_{1SEC}$  Weibull curves for WC-16% Co stress rate (R), and stepped loading (S) data, transformed using a value of  $n = 10$ .  $F$  - cumulative failure probability;  $\sigma_{1SEC}$  - constant stress necessary to induce a lifetime of one second. Dotted line - ground surfaces; solid line - polished surfaces.

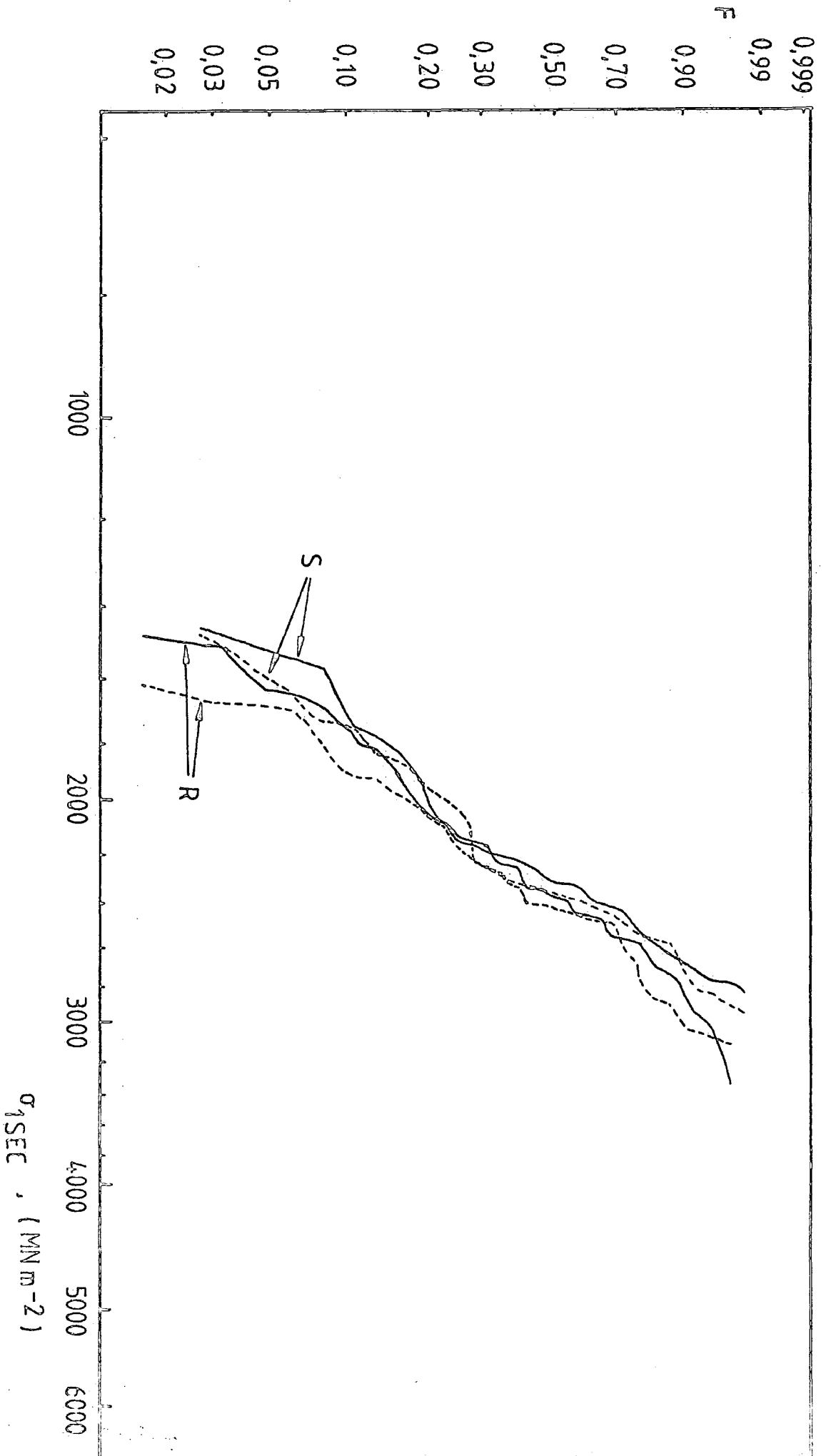


FIGURE 6.19: AS Figure 6.18 using a value of  $n = 30$ .

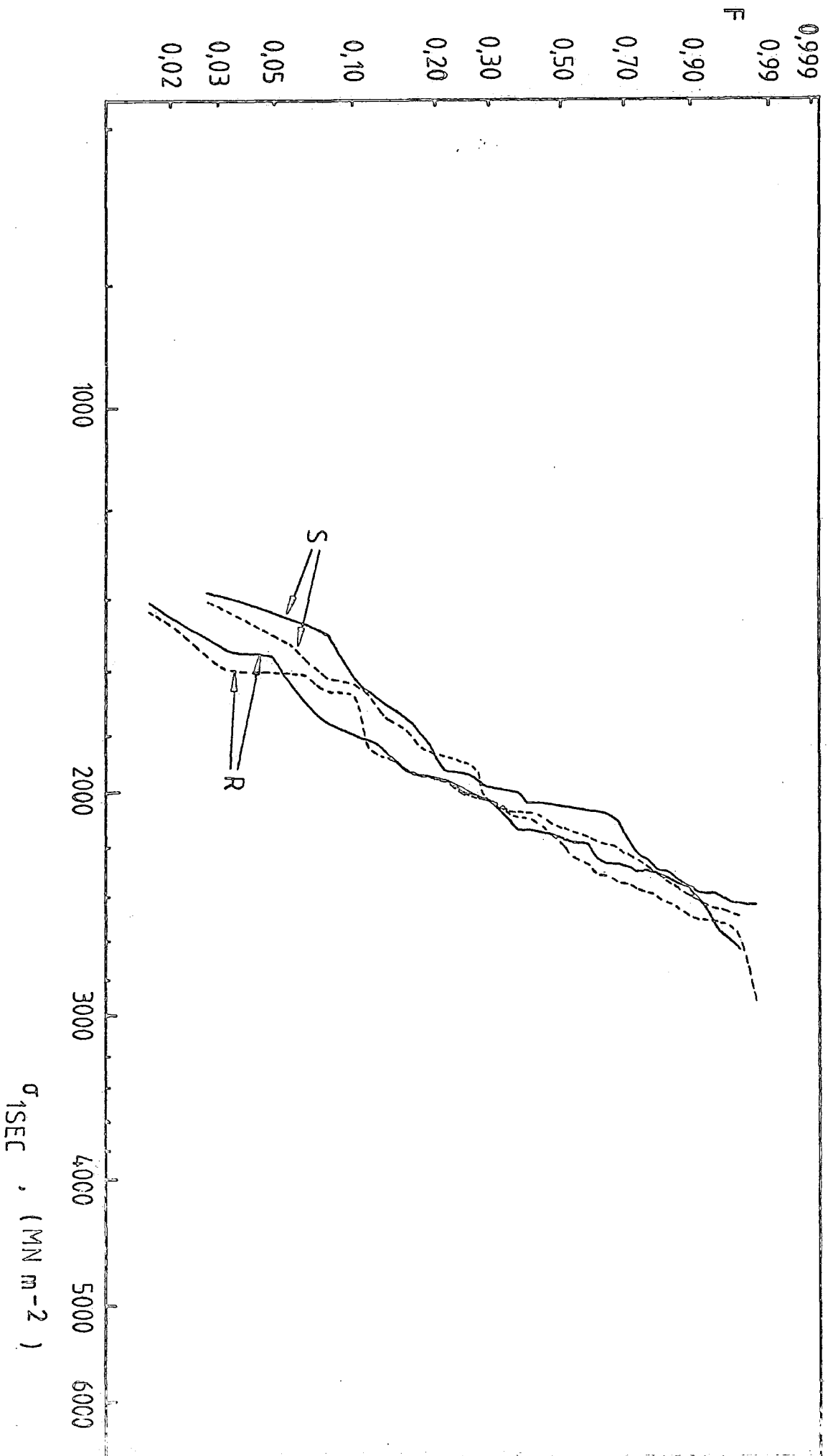


FIGURE 6.20: As Figure 6.18 using a value of  $n = 100$ .

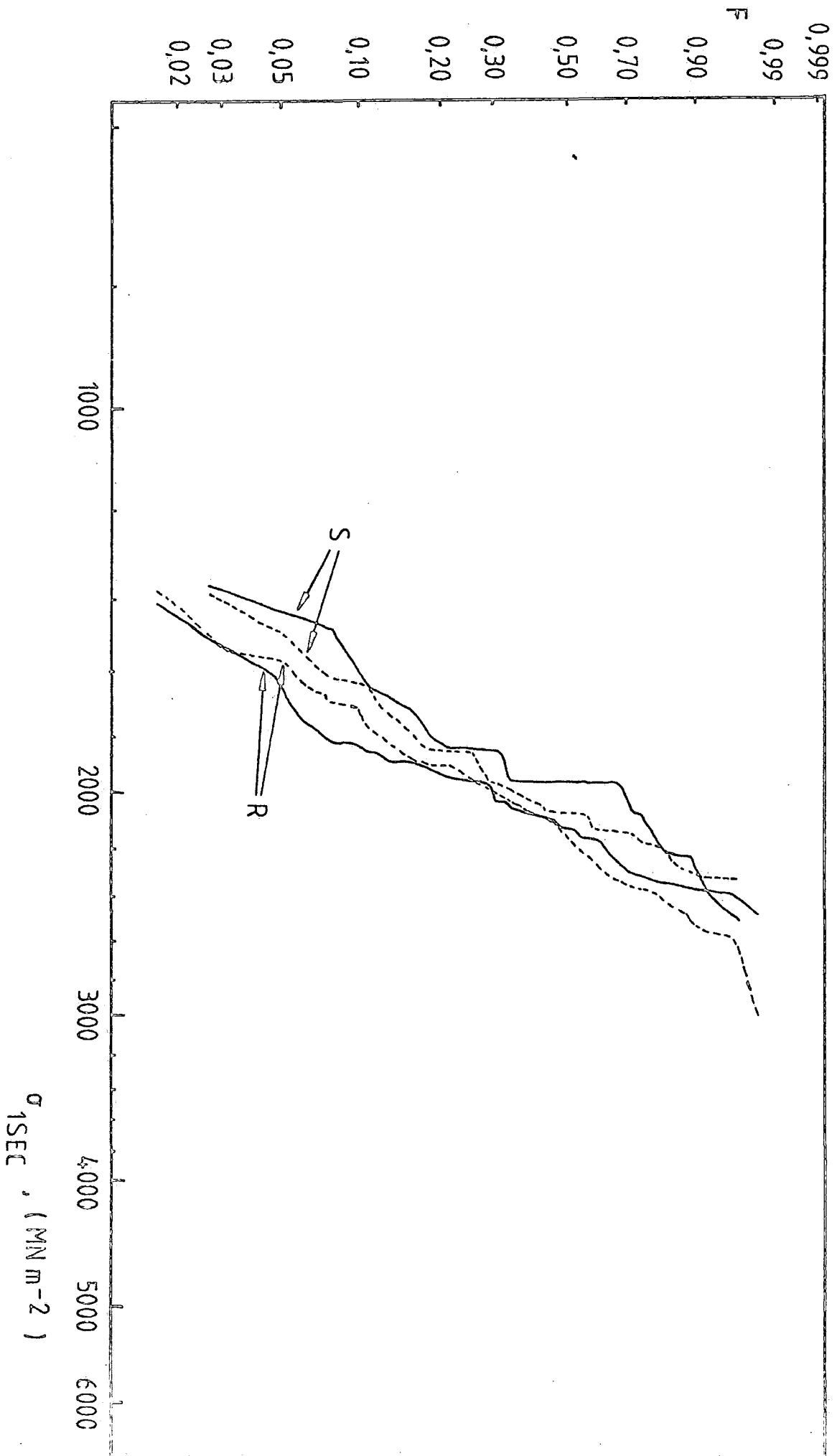


FIGURE 6.21: As Figure 6.18 using a value of  $n = 1000$ .

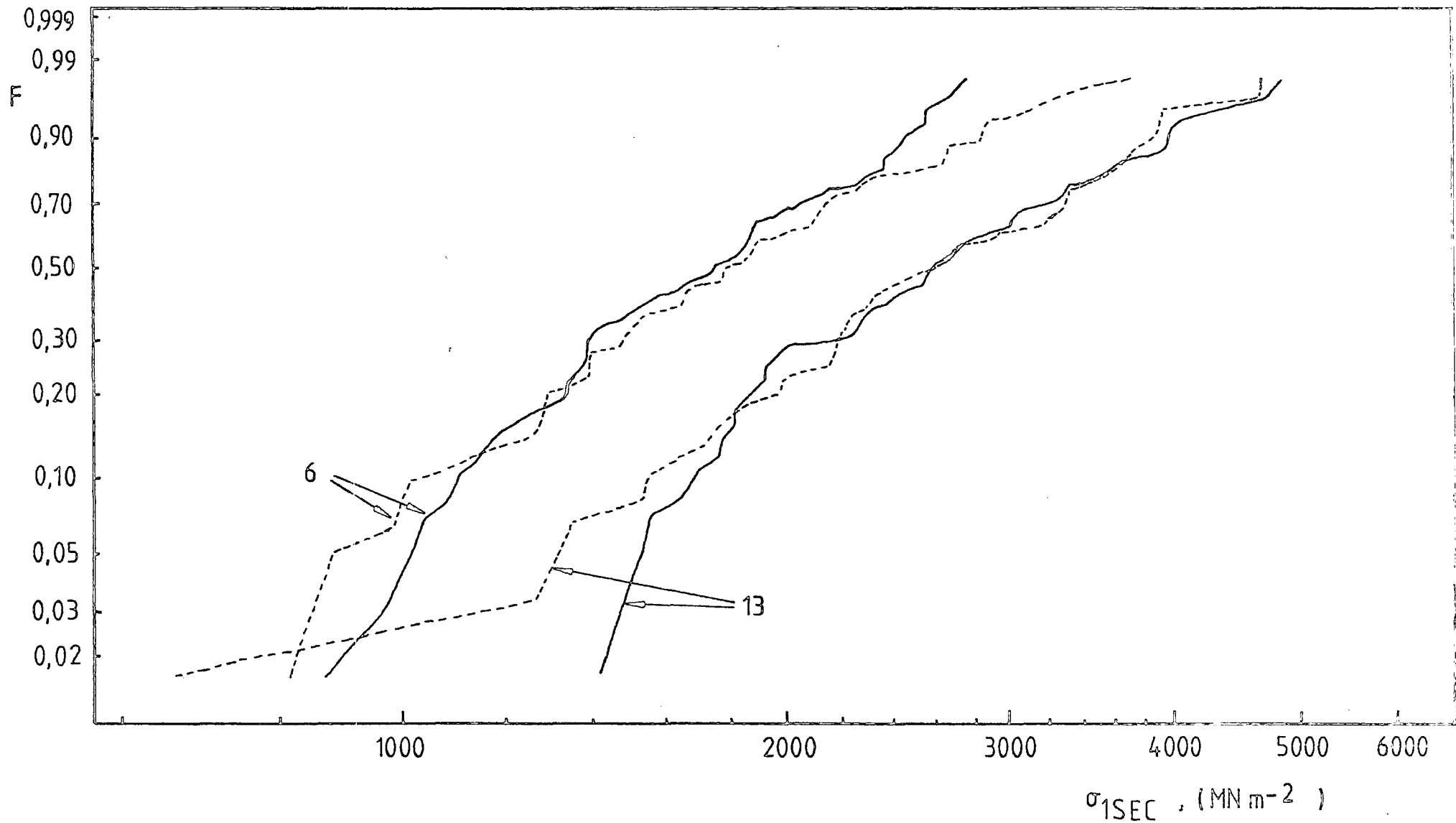


FIGURE 6.22:  $\sigma_{1\text{SEC}}$  Weibull curves for WC-6% Co (6), and WC-13% Co (13) stress rate data, transformed using a value of  $n = 10$ . F - cumulative failure probability;  $\sigma_{1\text{SEC}}$  - constant stress necessary to induce a lifetime of one second. Dotted line - ground surfaces; solid line - polished surfaces.

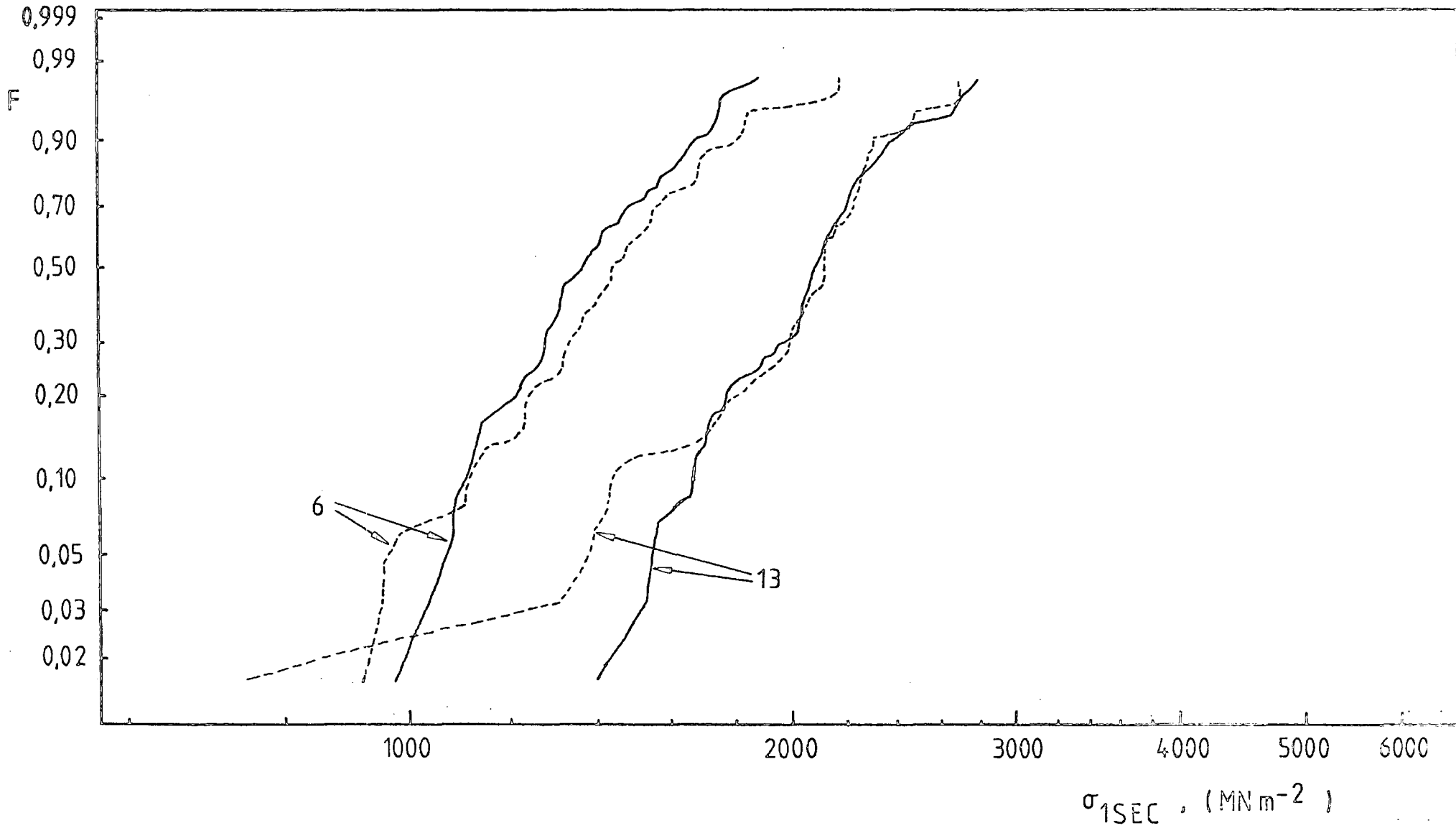


FIGURE 6.23: As Figure 6.22 using a value of  $n = 30$ .

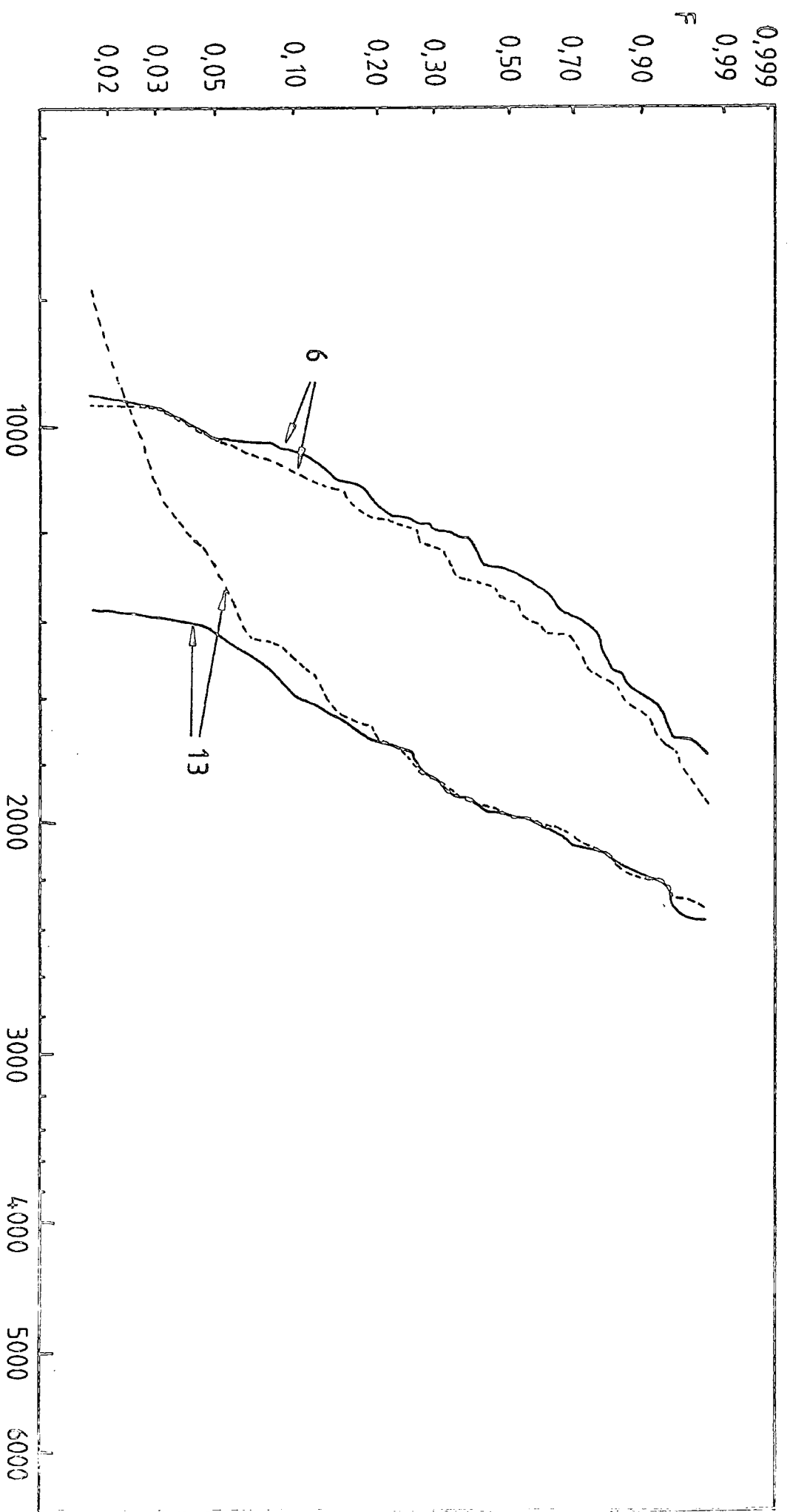


FIGURE 6.24: As Figure 6.22 using a value of  $n = 100$ .

$\sigma_{1SEC} \text{ , (MN m}^{-2} \text{ )}$

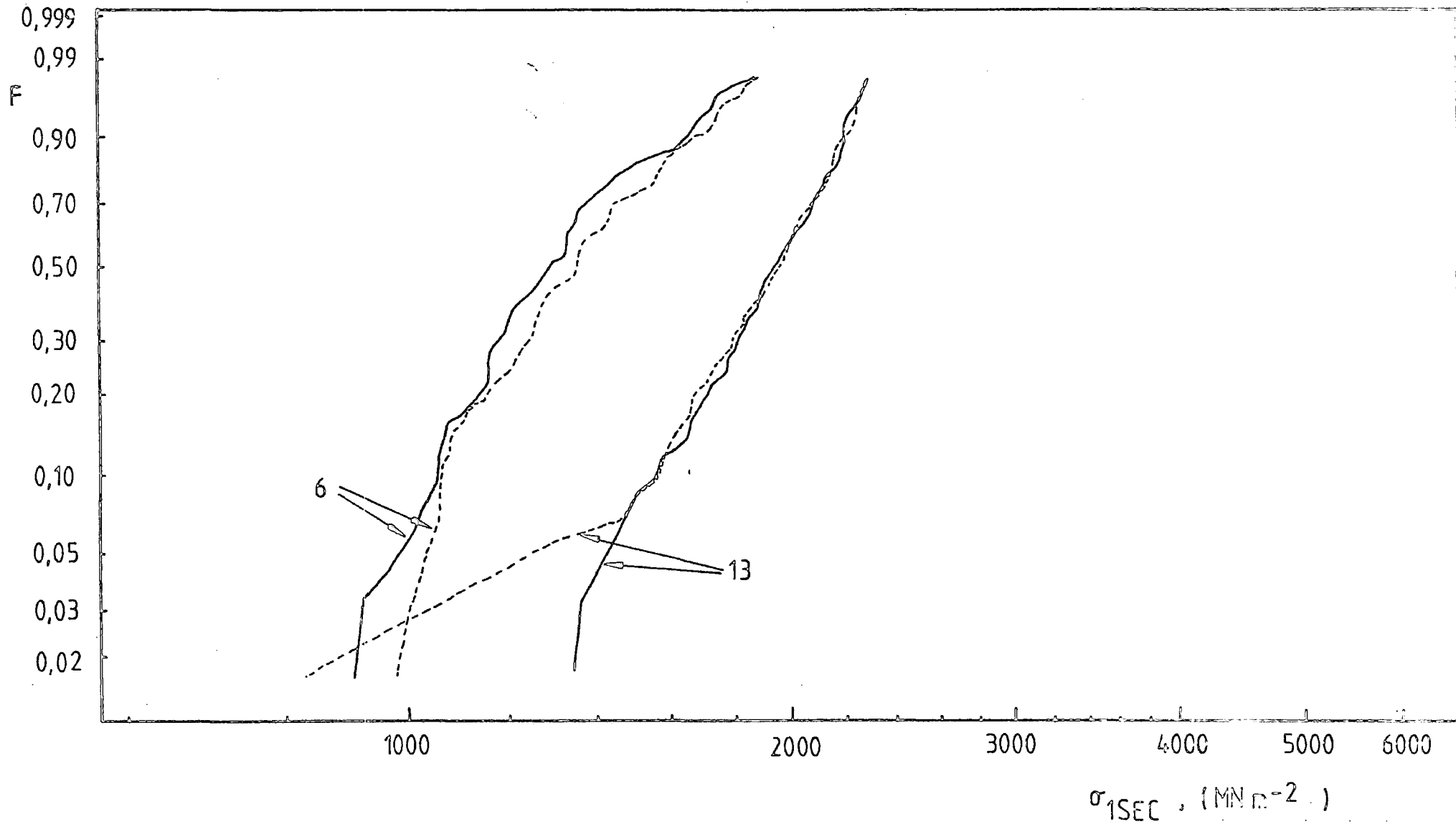


FIGURE 6.25: As Figure 6.22 using a value of  $n = 1000$ .

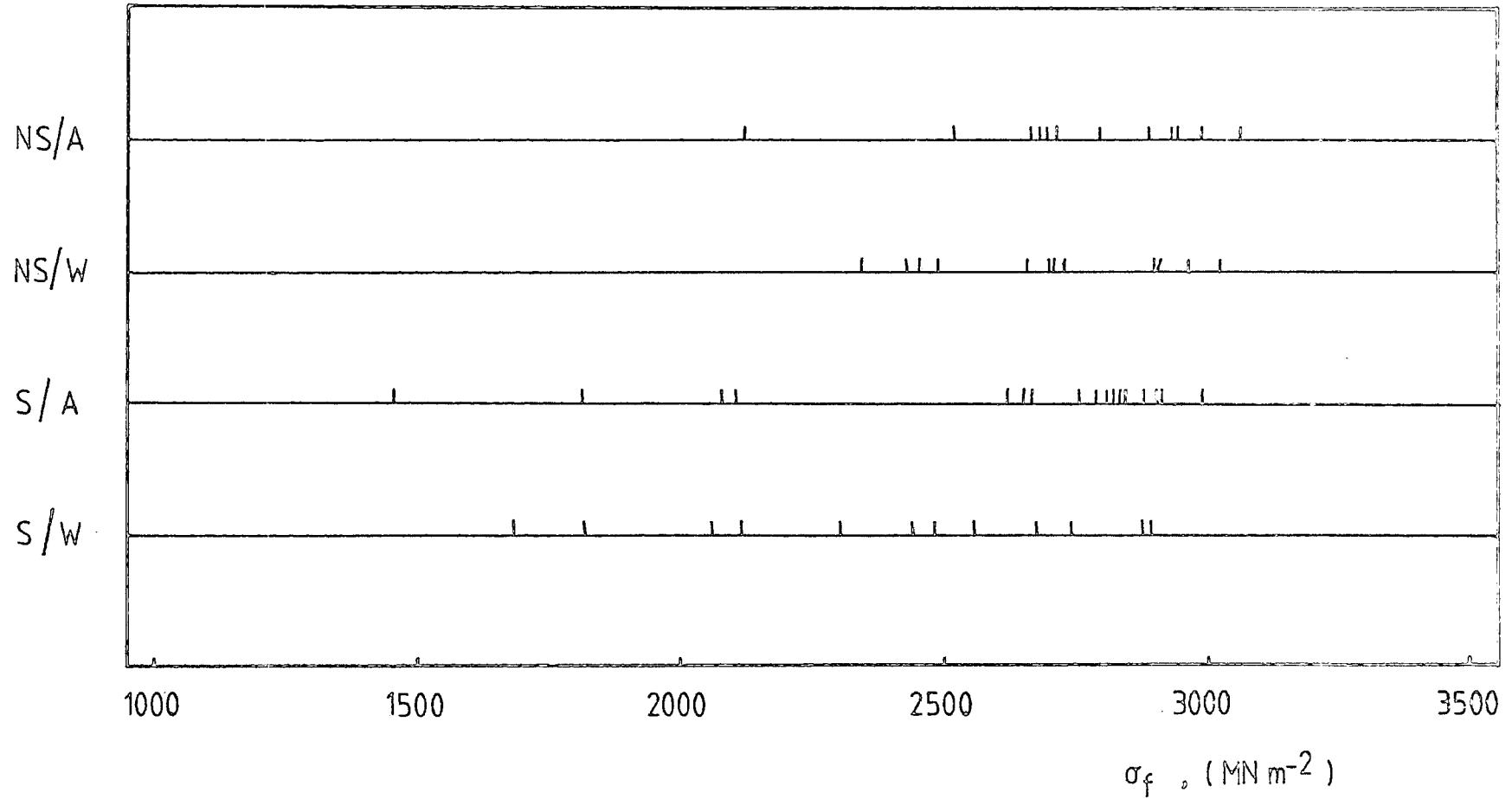


FIGURE 6.26: Strengths ( $\sigma_f$ ) recorded from stress rate tests at  $2\text{MN/m}^2\text{s}$  on WC-13% Co specimens at  $20^\circ\text{C}$ , in laboratory air (A), and distilled water (W), both with (S) and without (NS) a presoak of 150 hours in distilled water - preliminary environmental test data.

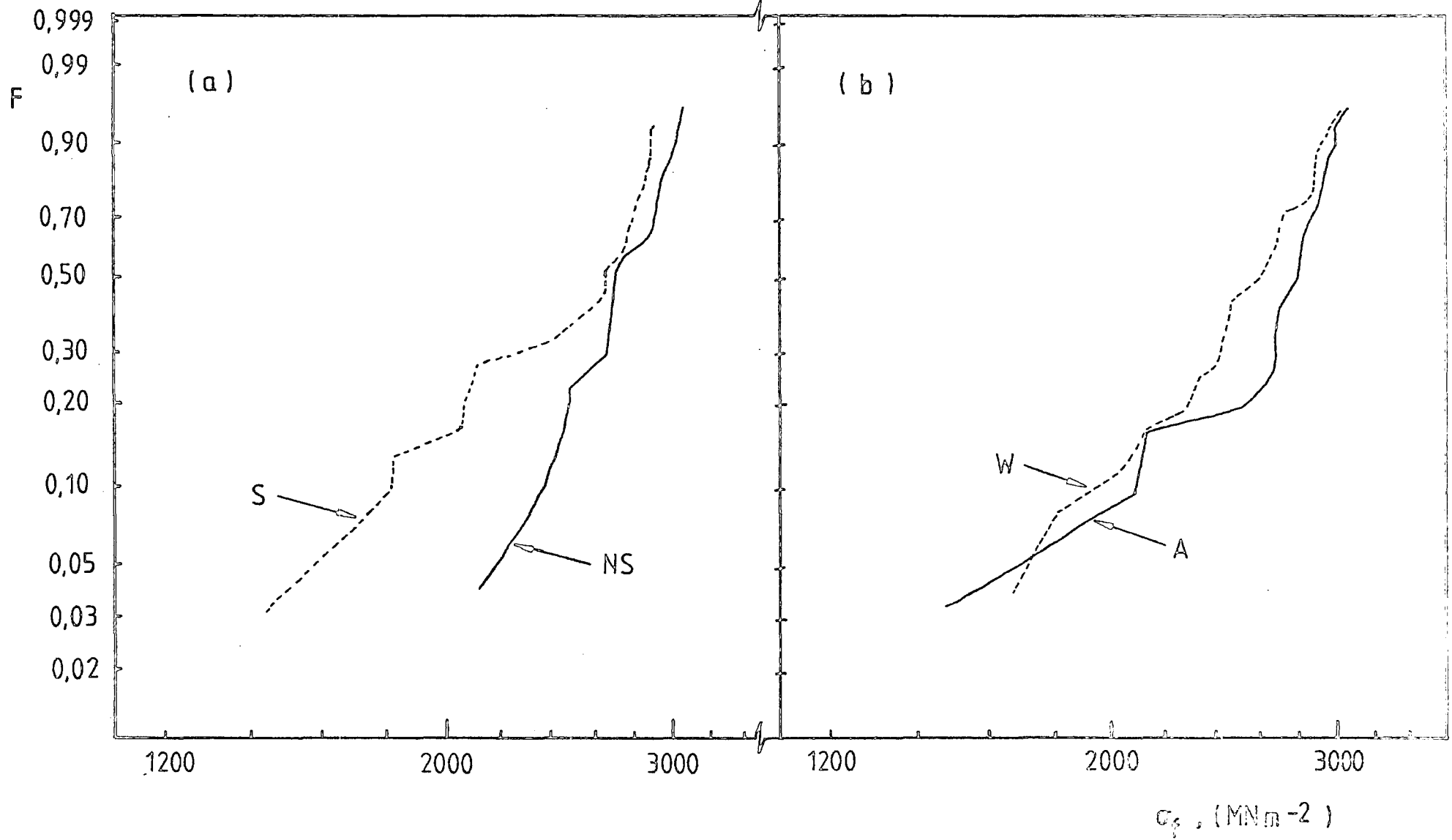


FIGURE 6.27: Weibull diagrams for preliminary environmental test data. (a), according to use of presoak (S), or not (NS), but independent of test environment; (b) according to test environment, laboratory air (A) or distilled water (W) but independent of use of presoak or not. F - cumulative failure probability;  $\sigma_f$  - fracture

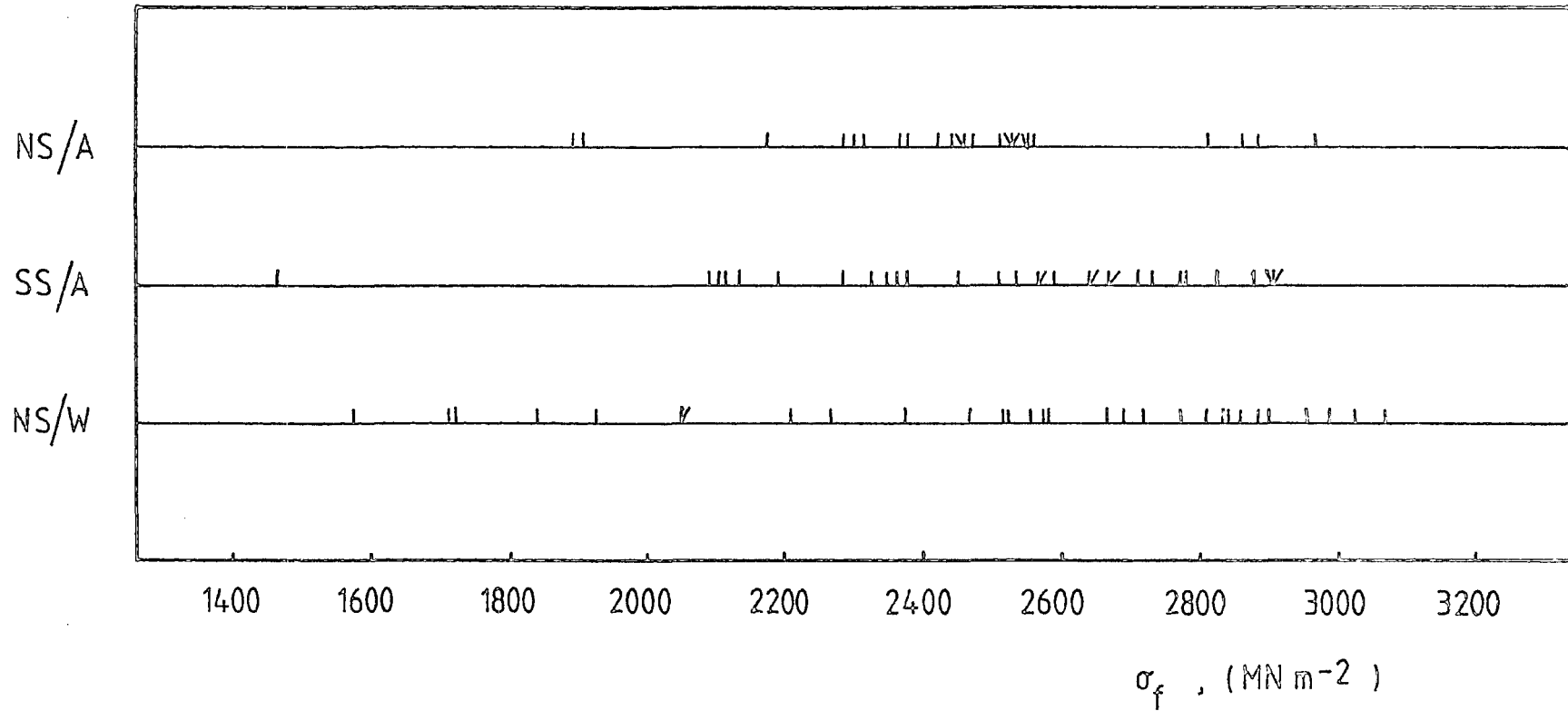


FIGURE 6.28: Strengths ( $\sigma_f$ ) recorded from stress rate tests at  $1 \text{ MN/m}^2\text{s}$  on WC-16% Co specimens at  $20^\circ\text{C}$ , in laboratory air with no presoak (NS/A), in laboratory air with a presoak in distilled water for 40 minutes (SS/A), and in distilled water with no presoak (NS/W) - main environmental test data.

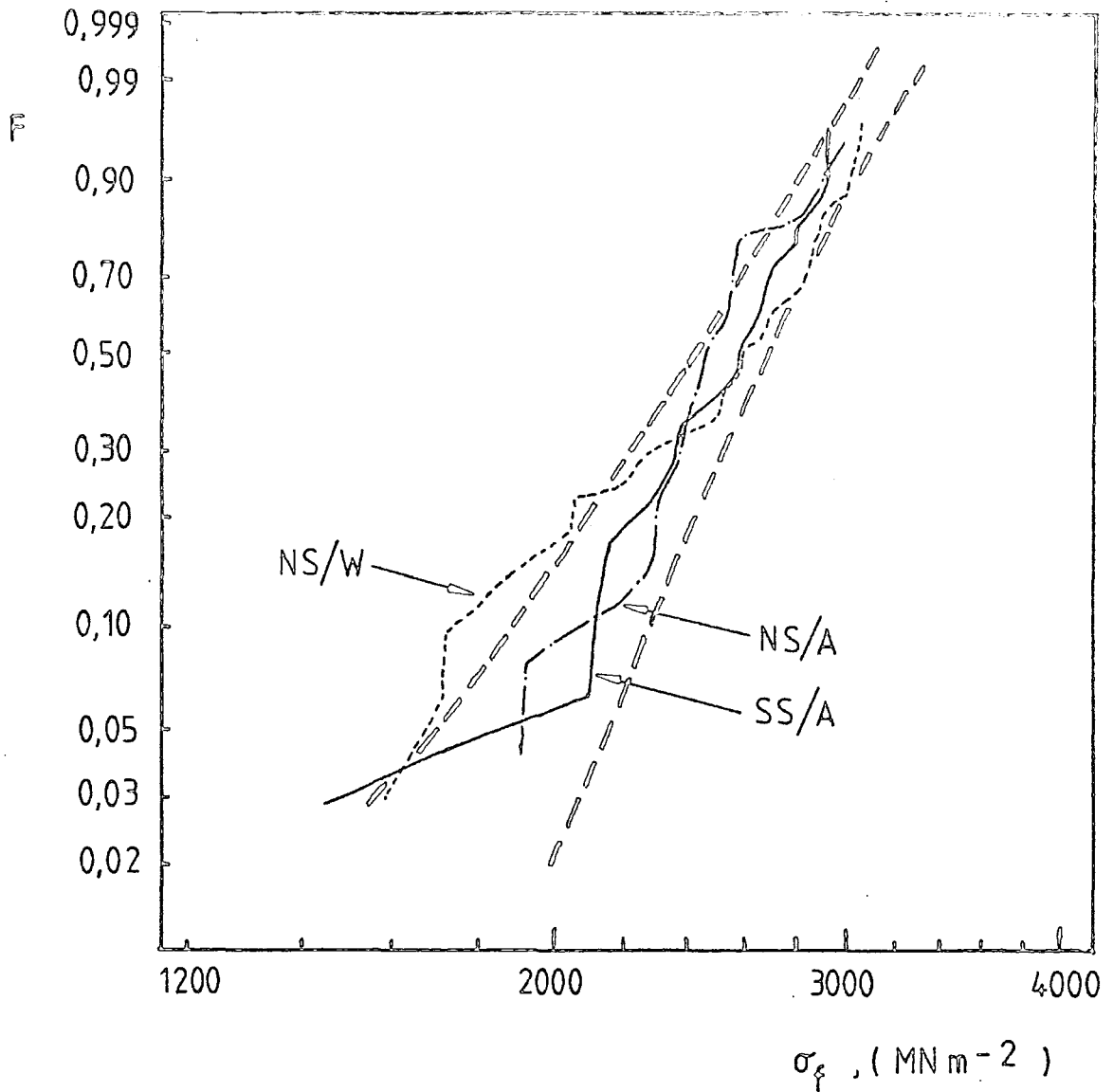


FIGURE 6.29: Weibull curves for main environmental test data, (see Figure 6.27 for details of symbols). Also shown (as thick dotted lines) are 5 and 95% confidence bands constructed about the best straight line passing through the SS/A data.  $F$  - cumulative failure probability;  $\sigma_f$  - fracture strength.

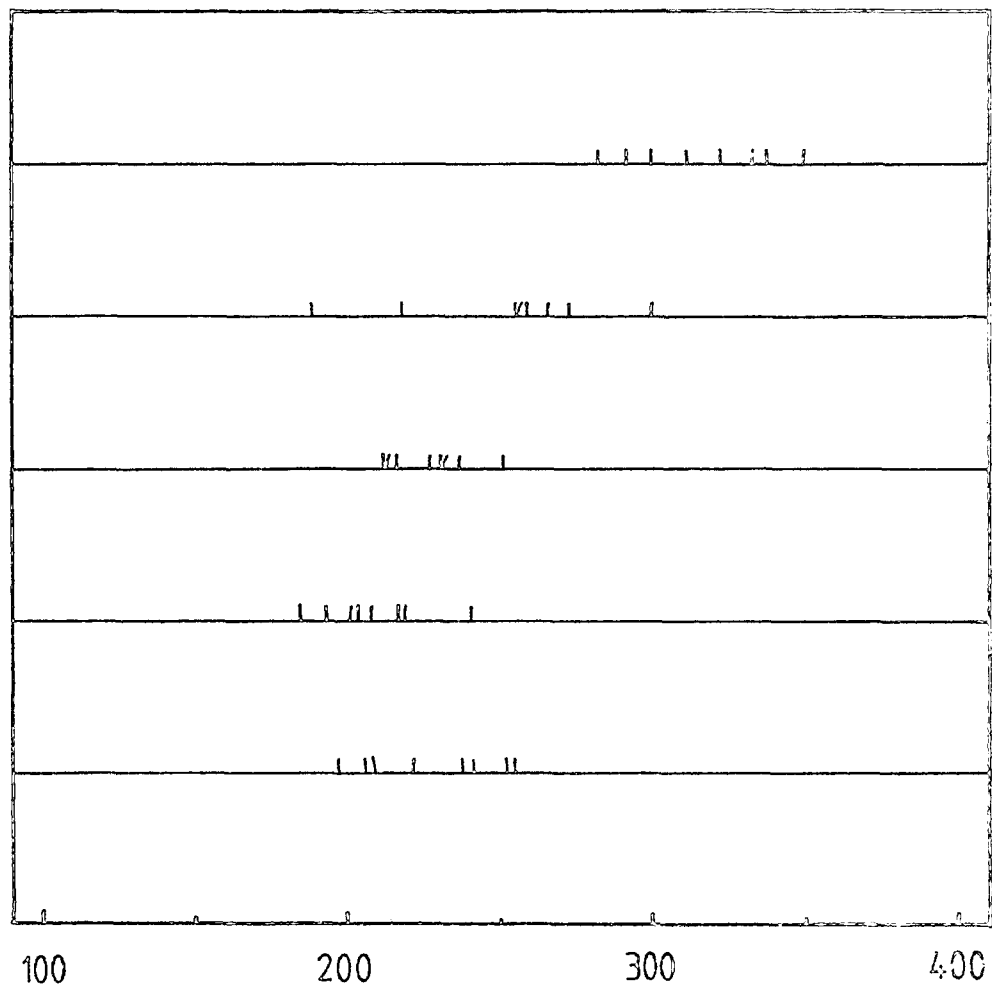
$$NS/A/\dot{\sigma} = 230 \text{ MN m}^{-2} \text{ s}^{-1}$$

$$NS/R/\dot{\sigma} = 230 \text{ MN m}^{-2} \text{ s}^{-1}$$

$$NS/R/\dot{\sigma} = 2,3 \text{ MN m}^{-2} \text{ s}^{-1}$$

$$NS/R/\dot{\sigma} = 0,023 \text{ MN m}^{-2} \text{ s}^{-1}$$

$$S/R/\dot{\sigma} = 2,3 \text{ MN m}^{-2} \text{ s}^{-1}$$



$\sigma_f$  , (MN m<sup>-2</sup>)

FIGURE 6.30: Strengths ( $\sigma_f$ ) recorded from stress rate ( $\dot{\sigma}$ ) tests on  $\text{Al}_2\text{O}_3$  specimens at  $20^\circ\text{C}$  in laboratory air (A), and Ringers Solution (R), both with (S) and without (NS) a presoak for one hour in Ringers Solution.

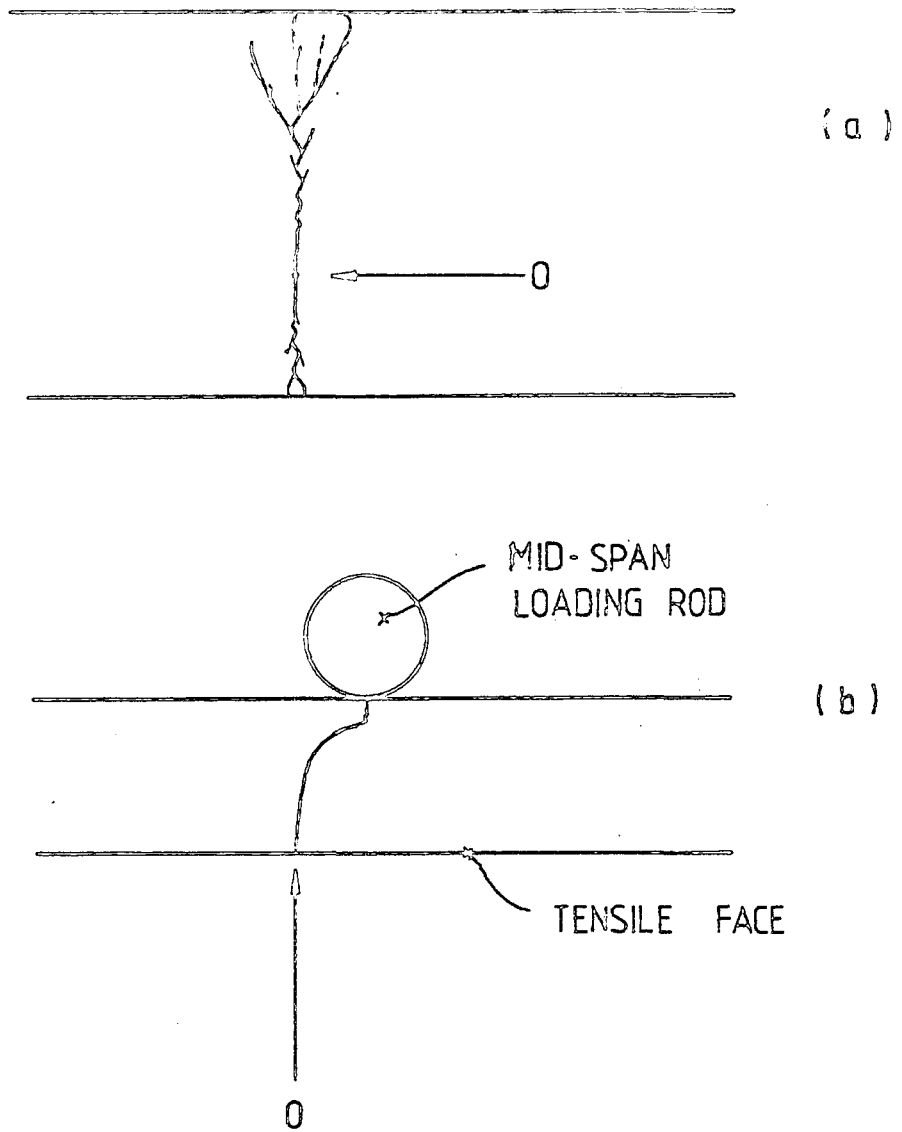


FIGURE 6.31: External views of a fractured bend specimen drawn diagrammatically. (a) tensile face; (b) side view. O indicates the site of fracture initiation.

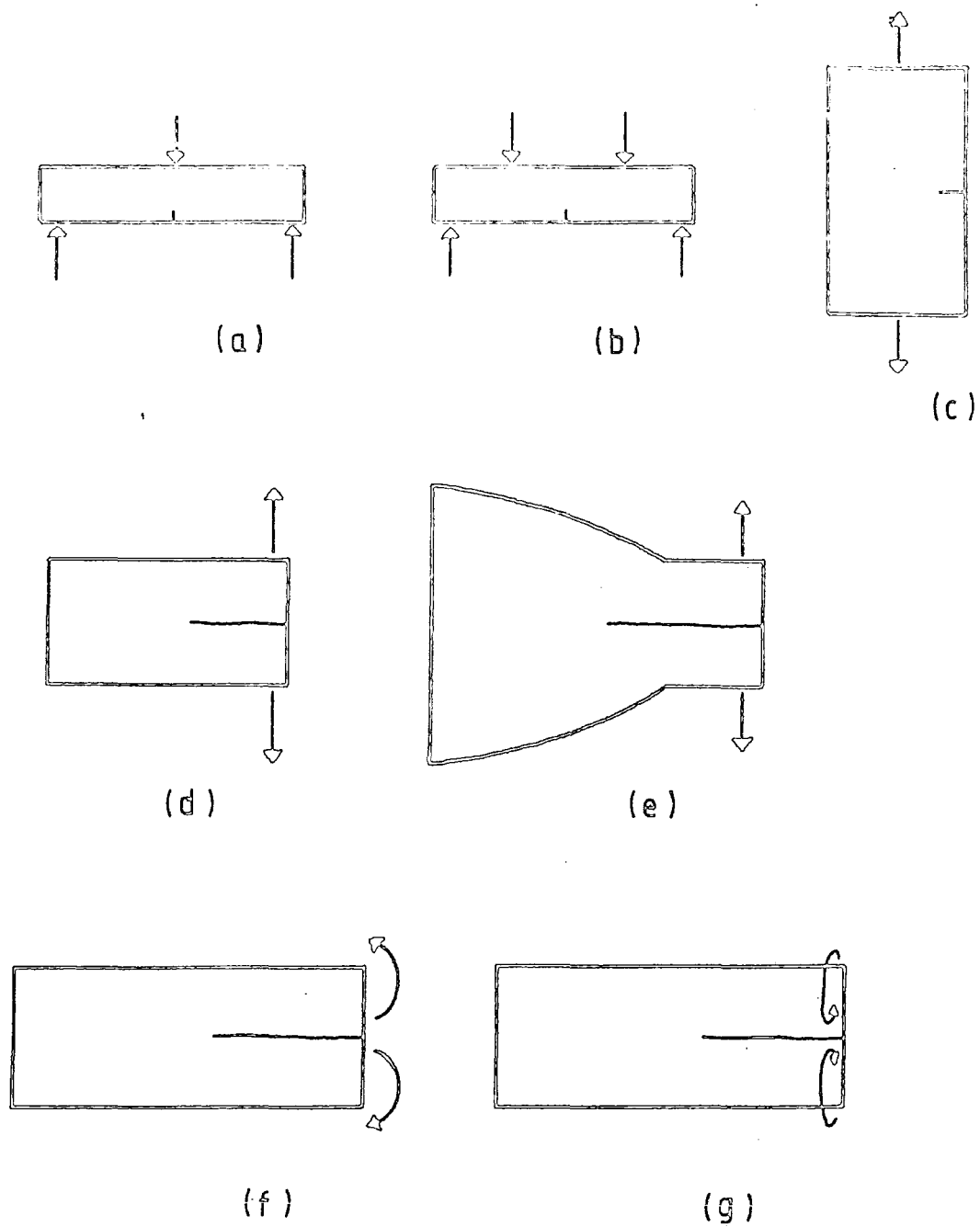


FIGURE 7.1: Common large crack technique configurations. (a), edge cracked three point bend; (b) edge cracked four point bend; (c) compact tension; (d), double cantilever beam; (e), tapered double cantilever beam; (f), constant moment; (g), double torsion.

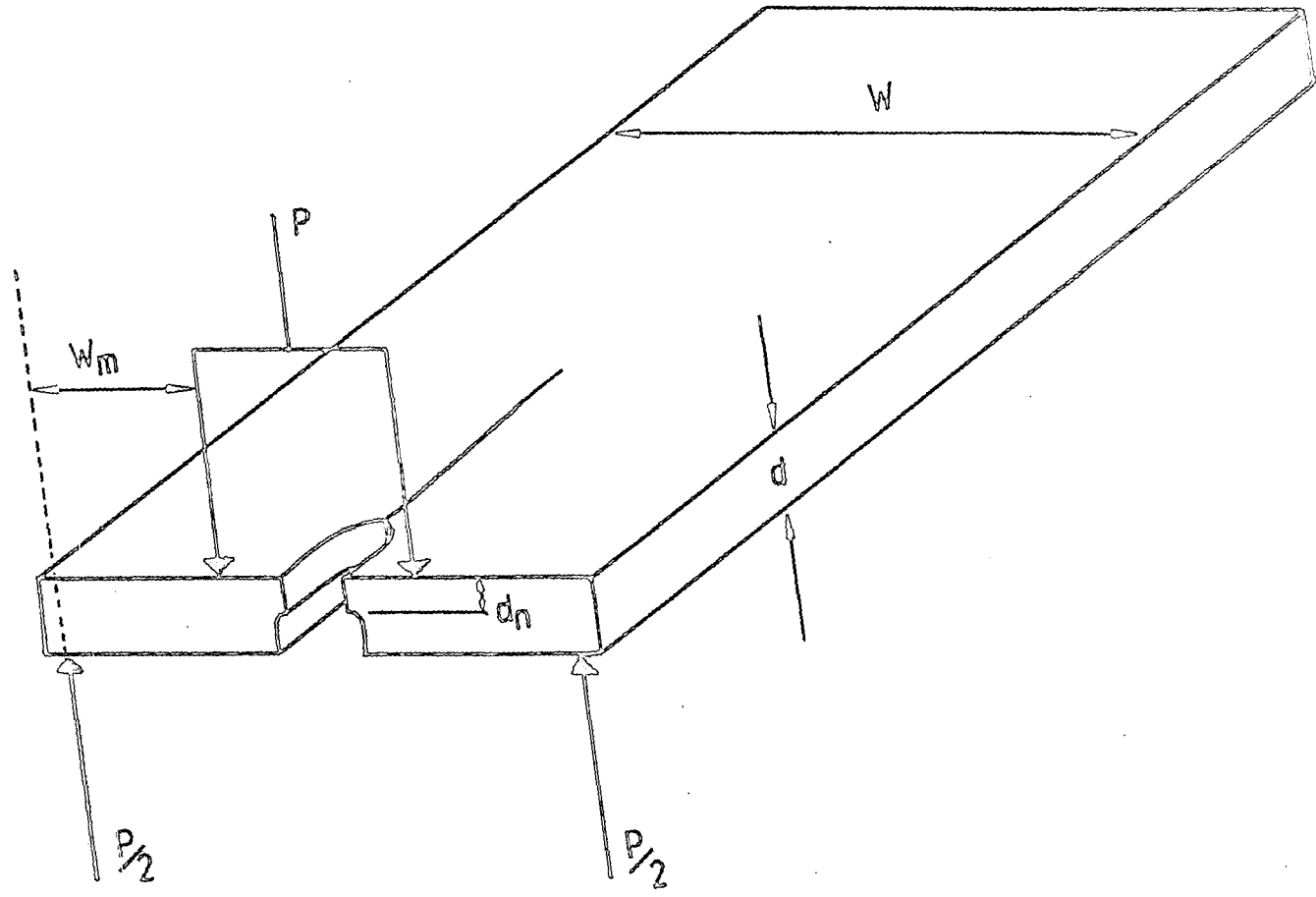


FIGURE 7.2: The double torsion specimen. (Symbols are described in the text.)

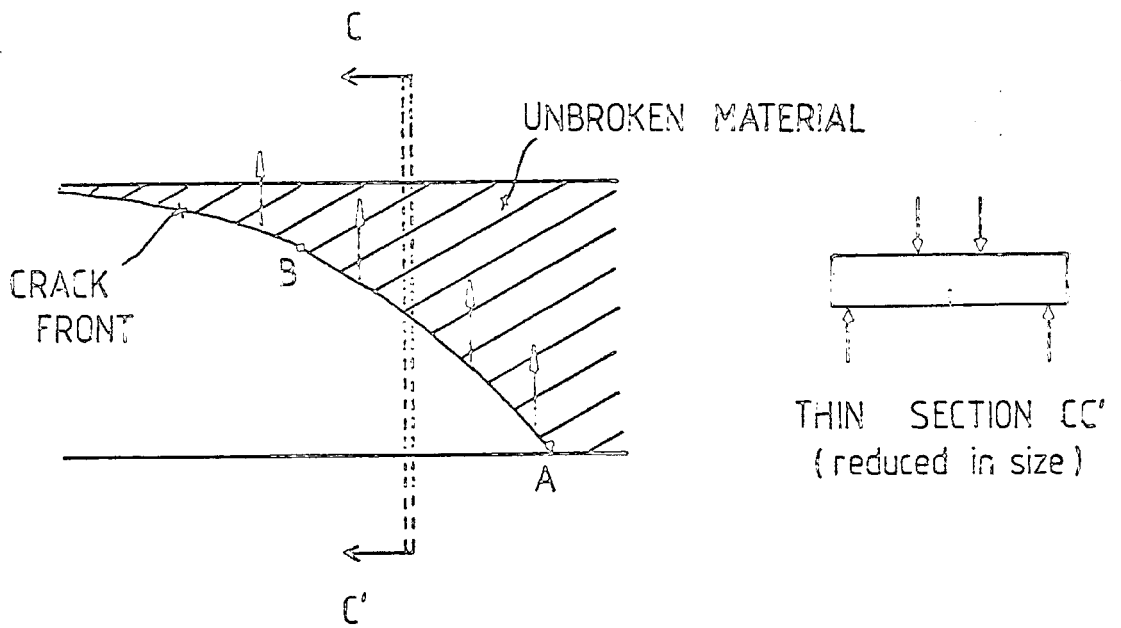


FIGURE 7.3: Double torsion crack front, drawn diagrammatically to show direction of cracking. (Symbols are described in the text.)

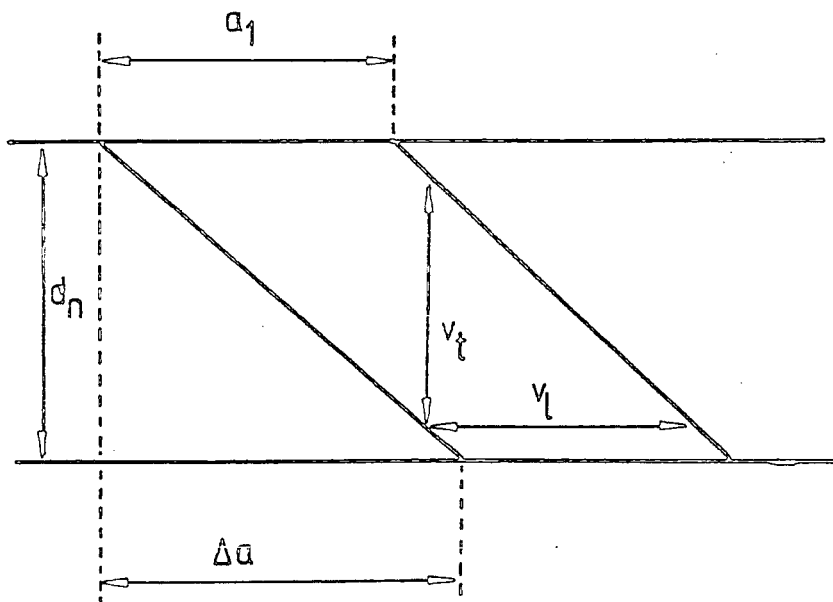


FIGURE 7.4: Double torsion crack growth model.  $a_1$  is the extent of lengthwise cracking in unit time. (Other symbols are described in the text.)

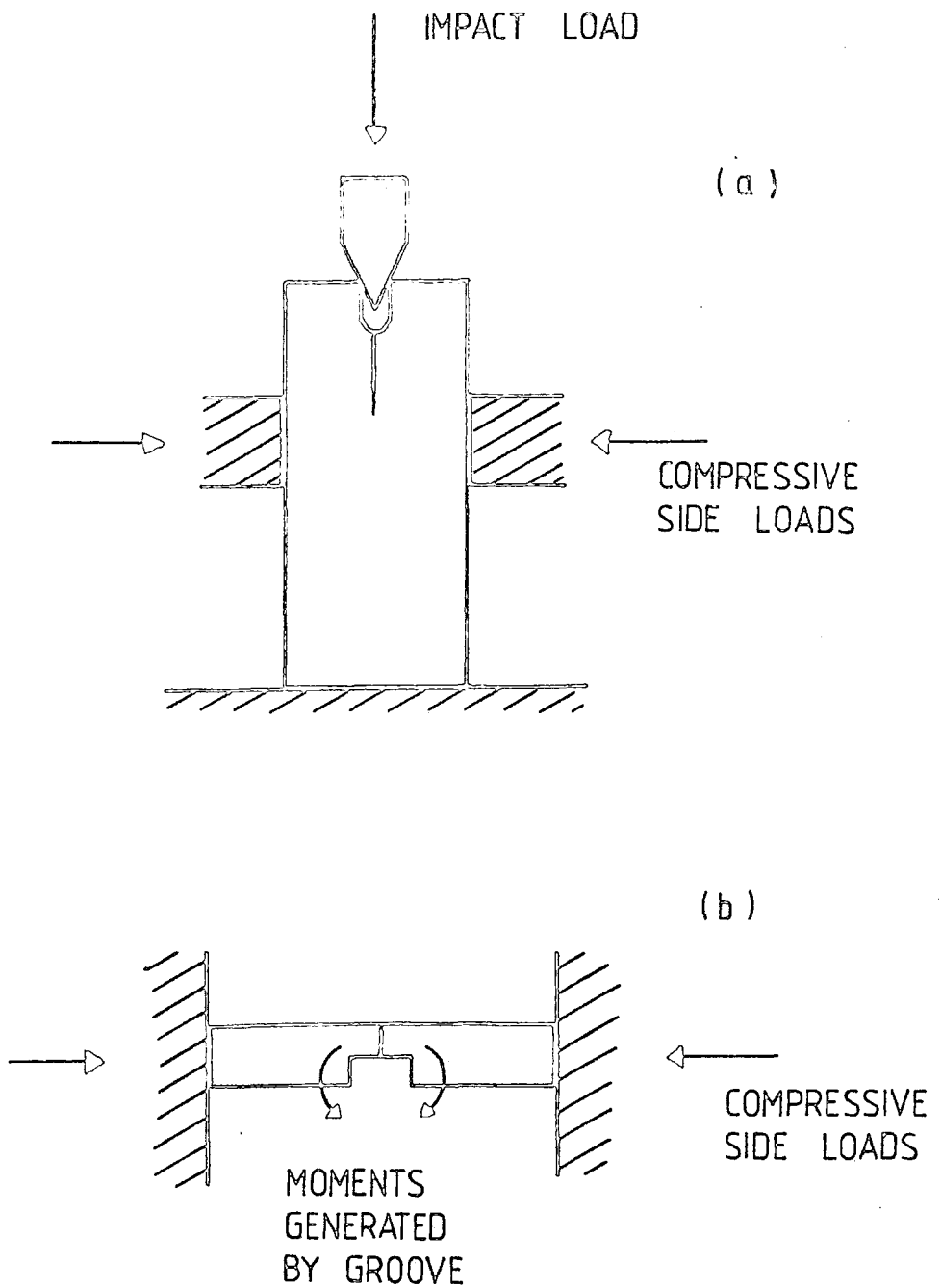


FIGURE 7.5: Impact loading technique for precracking double torsion specimens. (a), general scheme; (b), view from top, showing moments generated by the groove under compressive side loads (tending to open the crack).

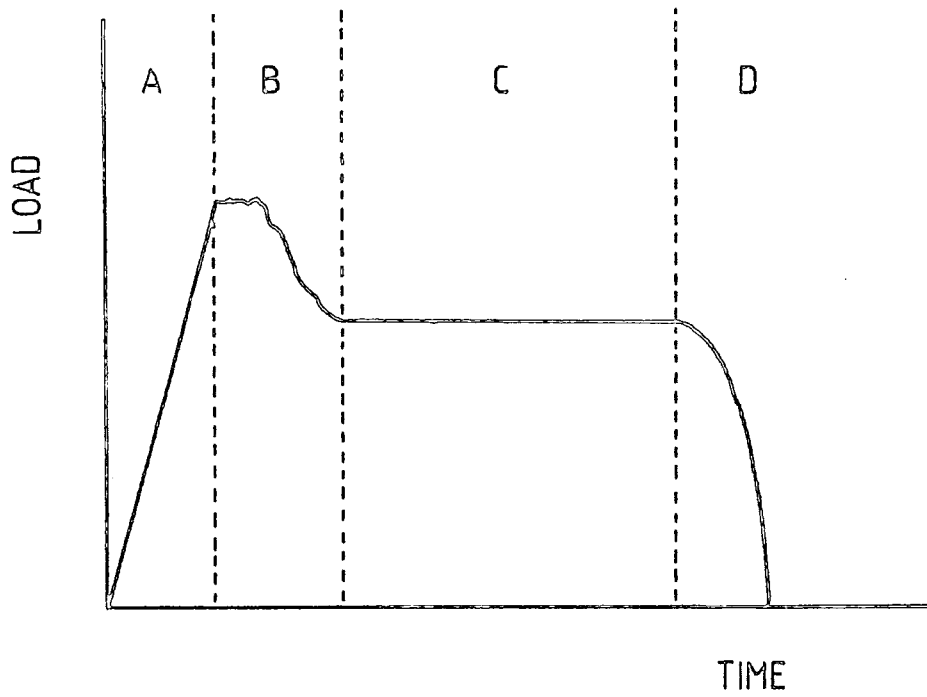


FIGURE 7.6: Typical load-time record for crack growth through a double torsion specimen loaded under a constant displacement rate.

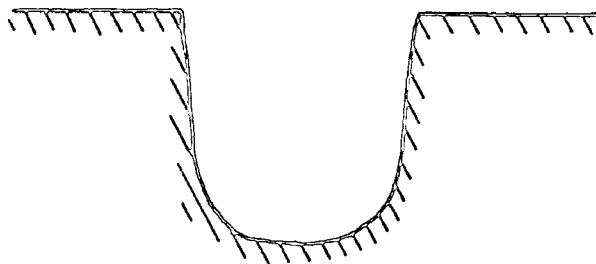


FIGURE 7.7: Approximate shape, in cross-section of crack-guiding grooves in double torsion specimens used in this study.

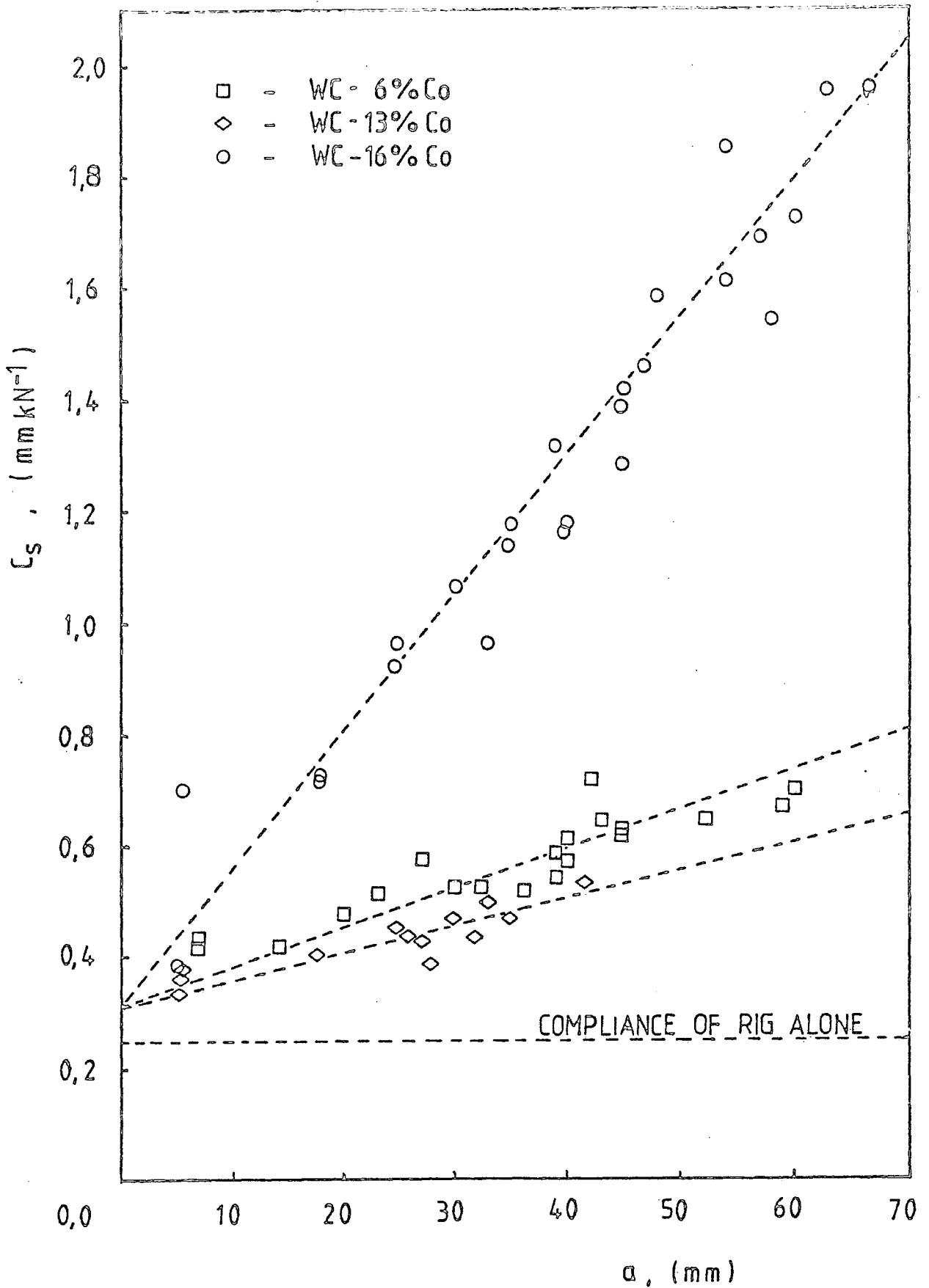


FIGURE 7.8: Compliance calibration diagram for double torsion specimens.  $C_s$  - compliance of specimen and rig;  $a$  - crack length.

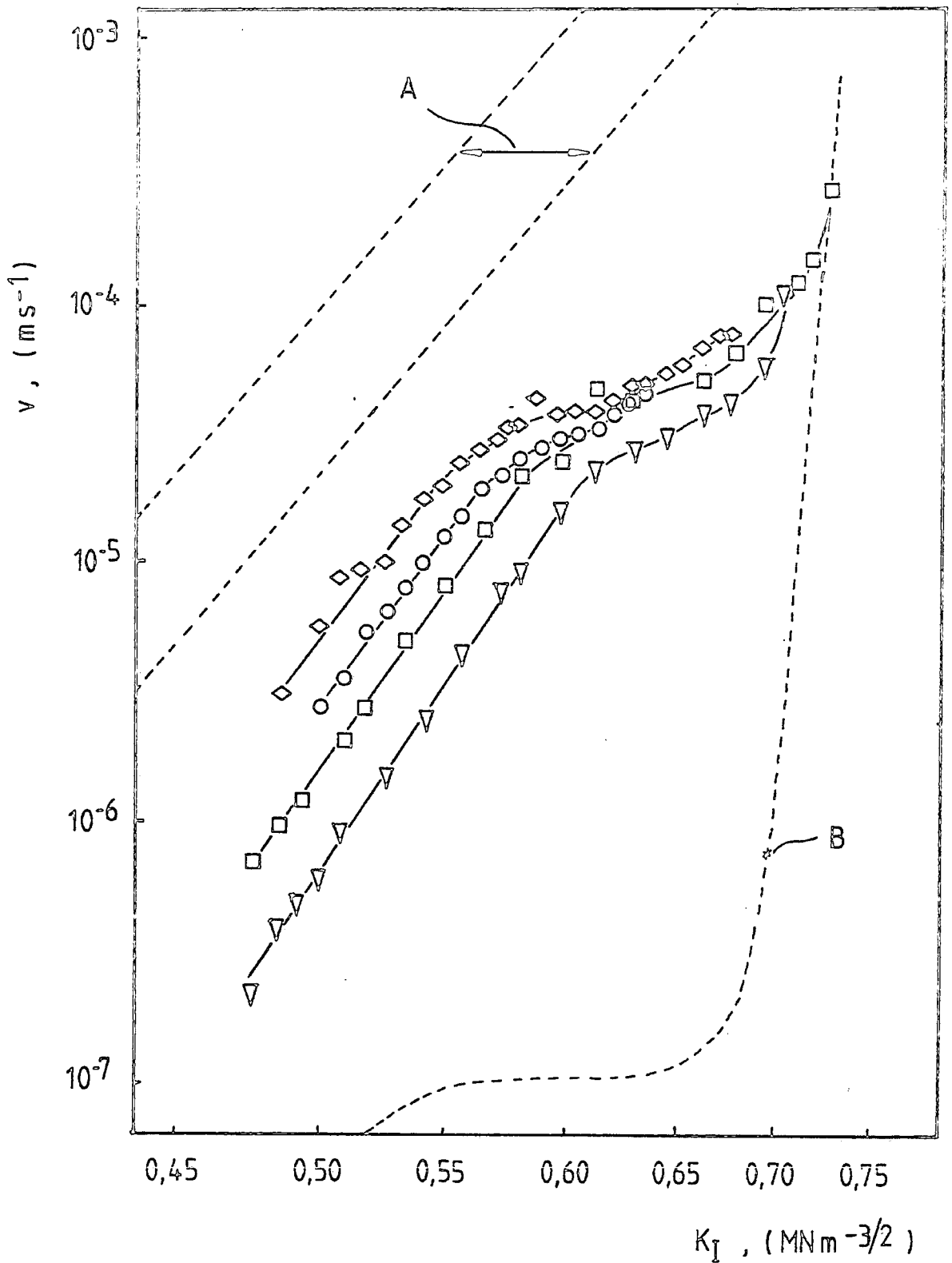


FIGURE 7.9:  $K_I$ - $v$  diagram for soda-lime glass at  $20^\circ\text{C}$  in laboratory air. Also shown are the spread of results from tests in distilled water (A), and results from tests in toluene (both at  $25^\circ\text{C}$ ) obtained by Evans (1972).  $K_I$  - stress intensity factor in crack opening mode (I);  $v$  - crack tip velocity.

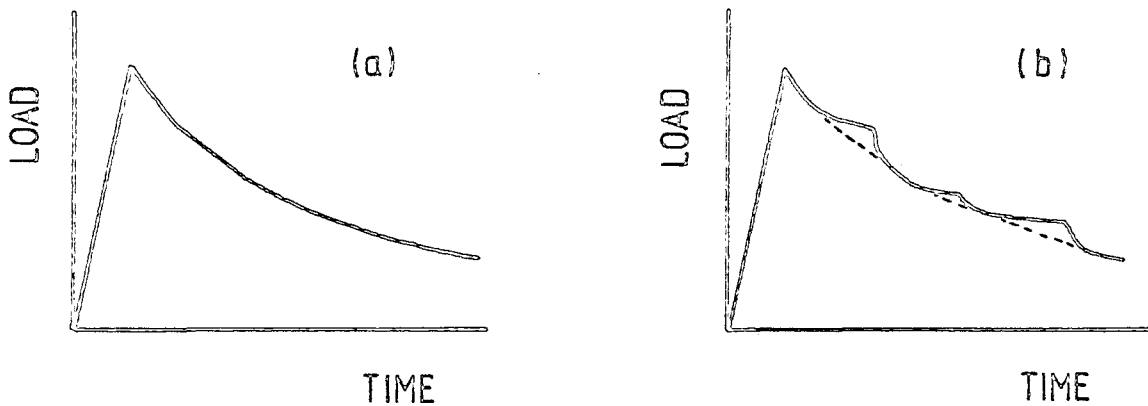


FIGURE 7.10: Typical form of load relaxation curves for (a), soda-lime glass, and (b), WC-Co materials.

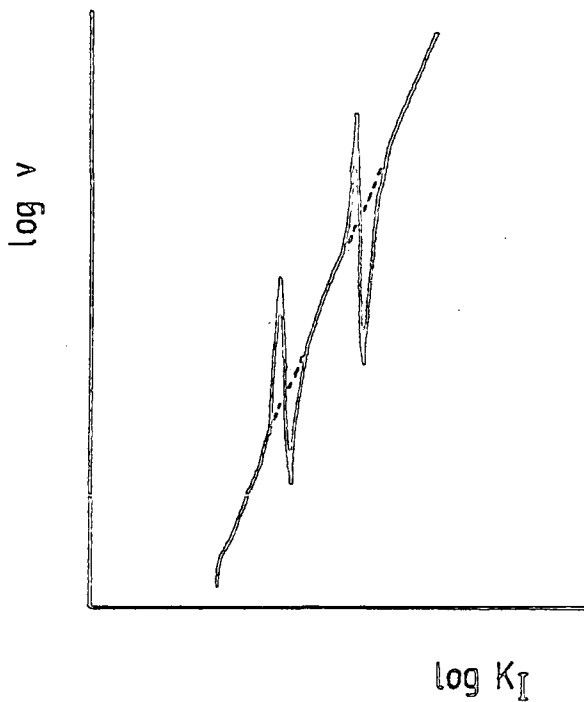


FIGURE 7.11: Typical form of  $K_I$ - $v$  diagram for WC-Co materials, showing the effect of "jumps" in load relaxation curves.

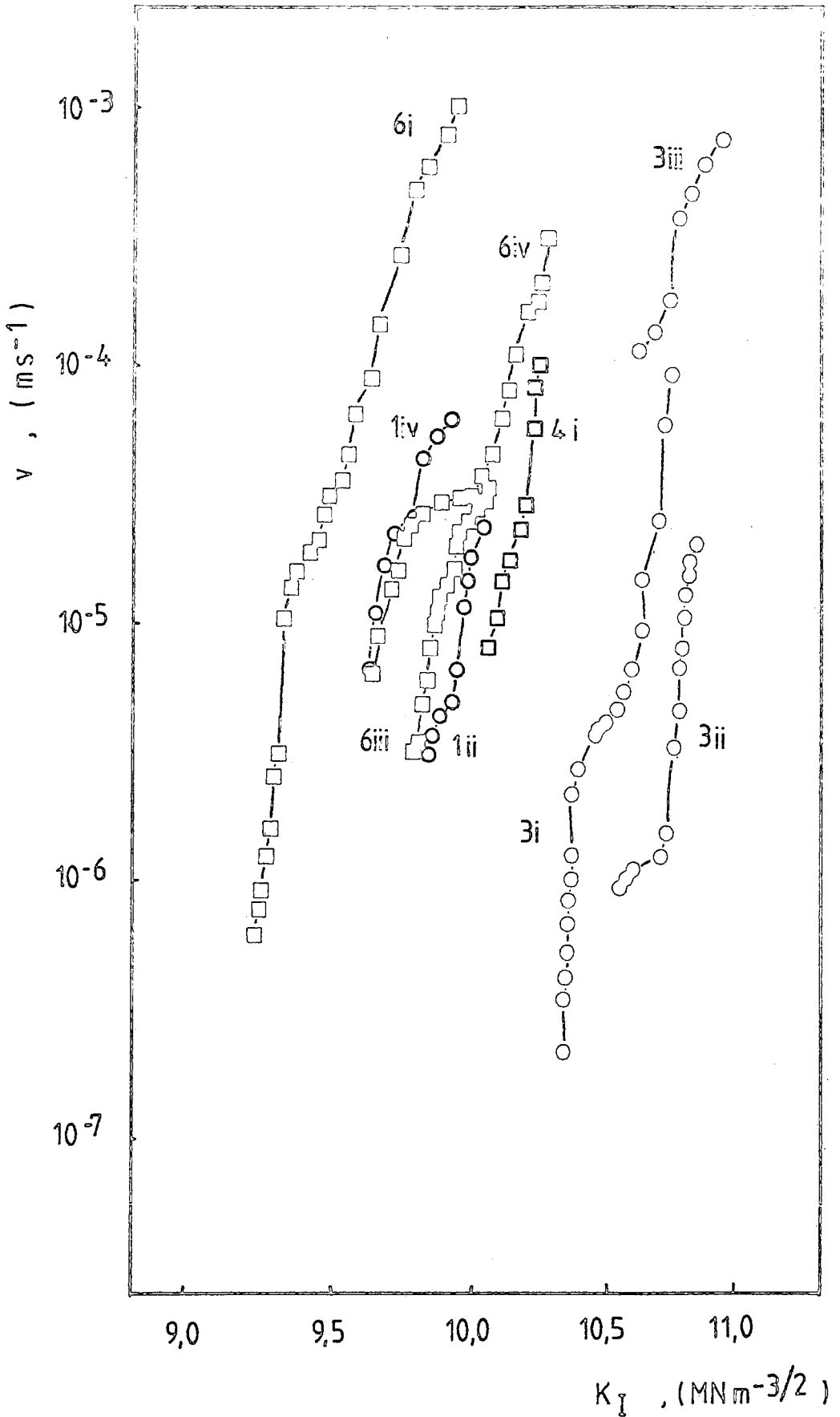


FIGURE 7.12:  $K_I$ - $V$  diagram for WC-6% Co at 20°C in laboratory air. Measurements from the same specimen are represented by the same symbol on the diagram. Adjacent numbers refer to, firstly, the specimen test number followed by the load relaxation number (in Roman numerals).

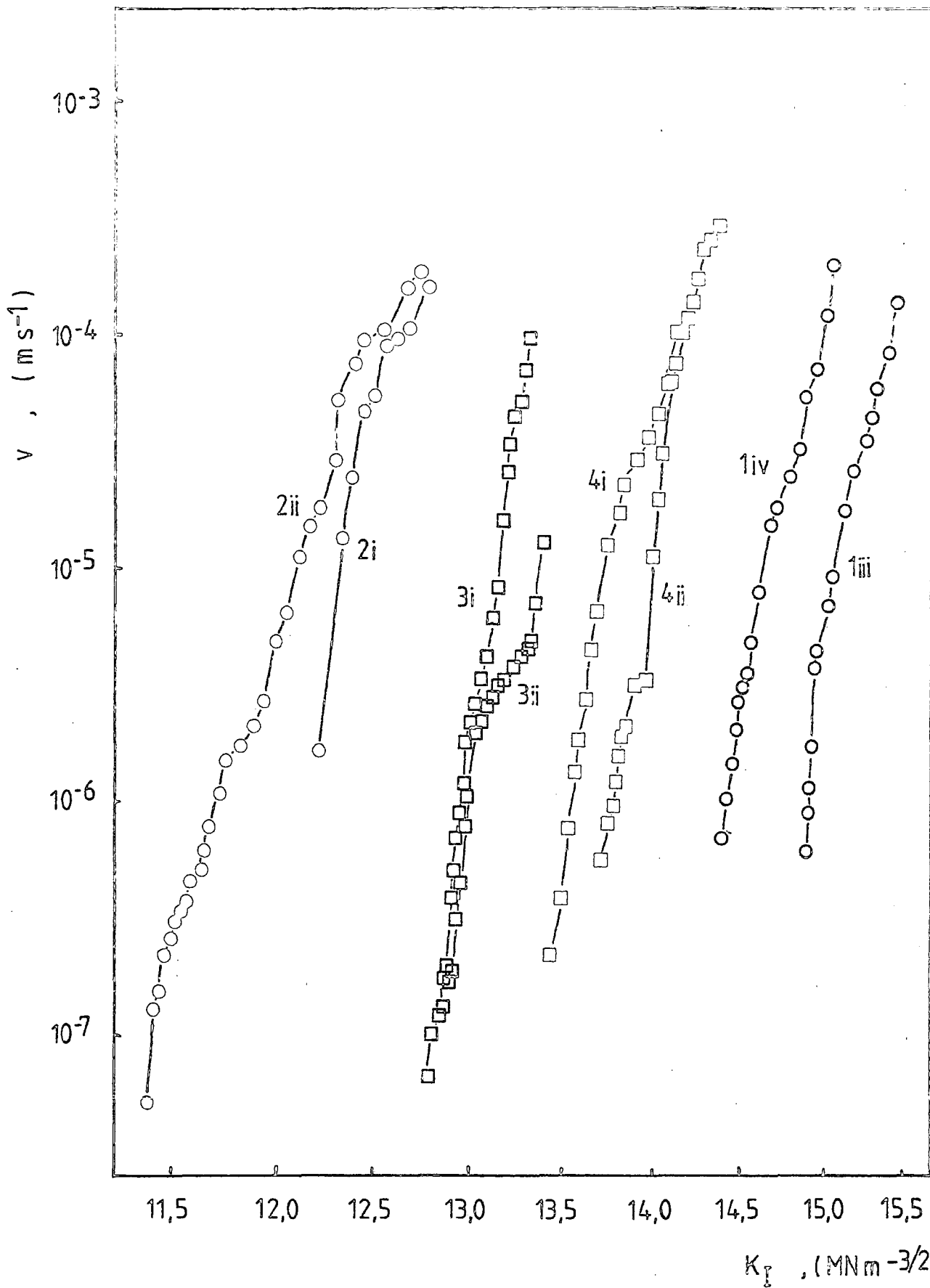


FIGURE 7.13:  $K_I$ - $v$  diagram for WC-16% Co at 20°C in laboratory air. See Figure 7.12 for details.

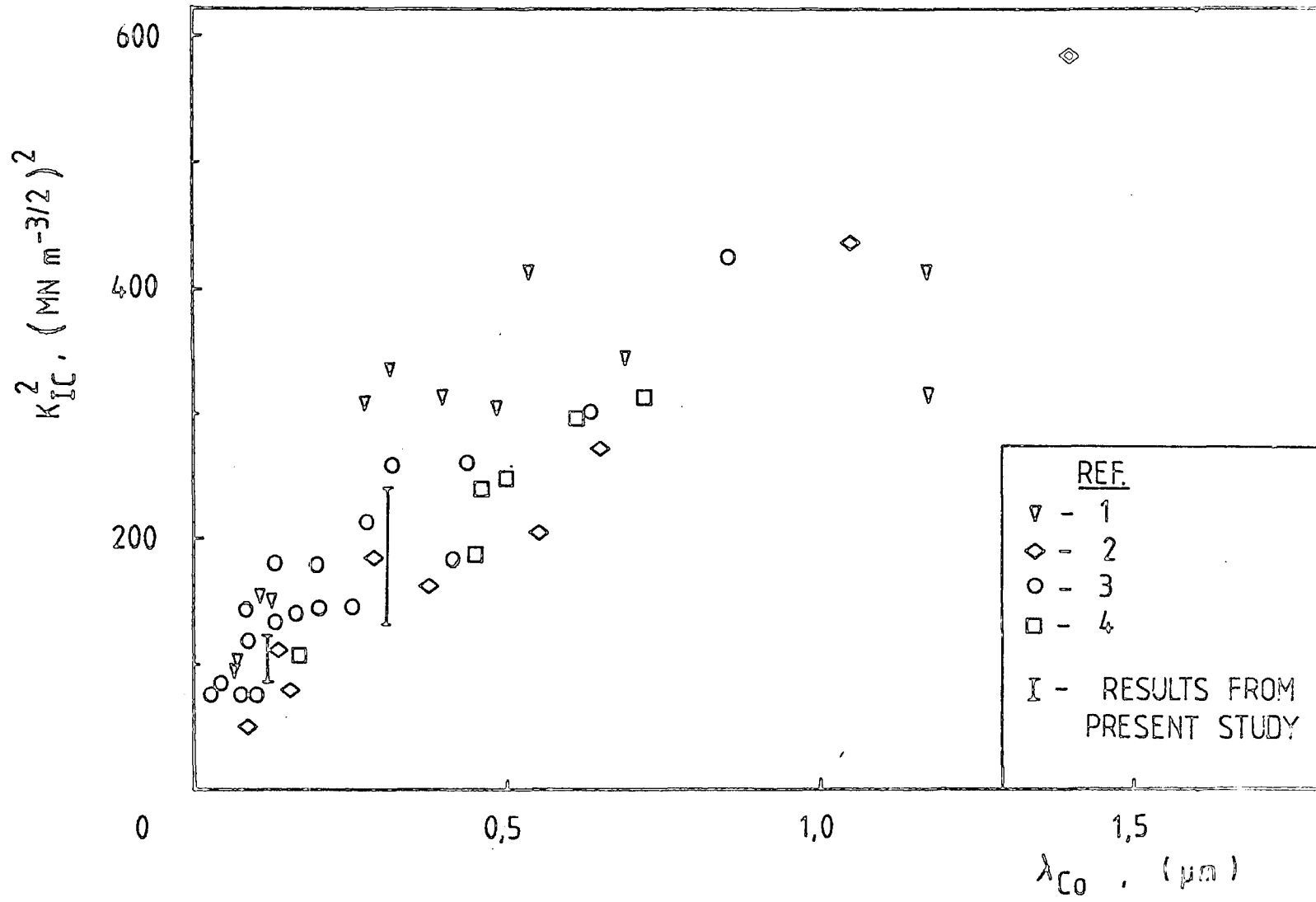


FIGURE 7.14: Ranges of  $K_I$  measured from double torsion slow crack growth tests on WC-6% Co and WC-16% Co compared with values of  $K_{IC}$  for WC-Co materials, found in the literature. (Refs: 1 - Inglestrom, Nordberg (1974); 2 - Lueth (1974); 3 - Chermant, Osterstock (1976); 4 - Murray (1977))

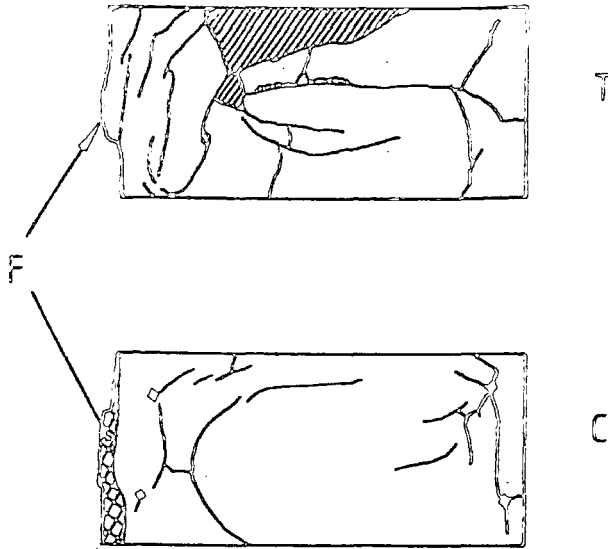


FIGURE 7.15: Cracked surfaces of the first WC-16% Co specimen to be soaked in a 10% solution of nitric acid - after 3 days. F, fracture face; T, tensile face; C, compressive face. Shaded regions indicate where chips have broken away.

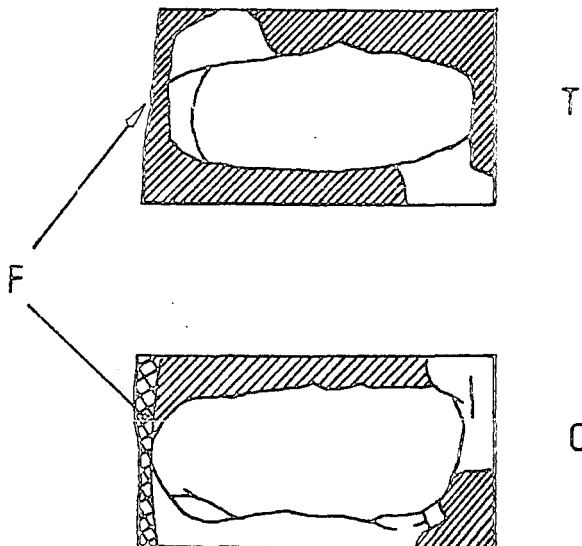


FIGURE 7.16: Cracked surfaces of the first WC-13% Co specimen to be soaked in a 10% solution of nitric acid - after 1 day. (See Figure 7.15 for details of symbols.)

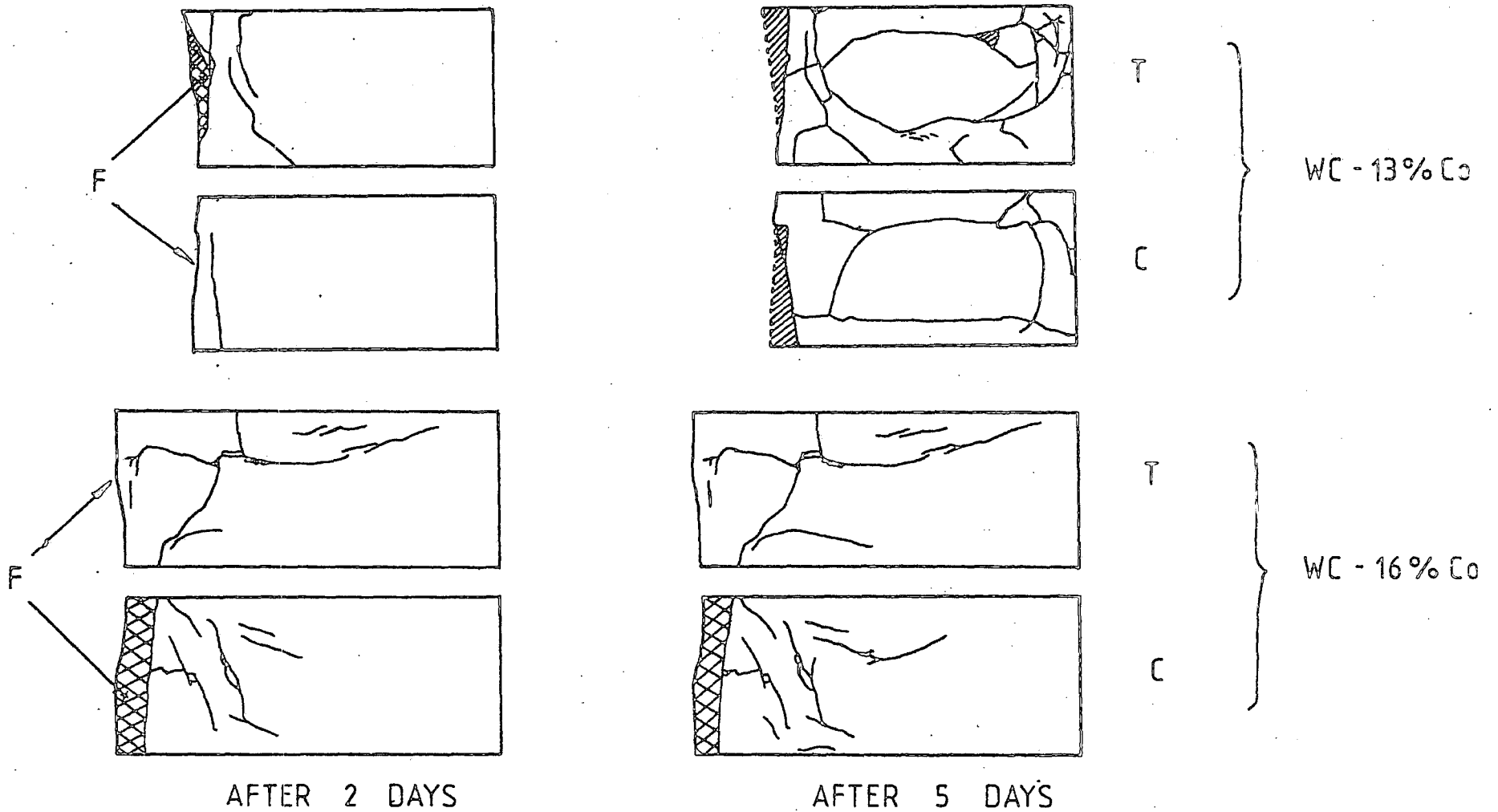


FIGURE 7.17: Cracked surfaces of the second WC-13% Co and WC-16% Co specimens to be soaked in a 10% solution of nitric acid - after 2, and 5 days (see Figure 7.15 for details of symbols).

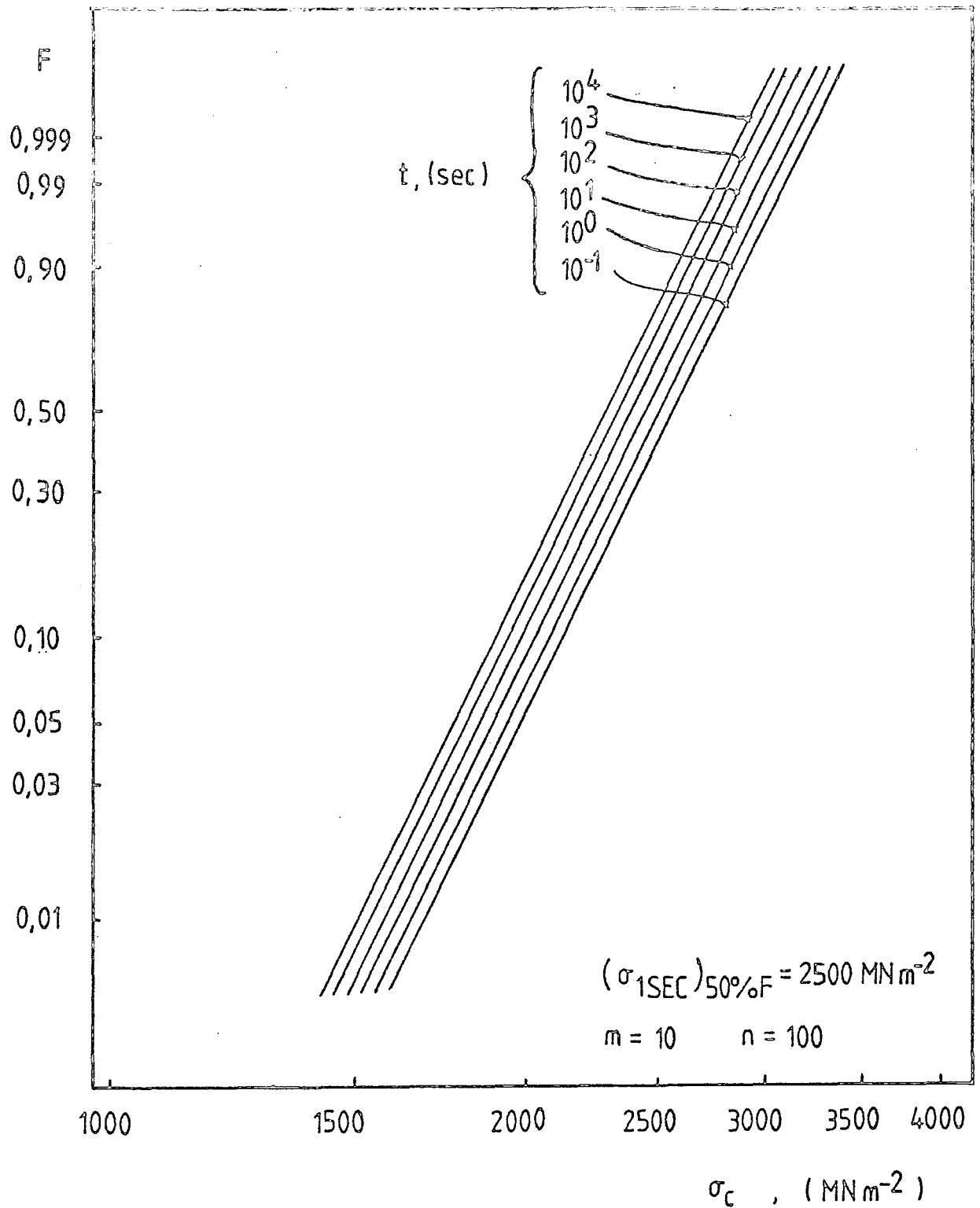


FIGURE 8.1: Typical SPT diagram for WC-Co materials in ambient conditions.  $F$  - cumulative failure probability;  $\sigma_c$  - constant applied stress;  $t$  - lifetime.

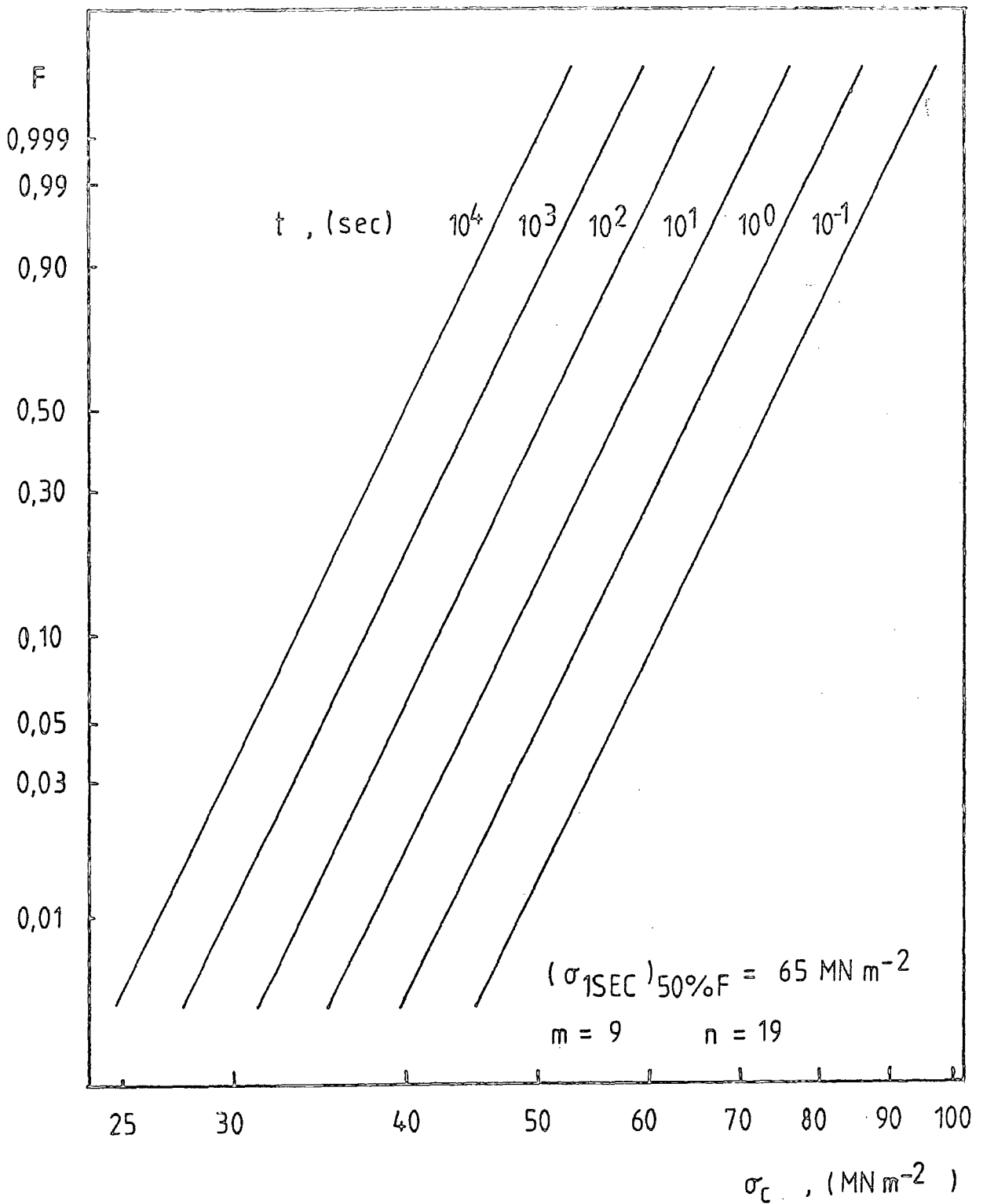
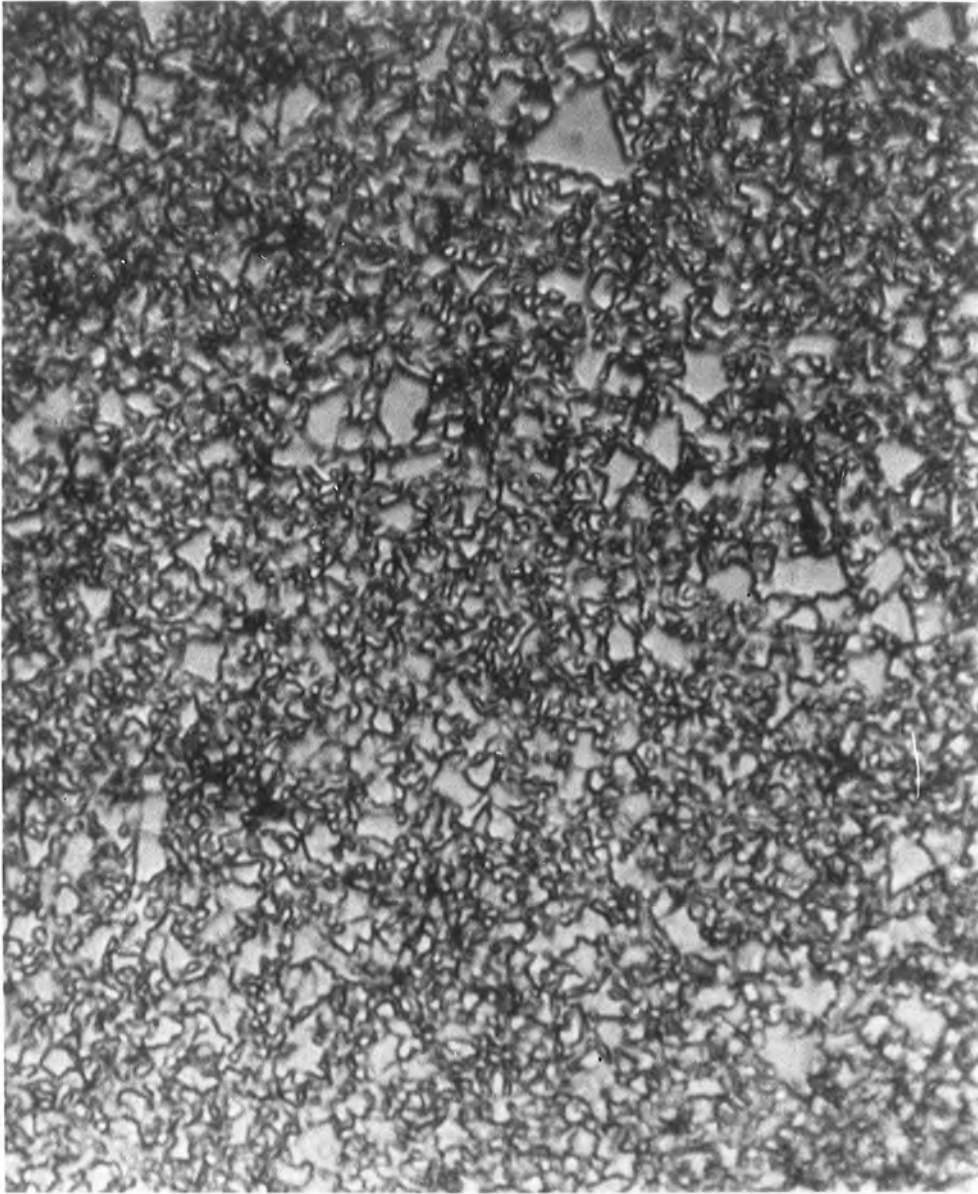


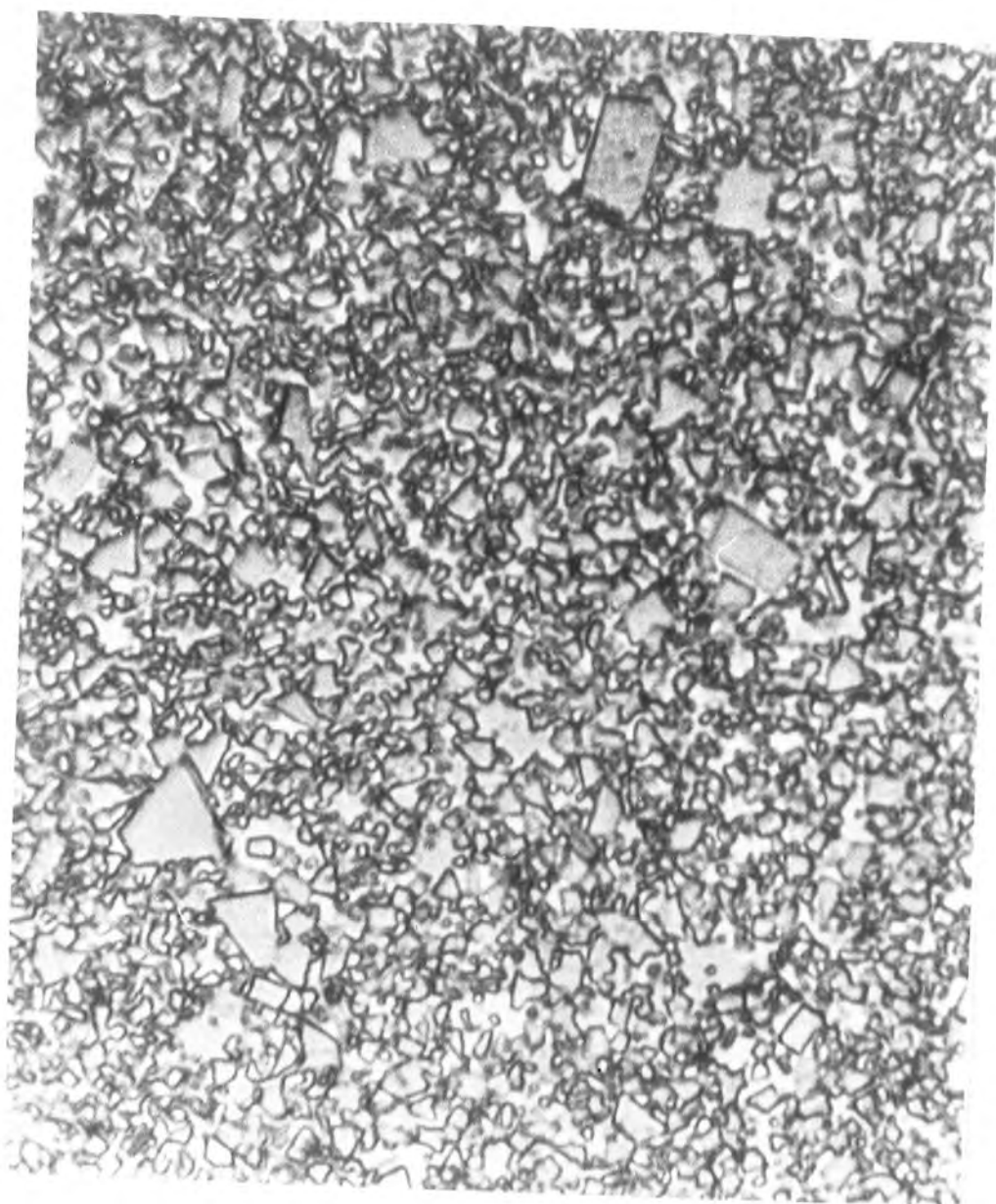
FIGURE 8.2: SPT diagram for soda-lime glass in laboratory air at 20°C.  $F$  - cumulative failure probability;  $\sigma_c$  - constant applied stress;  $t$  = lifetime.





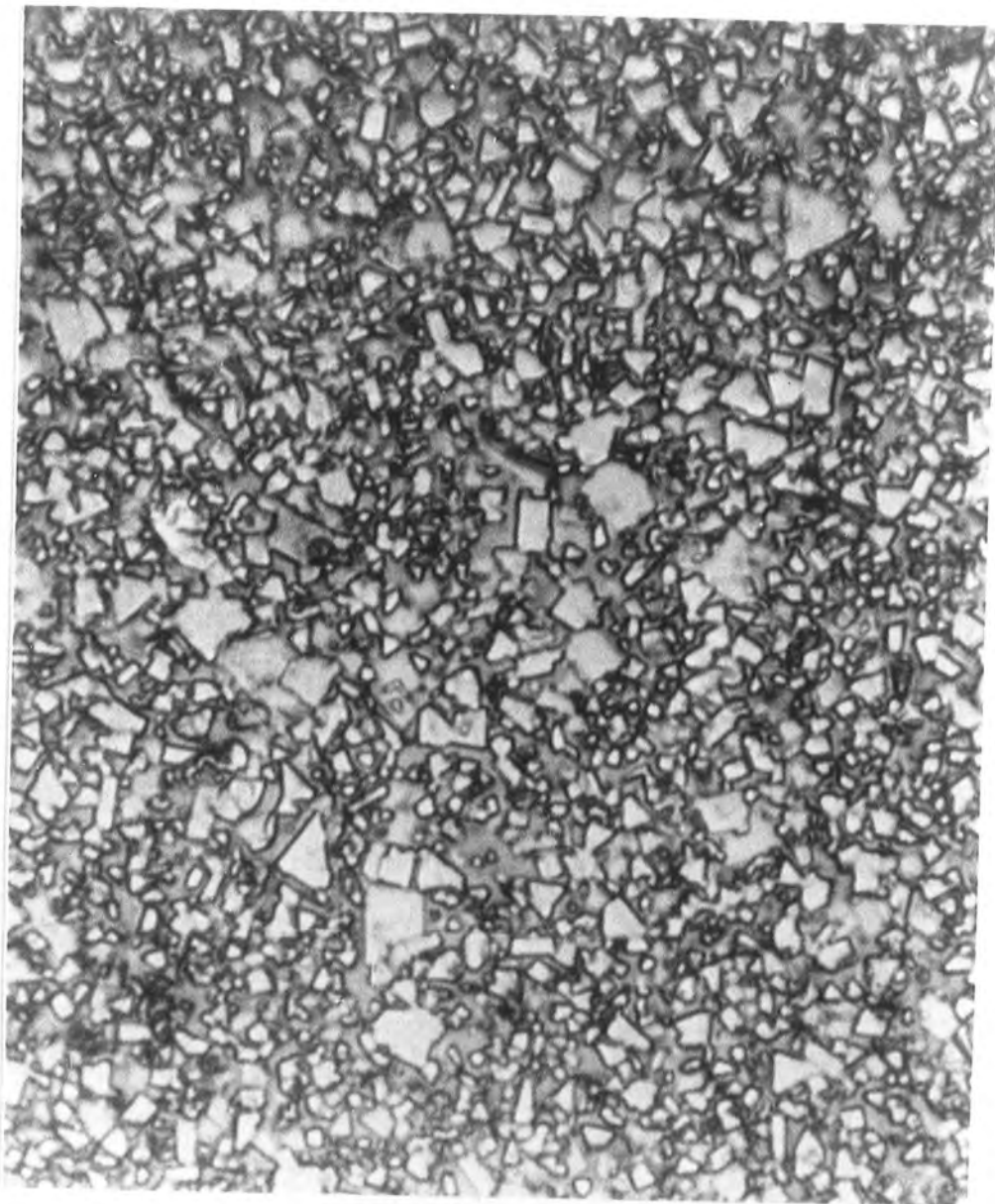
10  $\mu\text{m}$

PLATE 5.1: Etched surface of WC-6% Co.



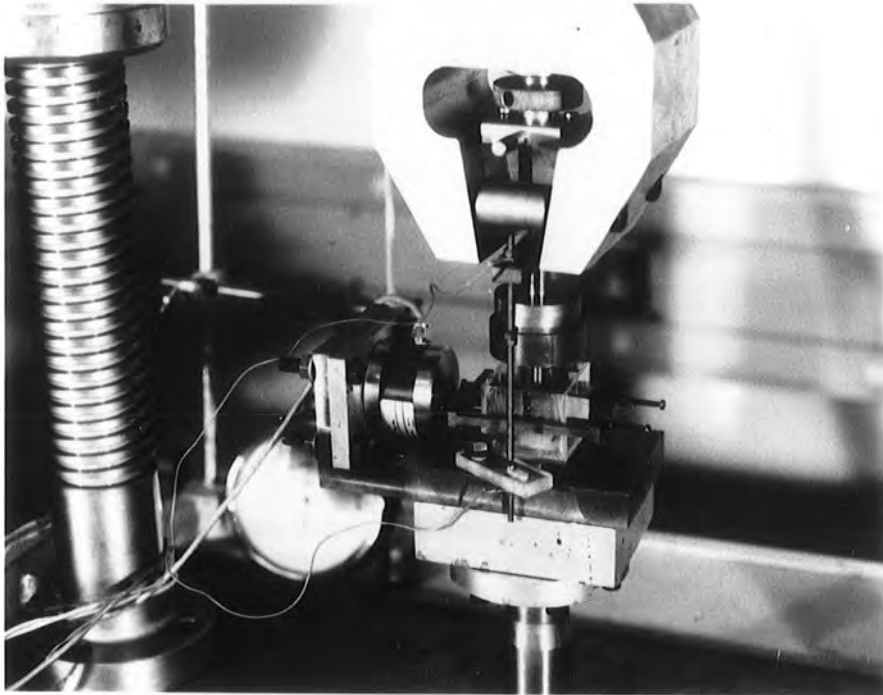
10  $\mu\text{m}$

PLATE 5.2: Etched surface of WC-13% Co.

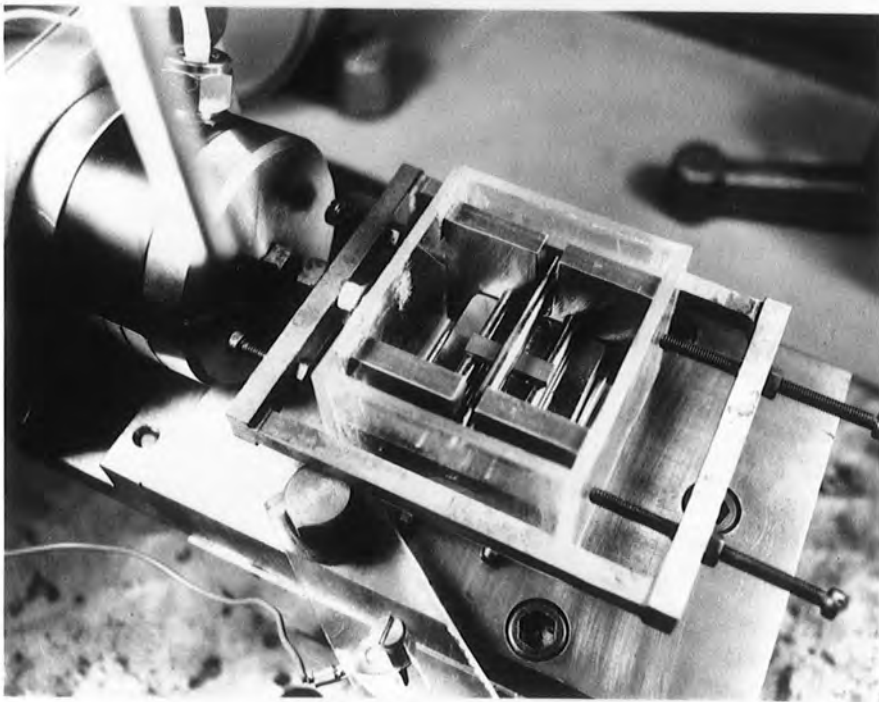


10  $\mu\text{m}$

PLATE 5.3: Etched surface of WC-16% Co.

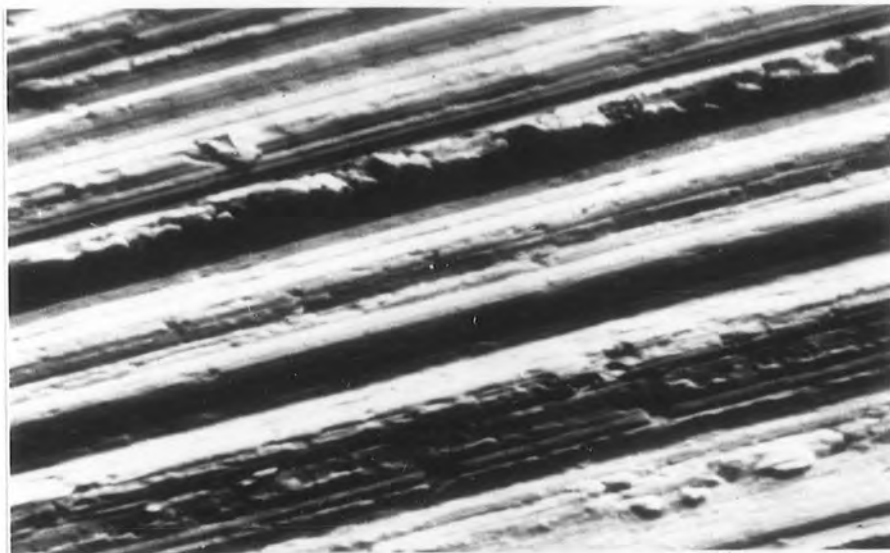


(a)



(b)

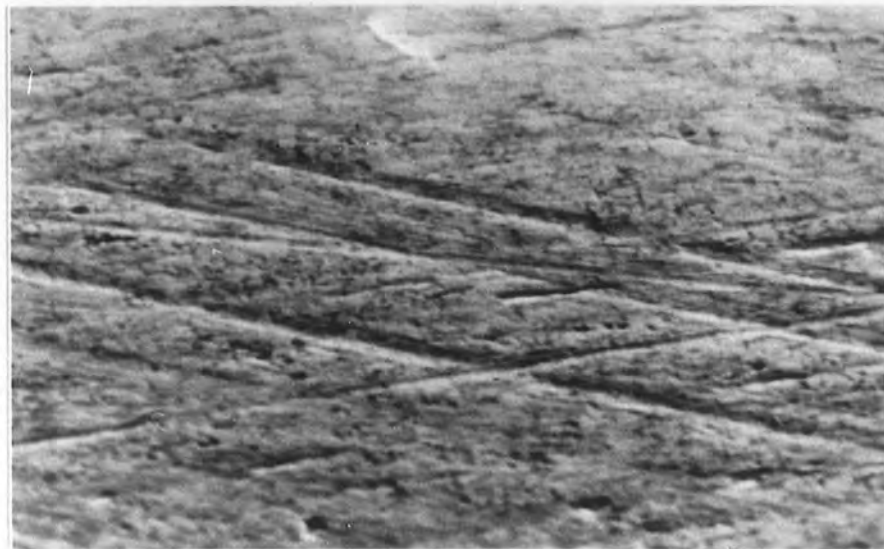
PLATE 6.1: The three point bend rig. (a) with load applied; (b) with the top portion removed to show the specimen, loading rods, alignment formers and environmental box.



(a)



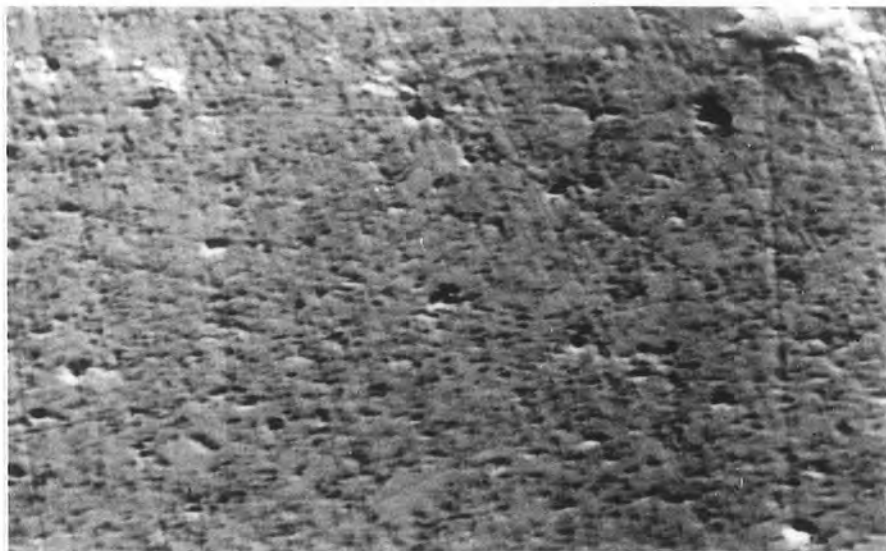
(b)



(c)

10  $\mu$ m  
|-----|  
 \   
 (all)

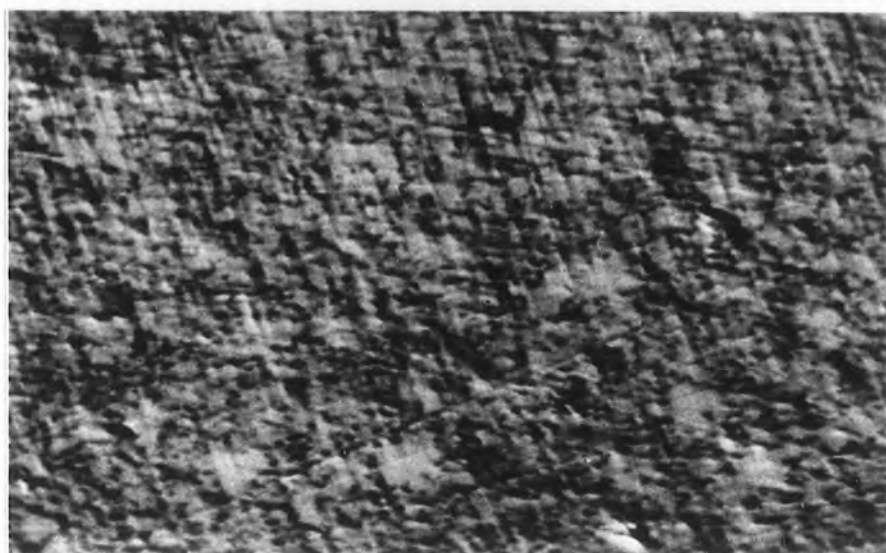
PLATE 6.2 : Scanning electron micrographs of the surfaces of bend specimens with a ground finish. (a) WC-6% Co; (b) WC-13% Co; (c) WC-16% Co.



(a)



(b)

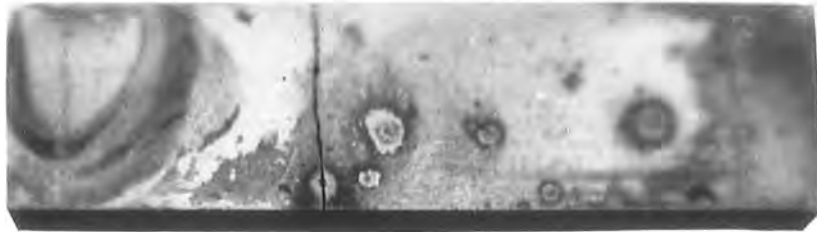


(c)

10  $\mu$ m  
|-----|  
  \  
  (all)

PLATE 6.3:

Scanning electron micrographs of the surfaces of bend specimens with a polished finish. (a) WC-6% Co; (b) WC-13% Co; (c) WC-16% Co.



5 mm

PLATE 6.4:

WC-13% CO specimen loaded to failure after a presoak of 150 hours in distilled water. Excessive discolouration around surface flaws, and the critical flaw on the line of fracture can be clearly seen.

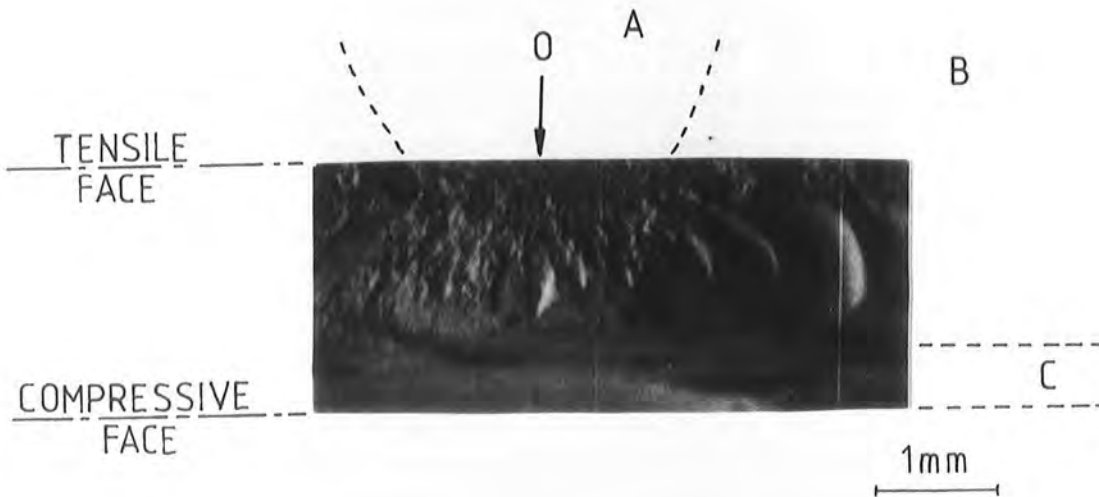
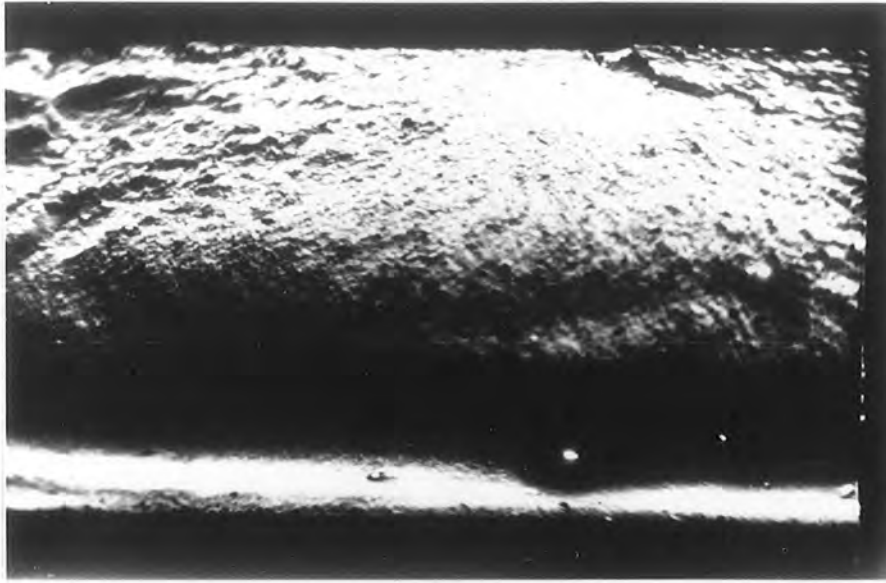


PLATE 6.5:

WC-16% specimen fracture face showing the approximate location of fracture initiation (O), the smooth elliptical region (A), the outer rough region (B) and the final ligament to be broken (C).



(a)

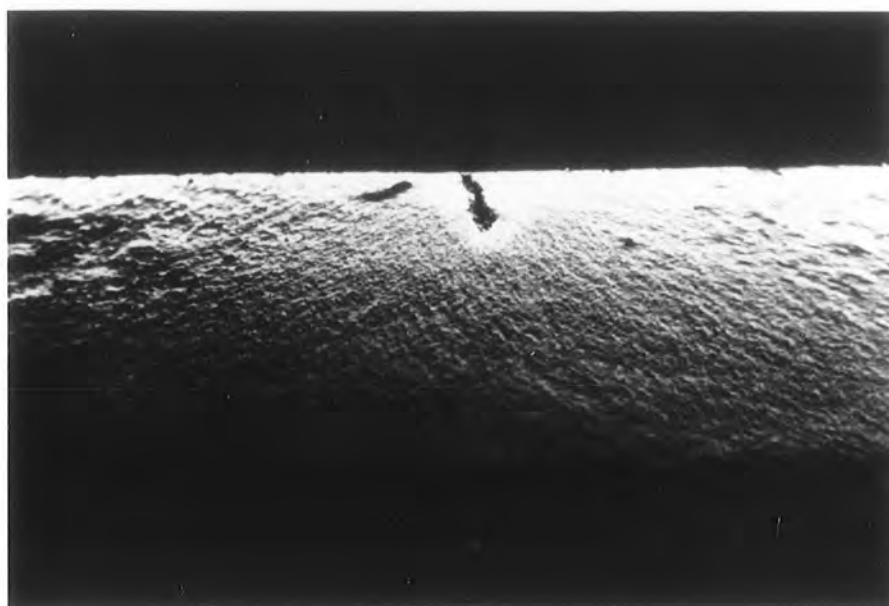
400 μm



(b)

40 μm

PLATE 6.6: Scanning electron micrograph of a WC-16% Co specimen fracture face containing a large surface flaw. (a) general view; (b) close-up of flaw.



(a)

400 $\mu$ m

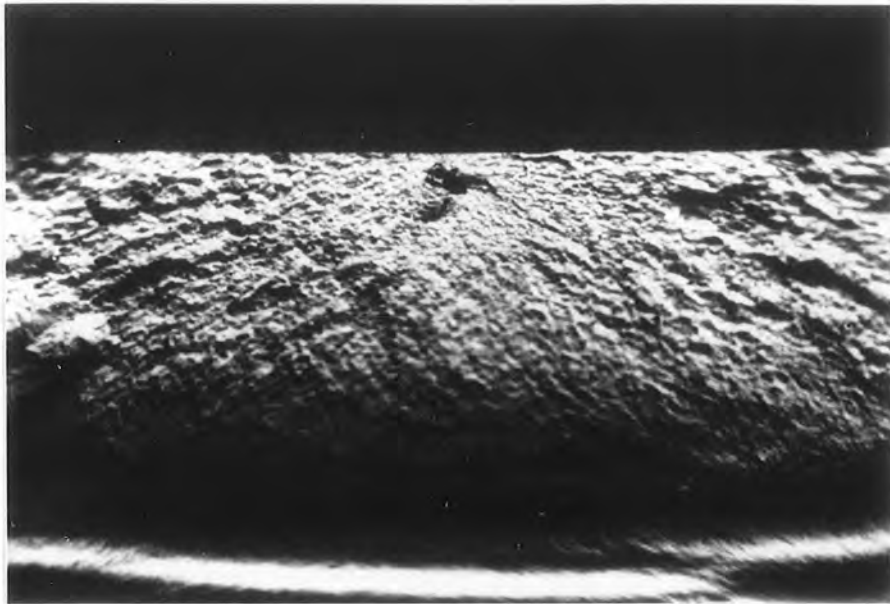


(b)

40 $\mu$ m

PLATE 6.7:

Scanning electron micrographs of a WC-16% Co specimen fracture face containing an extremely large surface flaw. (a) general view; (b) close-up of flaw. (An enlargement of this flaw appears on the Frontispiece.)



(a)

400 μm



(b)

100 μm

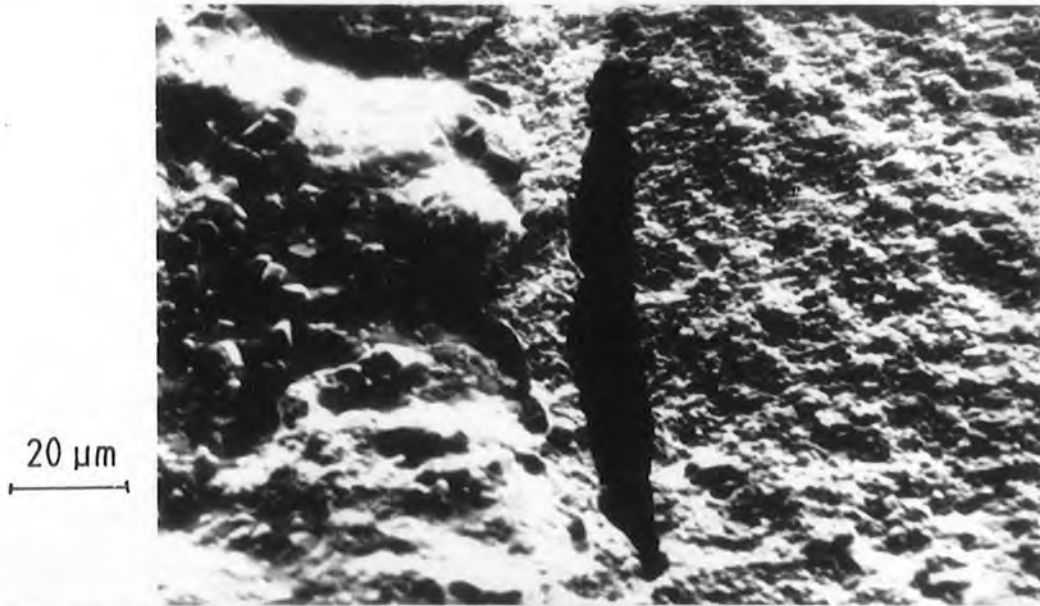
PLATE 6.8:

Scanning electron micrographs of a WC-16% Co specimen fracture face containing a sub-surface flaw. (a) general view; (b) close-up of flaw.



(a)

200  $\mu\text{m}$



20  $\mu\text{m}$

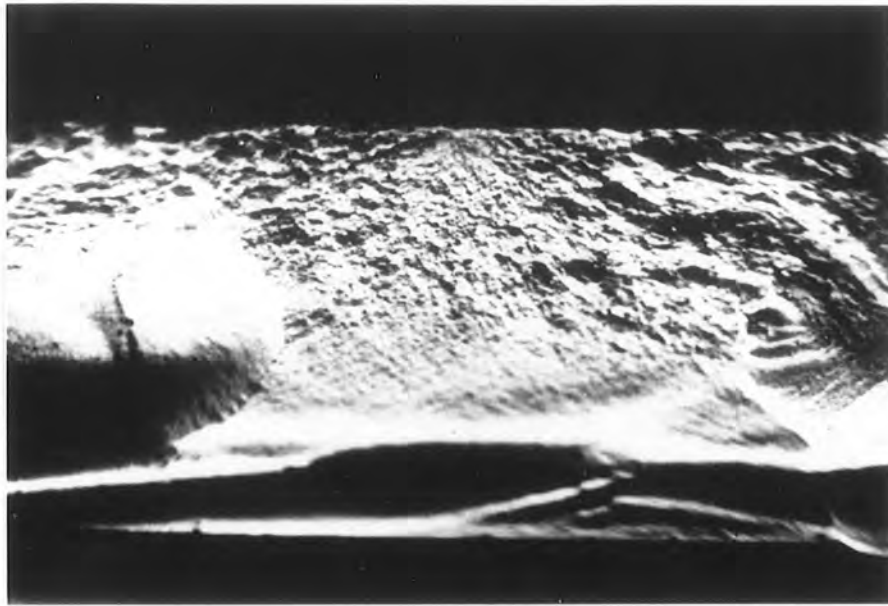


(b)

20  $\mu\text{m}$

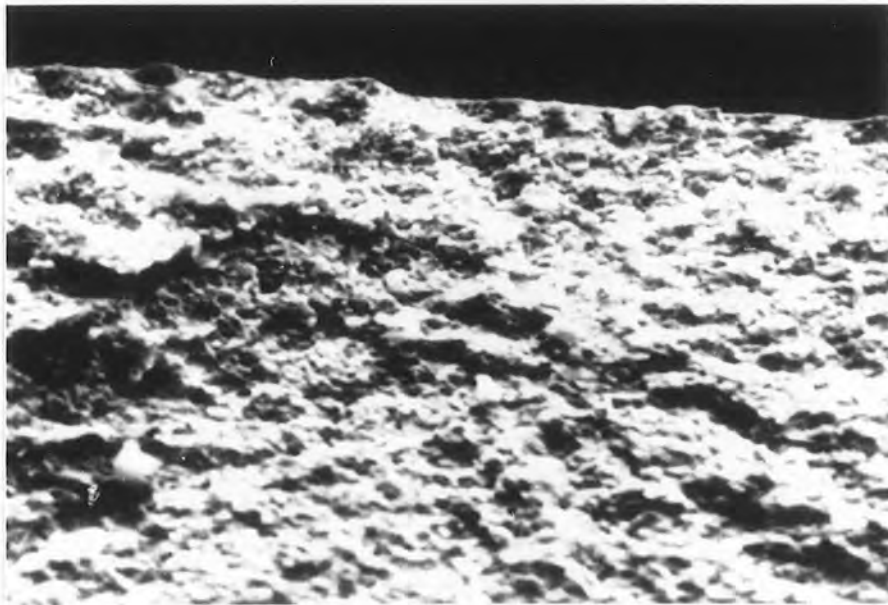
PLATE 6.9:

Scanning electron micrographs of a WC-6%Co specimen fracture face containing a large sub-surface multiple flaw system. (a) general view; (b) close-ups of crescent-shaped voids.



(a)

400  $\mu\text{m}$



(b)

20  $\mu\text{m}$

PLATE 6.10:

Scanning electron micrographs of a WC-16% Co specimen fracture face on which no large flaw was detected. (a) general view; (b) close-up of apparent site of fracture initiation.

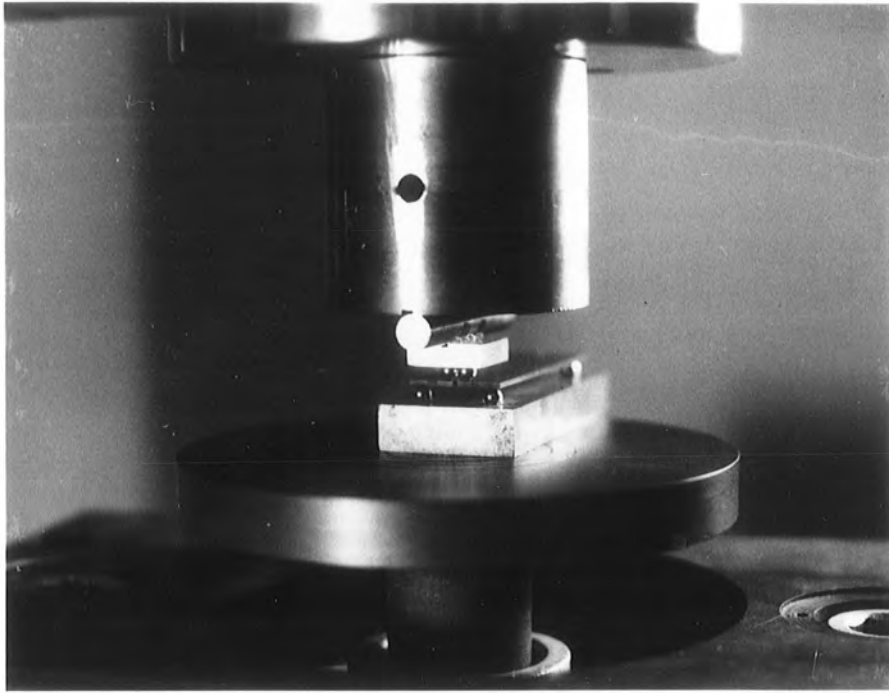


PLATE 7.1: The double torsion rig.

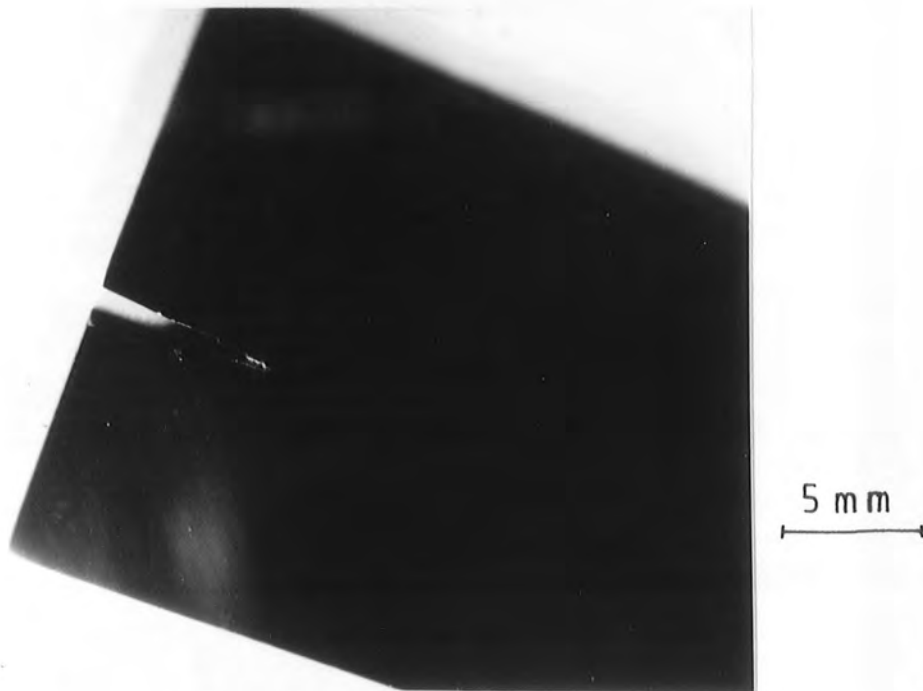


PLATE 7.2: WC-6% Co double torsion specimen with a machined notch sharpened by spark erosion.

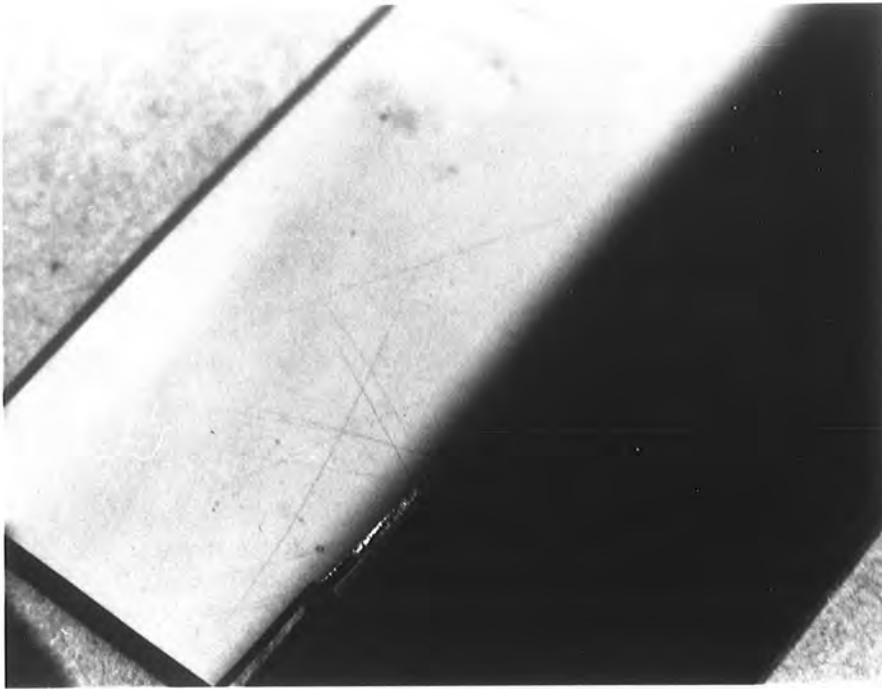


PLATE 7.3: The "kink" on the compressive ungrooved face of a double torsion specimen, highlighted by the reflected boundary of a dark object.

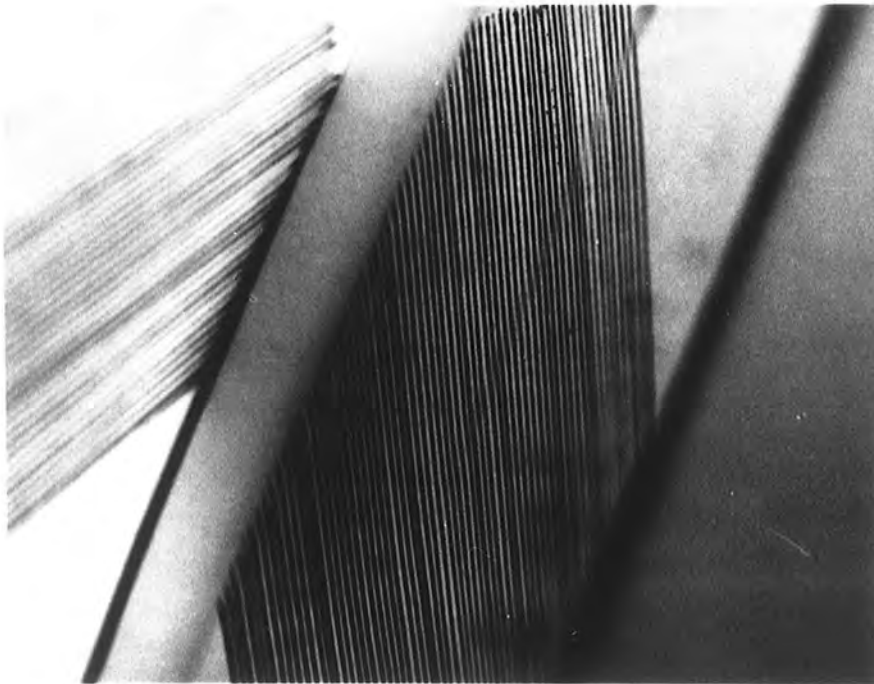
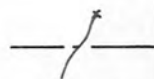
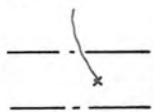
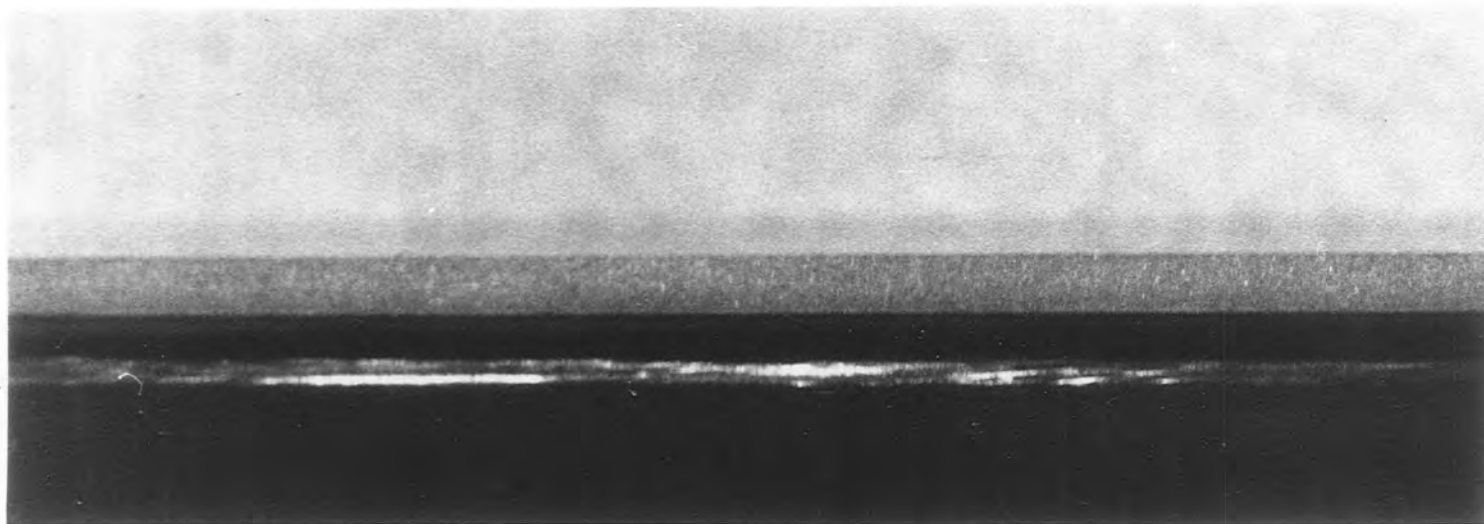


PLATE 7.4: Observation of the "kink" using reflections of a parallel line grid seen in the surface of the specimen. (The crack may be seen by viewing the Plate obliquely along the grid lines.)

FRACTURE  
FACE



GROOVE  
WALL



2 mm

PLATE 7.5: Fracture face of a WC-6% Co double torsion specimen.

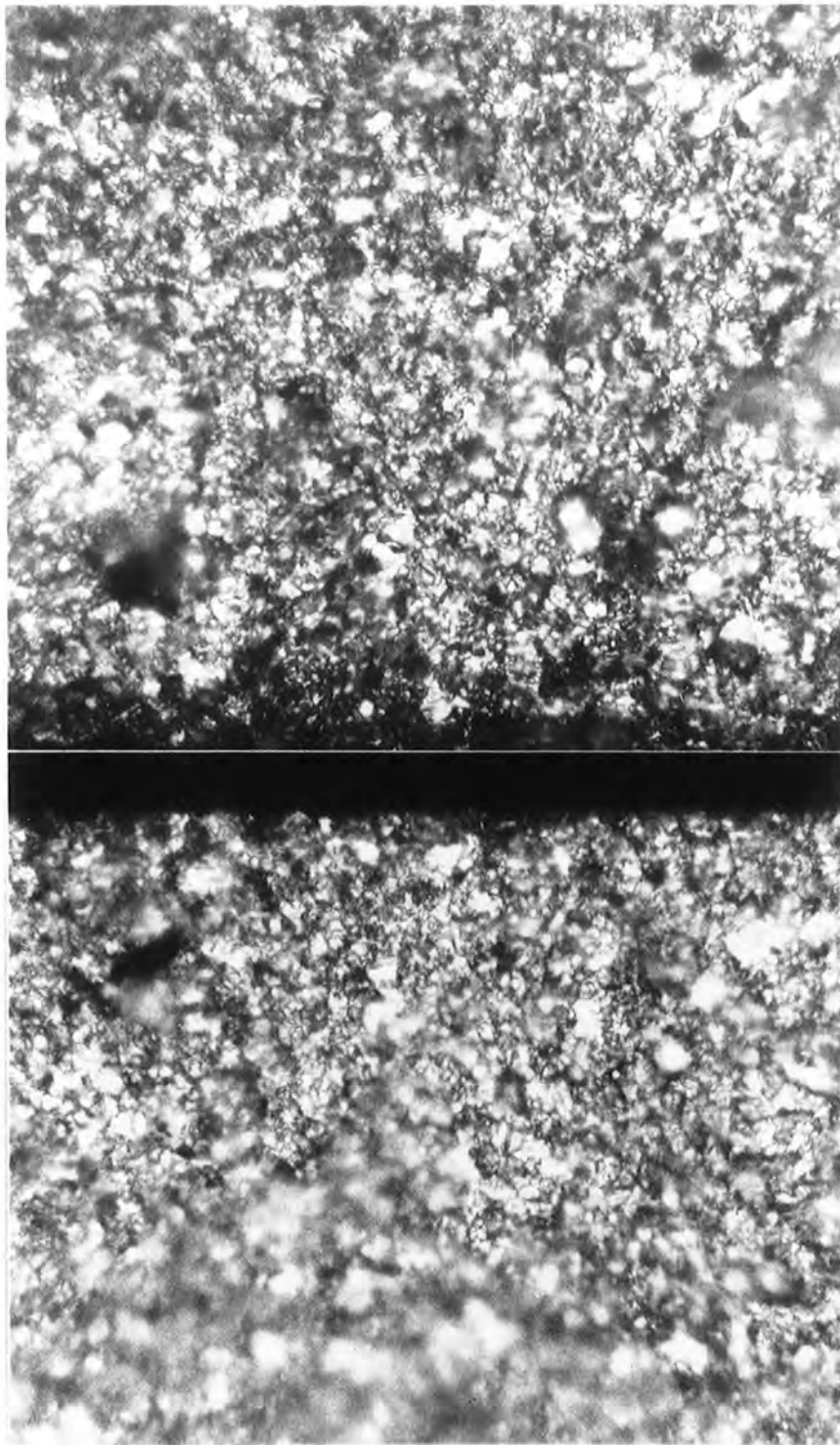
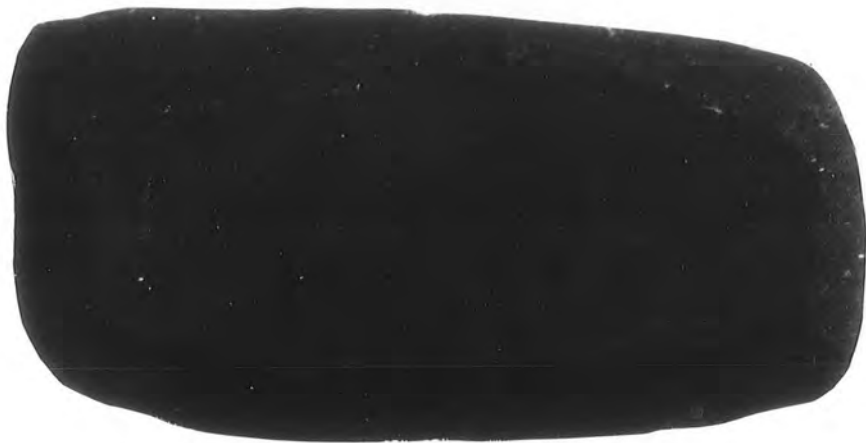
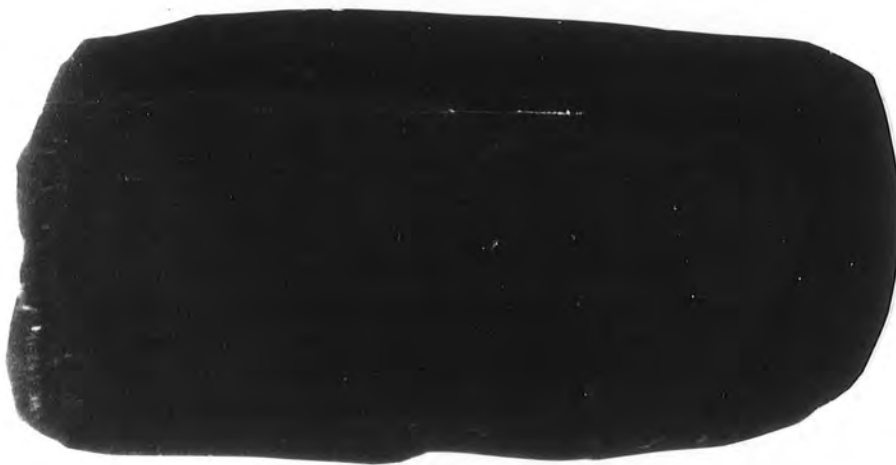


PLATE 7.6: Matching portions of the two fracture faces of a WC-16% Co double torsion specimen.



(a)

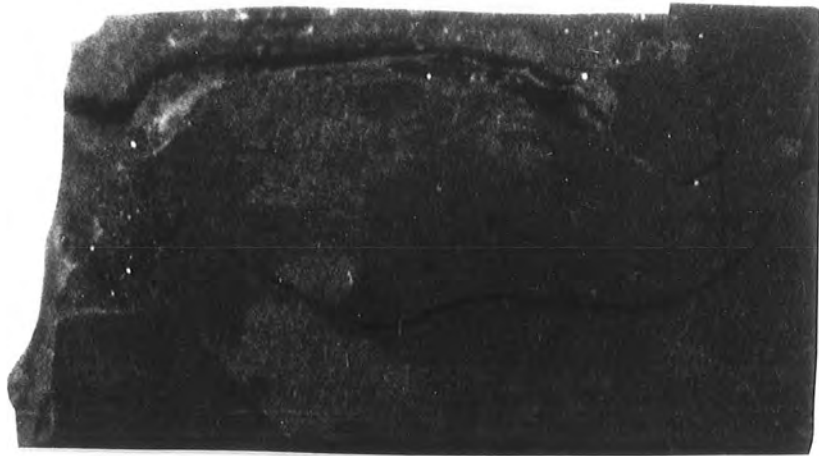
2 mm



(b)

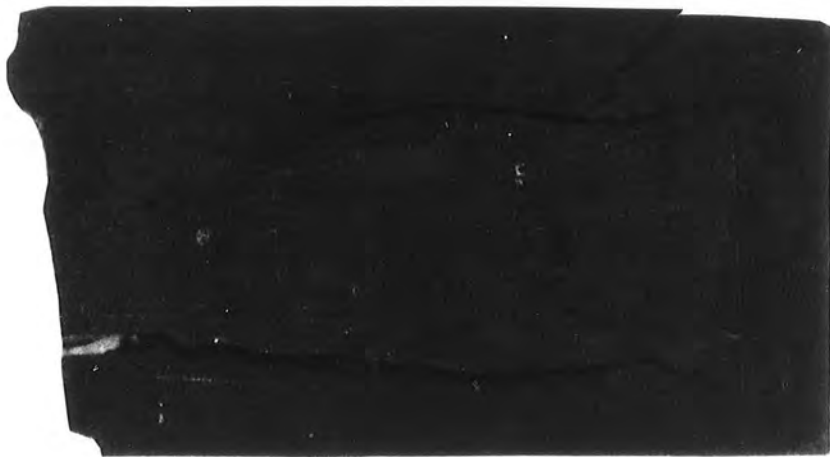
PLATE 7.7:

The first WC-13% Co specimen to be soaked in a 10% solution of nitric acid - after 14 days. The edges have broken away to leave the specimen in the shape of a lozenge. (a) tensile face; (b) compressive face.



( a )

2 mm



( b )

PLATE 7.8: The second WC-13% Co specimen to be soaked in a 10% solution of nitric acid - after 14 days. (a) tensile face; (b) compressive face.